STRUCTURES OF WERNER CLATHRATES

A thesis submitted to the

UNIVERSITY OF CAPE TOWN

in fulfilment of the requirements for the degree of

DOCTOR OF PHILOSOPHY

by

MICHAEL WILLIAM TAYLOR
B.SC.(HONS.) (CAPE TOWN)

Department of Physical Chemistry
University of Cape Town
Rondebosch 7700
South Africa

December 1988

ACKNOWLEDGEMENTS

I would like to thank:

Professor L.R. Nassimbeni for his patient supervision, advice and opportunities presented to me.

Dr. M.L. Niven for her helpful discussions and time freely given.

My colleagues in the Long Room for their patience, good spirits and friendly words.

My wife Susan, whose constant love, support and inspiration during the past six years has made this all possible.

My parents for all their enthusiasm and encouragement.

The University of Cape Town, C.S.I.R. (Pretoria) and Mintek (Randburg) for the financial assistance.

This work is dedicated to my wife

PUBLICATIONS AND CONFERENCE PROCEEDINGS

Parts of this work have been published:

1) Studies in Werner Clathrates. Part 7. Structures of bis(isothiocyanato)tetrakis(4-phenylpyridine)nickel(II) and its clathrates with *ortho*-Xylene, *meta*-Xylene and *para*-Xylene + Dimethylsulphoxide.
L.R. Nassimbeni, M.L. Niven and M.W. Taylor,
Inorg. Chim. Acta, **132**, 67 (1987).

2) Studies in Werner Clathrates. Part 9. Structures with bis(isothiocyanato)tetrakis(4-phenylpyridine)nickel(II) as host.
L.R. Nassimbeni, M.L. Niven and M.W. Taylor,
J. Chem. Soc., Dalton Trans., in press.

3) Studies in Werner Clathrates. Part 10. Structures of bis(isothiocyanato)bis(4-methylpyridine)bis(4-phenylpyridine) nickel(II) with acetylacetone and 1-chlorobutane.
L.R. Nassimbeni, M.L. Niven and M.W. Taylor,
J. Coord. Chem., in press.

4) Studies in Werner Clathrates. Part 11. Structure and thermal analysis of bis(isothiocyanato)tetrakis(4-phenylpyridine) nickel(II) benzene clathrate (1:4).
L.R. Nassimbeni, M.L. Niven and M.W. Taylor,
Acta Cryst., in press.

5) Studies in Werner Clathrates. Part 12. Structures of four novel but non-clathrating complexes.
L.R. Nassimbeni, M.L. Niven and M.W. Taylor,
Acta Cryst., submitted.

Parts of this work have been presented to:

The South African Chemical Institute - Young Chemist's meeting, University of Cape Town, July 1985.

The South African Crystallographic Society, CSIR, Pretoria, January 1986.

The American Crystallographic Association, McMaster University, Hamilton, Ontario, Canada, 22-27 June 1986.

The Fourteenth International Congress of Crystallography, Perth, Australia, 12-20 August, 1987.

ABSTRACT

This work is predominantly devoted to the 4-phenylpyridine ligand and the role that it plays in the formation of a series of inorganic coordination complexes termed Werner Clathrates. The synthesis and characterization by single crystal X-ray diffraction techniques are reported for 18 structures, the majority of which, upon crystallization, have the ability to include solvent or guest molecules within the host framework. The compounds are divided into four broad classes with the host complex of each as follows:

Class A $[Ni(NCS)_2(4\text{-}PhPy)_4]$

Class B $[NiCl_2(4\text{-}PhPy)_4]$

Class C $[Ni(NCS)_2(4\text{-}MePy)_2(4\text{-}PhPy)_2]$

Class D $[NiX_2(dmso)_2(4\text{-}PhPy)_2]$ where $X = NCS^-$ or Cl^-

and $[Ni(NCS)_2(4\text{-}RPy)_4]$ where R = 4-*t*-Bu or 4-Bz.

The guest molecules, anionic ligand and substituent on the pyridine ligand have all been varied to try to establish the role that they each play in the formation of a structure. Much effort has been spent on the location and refinement of disordered guest molecules. Use has been made of statistical disorder and molecular scattering factors to try and successfully model these guests.

The shapes of the cavities containing the guest molecules have been mapped by volume calculations and comparisons made between the packing of the compounds. Several of the complexes pack in space groups which are subsets of others and attempts have been made to determine the cause of the reduction in symmetry.

A new technique to analyze competition experiments, with two guest solvents competing for occupation of the voids within the host lattice, has been established. Preliminary results for competition between *p*-xylene/benzene, *p*-xylene/toluene and *p*-xylene/ethylbenzene with the host complex $[Ni(NCS)_2(4\text{-ViPy})_4]$ are reported. The ability of the host complex $[Ni(NCS)_2(4\text{-MePy})_2(4\text{-PhPy})_2]$ to separate a series of straight chain alcohols is demonstrated. The preference, by this host complex, for guest molecules containing a linear skeleton of 5 non-hydrogen atoms, is explained in terms of potential energy and residual volume calculations.

Thermal analysis, consisting of thermogravimetry and differential thermal analysis, has been performed on several of the compounds. Temperatures of guest release, host decomposition and the enthalpies involved at each of these steps are reported.

ABBREVIATIONS USED IN THIS WORK

4-ViPy	4-Vinylpyridine.
4-PhPy	4-phenylpyridine
4-MePy	4-methylpyridine
4-EtPy	4-ethylpyridine
4-BzPy	4-benzylpyridine
4-*t*-BuPy	4-tertiarybutylpyridine
dmso	dimethylsulphoxide
MeOH	methanol
EtOH	ethanol
acac	acetylacetone
e.s.d.	estimated standard deviation
s.o.f.	site occupancy factor

TABLE OF CONTENTS

CHAPTER ONE

INTRODUCTION

The history of Inclusion Compounds can now be traced back to 1823 when Faraday[1.1] reported the preparation of the chlorine clathrate hydrate. The nineteenth century literature carries several other observations which today are recognized as significant in the field of inclusion compounds. These include the preparation of graphite intercalates[1.2] in 1841; the (unexpected) preparation of the β-quinol clathrate with H_2S[1.3] in 1849, and with SO_2[1.4] in 1859 and formic acid plus carbon monoxide[1.5] in 1886; the preparation of cyclodextrin inclusion compounds[1.6] in 1891 and the preparation of a nickel cyanide ammonia inclusion compound with benzene[1.7], now known as the Hofmann inclusion compound, in 1897.

For nearly fifty years, from the beginning of this century, many authors still reported an apparent "variable composition" for their synthesized compounds. The preparation of the tri-*o*-thymotide benzene inclusion compound[1.8] in 1909; clathrates of Dianin's compound[1.9] in 1914; choleic acid inclusion compounds[1.10] in 1916 and the urea inclusion compounds[1.11] in 1940 were all reported with little or no understanding as to the nature or spatial arrangements of the compounds.

Although confirmation was still almost another twenty years in coming, Hofmann gave the first suggestion of voids within a complex in 1928[1.44] when he wrote the formula of his compound as $Ni(CN)_2.NH_3.C_6H_6$ but added that one might conclude that strict spatial requirements conditioned the

uptake of benzene (or its equivalent) into the "luckenhafte Komplex $Ni(CN)_2NH_3$" from which he dropped the dot. Here was the suggestion of voids associated with the other dot.

It was only in 1948 with the publication of the famous paper by H.M. Powell[1.12], in which he revealed the structure of the β-quinol complex with sulphur dioxide, that it was confirmed that one molecule was completely surrounded by another without any ordinary chemical bond existing between the two. The word "clathrate" arising from an ancient word "*clathratus*", meaning closed or protected by the crossbars of a trellis, was introduced and has gained respectability by being included in the *Oxford English Dictionary.*

Inclusion compounds are formed when a particular type of molecule is able to include another molecule, usually smaller, spatially within its structure, leaving the bonding systems of both components unaffected. The enclosing molecular network and the enclosed species have been termed "host" and "guest" respectively. An essential characteristic of the host molecule is, therefore, its ability to form a structure with hollow spaces of large enough dimensions to house the prospective guests.

The number of abstracts appearing under "Clathrate" or "Inclusion Compound" sections in *Chemical Abstracts* has risen dramatically over the past few years. Fig 1.1 shows the annual distribution of these abstracts (1948 - 1981); zeolites and all compounds described as "solvates" have been excluded. With the number of different types of host-guest

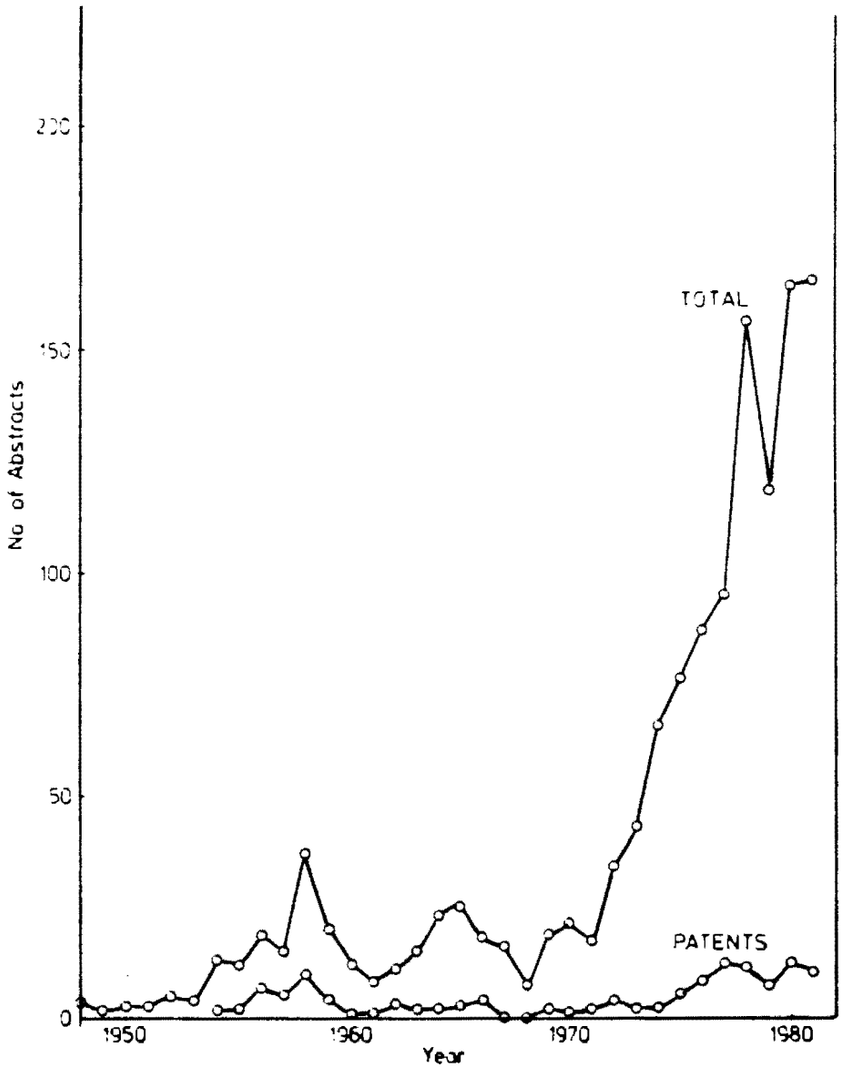

Fig. 1.1 The annual distribution of abstracts on inclusion compounds, excluding zeolites and 'solvates', 1948-1981.

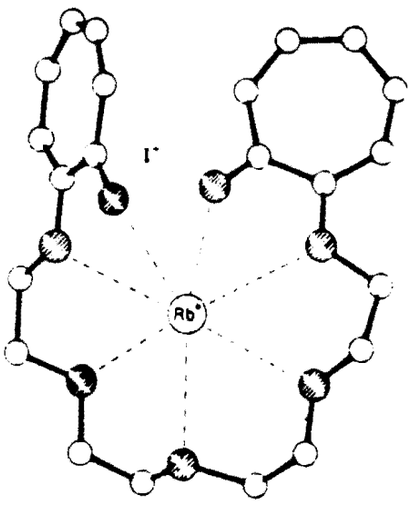

Fig. 1.2 An example of an open-chain polyether, wrapped around a rubidium cation to enable direct interactions with all seven oxygen atoms.

compounds increasing annually, classification has become extremely confusing and terms such as tweezer molecules, spherands, octopus molecules and even "Mobius Strip" molecules abound in the literature. In 1983, Weber and Josel[1.13] suggested a new form of classification based upon the following criteria: a) host-guest **type** and host-guest **interaction**, b) **topology** of the host-guest aggregate and c) dependence on the **number** of the various components forming the aggregate.

The first division is between the extremes of **complex**, which are derived from a coordination between host and guest, and **clathrates**, where the guest is retained by steric barriers formed by the host lattice. Examples of complexes are crown ethers, first synthesized by C.J. Pedersen[1.14] and which have the outstanding ability to complex with metal ions illustrated in Fig 1.2, and the cryptands, introduced by J M Lehn[1.15].

Host-guest compounds formed by: Dianin's compound (Fig 1.3); urea, schematically represented in Fig 1.4 showing cavity and guest sizes; and graphite intercalated with K (Fig 1.5) are typical examples of clathrates. The decomposition of clathrates in solution is another way of distinguishing between them and complexes which retain their identity in solution.

The broad division between complexes and clathrates is such that many compounds fall somewhere in between them. If they have a dominant clathrate character but display a certain degree of coordinative

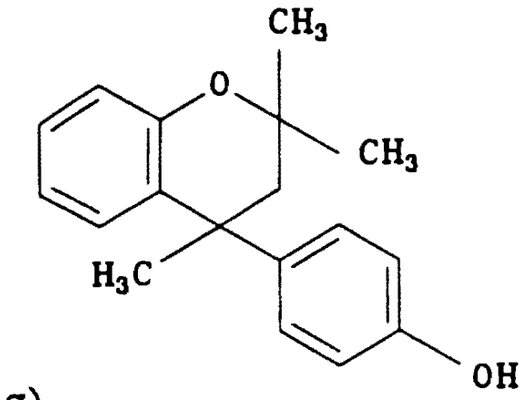

a)

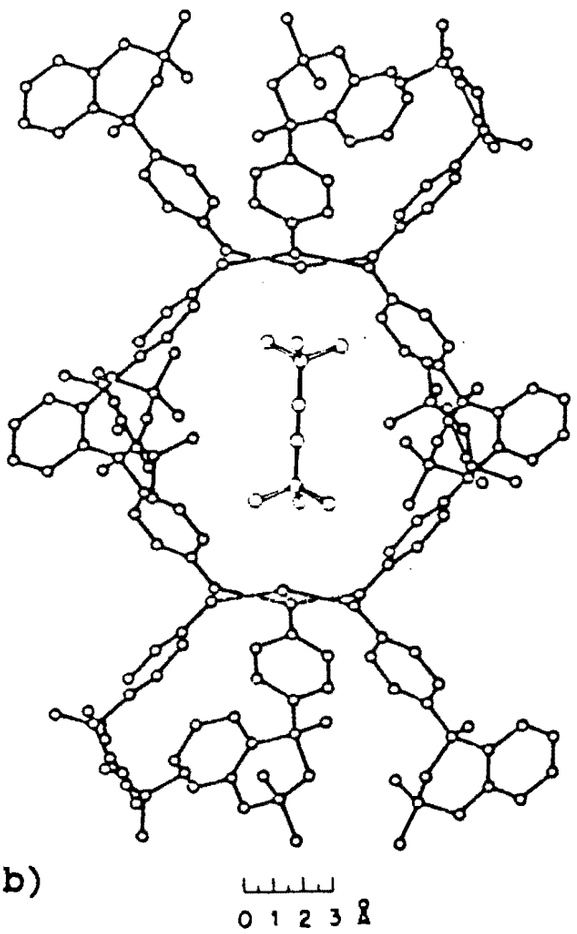

b)

Fig. 1.3 a) Dianin's compound : 4-*p*-hydroxyphenyl-2,2,4-trimethyl chroman.
b) A view normal to the c-axis of the thio derivative, showing a guest molecule in the cavity. Two host molecules have been excluded (except for their hydroxy-oxygen atoms) for clarity.

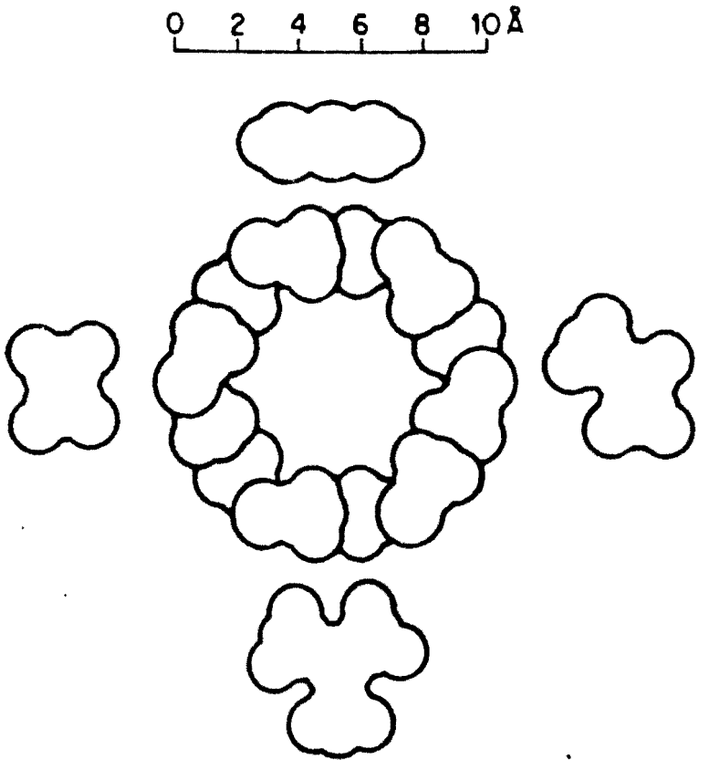

Fig. 1.4 Cross section of the cavity in the urea channel compared with the size of *n*-octane (left), benzene (top), 3-methylheptane (right) and 2,2,4-trimethylpentane (bottom).

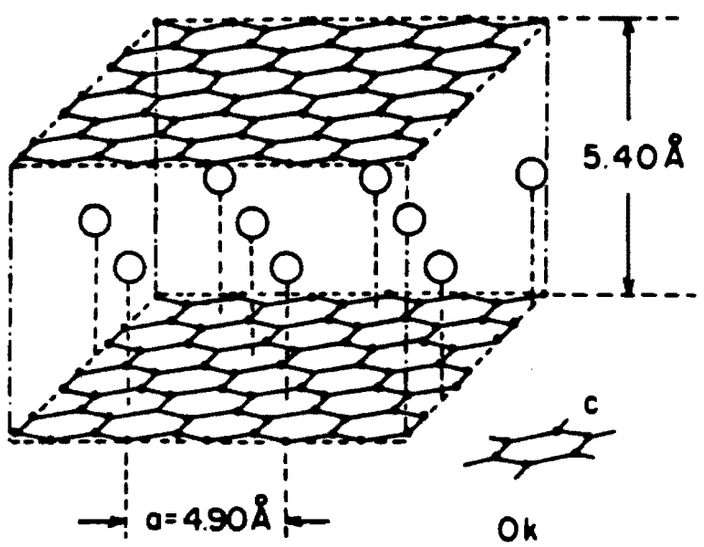

Fig. 1.5 Potassium in graphite - C_8K. The planar distance of graphite has increased from 3.35Å to 5.40Å to accommodate the K atoms.

participation, these are termed **coordinato clathrates**; when the reverse situation is applicable, they are called **clathrato complexes**.

The topological aspect distinguishes between compounds where the host molecule forms a cavity, termed **cavitates**, and **adducts** which do not contain a host cavity. The degree of encapsulation for cavitates can be broken down into five classes, which are, in order of increasing encapsulation;

I) **Intercalate** type which forms two dimensional open layer or sandwich structures, an example of which is the previously displayed aggregate consisting of graphite and potassium.

II) **Coronate** (or **podate**) type which forms a ring-like cavity of which the crown ether illustrated previously in Fig 1.2 is an example.

III) **Tubulates** - the cavity is a one dimensional open channel. The urea/β-paraffin inclusion compound is an example of this large class of compounds.

IV) **Aediculate** (from the Latin "aedicula" meaning niche, pocket) - the host molecule is generally much larger than the guest (*e.g.* protein host) and by folding back on itself, it forms a "pocket" into which the guest fits. Many biochemical systems operate using compounds in this class. Fig 1.6 shows some of the principle groups in the LDH active centre showing lactate and NAD^+ binding.

V) **Cryptate** - the cavity is completely enclosed by the host network. For example Dianin's host-guest compound (Fig 1.3).

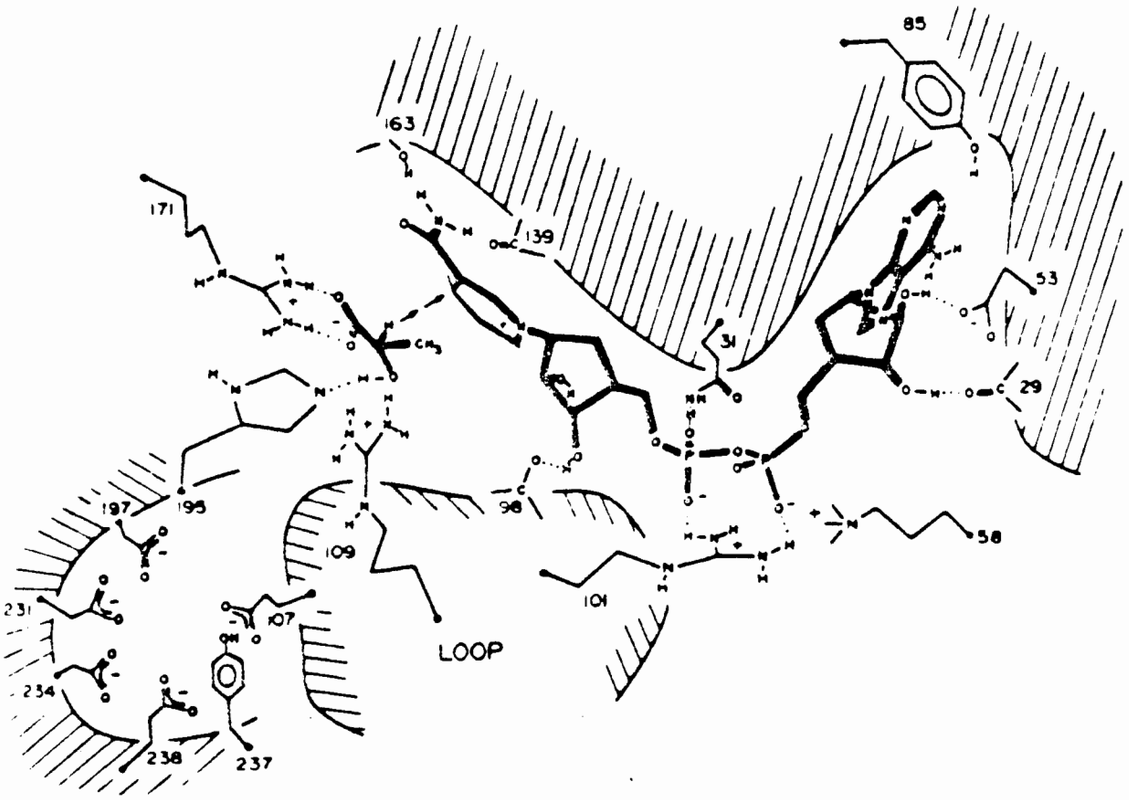

Fig. 1.6 Diagrammatic representation of the principle groups in the LDH active centre showing lactate and NAD^+ binding.

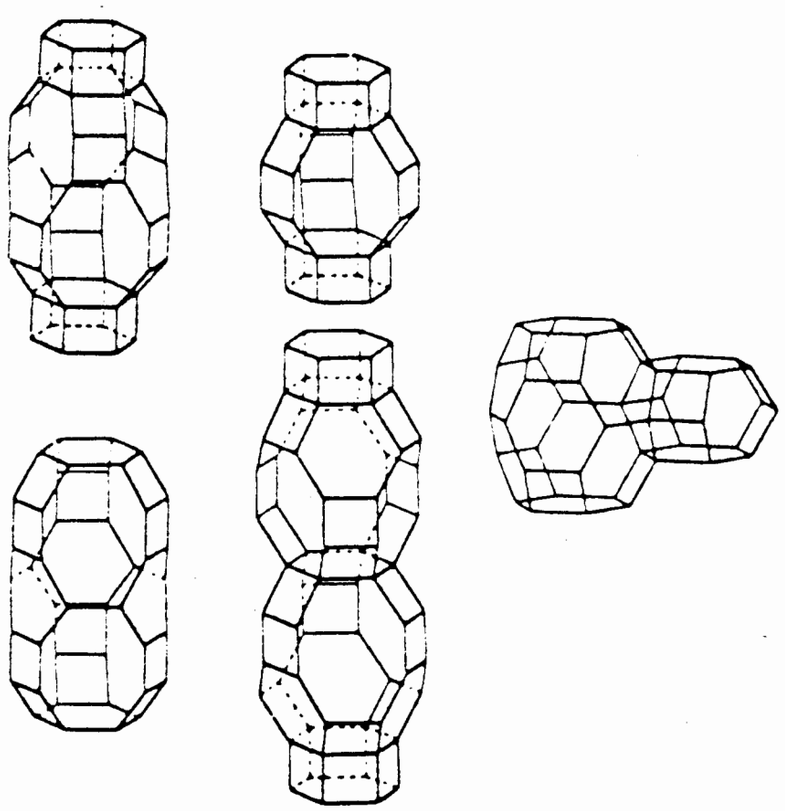

Fig. 1.7 Line drawings of cavities present in some zeolites to illustrate the diversity in size and shape.

Another subdivision is possible: using numerical aspects of the host-guest aggregate. A binary aggregate would include two individual molecular or ionic components and this classification can itself be broken down to include the number of host molecules and the number of guest moieties.

Unfortunately, the above scheme of classification has not become widely accepted and there appears to be a reluctance in the literature to depart from the terms "clathrate" or "inclusion compounds" to describe almost all compounds containing host and guest molecules. Whatever they are called, "clathrates" (used in its broadest sense) are emerging on the chemical scene to take a place of increasing importance. Their formation is novel, their properties unique and their potential uses very varied.

The extreme diversity of host-guest compounds makes any attempt to present a comprehensive survey of all structures within a single chapter very difficult. Thus the object of this introduction is to provide a working knowledge of the various types of inclusion compounds, their unusual behaviour and some of their extensive applications.

The most stable and technically the most useful family of host crystals are the porous tectosilicates, which comprise the **zeolites** and several crystalline silicas having the same framework topologies as certain zeolites. About 60 different zeolite framework topologies are available and many more have been constructed as models and await synthesis. This variety of structure owes its existence to the ease of linking

tetrahedra of SiO_2 and AlO_4^- to make numerous space patterns. Zeolites, which are natural clay minerals, are used to upgrade gasoline, to dry gases commercially, in shape-selective catalysis, as storage media for certain types of nuclear waste, as heat pumps and for many other industrial applications. Line drawings of cavities present in some zeolites are shown in Fig 1.7.

Another large class of inclusion compounds and one in which intense interest is being displayed is that of the cyclodextrins (CD). These are cycloamyloses consisting (predominantly) of six (α), seven (β) or eight (γ) sugar units in α-1,4 linkage. The height of these truncated-cone shaped molecules is constant at 8Å but the internal diameter varies from 5Å in the α-CD to 8Å in the γ-CD. One of the most important features of cyclodextrins concerns the distribution of the hydrophilic and hydrophobic groups. Hydroxyl groups occupy both rims of the cone and render the CDs soluble in aqueous solution. The interior of the cavity is hydrophobic and thus, in solution, these cavities provide a hydrophobic matrix in hydrophilic surroundings. The unique properties of the CD cavity explain some of the unusual features of these molecules. They form inclusion complexes rather unspecifically with a wide variety of guest molecules, even in solution; the only obvious requirement is that the guest must fit into the cavity - albeit only partially. Thus their uses are extremely diverse. Cyclodextrins can be used to stabilize food flavours and fragrances *e.g.* a vanillin-glucose mixture lost all aroma after 240 days whilst no detectable loss was observed after two years for the vanillin-CD analogue[1.16]; cyclodextrins with fragrant substances such as lavender oil have been added to plastics[1.17] to

promote long lasting fragrance. CDs are also used to improve food quality and technology *e.g.* the formation of white precipitate in bamboo shoots canned in water is prevented by adding 0.01-2% β-cyclodextrin[1.18]. The chemical structure, indicating the cavity size is shown in Fig 1.8 which illustrates a β-cyclodextrin.

Another class of compounds, that of the choleic acids, shows similar hydrophilic/phobic character as displayed by the cyclodextrins. 3α,12α-Dihydroxy-5β-cholan-24-oic acid (deoxycholic acid, DCA) is a very versatile host lattice forming inclusion compounds with a wide variety of guest molecules; these include: a 2:1 complex with bromobenzene[1.19], a 3:1 complex with phenanthrene[1.20] and a 4:1 complex with azo dyes[1.21]. The molecules of DCA pack as bilayers (Fig 1.9) with each layer linked by head-to-tail hydrogen bonds and the guest molecules located in channels between adjacent bilayers.

Macrocyclic polyethers (termed "crown" ethers because of the appearance of their molecular models) have remarkable complexing properties towards metal cations, primary alkylammonium salts and other neutral as well as charged potential substrates and have provided new challenges in chemistry during the past 15 years. It is hoped that the process of structured molecular complexation, which is central in enzyme chemistry, may be better understood by developing methods for new design and synthesis of macrocyclic host molecules. The possible applications of crown-ether macrocycles, as model compounds in reactions of stereoselective complexation, ion-transport and molecular catalysis have received much attention recently. The ability of these compounds to

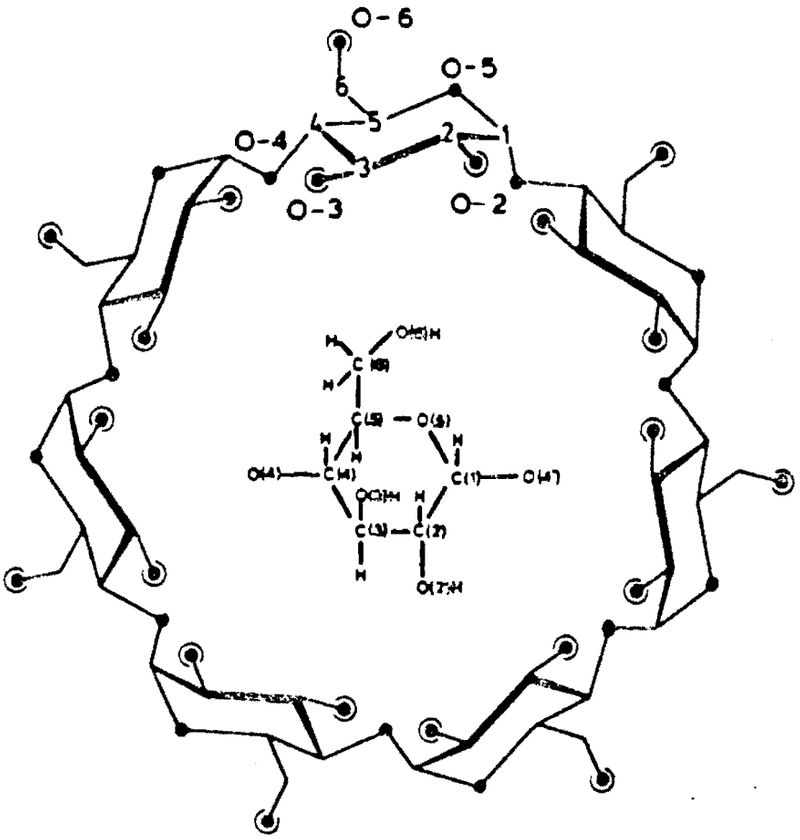

Fig. 1.8 Chemical structure of β-cyclodextrin with oxygen (●) and hydroxy groups (◉) marked. All glucoses are in C_1 chair form.

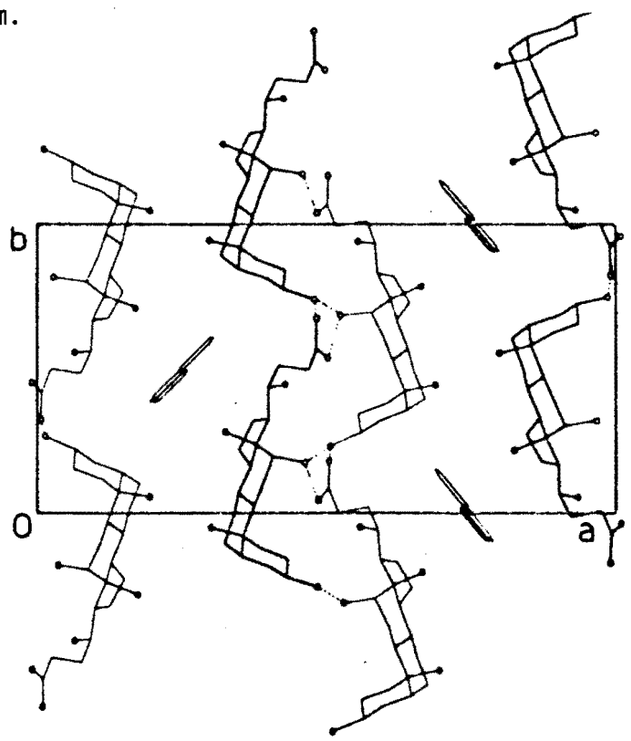

Fig. 1.9 Molecular packing of deoxycholic acid, viewed along *c*, containing phenanthrene as guest molecules. Black and open circles represent methyl groups and oxygen atoms respectively and hydrogen bonding is represented by dashed lines.

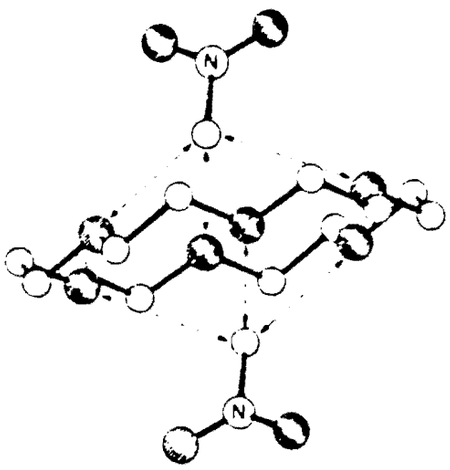

Fig. 1.10 Molecular structure of the 1:2 18-crown-6 complex with nitromethane showing close contacts between each methyl group of the guests and alternate oxygens of the host.

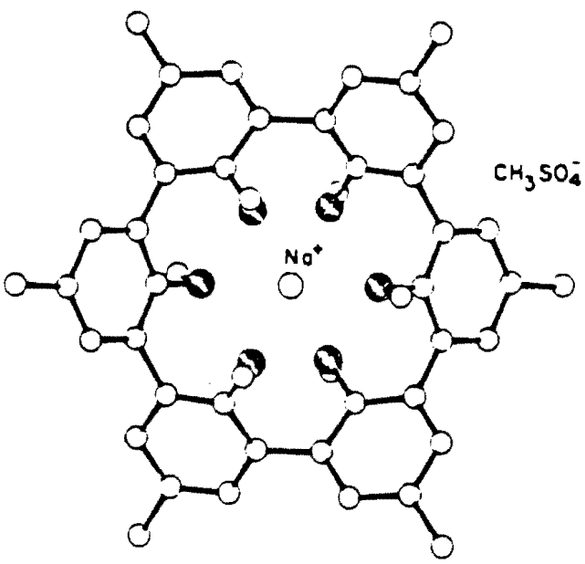

Fig. 1.11 Structure of the spherand cyclohexametaarylene with a sodium ion contained in the cavity.

coordinate organic guests *via* hydrogen bonds to the ether oxygens, such as the 2:1 adduct between nitromethane and 18-crown-6 (Fig 1.10), as well as their ability to insert cations into the cavity (Fig 1.11), which provide model compounds for studies of cation transport across membranes[1.22], allow these inclusion compounds to have extremely diverse properties.

Hofmann-type clathrates, of the general formula, $M(NH_3)_2M'(CN)_4.2G$, where M = Mn-Cu, M′ = platinum group metals and G = small aromatic molecule, have a layered structure of two-dimensional extended metal sheets with ammonia molecules protruding above and below the sheets. The guest molecules are trapped between adjacent sheets. Modifications to the host compounds by replacement of the amino ligands with ambidentate ligands, or replacement of the square planar Ni by a tetrahedral metal serve to alter the stoichiometry and size of the guest types taken up, *e.g.* by changing M from Ni to Mn allows biphenyl to be included as opposed to the classic Hofmann clathrate which contains benzene (Fig 1.12).

Clathrate compounds have been used to enclathrate radioactive or highly toxic material. One of the products of ^{235}U fission is ^{85}Kr with a half life of about 10 years, and the inclusion of this radioactive material in a hydroquinone cage[1.23] so that it can be finely powdered allows its safe and easy handling. Highly toxic organo-mercurials such as dimethyl mercury[1.24] may be handled with comparative safety in the form of its clathrate with thiachroman, a structural modification of Dianin's compound.

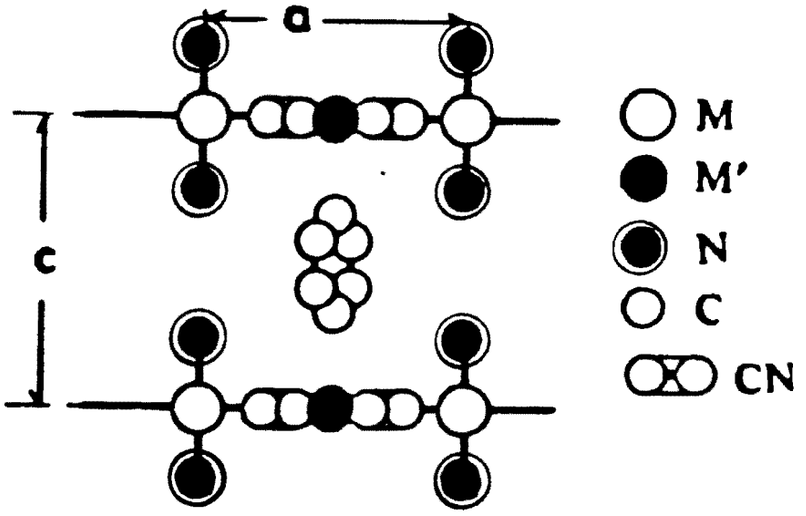

Fig. 1.12 The structure of the Hofmann-type inclusion compound $Ni(NH_3)_2Ni(CN)_4.2C_6H_6$.

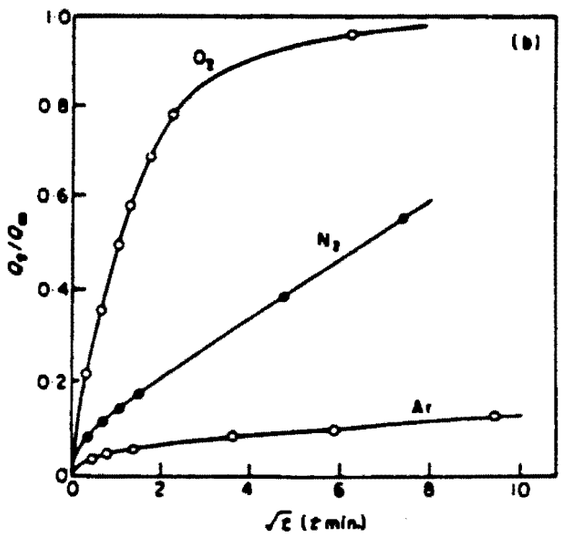

Fig. 1.13 Sorption rates of O_2, N_2, and Ar in a narrow port Ca-mordenite at 195K.

The field of superconductors has, during the past 18 years, attracted much attention to intercalation compounds. 2H-tantalum disulphide (2H-TaS_2) is a superconductor at 0.8K and can be intercalated with organic compounds[1.25] which have the effect of enhancing the superconducting transition temperature (T_c). Intercalation of glycinamide hydrochloride in 2H-TaS_2, for example, raises T_c to 4.1K[1.26].

Clay minerals, such as smectites and vermiculites, can be permanently opened and made porous by exchanging interlayer cations with suitably large globular ions. By varying the size, charge and shape of the entering ion, as well as the cation exchange capacity of the clay mineral, the molecular sieve character of the expanded clay mineral sorbents can be altered as required. Fig 1.13 shows the dramatic difference in rate of uptake of O_2, N_2 and Ar in a narrow port Ca-mordenite at 195K[1.27].

The examples presented thus far of host-guest compounds have shown the wide range of cavity types displayed in these compounds. One class of compounds, however, shows this wide range of encapsulation within itself; ranging from complete encapsulation to open one dimensional cavities. Werner clathrates, named for Alfred Werner, a pioneer in coordination chemistry, are inclusion compounds consisting of a host framework of the general formula MX_2L_4; where M is a divalent transition metal cation *e.g.* Mn^{2+},Fe^{2+}, Co^{2+}, Ni^{2+}, Cu^{2+}, Zn^{2+}, Cd^{2+}; X is an anionic ligand *e.g.* NCS^-, NCO^-, CN^-, NO_3^-, halide; and L is an

electrically neutral substituted pyridine, α-arylalkyamine or isoquinoline. By varying these constituents, the number of possible different MX_2L_4 complexes which can theoretically be synthesized runs into the thousands. The complexes studied most extensively thus far, have the general formula $[Ni(NCS)_2(4\text{-}RPy)_4]$ with R typically representing an alkyl group. The size and chemical composition of guest components vary from atoms of the noble gases[1.28] through to relatively large aromatic molecules[1.29]. It was the paper by Schaeffer *et al*[1.29] in 1957 that stimulated interest in Werner Clathrates, in which their use in the separation of various aromatic hydrocarbons from petroleum fractions was announced.

Apart from their ability to enclathrate a wide variety of guest molecules, Werner clathrates have another major advantage in that their synthesis is usually very simple. For the isothiocyanate derivative, simple addition of an SCN^- salt to a nickel hydrate followed by addition of the substituted pyridine is all that is required to precipitate the host powder complex. Crystallization of the host in the presence of a guest is usually sufficient to obtain the clathrate.

Werner clathrates have been used to separate isomers[1.30] and the Union Oil Company built a pilot plant for the separation of the *meta* and *para* isomers of xylene using the selectivity of the $[Ni(NCS)_2(4\text{-}MePy)_4]$ host for the *para* isomer. Recently Smith and coworkers[1.31] showed that this host compound displays a small preference for the deuterated species of *p*-xylene but that this preference is not sufficient to allow realistic separation of the isotopes.

For all clathrates of the form $[Ni(NCS)_2(4\text{-}RPy)_4.nG]$ (G = guest molecule), the host molecule has distorted octahedral coordination about the nickel atom which is bonded to the six ligands through their nitrogen atoms. Interactions between ligands in this overcrowded central region allows for only a limited number of stable conformations with the pyridine ligands twisted from their coplanar arrangement. The NCS^- group, is frequently bent about the nitrogen atom and this angle is governed in part by non-bonded interactions. The N-C-S moiety is typically linear and there are thus two possible extremes for the arrangement of the anionic moieties.

i

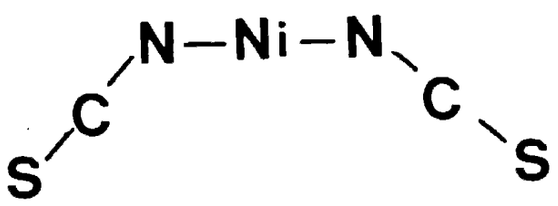

&

ii

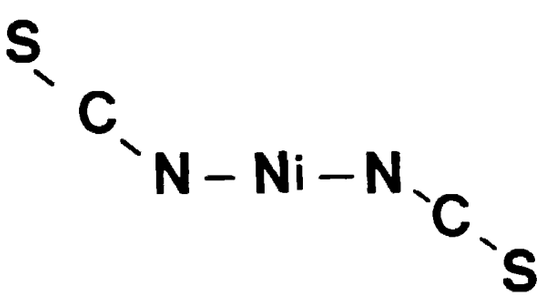

Variation between these extremes causes the S atom to move by as much as 1.4Å.

The role that the substituent on the pyridine plays in the molecular packing is not obvious. Its presence is not essential to form clathrates *e.g.* $Co(NCS)_2Py_4$ forms inclusion compounds with iodine[1.32] and

iodoform[1.33]. However there are many more clathrates known when the hydrogen in the 4-position of the pyridine is replaced by, for example, a methyl group. The added bulkiness of the substituent obviously promotes the formation of interstitial space between host molecules during crystallization and to ensure that the system remains energetically favourable, guest molecules fill this space. For a substituent larger than a methyl group, the orientation of the substituent adds another variable to the host conformation. This is demonstrated by the 4-EtPy derivative which forms two different phases, neither of them clathrates, which differ merely in the orientation of some of the ethyl groups[1.34].

It would thus appear that in order to increase the size of the cavities, and hence induce either a higher guest:host ratio or improve the ability of the host to include larger guest molecules, an increase in the size of the substituent would be logical.

The 4-MePy derivative has been studied extensively and its physico-chemical properties have been reviewed by Lipkowski[1.35]. The 4-ViPy derivative has recently received much attention[1.36,1.37] and the ability of the isothiocyanate sulphur to participate in secondary bonding with iodine has been displayed[1.38]. An extremely versatile ligand and one which has shown remarkable diversity in its clathrating ability is the 4-ethyl substituted pyridine[1.34].

This work is largely dominated by the 4-PhPy derivative, with both NCS^- and Cl^- as the anionic ligand. Other prospective host compounds, those

containing the 4-*t*-BuPy and the 4-BzPy ligands, have been studied. Unfortunately the latter two derivatives, which are longer or bulkier than the 4-PhPy derivative, could not be crystallized with a guest molecule included within the host framework. Thus an increase in size of the substituent on the pyridine does not necessarily improve the host's capabilities of forming a clathrate.

The nomenclature[1.39] 'α-phase' for a non-clathrating lattice type (clathrand) and 'β-phase' for a porous clathrating type has been widely adopted. More specifically, the term β-phase indicates the packing arrangement adopted by many of the 4-Me, 4-Et and 4-Vi pyridine clathrates when they crystallize in the tetragonal $I4_1/a$ space group. However, thus far, no particular packing arrangement has appeared to predominate for the 4-PhPy clathrate, nor have any crystals formed in the $I4_1/a$ space group. Therefore, in this work, the term α-phase refers to a non-clathrating complex whilst β-phase refers to any system where a guest molecule has been included within the host framework.

Although Werner Clathrates have only been industrially applied in the two instances: firstly by the Union Oil Company mentioned previously and secondly in the Labofina process for separating *m*- and *p*-xylene using $[Ni(NCS)_2(\alpha$-(*m*-chlorophenyl)ethylamine$)_4]$[1.40], the search is still on for a host lattice that will either be specific for a particular molecule, isomer or isotopomer, or one that will selectively enclathrate a particular group of organic compounds with a high guest:host ratio.

Methods to determine the specificity of a complex are not trivial. Firstly it must be demonstrated that the host can consistently enclathrate a guest molecule with a specific host:guest ratio. Generally this requires a crystal structure determination to be carried out on the clathrate and consequently suitable single crystals must be grown. Once it has been proved that a particular host can include a guest (or guests), competition experiments must be devised to demonstrate that the uptake of one guest is preferred over that of others. Smith and coworkers have published several results pertaining to the $[Ni(NCS)_2(4\text{-}MePy)_4]$ host and its preference for particular guest molecules over others[1.31,1.41,1.42]. Their experiments involve continual mixing of the host and competing guests until equilibrium is reached, and then analyzing both solid and liquid phases for each of the guests. Comparison of the guest ratios in each phase reveals the selectivity of the host towards one of the guest molecules. In this work further competition experiments are reported (Chapter 5) with the 4-ViPy derivative as the host complex.

The success of some Werner Clathrates to separate mixtures on a small scale *e.g.* benzene and thiophene which by other techniques are extremely difficult to separate, has been displayed chromatographically[1.43]. Reported in this work are some results showing the preference of the mixed base host complex $[Ni(NCS)_2(4\text{-}MePy)_2(4\text{-}PhPy)_2]$ towards molecules containing a 5-atom skeleton. Thus this particular host will separate butanol from other alcohols when used in a filled column in a gas chromatograph.

Work covered in this report will be added to the rapidly increasing 'data-bank' of knowledge on Werner Clathrates. Hopefully, one day, it will be possible to consult the data-bank to establish which host complex will most successfully separate a particular mixture of guest solvents to isolate the desired product.

REFERENCES

1.1 M. Faraday, *Quart. J. Sci.*, 15, 71 (1823).

1.2 C. Schafhautl, *J. Prakt. Chem.*, 21, 129 (1841).

1.3 F. Wohler, *Ann. Chem. Liebigs*, 69, 297 (1849).

1.4 A. Clemm, *Ann. Chem. Liebigs*, 110, 357 (1859).

1.5 F. Mylius, *Ber. Bunsenges Phys. Chem.*, 19, 999 (1886).

1.6 A Villiers, *C.R. Hebd. Sceances Acad. Sci.*, 112, 536 (1891)

1.7 K.A. Hofmann and F. Kuspert, *Z. Anorg. Allg. Chem.*, 15, 204 (1897).

1.8 R. Spallino and G. Provenzal, *Gass. Chim. Ital.*, 39, 325 (1909).

1.9 A.P. Dianin, *J. Soc. Phys. Chem. Russe*, 46, 1310 (1914).

1.10 H. Wieland and F. Sorge, *Z. Physiol. Chem. Hoppe-Seyler's*, 97, 1 (1916).

1.11 M.F. Bengen, German Patent Application, OZ 123438 (1940).

1.12 H.M. Powell, *J. Chem. Soc.*, 61 (1948).

1.13 E. Weber and H. -P. Josel, *J. Incl. Phenom.*, 1, 79 (1983).

1.14 C.J. Pedersen, *J. Am. Chem. Soc.*, 89, 2495 ,7017 (1967).

1.15 B. Diethrich, J. -M. Lehn and J.P. Sauvage, *Tetrahedron Lett.*, 2885 (1969).

1.16 J. Szettli, L. Szente and E. Banky-Elod, *Acta. Chim. Acad. Sci. Hung.*, 101, 27 (1979).

1.17 K.K. Kyoshin, *Chem. Abst.*, 93, P221523v (1980).

1.18 Takeda Chem. Ind. Ltd., Japan Kokai, 81,78,574 (1981)

1.19 A. Damiani, E. Giglio, N. Morosoff, R. Puliti and I. Rosen, *Ric. Sci.*, 37, 42 (1967).

1.20 W. MArx and H. Sobotka, *J. Org. Chem.*, 1, 275 (1936).

1.21 G. Cilento, *J. Am. Chem. Soc.*, 72, 4272 (1950).

1.22 J. Rebek, Jr. and R.V. Wattley, *J. Am. Chem. Soc.*, 102, 4853 (1980).

1.23 D.J. Chleck and C.A. Ziegler, *Nucleonics*, 17(9), 130 (1959).

1.24 R.J. Cross, J.J. McKendrick and D.D. MacNicol, *Nature*, **245**, 146 (1973).

1.25 R.F. Gamble, F.J. Di Salvo, R.A. Klemm and T.H. Geballe, *Science*, **168**, 568 (1970).

1.26 G. Acosta and N.M. Chapela, *J. Incl. Phenom*, **3**, 9 (1985).

1.27 R.M. Barrer, *Zeolites and Clay Minerals as Sorbents and Molecular Sieves*, Academic Press, p 290 (1978).

1.28 S.A. Allison and R.M. Barrer, *J. Chem. Soc.*, **A**, 1717 (1969).

1.29 W.D. Schaeffer, W.S. Dorsey, D.A. Skinner and C.G. Christian, *J.Am. Chem. Soc.*, **79**, 5870 (1957).

1.30 P. Starzewski and J. Lipkowski, *Pol. J. Chem.*, **53**, 1869 (1979).

1.31 H.L. Wiener, L. Ilardi, P. Liberati, L. Dengler, S.A. Jeffas, S. Saba and N.O. Smith, *J. Incl. Phenom.*, **4**, 415 (1986).

1.32 H. von Hartl and S. Steidl, *Z. Naturforsch*, **32B**, 6 (1977).

1.33 H. von Hartl and S. Steidl, *Acta. Cryst.*, **B36**, 65 (1980).

1.34 M.H. Moore, L.R. Nassimbeni and M.L. Niven, *J. Chem. Soc., Dalton Trans.*, 2125 (1987).

1.35 J. Lipkowski in *Inclusion Compounds*, eds. J.L. Atwood, J.E.D. Davies and D.D. MacNicol, Academic Press, London, Vol. 1, ch. 3 (1984).

1.36 M.H. Moore, L.R. Nassimbeni ,M.L. Niven and M.W. Taylor, *Inorg. Chim. Acta.*, 115, 211 (1986).

1.37 M.H. Moore, L.R. Nassimbeni and M.L. Niven, *Inorg. Chim. Acta.*, 131, 45 (1987).

1.38 L.R. Nassimbeni, M.L. Niven and A.P. Suckling, *Inorg. Chim. Acta.*, submitted.

1.39 M.I. Hart and N.O. Smith, *J. Am. Chem. Soc.*, 84, 1816 (1962).

1.40 J. Hanotier, *Ind. Chim. Belg.*, 31, 19 (1966).

1.41 S.E. Ofodile, R.M. Kellet and N.O. Smith, *J. Am. Chem. Soc.*, 101:26, 7725 (1979).

1.42 S.E. Ofodile and N.O. Smith, *J. Phys. Chem.*, 87, 473 (1983).

1.43 D. Sybilska and E. Smolkova-Keulemansova in *Inclusion Compounds* eds. J.L. Atwood, J.E.D. Davies and D.D. MacNicol, Academic Press, New York, Vol. 3, ch 6 (1984).

1.44 K.A. Hofmann in 'Lehrbuch der Anorganischen Chemie' (1928)

CHAPTER TWO

CHAPTER TWO

EXPERIMENTAL

The 18 compounds reported in this work can be divided into 4 broad classes as follows:

A) the α and β phases of $[Ni(NCS)_2(4\text{-}PhPy)_4]$

B) the β phases of $[NiCl_2(4\text{-}PhPy)_4]$

C) the β phases of $[Ni(NCS)_2(4\text{-}MePy)_2(4\text{-}PhPy)_2]$

D) various α phases of the type:

$[NiX_2(dmso)_2(4\text{-}PhPy)_2]$ where X = NCS^- or Cl^-

$[Ni(NCS)_2(4\text{-}RPy)_4]$ where R = *t*-Bu or Bz

Table 2.1 lists all compounds reported, with host and guest formula, their respective code names and their classes. This table is repeated on the fold out section located on the inside back cover of this work for ease of reference.

The main technique used to analyze both the molecular and crystal structure of these compounds is single crystal X-ray diffraction. The theory behind this technique is not discussed in this work as there are many excellent texts, of which 'Crystal Structure Analysis' by J.P. Glusker and K.N. Trueblood, (Oxford University Press, 1985) and 'X-ray Structure Determination' by G.H. Stout and L.H. Jensen (MacMillian, London, 1968), are highly recommended to the interested reader.

TABLE 2.1 Compound Classes, Numbers and Codenames for all Structures reported in this work.

HOST	COMPOUND	GUEST	CODE.
Class A			
$[Ni(NCS)_2(4\text{-}PhPy)_4]$	I	-	PHEN
	II	*o*-xylene	PHENOX
	III	*m*-xylene	PHENMEX
	IV	*p*-xylene + dmso	PHENPAX
	V	4-PhPy + 2-methoxyethanol	DILUT
	VI	4-PhPy + dmso	PHENALC
	VII	Phenylacetylene + dmso	PHENACR
	VIII	Benzene	PHENBEN
Class B			
$[NiCl_2(4\text{-}PhPy)_4]$	IX	Methanol	PHENSAY
	X	*m*-xylene	FENMEX
	XI	*p*-xylene	FENPAX
	XII	4-PhPy	FENTET
Class C			
$[Ni(NCS)_2(4\text{-}MePy)_2(4\text{-}PhPy)_2]$	XIII	Acetylacetone	DIEC
	XIV	1-chlorobutane	DECAME
Class D			
$[Ni(NCS)_2(dmso)_2(4\text{-}PhPy)_2]$	XV	-	METAG
$[NiCl_2(dmso)_2(4\text{-}PhPy)_2]$	XVI	-	PHENDIM
$[Ni(NCS)_2(4\text{-}t\text{-}BuPy)_4]$	XVII	-	TERB
$[Ni(NCS)_2(4\text{-}BzPy)_4]$	XVIII	-	BENNEY

2.1 SYNTHESIS

2.1.1 Synthesis of the host powder complexes $[Ni(NCS)_2L_4]$

where L = 4-BzPy, 4-MePy, 4-PhPy or 4-*t*-BuPy.

The host complexes were synthesized by the method of Schaeffer *et al*[2.1] with minor variations as follows.

Method 1.

To an aqueous solution (50ml) of $NiCl_2.6H_2O$ (8.4mmole) was added KSCN (16.8mmole). The substituted pyridine (4-BzPy, 4-*t*-BuPy or 4-MePy), or the substituted pyridine dissolved in a minimum of methanol (4-PhPy), (37mmole) was added dropwise with constant stirring. A blue precipitate of the host powder complex formed, and the mixture was stirred for an additional 30 minutes before being filtered, washed thoroughly with water and dried overnight in a desiccator.

Method 2.

To an alcoholic solution (50ml methanol) of $NiCl_2.6H_2O$ (8.4mmole) was added KSCN (16.8mmole). The white precipitate of KCl which formed was filtered and the substituted pyridine (4-PhPy), dissolved in a minimum of methanol, was added slowly to the filtrate. The blue host powder which formed was filtered, washed with methanol and dried as in Method 1. The filtrate was retained, for further recovery of host, as it was very light blue in colour.

2.1.2 Synthesis of the host powder complex $[NiCl_2(4\text{-}PhPy)_4]$

This host powder complex was prepared in a similar manner to that described in Method 2 with the exception that no KSCN was added. After the blue precipitate had been filtered, washed and dried, the filtrate was concentrated by evaporation until further precipitation was induced, which was also filtered and treated as before.

2.2 CLATHRATE FORMATION.

2.2.1 Class A. $[Ni(NCS)_2(4\text{-}PhPy)_4]$

Compound (I), the α-phase complex, was formed by the slow evaporation, at room temperature, of the filtrate retained from Method 2 of the previous section. Small blue needle-shaped crystals, congregated in clumps, formed after several days. Suitable single crystals were mounted on glass fibres and covered with a thin layer of cyanoacrylate glue to prevent deterioration in the atmosphere.

Compounds (II)-(VIII) were prepared by dissolving the host powder complex $[Ni(NCS)_2(4\text{-}PhPy)_4]$ in a suitable solvent, and then layering the resulting solution with the intended guest, or if the guest is a solid, with the guest dissolved in methanol.

Unlike the 4-MePy, 4-EtPy and 4-ViPy derivatives, the 4-PhPy host complex is soluble in only a few solvents. This factor necessitated the use of a co-solvent which, unfortunately, introduces the possibilities

of mixed guests being included or even the co-solvent exclusively being included in the clathrate.

Solubility tests with over 20 common organic solvents indicated that only dmso, 2-methoxyethanol and methanol could be considered as suitable co-solvents. The host complex is soluble in hot dmso (0.154g/ml @ 50°C) and slightly less so in hot 2-methoxyethanol (0.086g/ml @ 50°C). All other solvents were deemed to be unsuitable as less than 0.01g host complex would dissolve in 1ml solvent even when heated to boiling point.

Compound (II)-(IV) and (VI)-(VIII) were crystallized by dissolving the host complex in hot dmso whilst compound (V) was crystallized from hot 2-methoxyethanol.

All layered solutions were stoppered and allowed to stand at room temperature for about 2 weeks. If no crystals had formed after this period, slow evaporation of the resulting solution was allowed. For all seven compounds, blue plate-like crystals formed amongst an amorphous sediment within 1 month of the initial layering.

Crystals of suitable size were cut from the plates and mounted in Lindemann capillaries with mother liquor, to prevent deterioration by the desorption of the guest solvent. Deterioration was rapid in many instances and if the crystals were out of contact with their mother liquor for a period of greater than five minutes, the crystals would crack and therefore be unsuitable for X-ray diffraction. Thus within this period, crystals had to be removed from the vial, selected for

their ability to uniformly extinguish plane polarized light, cut, and wedged inside a capillary in a position so as not to interfere with the sealing process, before mother liquor could be introduced. Sealing of the Lindemann capillaries was also often difficult. Many of the solvents used are inflammable and thus the flame used to seal the capillary had to be hot enough to melt the glass before the solvent ignited. It could not be too hot however, or else it would boil the solvent which would either dislodge the crystal or cause it to dissolve. Sealing wax was often used to ensure complete closure of both ends of the capillary.

2.2.2 Class B. $[NiCl_2(4\text{-}PhPy)_4]$

Clathrates were formed from the host compound by layering a saturated methanolic solution of $[NiCl_2(4\text{-}PhPy)_4]$ with a solution of the intended guest. The layered solutions were treated as previously described in the Class A clathrates with similar results.

2.2.3 Class C $[Ni(NCS)_2(4\text{-}MePy)_2(4\text{-}PhPy)_2]$

Formation of clathrates in this class involved dissolving the solid host complex $[Ni(NCS)_2(4\text{-}MePy)_4]$ (4mmole) in *ca.* 20 ml 2-methoxyethanol by heating to 60°C. To this hot solution, 4-PhPy (15mmole) dissolved in a minimum of methanol was added slowly . The solution was allowed to cool and then carefully layered with the intended guest solvent. The stoppered vials were allowed to stand at room temperature, and after about 10 days blue prismatic-shaped crystals formed.

2.2.4 Class D. $[NiX_2(dmso)_2(4\text{-}PhPy)_2]$ or $[Ni(NCS)_2(4\text{-}RPy)_4]$

where X = NCS^- or Cl^-, and R = 4-*t*-BuPy or 4-BzPy

For compounds (XV) and (XVI) the respective host complexes $[Ni(NCS)_2(4\text{-}PhPy)_4]$ and $[NiCl_2(4\text{-}PhPy)_4]$ were dissolved in hot dmso. The solutions were then allowed to slowly evaporate at room temperature. After a few days, purple-blue diamond shaped crystals formed in the solution containing the isothiocyanate derivative. This clathrate had been characterized previously[2.2] and thus the solution was allowed to continue to evaporate for several months. In both solutions, after about 1 month, tiny conglomerates of needle-shaped crystals appeared; these grew with time until suitable crystals were obtained after about 3 months.

For compounds (XVII) and (XVIII), attempts to form β-phase clathrates failed even when the host complexes, $[Ni(NCS)_2(4\text{-}t\text{-}BuPy)_4]$ and $[Ni(NCS)_2(4\text{-}BzPy)_4]$ respectively, were dissolved in a variety of solvents (dmso, $CHCl_3$, thf, 2-methoxyethanol, ethanol) and layered with a variety of guests. The $CHCl_3$ solutions for both complexes produced suitable blue monoclinic-shaped crystals after approximately 1 week of standing of a solution layered with diethylether.

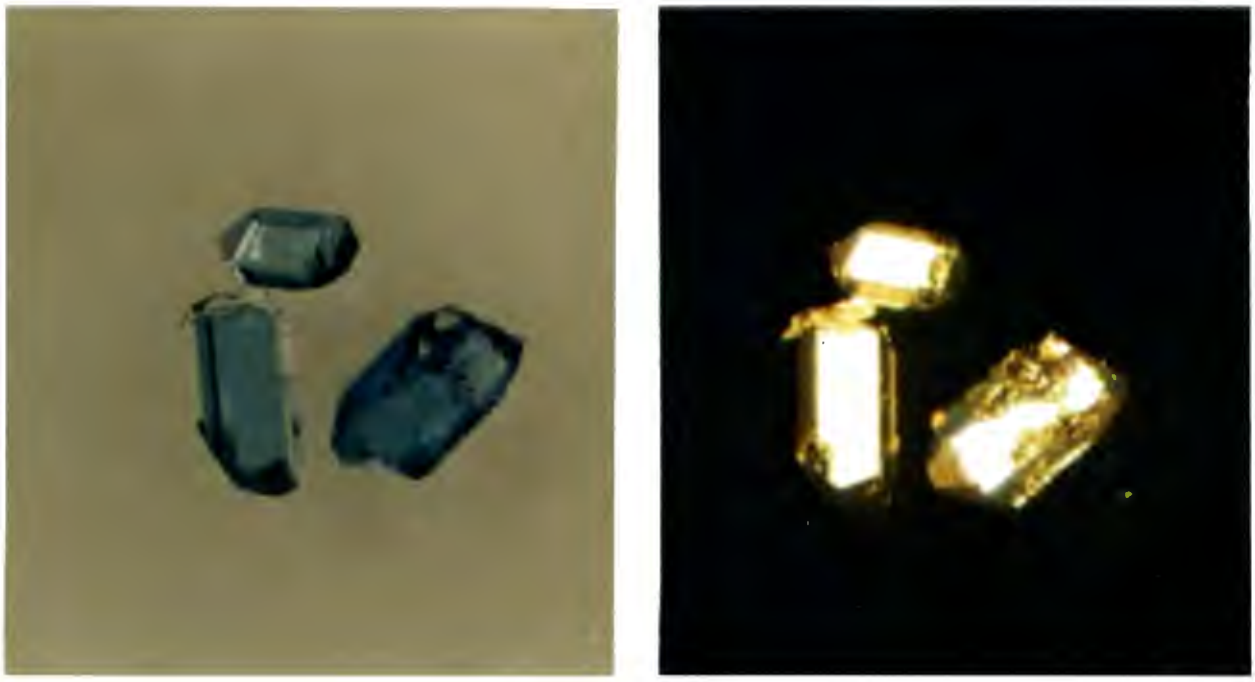

a b

Photograph 1 Crystals of Compound (XVIII) illuminated with: a) overhead and b) plane polarized light.

Photograph 2 Crystals of Compound (XIII) after 10 minutes exposure to the atmosphere.

2.3 ANALYSES

2.3.1 Microanalysis

Elemental analysis was carried out to determine the percentages of carbon, hydrogen and nitrogen. All analyses were performed on an Hereaus Universal Combustion Analyser, Model CHW-MICRO.

The analysis of each host powder complex was determined after synthesis and these are listed in Table 2.2. Owing to the inability of purifying the host complexes by recrystallization (possible clathrate formation prevents this), this technique was employed to confirm the gross composition of the complex, rather than the absolute purity. Thus relatively large deviations between calculated and measured percentages were tolerated.

Microanalysis could not be used on the clathrate crystals to determine composition for two reasons:

a) Owing to the continual desorption of the guest solvent, the crystals deteriorate rapidly on standing in the atmosphere and, within 5 minutes, they have become amorphous solids retaining their gross morphology but not their crystallinity because of cracking.

b) Even with suitably stable clathrates, the host:guest stoichiometry is variable and thus accurate calculation of empirical formulae is impossible.

Table 2.2 Comparison between calculated and observed elemental percentages for the host powder complexes.

	% Measured			% Calculated		
	C	H	N	C	H	N
Host						
$[Ni(NCS)_2(4\text{-}PhPy)_4]$	69.0	4.6	9.3	69.3	4.5	10.6
$C_{46}H_{36}N_6NiS_2$						
$[NiCl_2(4\text{-}PhPy)_4]$	71.5	5.2	6.8	70.3	4.8	7.5
$C_{44}H_{36}N_4NiCl_2$						
$[Ni(NCS)_2(4\text{-}t\text{-}BuPy)_4]$	62.7	7.5	10.1	63.8	7.3	11.7
$C_{38}H_{52}N_6NiS_2$						
$[Ni(NCS)_2(4\text{-}BzPy)_4]$	70.8	5.5	9.2	70.5	5.2	9.9
$C_{50}H_{44}N_6NiS_2$						
$[Ni(NCS)_2(4\text{-}MePy)_4]$	57.8	5.2	14.9	57.0	5.1	15.4
$C_{26}H_{28}N_6NiS_2$						

2.3.2 Density Measurements

Accurate density measurements of small single crystals of the clathrates were employed to determine host:guest ratios. Two techniques were employed, both utilizing the same principle, to determine the density of a crystal.

Method 1. Density column.

A linear density column containing water and saturated KI solution was prepared and calibrated with oil droplets of predetermined density. A density measurement of a crystal could be carried out in a matter of seconds once the crystal had been immersed beneath the surface of the liquid. This method is rapid and thus decomposition of the clathrate is insignificant, but it suffers from the disadvantage that air droplets adhere tightly to the surface of the crystal and are difficult to dislodge before the crystal descends the column.

Method 2. Flotation method.

This method involved adding KI solution to a crystal immersed in water and shaking after each addition. Once the crystal was suspended in an homogeneous solution, the density of the solution was determined using a PAAR DMA 35 densitymeter. This method is slower than the density column technique and thus decomposition may become significant but the advantage lies in being able to dislodge all air droplets from the crystal.

2.3.3 Thermal Analysis

Thermal analysis, in the form of Thermal Gravimetric Analysis (TGA) and Differential Thermal Analysis (DTA), was performed on certain clathrates to try and gain a better understanding of their physico-chemical properties. These include:

a) confirmation of the stoichiometry of host:guest ratio.

b) the temperature at which the guest is liberated.

c) the energy required (or evolved if exothermic) to cause guest liberation; this is proportional to the area under the DTA curve. By comparison with standards of known ΔH values, the enthalpy of the reaction can be calculated.

d) the pathway of the breakdown of the host lattice.

Before any thermograms were carried out, crystals of the complex were removed from their mother liquor, dried by gentle patting with paper tissue and quickly weighed. Sample weight was approximately 10mg for each run, and the temperature range was typically 40-400°C at a heating rate of 10°C/min. Throughout the run, nitrogen was passed through the cell at a flow rate of 60ml/min. The reference material used in each case was inert alumina (Al_2O_3).

Owing to the construction of the sample holder assembly (illustrated in Fig 2.1) the platinum crucibles, containing sample and reference materials, are located directly on top of the thermocouple. Thus only the furnace temperature can be measured directly. It was therefore

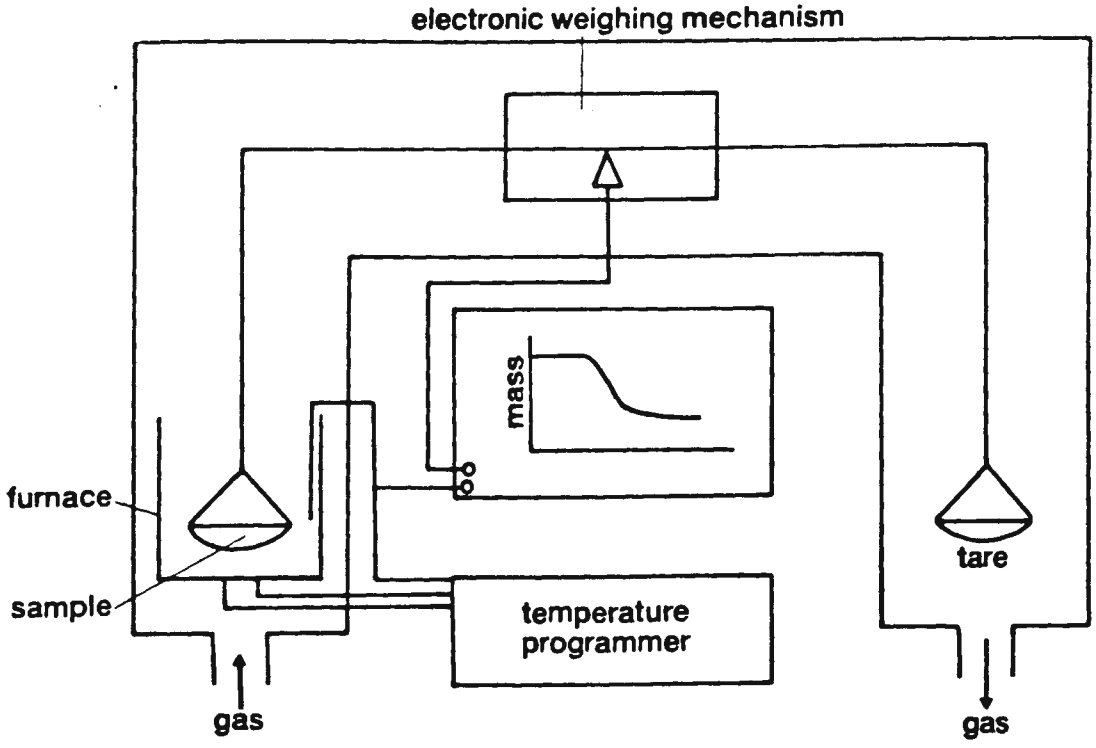

Fig 2.1a Schematic diagram of a thermobalance.

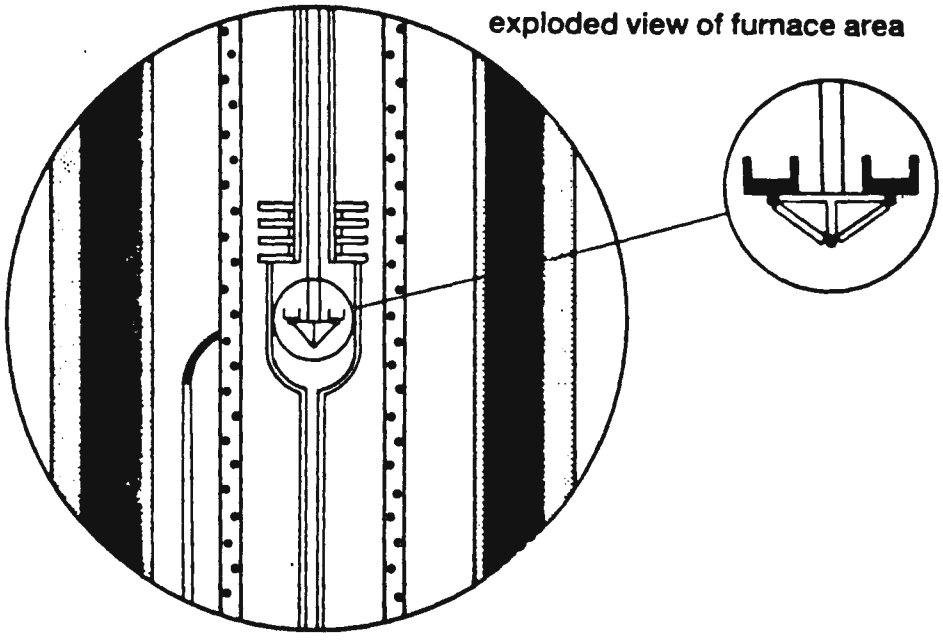

Fig 2.1b The sample holder assembly of the Stanton-Redcroft Thermal Analyser.

necessary to prepare a calibration curve to convert furnace temperature to sample temperature. This is discussed in greater detail in Chapter 5. All thermograms were performed on a Stanton-Redcroft Thermal Analyser, model STA 780. Unfortunately access to this machine was only permitted towards the latter half of this project, and even then access was limited. Thus not all compounds reported in this work could be analyzed using this technique.

2.3.4 X-ray Analysis

Single crystals of suitable size and quality were isolated or cut and mounted in Lindemann capillaries, with mother liquor to prevent deterioration by the desorption of the guest solvent.

Preliminary cell parameters and space group symmetry were established photographically using nickel filtered CuK_α radiation (λ = 1.5418Å) on a Stoe camera. Accurate lattice constants were obtained by least-squares analysis of several (*ca.* 25) high θ reflections collected and centered on a Enraf Nonius CAD4 diffractometer with graphite monochromated MoK_α radiation (λ = 0.7107Å). In all cases, scans were in the ω-2θ mode with a final acceptance limit of 20σ at $20°min^{-1}$ in ω and a maximum recording time of 40s. The vertical aperture length was fixed at 4mm and for each structure:

1) the aperture width (mm) was set according to the formula $(x + 1.05\tan\theta)$
2) the scan width ($\Delta\omega/°$) was set according to $(y + 0.35\tan\theta)$

For each data collection the intensities of 3 reference reflections were monitored every 100 measured reflections to check crystal stability and centering was checked every hour. All intensities were corrected by a Lorentz polarization factor, and an empirical absorption correction[2.3] was applied to all compounds which had not decomposed during the data collection. Crystal data as well as experimental and refinement parameters for each structure are listed in the following tables which are given at the end of this chapter:

Class	Crystal data	Expt. & Refinement
A	2.3 - 2.5	2.3a - 2.5a
B	2.6 - 2.7	2.6a - 2.7a
C	2.8	2.8a
D	2.9 - 2.10	2.9a - 2.10a

2.4 COMPUTATION

All structures (except for compound (XVII)) were solved by the heavy-atom technique using the SHELX-76[2.4] or SHELXS-86[2.5] program system. Compound (XVII) was solved using the direct methods option of the SHELXS-86 program. Refinement for all structures was carried out by full-matrix least-squares using the SHELX-76 program. If atoms, placed on sites of symmetry, were refined anisotropically, symmetry restrictions on their thermal parameters were applied according to Peterse and Palm[2.6]. Atomic radii calculated by Pauling[2.7] were used whilst complex neutral scattering factors for all non-hydrogen atoms were taken from Cromer and Mann[2.8] and those for hydrogen from Stewart *et al*[2.9]. Dispersion corrections are taken from Cromer and Liberman[2.19].

space, and counting the number of points inside at least one of the spheres described by the atomic radii of the atoms present, it is possible to calculate the molecular volume. Knowing which points are occupied allows mapping of areas which are empty *i.e.* the cavities in which the guest molecules are situated, if the calculation is performed on the host part of the structure alone.

The program NORMAL of the suite MULTAN 78[2.17] was used to calculate the spherically-averaged molecular scattering factors for certain guest molecules which displayed severe disorder and could not be described by chemically sensible models.

All computations, with the exception of ALCHEMY, were performed on the SPERRY 1108/76 mainframe computer situated at the University of Cape Town. ALCHEMY runs on an IBM/XT PC or clone fitted with EGA, colour monitor, hard disk and mouse.

2.5 GAS CHROMATOGRAPHY

Gas chromatography was used to establish whether certain clathrates are sufficiently selective in their retention of guest molecules to be considered as molecular sieves. This technique was also employed to ascertain the ratios of guest molecules retained in competition experiments, which is described in detail in Chapter 5.

For the 'molecular sieve' experiments, a packed column of the clathrate was prepared by mixing dried, crushed and sieved (80-100mesh) crystals

of the complex with an inert support packing (Chromosorb W, 100-120mesh) to form a 30% w/w homogeneous mixture. The effectiveness of a particular clathrate as a 'sieve' can be determined by its ability to retain guest solvents for varying times. Thus when a mixture of guests is injected into the column, the solvents are eluted individually and their retention times (equivalent to their order of elution) give an indication of the clathrates' preference to include the guest.

For the competition reactions, gas chromatography was used as an analytical technique to determine quantities of each guest solvent in the mixture. For this, a commercial packing (10% Silicone SE-30) was used to separate the solvents.

All runs were performed on a Pye Unicam PU 4500 Chromatograph, equipped with a Flame Ionizer Detector (FID) with output plotted on a pen recorder. Nitrogen was used as the carrier gas (30ml/min) and the flame of the detector was supported by an air/hydrogen mixture. Sample aliquots and temperature conditions are given for each run in the relevant sections.

2.6 COMPETITION EXPERIMENTS

The method described by Minton and Smith[2.18] was employed with modifications. These modifications were first checked by conducting the same experiments as described by Minton and Smith namely competition between *p*-xylene/ethylbenzene, *p*-xylene/toluene and *p*-xylene/benzene using $[Ni(NCS)_2(4\text{-}MePy)_4]$ as the host complex.

The host complex was prepared as described in Section 2.1.1. 2mmoles (1.094g) of the dried complex were placed in 12mm Pyrex tubes. Known mixtures of the two guests plus a co-solvent (*n*-pentane) were added to the host, the mixture frozen with liquid nitrogen and the tubes sealed. The co-solvent was added to increase the quantity of the liquid phase without increasing the host:guest ratio. The solvent *n*-pentane was chosen because it does not become included in the clathrate and it does not interfere with elutants from the gas chromatograph.

The sealed tubes were tumbled for several months whilst the analytical technique of determining ratios of solvents was perfected. The apparatus used for the tumbling is displayed in Photographs 5 and 6. Once a suitable calibration curve had been obtained for the various competing mixtures, the tubes were again frozen and opened. Once melted, the liquid was centrifuged and then analyzed by gas chromatography to determine the ratio of the guests in the liquid phase (R_L). Knowing the amount of host present, the amount of each guest added initially, and the stoichiometry for the host:guest ratio, considering each guest individually, it is possible to calculate the ratio of the guests in the solid phase (R_S).

This technique was employed because one analysis could determine both R_S and R_L. Care had to be taken to ensure that the number of moles of each guest added was greater than the number of moles of the host or else it would not be a true competition experiment. Various ratios of each combination of guests were chosen but the range was such that even small differences in R_L would be detectable. The range of ratios for guest

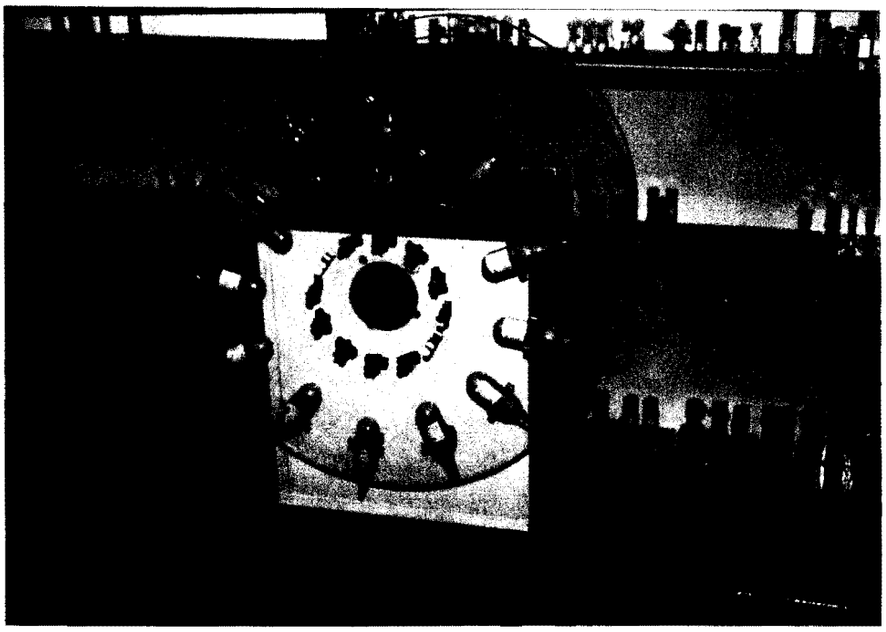

Photograph 5 The tumbling apparatus, capable of holding 24 tubes, as used in the competition experiments.

Photograph 6 Close up of individual sealed tubes indicating the solid and liquid phases.

combinations varied from 1:5 through to 5:1 with the amount of co-solvent present constant as approximately 10 times the sum of the number of moles of guest.

Once the validity of this technique had been demonstrated, it was hoped to use it on a series of guest combinations with the $[Ni(NCS)_2(4\text{-}PhPy)_4]$ host complex. However the number of guest combinations that satisfied the following criteria for this complex, were too small to be able to determine any trends. The criteria for selection were:

a) each guest must individually form a 1:1 host:guest complex,

b) the guest solvents must be mutually soluble and soluble in *n*-pentane,

c) the peaks upon elution from the G.C. must be sufficiently resolved to allow accurate determination of their individual areas.

Owing to the paucity of suitable guest combinations for the 4-PhPy derivative host complex, provisional work was undertaken with the 4-ViPy complex, for which more guest combinations could be found, even though this host complex was only partially related to the main theme of this work.

Thus the above experiments were repeated using 2mmoles of the 4-ViPy host complex and the following guest combinations: *p*-xylene/benzene, *p*-xylene/ethylbenzene and *p*-xylene/toluene.

A calibration curve for each combination was constructed for R *vs* A where R is the mole ratio of the guests and A the ratio of their areas

as determined by G.C. Mole ratios in the range 0.2-5 for each pair of solvents were diluted with approximately a ten fold excess of *n*-pentane. Each sample was analyzed repeatedly (at least three times) until the deviation of the mean was less than 2%. For each run, the column was maintained isothermal at 80°C. The peaks were recorded on pen plotter which was adjusted to give maximum deflection for the largest (guest) peak in a particular guest combination. The co-solvent, *n*-pentane, was eluted first and did not interfere with any of the other peaks. The area of the peaks was determined by the method of "cutting and weighing".

Checks were initially done to ensure that the ratio of the areas for a particular sample was independent of the volume of the aliquot. Thus runs were performed with the same sample but varying the sample injection size from 1-5μl in 0.5μl intervals. These proved that, within a precision of 5%, the ratio of the areas of the eluted peaks was independent of the sample size.

Altering the flow rate of the gases supporting the flame (air and hydrogen) only altered the calibration graph if they were varied dramatically. By ensuring that the flow rate of both gases was constant, the flame could be repeatedly extinguished and relit without significantly affecting the quantitative results. Thus once a calibration graph had been established, it could be used on samples which had been analyzed using a different flame.

Tests were also performed to check if varying the co-solvent concentration had any effect on the area ratio. Runs performed on

samples containing an excess of *n*-pentane varying from 0 to 20 times, showed that problems only occurred when the peak of the co-solvent became so big that it interfered with the benzene peak. Thus as long as the *n*-pentane was present in about a ten-fold excess over the sum of the other guests, no variation in the ratio of the areas was detected.

Thus for a particular experiment, for guest A and B which satisfy the previous criteria, let:

m_S = number of moles of Host powder,

m_A^T = total number of moles of A

m_B^T = total number of moles of B

m_A^L = number of moles of A in liquid phase

m_B^L = number of moles of B in liquid phase

m_A^C = number of moles of A which are enclathrated

m_B^C = number of moles of B which are enclathrated.

Known are m_S - mass of host

m_A^T - mass of A added to host

m_B^T - mass of B added to host

can measure $m_A^L/m_B^L = R_L$ from G.C. (from area ratio).

Want $R_S = m_A^C / m_B^C$. therefore must calculate m_A^C & m_B^C.

Thus:

1) $m_A^T = m_A^L + m_A^C$

2) $m_B^T = m_B^L + m_B^C$

3) $m_A^L = R\ A\ m_B^L$

4) $m_S = m_A^C + m_B^C$ (both A & B form 1:1 H:G complex)

or $m_B^C = (m_S - m_A^C)$

Therefore

1) becomes $m_A^T = (m_B^L \times R) + m_A^C$

2) becomes $m_B^T = m_B^L + (m_S - m_A^C)$

Adding 1) and 2)

5) $m_A^T + m_B^T = m_B^L(R+1) + m_S$.

We want m_A^C and m_B^C.

Rearranging 5)

$$m_B^L = (m_A^T + m_B^T - m_S) / (R+1)$$

from 1) $m_A^C = m_A^T - m_A^L$

3) $m_A^L = m_B^L \times R$.

Hence

$$m_A^C = m_A^T - R \times ((m_A^T + m_B^T - m_S) / (R+1)).$$

From 2) $m_B^C = m_B^T - m_B^L$

therefore

$$m_B^C = m_B^T - ((m_A^T + m_B^T - m_S) / (R+1)).$$

Knowing m_A^C and m_B^C it is therefore possible to calculate R_S.

TABLE 2.3 Crystal data for Compounds (I), (II) and (III).

Host: $[Ni(NCS)_2(4\text{-}PhPy)_4]$

Compound	I	II	III
Guest 1	-	*o*-xylene	*m*-xylene
Guest 2	-	-	-
H : G1 : G2 ratio	- : - : -	1 : 2 : -	1 : 2 : -
M_r /gmol^{-1}	795.7	1008.1	1008.1
D_m /gcm^{-3}	1.29	1.26	1.18
D_c /gcm^{-3}	1.29	1.24	1.20
$\mu(MoK_\alpha)$/cm^{-1}	5.67	4.37	4.24
F(000)	3312	4240	2120
Space Group	Pbca	Fdd2	C2/c
a /Å	12.846(7)	10.376(10)	10.610(5)
b /Å	16.160(2)	44.414(20)	23.181(14)
c /Å	39.377(8)	23.436(50)	22.950(4)
α /°	90	90	90
β /°	90	90	99.63(4)
γ /°	90	90	90
Vol./Å^3	8174.3	10800.2	5565.1
Z	8	8	4

TABLE 2.3A Experimental and Refinement Parameters for Compounds (I), (II) and (III).

Compound	I	II	III
Crystal dimensions/mm	.12x.16x.18	.47x.47x.25	.31x.38x.47
θ range scanned/°	1-25	1-25	1-25
Ave Transmission /%	-	-	98.4
Crystal Stability /%	0.2	10.0	3.2
Scan width[a]	0.84	0.74	0.74
Aperture width[b]	1.25	1.15	1.11
Vert. Aperture length/mm	6	4	4
Max. recording time/s	80	50	40
Total no. reflections	7948	2135	5174
Total no. observed	1788[c]	1697[d]	3037[d]
No. variables	226	160	155
R	0.0900	0.1286	0.0915
R_w	0.0691	0.1259	0.0894
Weighting scheme,w	$(\sigma^2F)^{-1}$	$(\sigma^2F)^{-1}$	$(\sigma^2F)^{-1}$

a Scan width, $\Delta\omega = (y+.35\tan\theta)°$

b Aperture width = $(x+1.05\tan\theta)$ mm

c $I_{rel} > /2\sigma I_{rel}$

d $I_{rel} > 2\sigma I_{rel}$

TABLE 2.4 Crystal data for Compounds (IV), (V) and (VI).

Host: $[Ni(NCS)_2(4\text{-}PhPy)_4]$

Compound	IV	V	VI
Guest 1	*p*-xylene	4-PhPy	4-PhPy
Guest 2	dmso	2-methoxyethanol	dmso
H : G1 : G2 ratio	1 : 1 : 2	1 : 1 : 1	1 : 1 : 1
M_r /gmol^{-1}	1058.1	1027	1029
D_m /gcm^{-3}	1.21	1.242	1.235
D_c /gcm^{-3}	1.16	1.24	1.23
$\mu(MoK_\alpha)$/cm^{-1}	3.85	4.34	4.18
F(000)	859	2071.9	1688
Space Group	$P\bar{1}$	$P2_1/n$	$P2_1/n$
a /Å	10.149(13)	10.085(3)	10.150(5)
b /Å	12.234(38)	23.723(4)	24.073(5)
c /Å	27.014(8)	23.266(7)	23.049(14)
α /°	99.60(13)	90	90
β /°	95.27(7)	99.19(3)	98.62(4)
γ /°	111.55(16)	90	90
Vol./Å^3	3032.8	5495.3	5568.2
Z	2	4	4

TABLE 2.4A Experimental and Refinement Parameters for Compounds (IV), (V) and (VI)

Compound	IV	V	VI
Crystal dimensions/mm	.28x.28x.47	.19x.19x.31	.38x.31x.25
θ range scanned/°	1-25	1-23	1-25
Ave Transmission /%	95.7	-	0.78
Crystal Stability /%	3.4	7.5	3.1
Scan width[a]	0.78	1.44	0.74
Aperture width[b]	1.13	1.56	1.35
Vert. Aperture length/mm	4	3	6
Max. recording time/s	40	50	60
Total no. reflections	10874	4561	65490
Total no. observed	6724[d]	2569[d]	3059[d]
No. variables	310	302	305
R	0.1267	0.1073	0.1067
R_w	0.1289	0.0915	0.1057
Weighting scheme,w	$(\sigma^2F)^{-1}$	$(\sigma^2F)^{-1}$	$(\sigma^2F)^{-1}$

a Scan width, $\Delta\omega = (y+.35\tan\theta)°$

b Aperture width = $(x+1.05\tan\theta)$ mm

c $I_{rel} > \sqrt{2}\sigma I_{rel}$

d $I_{rel} > 2\sigma I_{rel}$

TABLE 2.5 Crystal data for Compounds (VII) and (VIII).

Host: $[Ni(NCS)_2(4\text{-}PhPy)_4]$

Compound	VII	VIII
Guest 1	Phenylacetylene	Benzene
Guest 2	dmso	-
H : G1 : G2 ratio	1 : 2 : 1	1 : 4 : -
M_r /gmol^{-1}	1077	1108
D_m /gcm^{-3}	1.209	1.235
D_c /gcm^{-3}	1.19	1.22
$\mu(MoK_\alpha)$/cm^{-1}	3.95	3.95
F(000)	2151.9	582.0
Space Group	C2/c	$P\bar{1}$
a /Å	10.065(7)	9.52(1)
b /Å	24.147(8)	12.19(3)
c /Å	24.743(11)	13.72(2)
α /°	90	100.3(1)
β /°	94.00(6)	90.3(1)
γ /°	90	105.9(2)
Vol./Å^3	5998.0	1504.0
Z	4	1

TABLE 2.5A Experimental and Refinement Parameters for Compounds (VII) and (VIII).

Compound	VII	VIII
Crystal dimensions/mm	.47x.44x.38	.56x.59x.56
# range scanned/°	1-20	1-20
Ave Transmission /%	-	-
Crystal Stability /%	8.0	55.4
Scan width[a]	1.04	1.00
Aperture width[b]	1.35	1.30
Vert. Aperture length/mm	4	6
Max. recording time/s	40	30
Total no. reflections	2973	4716
Total no. observed	1945[d]	3782[d]
No. variables	161	159
R	0.1074	0.1137
R_w	0.1043	0.0931
Weighting scheme,w	$(\sigma^2F+.01F^2)^{-1}$	$(\sigma^2F)^{-1}$

a Scan width, $\Delta\omega = (y+.35\tan\theta)°$

b Aperture width = $(x+1.05\tan\theta)$ mm

c $I_{rel} > \sqrt{2}\sigma I_{rel}$

d $I_{rel} > 2\sigma I_{rel}$

TABLE 2.6 Crystal data for Compounds (IX) and (X) .

Host: $[NiCl_2(4\text{-}PhPy)_4]$

Compound	IX	X
Guest 1	CH_3OH	*m*-xylene
Guest 2	-	-
H : G1 : G2 ratio	1 : 1 : -	1 : 2 : -
M_r /gmol^{-1}	783	963
D_m /gcm^{-3}	1.289	1.232
D_c /gcm^{-3}	1.29	1.23
$\mu(MoK_\alpha)$/cm^{-1}	6.02	4.73
F(000)	1632	1012
Space Group	$P2_12_12_1$	$P\bar{1}$
a /Å	12.470(4)	12.747(12)
b /Å	16.550(5)	12.888(3)
c /Å	19.525(2)	16.817(3)
α /°	90	90.05(2)
β /°	90	102.21(5)
γ /°	90	92.38(5)
Vol./Å^3	4029.6	2596.7
Z	4	2

TABLE 2.6A Experimental and Refinement Parameters for Compounds (IX) and (X) .

Compound	IX	X
Crystal dimensions/mm	.28x.28x.38	.44x.41x.47
θ range scanned/°	1-25	1-25
Ave Transmission /%	97.8	95.3
Crystal Stability /%	5.2	3.6
Scan width[a]	0.94	1.00
Aperture width[b]	1.12	1.25
Vert. Aperture length/mm	6	6
Max. recording time/s	60	40
Total no. reflections	6702	7367
Total no. observed	5077[d]	5163[d]
No. variables	229	298
R	0.0565	0.0766
R_w	0.0529	0.0968
Weighting scheme,w	$(\sigma^2F)^{-1}$	$(\sigma^2F)^{-1}$

a Scan width, $\Delta\omega = (y+.35\tan\theta)°$

b Aperture width = $(x+1.05\tan\theta)$ mm

c $I_{rel} > /2\sigma I_{rel}$

d $I_{rel} > 2\sigma I_{rel}$

TABLE 2.7 Crystal Data for Compounds (XI) and (XII).

Host: $[NiCl_2(4\text{-}PhPy)_4]$

Compound	XI	XII
Guest 1	*p*-xylene	4-PhPy
Guest 2	-	-
H : G1 : G2 ratio	1 : 4 : -	1 : 1 : -
M_r /gmol^{-1}	1175	906
D_m /gcm^{-3}	1.19	1.270
D_c /gcm^{-3}	1.19	1.25
$\mu(MoK_\alpha)$/cm^{-1}	3.81	5.08
F(000)	2488	1848
Space Group	C2/c	C2/c
a /Å	9.692(2)	9.436(2)
b /Å	23.955(4)	23.841(14)
c /Å	28.385(2)	21.577(2)
α /°	90	90
β /°	96.40(4)	98.40(1)
γ /°	90	90
Vol./Å^3	6549.1	4801.6
Z	4	4

TABLE 2.7A Experimental and Refinement Parameters for Compounds (XI) and (XII).

Compound	XI	XII
Crystal dimensions/mm	.38x.38x.41	.35x.40x.50
θ range scanned/°	1-25	1-25
Ave Transmission /%	72.6	98.4
Crystal Stability /%	2.8	3.1
Scan width[a]	1.04	0.89
Aperture width[b]	1.14	1.12
Vert. Aperture length/mm	6	6
Max. recording time/s	40	40
Total no. reflections	4304	3464
Total no. observed	2694[d]	2501[d]
No. variables	164	128
R	0.1156	0.0910
R_w	0.1263	0.1154
Weighting scheme,w	$(\sigma^2F+.02F^2)^{-1}$	$(\sigma^2F+.02F^2)^{-1}$

a Scan width, $\Delta\omega = (y+.35\tan\theta)°$

b Aperture width = $(x+1.05\tan\theta)$ mm

c $I_{rel} > \sqrt{2}\sigma I_{rel}$

d $I_{rel} > 2\sigma I_{rel}$

TABLE 2.8 Crystal Data for Compounds (XIII) and (XIV).

Host: $[Ni(NCS)_2(4\text{-}MePy)_2(4\text{-}PhPy)_2]$

Compound	XIII	XIV
Guest 1	acetylacetone	1-chlorobutane
Guest 2	-	-
H : G1 : G2 ratio	1 : 1 : -	1 : 1 : -
M_r /gmol^{-1}	770	763
D_m /gcm^{-3}	1.269	1.268
D_c /gcm^{-3}	1.28	1.26
$\mu(MoK_\alpha)$/cm^{-1}	5.82	6.37
F(000)	1608	1592
Space Group	C2/c	C2/c
a /Å	10.541(2)	10.771(20)
b /Å	22.879(3)	23.027(9)
c /Å	16.814(2)	16.405(16)
α /°	90	90
β /°	99.85(1)	99.1(1)
γ /°	90	90
Vol./Å^3	3995.1	4107.6
Z	4	4

TABLE 2.8A Experimental and Refinement Parameters for Compounds (XIII) and (XIV).

Compound	XIII	XIV
Crystal dimensions/mm	.22x.22x.25	.19x.25x.44
θ range scanned/°	1-25	1-25
Ave Transmission /%	95.0	97.2
Crystal Stability /%	1.5	0.8
Scan width[a]	0.64	1.34
Aperture width[b]	1.11	1.47
Vert. Aperture length/mm	4	4
Max. recording time/s	40	40
Total no. reflections	2915	2782
Total no. observed	2086[d]	1419[d]
No. variables	132	139
R	0.0862	0.0746
R_w	0.0857	0.0664
Weighting scheme,w	$(\sigma^2F)^{-1}$	$(\sigma^2F)^{-1}$

a Scan width, $\Delta\omega = (y+.35\tan\theta)$°

b Aperture width = $(x+1.05\tan\theta)$ mm

c $I_{rel} > \sqrt{2}\sigma I_{rel}$

d $I_{rel} > 2\sigma I_{rel}$

TABLE 2.9 Crystal Data for Compounds (XV) and (XVI).

Compound	XV	XVI
Host	$[Ni(NCS)_2(dmso)_2(4\text{-}PhPy)_2]$	$[NiCl_2(dmso)_2(4\text{-}PhPy)_2]$
Guest 1	-	-
M_r /gmol^{-1}	640.7	595.7
D_m /gcm^{-3}	1.364	1.394
D_c /gcm^{-3}	1.37	1.39
$\mu(MoK_\alpha)$/cm^{-1}	8.62	9.78
F(000)	1256	596
Space Group	C2/c	$P2_1/c$
a /Å	10.016(1)	7.800(1)
b /Å	23.430(4)	8.250(1)
c /Å	13.290(9)	22.138(2)
α /°	90	90
β /°	96.94	95.15(1)
γ /°	90	90
Vol./Å^3	3096	1418.8
Z	4	2

TABLE 2.9A Experimental and Refinement Parameters for Compounds (XV) and (XVI).

Compound	XV	XVI
Crystal dimensions/mm	.15x.16x.24	.25x.28x.28
θ range scanned/°	1-20	1-25
Ave Transmission /%	-	98.7
Crystal Stability /%	0.5	0.4
Scan width[a]	0.890	0.84
Aperture width[b]	1.20	1.11
Vert. Aperture length/mm	4	6
Max. recording time/s	40	40
Total no. reflections	2917	2762
Total no. observed	2034[d]	1883[d]
No. variables	107	107
R	0.0588	0.0467
R_w	0.0623	0.0460
Weighting scheme,w	$(\sigma^2F)^{-1}$	$(\sigma^2F)^{-1}$

a Scan width, $\Delta\omega = (y+.35\tan\theta)°$

b Aperture width = $(x+1.05\tan\theta)$ mm

c $I_{rel} > \sqrt{2}\sigma I_{rel}$

d $I_{rel} > 2\sigma I_{rel}$

TABLE 2.10 Crystal Data for Compounds (XVII) and (XVIII).

Compound	XVII	XVIII
Host	$[Ni(NCS)_2(4\text{-t-BuPy})_4]$	$[Ni(NCS)_2(4\text{-BzPy})_4]$
Guest 1	-	-
M_r /gmol^{-1}	715.8	851.8
D_m /gcm^{-3}	1.132	1.298
D_c /gcm^{-3}	1.14	1.32
$\mu(MoK_\alpha)$/cm^{-1}	5.53	5.47
F(000)	3056	2015.9
Space Group	$I4_1/a$	Cc
a /Å	21.501(6)	9.686(6)
b /Å	21.501(8)	25.015(10)
c /Å	18.003(8)	17.728(9)
α /°	90	90
β /°	90	90.29(8)
γ /°	90	90
Vol./Å^3	8322.7	4295.4
Z	8	4

TABLE 2.10A Experimental and Refinement Parameters for Compounds (XVII) and (XVIII).

Compound	XVII	XVIII
Crystal dimensions/mm	.25x.25x.31	.19x.31x.31
θ range scanned/°	1-20	1-25
Ave Transmission /%	95.2	98.3
Crystal Stability /%	1.1	0.5
Scan width[a]	0.44	0.64
Aperture width[b]	1.12	1.13
Vert. Aperture length/mm	4	4
Max. recording time/s	40	40
Total no. reflections	8072	4003
Total no. observed	1599[d]	2819[d]
No. variables	159	252
R	0.0714	0.0563
R_w	0.1009	0.0567
Weighting scheme,w	$(\sigma^2F+0.01)^{-1}$	$(\sigma^2F)^{-1}$

a Scan width, $\Delta\omega = (y+.35\tan\theta)$°

b Aperture width = $(x+1.05\tan\theta)$ mm

c $I_{rel} > \sqrt{2}\sigma I_{rel}$

d $I_{rel} > 2\sigma I_{rel}$

REFERENCES

2.1 W.D. Schaeffer, W.S. Dorsey, D.A. Skinner and J. Christian, *J. Am. Chem. Soc.*, **79**, 5870 (1957).

2.2 L.R. Nassimbeni, S. Papanicolaou and M.H. Moore, *J. Incl. Phenom.*, **4**, 31 (1986).

2.3 A.C.T. North, D.C. Phillips and F.S. Mathews, *Acta. Cryst.*, **A24**, 351 (1968).

2.4 G.M. Sheldrick in 'Computing in Crystallography', Eds. H. Schenk, R. Olthof-Hazekamp, H. van Koningsveld and G.C. Bassi, Delft University Press, pp. 34-42 (1978).

2.5 G.M. Sheldrick in 'Crystallographioc Computing 3', Eds. G.M. Sheldrick, C. Kruger and R. Goddard, Oxford University Press, pp. 175-189 (1985)

2.6 W.J.A.M. Peterse and J.H. Palm, *Acta. Cryst.*,**20**, 147 (1966).

2.7 L. Pauling in 'The Nature of the Chemical Bond', Cornell University Press, Ithaca, New York.

2.8 D.T. Cromer and J.B. Mann, *Acta. Cryst.*, **A24**, 321 (1968).

2.9 R.F. Stewart, E.R. Davidson and W.T. Simpson, *J. Chem. Phys.*, 42, 3175 (1965).

2.10 W.D.S. Motherwell in 'PLUTO and PLUTOX programs for plotting molecular and crystal structures.' Cambridge University, England, unpublished.

2.11 'ALCHEMY', Molecular Modelling Software, Tripos Associates, Inc. (1987).

2.12 M. Nardelli, *Comput. Chem.*, 7, 95 (1983).

2.13 W.D.S. Motherwell in 'EENY Potential Energy Program', Cambridge University, England, unpublished.

2.14 E. Giglio, *Nature*, 222, 339 (1969).

2.15 N.V. Pavel, C. Quagliata and N. Scarcelli, *Z. Kristallogr.*, 144, 64 (1976).

2.16 A. Gavezzotti in 'OPEC Organic Potential Energy Calculations Program', *J. Am. Chem. Soc.*, 105 No. 16, 5220 (1983).

2.17 P. Main, S.E. Hull, L. Lessinger, G. Germain, J-P. Declercq and M.M. Woolfson in ' MULTAN 78. A System of Computer Programs for the Automatic Solution of Crystal Structures form X-Ray Diffraction Data', Universities of York, England and Louvain, Belgium (1978).

2.18 Sr.M.J. Minton and N.O. Smith, *J. Phys. Chem.*, **71 Number 11**, 3628 (1967).

2.19 D.T. Cromer and D. Liberman, *J.Chem. Phys.*, **53**, 1891 (1970).

CHAPTER THREE

STRUCTURE SOLUTION

For all eighteen compounds, the general method of solution of the crystal structure of the host molecule was similar, as was its subsequent refinement. The strategy for the location and refinement of the guest molecules (where present) however, varied considerably. The method used for each structure, which produced the best model of the guest is discussed later.

If the systematic absence of reflections in the data collection was such that there was ambiguity in the determination of the space group (*e.g.* C2/c vs Cc) then the space group with the higher symmetry was tried first. If the use of this space group failed to solve/refine the structure sensibly, then attempts were made in the alternative space group. Once the structure was fully refined in both space groups, various tests were carried out to establish the correct space group. This is described in detail for Compound (XVIII) later in this section for which the C2/c *vs* Cc ambiguity obtains.

For all the compounds where the structure was solved by the heavy-atom method, the Ni-Ni Patterson vector was always the highest non-origin peak in the Patterson calculation. Thus solving the Patterson map for the nickel atom proved to be unambiguous. When the nickel atom was located in a general position, insertion of its coordinates into a structure factor calculation was sufficient to allow suitable phasing to occur. The electron density maps thus calculated revealed peaks which could sensibly be ascribed to atoms in a reasonable model. When the

nickel atom was located on a special position, or near the origin, the structure factor calculation often required more than the solitary atom in order to phase correctly and thus for all compounds the Patterson map was carefully studied to try and determine the positions of the next heaviest atoms (S or Cl). The Ni-S and Ni-Cl distances are well known at ≈4.7Å and ≈2.4Å respectively. Thus, if in the Patterson map, the next highest non Ni-Ni vector was at a distance of ≈4.7Å (2.4Å) from the origin, that vector was solved for the position of the S (or Cl) atom.

Once the heavy atom(s) had been located, the assumption was made that it/they dominated the diffraction pattern, and the phase angle for each diffracted beam for the whole structure is approximated by that for the heavy atoms.

Insertion of the Ni, (and S or Cl atoms where applicable) into a structure factor calculation, followed by a difference electron density map, invariably yielded the positions of the remaining atoms of the isothiocyanate ligands as well as those of the pyridine rings. The peaks pertaining to the nitrogen atoms were usually higher than those corresponding to carbon atoms. A further difference Fourier, phased on all above mentioned atoms, typically located all the remaining atoms of the host molecule.

To speed up refinement in the early stages, all pyridine and phenyl rings were fixed as regular hexagons with bond distances of 1.39Å and refined as rigid groups with only rotational parameters for the pivot atoms and thermal parameters for all atoms permitted. Once all the

non-hydrogen atoms had been inserted into a difference electron density map following a structure factor calculation, and refined for a few least-squares cycles, this constraint was removed and all atoms were refined individually.

Final refinement of the host molecule involved anisotropic thermal parameters for all heavy atoms (Ni, S, Cl and O) and isotropic ones for all others. Hydrogen atoms were geometrically positioned and linked by a common temperature factor.

For all compounds where guest molecules were included, the host molecule had to be well refined before any sensible interpretation could be made of the remaining electron density peaks. The standard R value for the host alone varied considerably depending on the type of guest, the host : guest ratio as well as the degree of disorder of the guest molecule and the quality of the crystal as seen in the profile of the diffraction peaks.

The methods used to refine the guest molecules as well as any deviations from the above method for host refinement are discussed for each individual structure. Refinement was considered complete when three criteria were satisfied: i) all peaks in an electron density map greater than 0.5 $eÅ^{-3}$ had been accounted, ii) the final maximum shift/e.s.d. for refined parameters value was less than 0.05 and iii) the model made chemical sense *i.e.* realistic bond lengths and angles. Condition i) could not always be satisfied because of the disorder of the guest molecules and thus no single model could adequately describe the

complete electron density. Several models were tried and the best one selected even if its use resulted in some electron density remaining. This guest disorder and the lability of the terminal atoms of the substituted pyridines sometimes prevented condition ii) from being wholly satisfied.

The guest type, host : guest ratio, space group, number of molecules per unit cell and cell parameters are also summarized at the beginning of the discussion of each structure. Full details of the crystal data, and the experimental and refinement parameters were given in **Tables 2.3 - 2.10** and **Tables 2.3a - 2.10a** respectively at the end of the previous chapter. Fractional atomic coordinates for each compound are given in **Tables 3.1a-3.18a** at the end of this chapter.

All bond lengths, bond angles, torsion angles and fractional atomic coordinates for geometrically positioned hydrogen atoms are listed in **Appendix B**. Structure factors (F_o and F_c) are given in **Appendix C** whilst the analysis of variance for each compound is listed in **Appendix D**. All of these appendices are on microfiche which are in an envelope inside the back cover of this work.

3.1 CLASS A

Compound (I) $[Ni(NCS)_2(4\text{-}PhPy)_4]$, Pbca, Z = 8

a = 12.846, b = 16.160, c = 39.377Å, .

Crystals for this compound were very small and weakly diffracting with only 1788 out of 7948 being considered as significant at the $I_{rel} > \sqrt{2}\sigma I_{rel}$ level. With μR varying from minimum of 0.7 to a maximum of 1.0, the corresponding A^* values vary from 2.75 to 3.88 respectively for the theta range scanned and thus an absorption correction was deemed unnecessary. The structure was solved and refined as described in the general method. Although the ratio of number of parameters : number observed reflections was low (< 1:8), attempts to synthesize larger crystals proved to be unsuccessful and therefore no better data set could be obtained. The final maximum shift/e.s.d. ratio was 0.01, and no feature on a difference electron density map exceeded 0.54 $eÅ^{-3}$. Final coordinates are in **Table 3.1a**

Compound (II) $[Ni(NCS)_2(4\text{-}PhPy)_4].2o$-xylene,

H:G = 1:2, Fdd2, Z = 8

a = 10.376, b = 44.414, c =23.436Å.

The crystals of this compound suffered from severe decay during the data collection despite its being sealed in a capillary tube with mother liquor. The data were collected for the space group Fd2d and were thus transformed via the matrix (-1,0,0; 0,0,1; 0,1,0) to Fdd2. The absorption correction ranged from 40.9% to 96.0% with an average

transmission of 78.3%; this variation was deemed to be unacceptable especially as the decay was severely anisotropic and the data were therefore not corrected for absorption.

With Z = 8 it is necessary that the molecule lies on the diad at Wyckoff position *a* and it is the nickel atom and two 4-PhPy ligands that lie on this diad. The guest molecule lies in a general position and was initially refined as a regular hexagon with all atoms having a common temperature factor. These constraints were lifted for the final refinement.

Fdd2 is a polar space group and attempts were made to determine the absolute configuration of the structure. The host molecule was refined for many cycles with the imaginary term in the scattering factor expression ($\Delta f''$) equal to zero. Two parallel structure factor calculations (with no least-squares) were then performed; one with $\Delta f''$ as positive and the other with $\Delta f''$ as negative. A Hamilton test[3.1] was then performed on the R_G values obtained from these two runs. However, owing to the poor quality of the data, there was no significant difference in the R values obtained even at the 50% significance level. Thus it was not possible to determine the absolute configuration of the molecule and the coordinates reported in this work are those obtained from refinement with $\Delta f''$ as positive values as this is the default for the SHELX-76 program[3.8].

Final refinement of the molecule included geometrically placed H atoms on the guest molecule linked by a common temperature factor. The final

maximum shift/e.s.d. ratio was <0.01, and the largest residual electron density on the difference electron density map was 0.77 $eÅ^{-3}$ at a distance of 0.9Å from the nickel atom; this peak was attributed to inadequate modelling of the anisotropic thermal parameters. Final coordinates are in **Table 3.2a.**

Compound (III) $[Ni(NCS)_2(4\text{-}PhPy)_4].2m\text{-}xylene$,
H:G = 1:2, C2/c, Z = 4,
a = 10.610, b = 23.181, c = 22.950Å, β = 99.63°

Density measurements indicated that Z = 4 with host : guest ratio = 1:2 and the Patterson located the Ni atom on the diad at Wyckoff position *e*. Refinement of the structure yielded two 4-PhPy ligands also on the diad. The guest, which was in a general position and well ordered, emerged early on in the refinement, but even after full refinement, with H-atoms included, had thermal parameters considerably higher than those of the aromatic carbon atoms in the host molecule (0.131 *vs* $0.074Å^2$). The final maximum shift/e.s.d. ratio was 0.01, and no feature on a difference electron density map exceeded 0.47 $eÅ^{-3}$. Final coordinates are in **Table 3.3.**

Compound (IV) $[Ni(NCS)_2(4\text{-}PhPy)_4].1p\text{-xylene}.2dmso$,

H:G1:G2 = 1:1:2, $P\bar{1}$, Z = 2,

a = 10.149, b = 12.234, c = 27.014Å,

α = 99.60, β = 95.27, γ = 111.55°.

Density measurements of crystals of this compound indicated that Z = 2 with a host : guest ratio (for the intended guest = *p*-xylene) of 1:3. On refinement of the host molecule, which lies in a general position, it was noted that two unique cavities were formed. Contouring of the electron density maps of the channels revealed that a disordered *p*-xylene molecule was located in the one channel, whilst the other channel contained, surprisingly, two dmso molecules both disordered. The positions of the individual (non H) atoms of the dmso molecules could be located unambiguously as their electron density was clearly proportional to their atomic number. The site occupancy factors of the S atoms however, required careful refinement and the model of this disorder which yielded the best refinement is indicated in Fig 3.1.

The final maximum shift/e.s.d. ratio was 0.08, and although the highest feature on a difference electron density map was 1.0leÅ^{-3} this was in the vicinity of the sulphur atom of one of the dmso molecules and can be attributed to an imperfect model. Final coordinates are in **Table 3.4a**.

Compound (V) $[Ni(NCS)_2(4\text{-PhPy})_4].4\text{-PhPy}.2\text{-methoxyethanol}$

H:G1:G2 = 1:1:1, $P2_1/n$, Z = 4,

a = 10.085, b = 23.723, c = 23.266Å, β = 99.19°.

Density measurements indicated that if the only guest that had been included was 4-PhPy, then the H:G would be 1:1.5. However indications are that a guest molecule requires approximately twice its molecular volume as free space in order to be included in a cavity. Using values calculated by Kitaigorodskii[3.2] and approximating N: to CH, the volume occupied by a 4-PhPy molecule is 155Å^3. Thus an approximate figure for the required volume in order to include the molecule would be about 300Å^3. If we consider the α-phase structure (Compound (I)) to be the most efficiently packed "clathrate" ie. the one containing the least residual volume, then the volume/host molecule is 1021Å^3. Thus the volume available for the guest molecules in this compound is (5495/4 - 1021) = 353Å^3. It is therefore impossible for 1.5 molecules of 4-PhPy to fit into the residual volume available for the guest molecules, and the inclusion of the co-solvent, 2-methoxyethanol was suspected. The solution and refinement of the aromatic guest proved to be routine with the atoms appearing unequivocally in a difference electron density map. Contouring of an difference electron density map produced by a structure factor calculation, in which the aromatic guest had been included, revealed another guest molecule consisting of a 5 atom chain. Neither the electron density of the peaks nor the apparent bond distances could distinguish the oxygen from the carbon atoms of the 2-methoxyethanol molecule. Thus a two-fold statistically disordered rigid molecule (Fig. 3.2) was invoked for which the average atomic

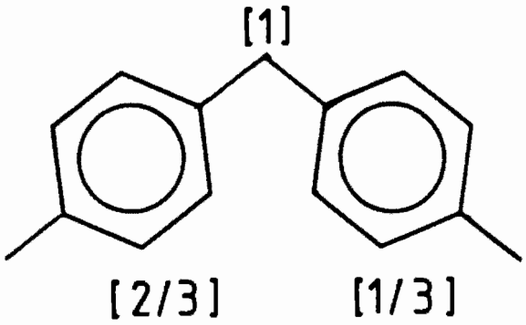

p-Xylene

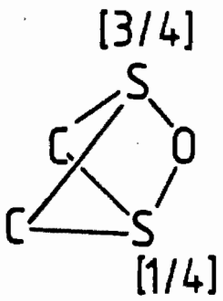

DMSO(1)

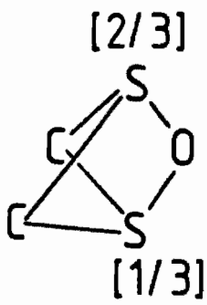

DMSO(2)

[ ] = Site Occupancy Factor

Fig 3.1 Schematic diagram to indicate the best model found to describe the disorder of the *p*-xylene and dmso molecules in Compound (IV).

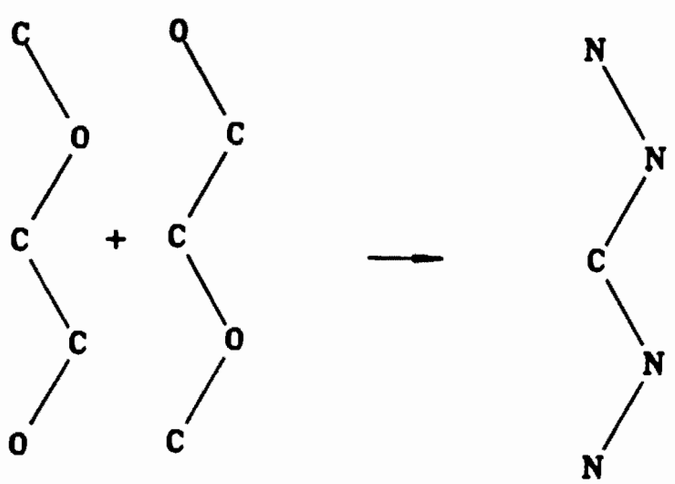

Fig 3.2 Two-fold static disorder of the 2-methoxyethanol molecule in Compound (V).

scattering factors of carbon and oxygen atoms, excepting the central carbon atom, were approximated as the atomic scattering factor of the nitrogen atom. Refinement as a rigid molecule accounted for all electron density peaks greater than $1eÅ^3$ whilst the final maximum shift/e.s.d. was <0.01. Final coordinates are in **Table 3.5a.**

Compound (VI) $[Ni(NCS)_2(4\text{-}PhPy)_4].4\text{-}PhPy.dmso$,
H:G1:G2 = 1:1:1, $P2_1/n$, Z = 4,
a = 10.150, b = 24.073, c = 23.049Å, β = 98.62°.

Solution and refinement of the host and aromatic guest molecules proved to be routine. Two high electron density peaks about 4Å apart (*ca* $4eÅ^{-3}$) with several smaller peaks (*ca* $1\text{-}2eÅ^{-3}$) associated with them indicated that dmso had been included as a second guest. Attempts to fit a model of dmso to the electron density peaks proved to be unsuccessful. Use was made of a spherically averaged scattering factor (g) as described by Jones *et al*[3.3] to model the dmso with atomic coordinates for dmso, including all H atoms, taken from the crystal structure determination of Thomas *et al*[3.4] This procedure is described in detail in Section 3.5, along with the function employed for the spherically averaged molecular scattering factor.

Use of this g function in a difference electron density map following a structure factor calculation with s.o.f.'s for each dmso = 0.5 and treated anisotropically led to a significant reduction in R, (12.5 to 10.7%) and also accounted for all the remaining electron density peaks greater than $0.5eÅ^{-3}$. Although the model of dmso had very high thermal

parameters, U_{equiv} *ca* 0.3Å^2, its inclusion was felt justified to describe the behaviour of the aliphatic guest molecule. The final maximum shift/e.s.d. ratio was <0.01. Final coordinates are in **Table 3.6a.**

Compound (VII) $[Ni(NCS)_2(4\text{-}PhPy)_4]$.2Phenylacetylene.dmso,
H:Gl:G2 = 1:2:1, C2/c, Z = 4,
a = 10.065, b = 24.147, c = 24.743Å, β = 94.0°.

Solution and refinement of the host and aromatic guest molecules proceeded routinely with the Ni atom and two pyridine ligands lying along the diad at Wyckoff position *e*. A high electron density peak (*ca* 6eÅ^3) situated at the centre of inversion at Wyckoff position *c*, indicated that dmso had been included in the lattice. The spherically averaged molecular scattering factor employed for Compound (VI) was again used and, as previously, led to a more satisfactory solution for the dmso molecule which was refined with anisotropic temperature factors and a site occupancy factor of 0.5. The final maximum shift/e.s.d. ratio was <0.01, and no feature on a difference electron density map exceeded 0.74 eÅ^{-3}. Final coordinates are in **Table 3.7a.**

Compound (VIII) $[Ni(NCS)_2(4\text{-}PhPy)_4].4Benzene$,

H:G = 1:4, $P\bar{1}$, Z = 1,

a = 9.52, b = 12.19, c = 13.72Å,

α = 100.3, β = 90.3, γ = 105.9°.

Considerable difficulty was experienced with the data collection of this compound because of the problems in securely mounting a crystal and retaining the mother liquor in the capillary. Crystals, even when firmly wedged in a sealed Lindemann capillary containing mother liquor, would move up the capillary over a period of days. (One such crystal "crept" up a distance of 7mm in 24 hours). Attempts to glue it in place within the capillary failed as the glue was dissolved by the solvent. The crystal was eventually mounted (after nearly a dozen attempts) in the following manner: a suitable crystal was cut, inserted into the capillary, firmly wedged and mother liquor introduced. A glass fibre, with the end rounded in a flame, was placed so that it just touched the bottom of the crystal. The lower end of the capillary containing this fibre was then sealed in a flame. Owing to the different constituents in the two types of glass, this sealing required careful manipulation. A similar glass fibre was then introduced into the top of the capillary and positioned so that it gently touched the top of the crystal. As before the capillary was sealed. This method prevented any gross movements of the crystal but minor variations in the crystal's position occurred throughout the data collection. During the data collection recentering of the crystal occurred nearly every 100 reflections and the variation in intensity of the standard reflections (a measure of the crystal stability) was greater than 50%. A decay correction was not

Photograph 3 A typical crystal of a clathrate mounted in a Lindemann capillary to prevent desorption of the guest.

Photograph 4 The wandering crystal!! - this crystal of Compound (VIII) moved from the place indicated by the probe upwards a distance of 7mm in 24 hours.

applied as decay was not isotropic and no absorption correction was applied.

The host molecule with the nickel atom situated on the centre of inversion at Wyckoff position *a* refined routinely. The two unique benzene guest molecules, situated in general positions, were refined as regular hexagons with common atomic temperature factors. The final maximum shift/e.s.d. ratio was 0.014, and although there was one peak on a difference electron density map of 0.98 $eÅ^{-3}$ this was in the vicinity of one of the guest molecules and can be ascribed to an imperfect model. Final coordinates are in **Table 3.8a.**

3.2 CLASS B

Compound (IX) $[NiCl_2(4\text{-}PhPy)_4]$.methanol,
H:G = 1:1, $P2_12_12_1$, Z = 4,
a = 12.470, b = 16.550, c = 19.525Å.

Refinement of the host molecule as well as the guest molecule, which was (surprisingly) completely ordered, proved to be routine. The host molecule can be centrosymmetric depending on the orientation of the pyridine and phenyl rings. Thus it was surprising to find that the host-guest complex had crystallized in a chiral space group. Possible reasons to account for this phenomenon are described in the next chapter when each structure is discussed in detail. Determination of the absolute configuration was carried out in the same manner as described for Compound (II). The Hamilton test revealed that we could disregard

the hypothesis, that the structure with Δf" negative was correct, at the 0.005% confidence level. Thus final refinement occurred with the imaginary terms of the atomic scattering factors positive. The final maximum shift/e.s.d. ratio was <0.01, and no feature on a difference electron density map exceeded 0.49 $eÅ^{-3}$. Final coordinates are in **Table 3.9a.**

Compound (X) $[NiCl_2(4\text{-}PhPy)_4].2m\text{-}xylene$,
H:G = 1:2, $P\bar{1}$, Z = 2,
a = 12.747, b = 12.888, c = 16.187Å
α = 90.05, β = 102.21, γ = 92.38°.

The complete refinement of this compound was routine. The host molecule was located in a general position as were the two independent guest molecules. These guest molecules were refined with hydrogen atoms and although the molecules were well ordered, the thermal parameters of the carbon atoms were, on average, three times higher than their counterparts in the host molecule. The average thermal parameters of one of the guest molecules was more than twice the value of the other (0.09 *vs* 0.2 $Å^2$) and for both molecules, the methyl carbons had higher parameters than the ring carbons.

The final maximum shift/e.s.d. ratio was 0.054, and no feature on a difference electron density map exceeded 0.72 $eÅ^{-3}$. Final coordinates are in **Table 3.10a.**

Compound (XI) $[NiCl_2(4\text{-}PhPy)_4].4p$-xylene,

H:G = 1:4, C2/c, Z =4,

a = 9.692, b = 23.955, c = 28,385Å, β = 96.40°.

Two unique guest molecules and the Ni and two pyridine ligands lying on the diad at Wyckoff position *e*, concurred in the high guest : host ratio. Refinement was routine with the guest molecules having common atomic temperature factors but no H atoms. The same observations as those of the previous compound concerning the thermal parameters were made for this compound.The final maximum shift/e.s.d. ratio was <0.01, and no feature on a difference electron density map exceeded 0.44 $eÅ^{-3}$. Final coordinates are in **Table 3.11a.**

Compound (XII) $[NiCl_2(4\text{-}PhPy)_4].4\text{-}PhPy$,

H:G = 1:1, C2/c, Z = 4

a = 9.436, b = 23.841, c = 21.577Å, β = 98.40°.

The host molecule lies at Wyckoff position *e*, with the Ni atom and two phenyl ligands lying on the diad. The molecule of the guest 4-PhPy is disordered and lies close to the centre of inversion at Wyckoff position *b*. The model which produced the most satisfactory refinement was obtained by fitting two separate regular hexagons to the peaks in an electron density map. Each hexagon represented half of the 4-PhPy molecule which was approximately 1.5Å away from the symmetry generated hexagon. The hexagons were refined as rigid bodies with the sum of their site occupancy factors equalling unity. Final refinement (without hydrogens on the guest molecules) revealed the abundance of the one

hexagon to be 45%. A diagram of the best model is shown in Fig 3.3. The final maximum shift/e.s.d. ratio was <0.01, and the highest feature on a difference electron density map was 0.81 $eÅ^{-3}$ which was in the vicinity of the guest molecule. Final coordinates are in **Table 3.12a.**

3.3 CLASS C

Compound (XIII) $[Ni(NCS)_2(4\text{-}MePy)_2(4\text{-}PhPy)_2]$.acac,
H:G = 1:1, C2/c, Z = 4,
a = 10.541, b = 22.879, c = 16.814Å, β = 99.85°.

With the host molecule again being located at Wyckoff position *e*, with the nickel atom and two 4-PhPy ligands lying on the diad, the refinement of the host was routine. Location of the guest molecule necessitated the contouring of electron density maps. The positions of the two oxygen atoms were located unambiguously as their electron density was significantly higher than that of the carbon backbone. The difference electron density corresponding to the C atoms however was diffuse and the best model, obtained by fixing bond distances as shown in Fig 3.4, resulted in high thermal parameters (*ca* .15$Å^2$) for all guest atoms. The molecule lies close to the centre of inversion at Wyckoff *d* and thus two-fold static disorder was invoked. The final maximum shift/e.s.d. ratio was 0.021, and the highest residual electron density in the final difference map was 0.81$eÅ^{-3}$ which, as often observed before, was in the region occupied by the guest molecule. Final coordinates are in **Table 3.13a.**

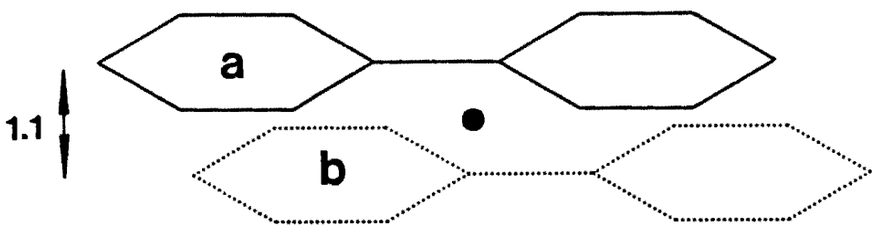

Fig 3.3 Disorder displayed by the 4-PhPy guest molecule of Compound (XII). Rings **a** and **b** inserted with s.o.f. = 1/2. Solid circle represents centre of inversion at Wyckoff position *b*. Interplanar distance in Å.

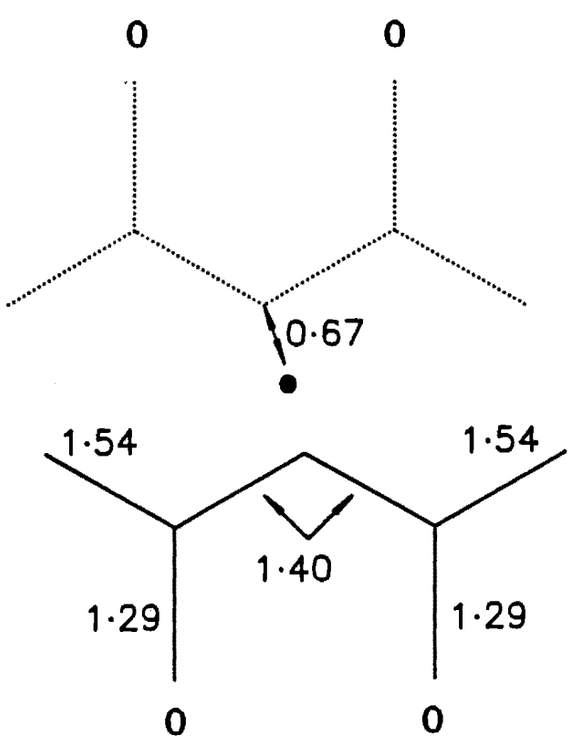

Fig 3.4 Bond distances (Å) of the rigid molecule used to describe the guest acetylacetone molecule of Compound (XIII). Solid circle represents the centre of inversion at Wyckoff position *d*.

Compound (XIV) $[Ni(NCS)_2(4\text{-}MePy)_2(4\text{-}PhPy)_2]$.1-chlorobutane,
H:G = 1:1, C2/c, Z = 4,
a = 10.771, b = 23.027, c = 16.405Å, β = 99.1°.

The host molecule lies in the same position as for Compound (XIII) and the guest molecule occupies a similar region. The contoured electron density map of the region of the guest molecule revealed three peaks which could be clearly interpreted as the three methylene carbons. The end peaks were, however, more diffuse with apparent bond distances of *ca* 1.6Å. Attempts were first made to refine the molecule as shown in Fig 3.5 but the terminal C and Cl peaks were continually merged and located in positions equidistant from the starting parameters. This required invoking of statistical disorder of these two atoms for which the average atomic scattering factor of the terminal C and Cl was approximated as the atomic scattering factor of the sodium atom. This is shown in Fig 3.6 along with bond distances used to refine the molecule as a rigid group. This molecule was again modelled with site occupancy factor of 0.5 as it lies close to the centre of inversion at Wyckoff position *d*. The "Na" atoms were refined anisotropically to try and indicate the dimension of the thermal motion of the atoms. Not surprisingly these parameters are extremely high ($U_{equiv} \approx 0.45Å^2$). The final maximum shift/e.s.d. ratio was 0.035, and no feature on a difference electron density map exceeded 0.56 $eÅ^{-3}$. Final coordinates are in **Table 3.14a.**

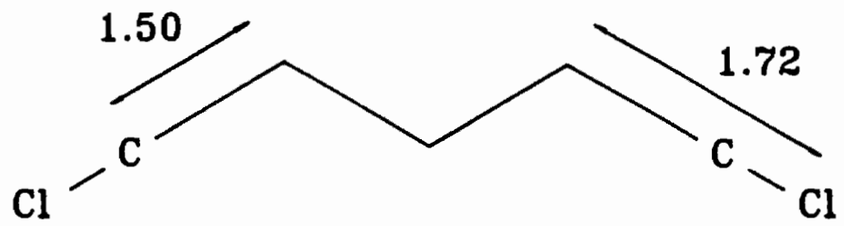

Fig 3.5 Initial model used to describe the two-fold statistically disordered 1-chlorobutane of Compound (XIV). Distances are in Å and the labelled atoms inserted with s.o.f.s equal to half those for the rest of the molecule.

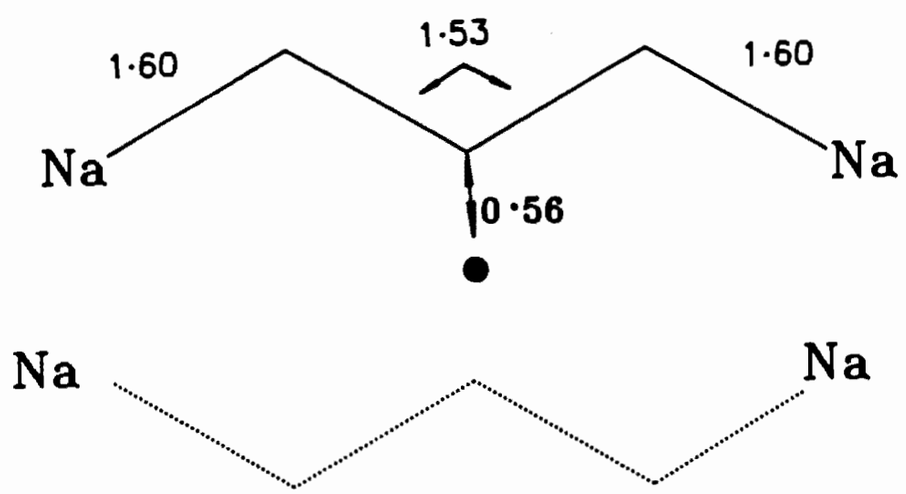

Fig 3.6 Bond distances (Å) of the rigid molecule used to finally describe the guest C_4H_9Cl molecule of Compound (XIV). Solid circle represents the centre of inversion at Wyckoff position *d*.

3.4 CLASS D

Compound (XV) $[Ni(NCS)_2(dmso)_2(4\text{-}PhPy)_2]$, C2/c, Z = 4,
a = 10.016, b = 23.430, c = 13.290Å, β = 96.94°.

The fact that crystals of this complex grew after crystals of $[Ni(NCS)_2(4\text{-}PhPy)_4].4dmso^{3.5}$ had formed indicated that something unusual had happened. The small volume of the cell (3096Å^3) and concomitant increase in density (1.364gcm^{-3}), when compared with that of other compounds (2921Å^3 (Z = 2) and 1.24gcm^{-3} for $[Ni(NCS)_2(4\text{-}PhPy)_4].4dmso$), suggested that one or more of the relatively large 4-PhPy ligands had either been substituted or displaced completely. The Patterson map revealed two vectors of comparable size after all the Ni-Ni vectors had been assigned. One was ≈4.5Å from the origin and could be assigned as the Ni to isothiocyanate S vector. The other vector was approximately 3.6Å from the origin and due to its electron density it was also suspected of also being a Ni-S vector. The Fourier synthesis, phased on the Ni and isothiocyanate S revealed a strong peak (ca.7eÅ^{-3}) in a position similar to that calculated from the Patterson map and a lesser peak (ca.3eÅ^{-3}) situated 2.1Å from the Ni and 1.5Å from the more intense peak. With this peak assigned as an oxygen atom it was confirmed that two pyridine ligands had been replaced by dmso molecules. The nickel atom, and the two remaining 4-PhPy ligands were located on the diad and final refinement was carried out with the methyl hydrogens geometrically placed in positions staggered with respect to the C-S bond and linked with a common temperature factor. The final maximum shift/e.s.d. ratio

was <0.01, and no feature on a difference electron density map exceeded 0.38 $eÅ^{-3}$. Final coordinates are in **Table 3.15a.**

Compound (XVI) $[NiCl_2(dmso)_2(4\text{-}PhPy)_2]$, $P2_1/c$, Z = 2,
a = 7.800, b = 8.250, c = 22.138Å, β = 95.19°.

Owing to the similarity in crystallizing technique for this compound and Compound (XV) and length of time for crystals to grow as well as the small volume of the unit cell and high density of the crystal it was suspected that the dmso had once again replaced two of the 4-PhPy ligands. Solution for the Ni-Ni vectors of the Patterson map yielded a Ni atom located on the centre of symmetry at Wyckoff position *a*. Final refinement occurred with one of each of NCS^-, dmso and 4-PhPy ligands inserted into a structure factor calculation followed by a difference electron density map. Methyl hydrogens were treated as for the previous compound. The final maximum shift/e.s.d. ratio was <0.01, and no feature on a difference electron density map exceeded 0.68 $eÅ^{-3}$. Final coordinates are in **Table 3.16a.**

Compound (XVII) $[Ni(NCS)_2(4\text{-}t\text{-}BuPy)_4]$, $I4_1/a$, Z = 8,
a = 21.501, c = 18.003Å,

Preliminary photographs of this structure indicated a triclinic cell with cell parameters a≈b≈c≈18Å, $\alpha \approx \beta \approx 60°$ and $\gamma \approx 75°$. Density measurements, using the volume of this triclinic cell, revealed that the number of host molecules in the unit cell was four *i.e.* 2 independent molecules per asymmetric unit. Although this triclinic cell was viewed with

suspicion, it was decided to proceed with the data collection, and to check for suitable transformations once the hemisphere of reflections had been collected. The triclinic cell:

$a = 17.669$, $b = 17.659$, $c = 18.003$Å

$\alpha = 59.41$, $\beta = 59.38$, $\gamma = 75.00°$

was then transformed using the following matrices:

i) $\begin{bmatrix} 1 & 1 & 0 \\ 1 & -1 & 0 \\ 0 & 0 & -1 \end{bmatrix}$ ii) $\begin{bmatrix} 1 & 0 & -1 \\ 0 & 1 & 0 \\ 1 & -1 & 1 \end{bmatrix}$

iii) $\begin{bmatrix} 0 & 1 & -1 \\ 1 & 0 & 0 \\ 1 & -1 & -1 \end{bmatrix}$ iv) $\begin{bmatrix} 1 & -1 & 0 \\ 1 & 1 & -1 \\ 0 & 0 & 1 \end{bmatrix}$.

The first matrix transforms to a monoclinic cell:

$a = 28.028$, $b = 21.506$, $c = 18.003$Å

$\alpha = 90.03$, $\beta = 129.92$, $\gamma = 89.97°$

However careful examination of reflections hkl and $h\bar{k}l$ showed that the required monoclinic equivalences were absent.

Matrices ii) and iii) transformed the triclinic cell to cells which were clearly not tetragonal and they were therefore discarded. Matrix iv) however yielded the following cell:

$a = 21.505$, $b = 21.496$, $c = 18.003$Å

$\alpha = 90.05$, $\beta = 89.97$, $\gamma = 89.98°$.

The equivalences hkl, $\bar{h}\bar{k}l$, $\bar{k}hl$ and $k\bar{h}l$ were carefully checked for six strong reflections and it was ascertained that the deviation was less that 10% between equivalent reflections. The structure was thus solved in the space group $I4_1/a$ which was indicated by the systematic absence of the transformed reflections.

The space group $I4_1/a$ has a choice of two origins and for this structure the second choice, on the $\bar{1}$ site, was chosen with the nickel being located on the diad at Wyckoff position *e*. The methyl hydrogens were treated as for Compound (XV). The final maximum shift/e.s.d. ratio was 0.039 and no feature on the electron density map exceeded $0.42eÅ^{-3}$. Final coordinates are in **Table 3.17a.**

Compound (XVIII) $[Ni(NCS)_2(4\text{-}BzPy)_4]$, Cc, Z = 4,
a = 9.686, b = 25.015, c = 17.728Å, β = 90.29°.

Systematic absence of reflections indicated that the space group for this compound was either the centrosymmetric C2/c or the non-centrosymmetric Cc. The structure was solved by the heavy-atom method in C2/c which indicated that the Ni was located on the diad at Wyckoff position *e*. Refinement, however, was unsuccessful with the conventional R failing to converge to beneath a value of 15%. For the Cc structure, with the nickel located at 0,y,0, the best model resulted in an R of 0.056. Thus for this compound, there was no difficulty in determining the correct space group. The final maximum shift/e.s.d. ratio was 0.05, and no feature on a difference electron density map exceeded 0.44 $eÅ^{-3}$. Final coordinates are in **Table 3.18a.**

For structures which were not as clear cut as the above complex *e.g.* Compound (XV), further tests were sometimes deemed necessary in order to resolve the C2/c *vs* Cc dilemma especially when the relevant E statistics were ambiguous. Refinements were completed in Cc with the nickel atom at 0,y,0 and in C2/c with the nickel of the diad at Wyckoff position *e* and

a standard Hamilton test performed on the two models. If there was any doubt in the interpretation of the statistical R thus obtained the following calculation, suggested by Professor F. Herbstein of Haifa Technion, Israel was performed.

For the centrosymmetric space group;

an atom A at x_A, y_A, z_A

with e.s.d.'s σx_A, σy_A, σz_A

is related by the symmetry element (-x, y, -x+1/2) to

an atom A^* at x^*, y^*, z^* also with

e.s.d.'s σx_A, σy_A, σz_A.

For Cc;

an atom B1 at x_{B1}, y_{B1}, z_{B1}

with e.s.d.'s σx_{B1}, σy_{B1}, $\sigma + z_{B1}$

(which has similar coordinates to atom A)

will have

an atom B2 at x_{B2}, y_{B2}, z_{B2}

with e.s.d.'s σx_{B2}, σy_{B2}, σz_{B2}

(which has similar coordinates to atom A^*).

Let $\Delta x_1 = (x_A - x_{B1})$ and $\Delta x_2 = (x^* - x_{B2})$

$\Delta y_1 = (y_A - y_{B1})$ and $\Delta y_2 = (y^* - y_{B2})$

$\Delta z_1 = (z_A - z_{B1})$ and $\Delta z_1 = (z^* - z_{B2})$

and $\Delta x = 1/2(\Delta x_1 + \Delta x_2)$

$\Delta y = 1/2(\Delta y_1 + \Delta y_2)$

$\Delta z = 1/2(\Delta z_1 + \Delta z_2)$

Let $(\overline{\sigma x}) = 1/2(\sigma x_A + \sigma x_{B1})$ or $1/2(\sigma x_A + \sigma x_{B2})$

$(\overline{\sigma y}) = 1/2(\sigma y_A + \sigma y_{B1})$ or $1/2(\sigma y_A + \sigma y_{B2})$

$(\overline{\sigma z}) = 1/2(\sigma z_A + \sigma z_{B1})$ or $1/2(\sigma z_A + \sigma z_{B2})$

Then $M_x = (\Delta x)/(\overline{\sigma x})$

$M_y = (\Delta y)/(\overline{\sigma y})$

$M_z = (\Delta z)/(\overline{\sigma z})$ for each atom.

If n = number of parameters

Then $\overline{M} = 1/n(\Sigma(M_x + M_y + M_z))$ for all parameters.

The correct space group is C2/c if $\overline{M} < 10$ and Cc if $\overline{M} > 10$ (the number 10 was chosen arbitrarily but it was considered sufficiently large to allow for high thermal motion within the crystal).

3.5 Molecular Scattering Factor

Many inclusion compounds, by their very nature, retain guest molecules within the host framework merely by steric effects as there are no formal covalent bonds between the host and guest molecules. Thus it is the shape of the cavity and the possibility of hydrogen bonds which govern the position and orientation of the guest molecule. If, however, a guest molecule is approximately spherical in shape, and hydrogen bonds

are not feasible, then although the molecule's position in the host's cavity is possibly determinable, its orientation will very likely be indeterminate. For compounds (VI) and (VII) this was the case for the guest dmso molecules. The difference electron density map showed either one large, roughly spherical diffuse peak of approximately $6e\text{Å}^{-3}$ or several smaller peaks in positions which did not make chemical sense.

The technique of a Molecular Scattering Factor (MSF) has been successfully used for the location of a two-fold disordered (+)-Camphor molecule in the 2:1 complex between deoxycholic acid and camphor[3.3]. Scattering from the camphor could be represented by the spherical average scattering factor *g*, calculated by the normalization program in MULTAN 78[3.7] using the Debye scattering formula:

$$g^2 = \sum_{p=1}^{N} \sum_{q=1}^{N} f_p \, f_q \, \frac{\sin(4\pi r_{pq} \sin\theta/\lambda)}{(4\pi r_{pq} \sin\theta/\lambda)}$$

where N is the number of atoms, r_{pq} the distance between atoms p and q, and f_p and f_q the atomic scattering factors of atoms p and q.

For the dmso molecule, coordinates from a crystal structure determination by Thomas *et al*[3.4] were used for an initial atomic model. A second model, derived from the first one, was tested to try and ascertain whether the centre of the dmso molecule was located on the centre of inversion in Compound (VII), or whether it was the sulphur atom which was located there. The first model, shown in Fig 3.7a, was used in MULTAN 78 to obtain the curve displayed in Fig 3.8. The second model, Fig 3.7b, was constructed by inverting the rest of the dmso molecule about the sulphur atom and allocating all the non S atoms a

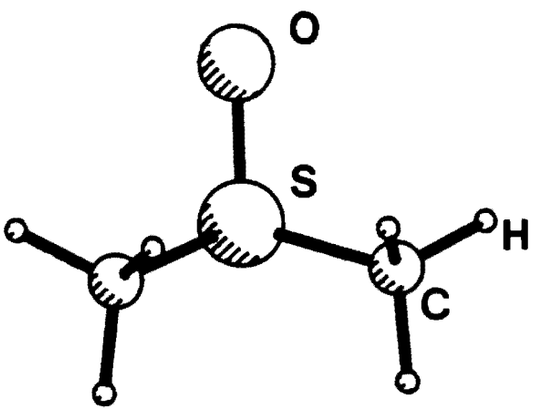

Fig 3.7a Model 1 used to determine the molecular scattering factor (MSF) for dmso.

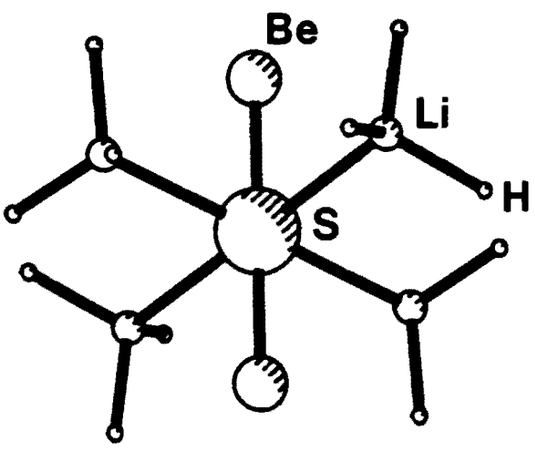

Fig 3.7b Model 2 used to determine the MSF for two-fold disordered dmso.

s.o.f. of a half, whilst that for S was unity. The NORMAL program, however, does not allow fractional s.o.f.s and therefore the model was changed to try and mimic the reduction in scattering power of the peripheral atoms. Thus the oxygen atoms were replaced by Be (oxygen has eight electrons and Be four), whilst the carbon atoms were replaced by Li (Z for C=6 and Li=3). The hydrogens were kept as hydrogens as there is nothing smaller in terms of number of electrons. Inputting this 'molecule' into NORMAL produced the curve displayed in Fig 3.9.

SHELX-76 requires the scattering factor to be in the form:

$$1)\ f(x) = a_1\exp(-b_1x^2) + a_2\exp(-b_2x^2) + a_3\exp(-b_3x^2) + a_4\exp(-b_4x^2) + c$$

where a_i, b_i and c are constants and $x = \sin\theta/\lambda$. The constants were obtained by the addition of normal distribution functions. For both models, output from NORMAL resulted in a graph (group scattering factor *vs* $\sin\theta/\lambda$) containing three maxima. For each peak (i = 1-3):

a_i = m_i (maximum) - c_i (minimum).

a_i was divided into the ratio 4:6 and the $\sin\theta/\lambda$ value (s_i) obtained from the intercept of this division on the curve.

Then $b_i = 1/(2s_i^2)$.

For successive peaks, $c_i = m_{(i+1)}$ with c_3 = c in equation 1). This determination of constants is illustrated in Fig 3.10. When the plot of f(x) from equation 1) *vs* $\sin\theta/\lambda$ is compared to the original output from NORMAL (Fig 3.8 for model 1 and 3.9 for model 2) the match is very good.

Thus the molecular scattering factor (g) (model 1)

$$f(x) = 31.8\exp(-52.06x^2) + 3.2\exp(-2.4x^2) + 1.2\exp(-1.15x^2) + 5.8$$

was used in SHELX-76 to describe the scattering power of the whole dmso molecule in Compound (VI) and (VII). With this term inserted into a structure factor calculation followed by an difference electron density map and treated anisotropically, the standard R was reduced from 12.1% to 10.7% and accounted for all the remaining peaks in the electron density map greater than $0.5eÅ^{-3}$.

For Compound (VII), both models were tried. Model 1 successfully reduced R from 12.5% to 10.7% with $U_{equiv} = 0.267Å^2$. Model 2 using the formula:

$$f(x) = 38.2\exp(-67.6x^2) + 3.3\exp(-2.62x^2) + 2.18\exp(-.96x^2) + 4.68$$

also reduced the R but not so dramatically (from 12.5% to 11.4%) but the thermal parameters were better ($U_{equiv} = 0.197Å^2$). These results indicate that the dmso molecule in Compound (VII) is best modelled by assuming that the centre of the molecule is located on the 1 site and not the S atom.

Model 1 is much smaller than model 2 and although the total number of electrons in model 2 is higher (48 vs 42) the electron density is higher for the former model. The tolerance, for model 1, in the positioning of the dmso 'molecule' is smaller than for the latter model and this will

cause higher thermal parameters but, if the correct position is found, a better R will result.

Fig 3.11 compares the g functions for both models. In the usable range of θ values ($\sin\theta/\lambda$ varying from $\approx$0.1 to 0.5), the agreement between the models is good with model 2 giving less scattering power at the higher θ values. This is in agreement with the empirical predictions made earlier.

Once both Compound (VI) and (VII) had been fully refined using the g function obtained for model 1, a further structure factor calculation followed by a difference electron density map was performed with the spherically scattering dmso molecule removed. The peaks thus obtained however, still did not make any chemical sense and thus final refinement was carried out for both compounds with the single giant dmso 'atom' to describe the aliphatic guest molecule.

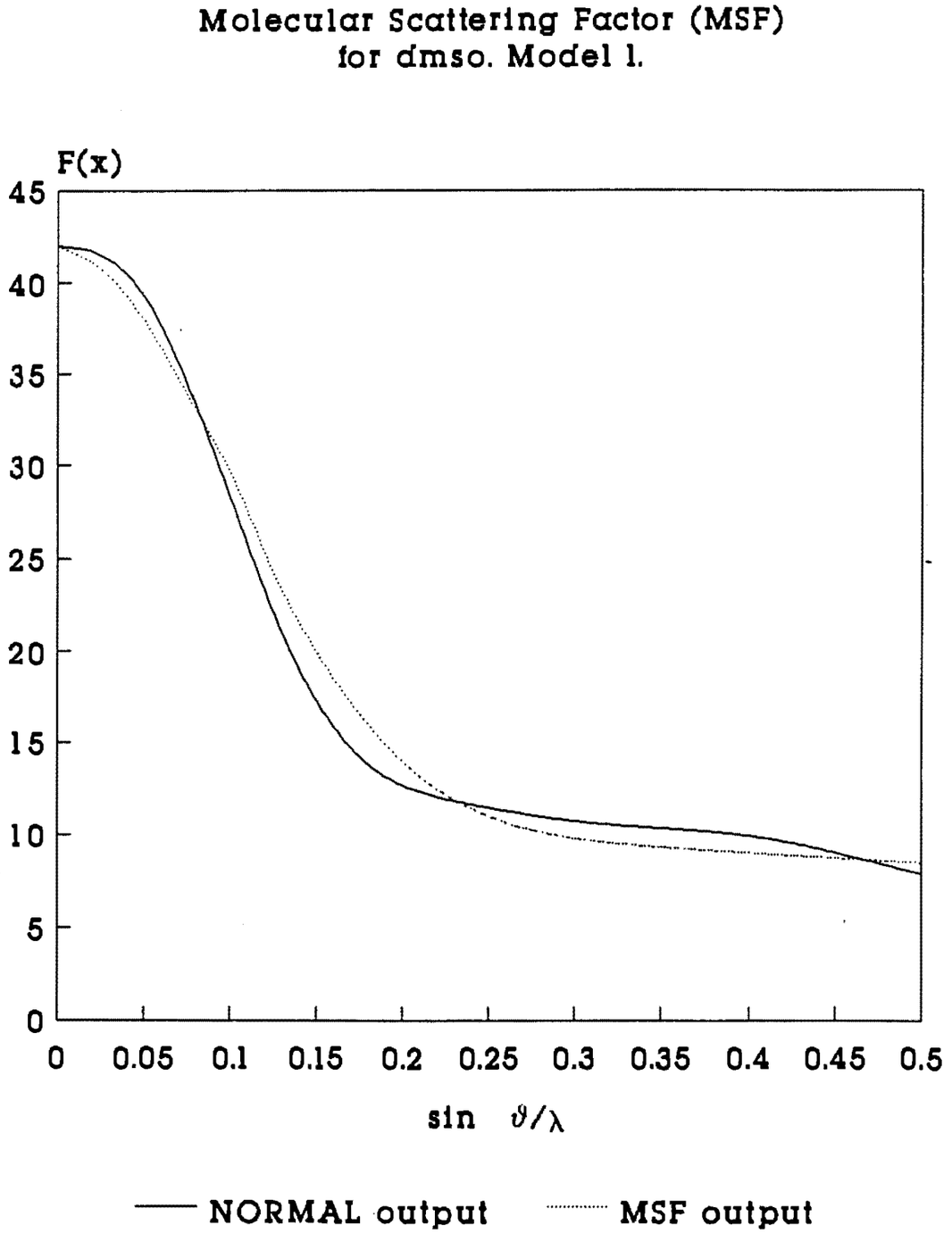

Fig 3.8 Comparison between output from NORMAL and input to SHELX for the MSF of model 1.

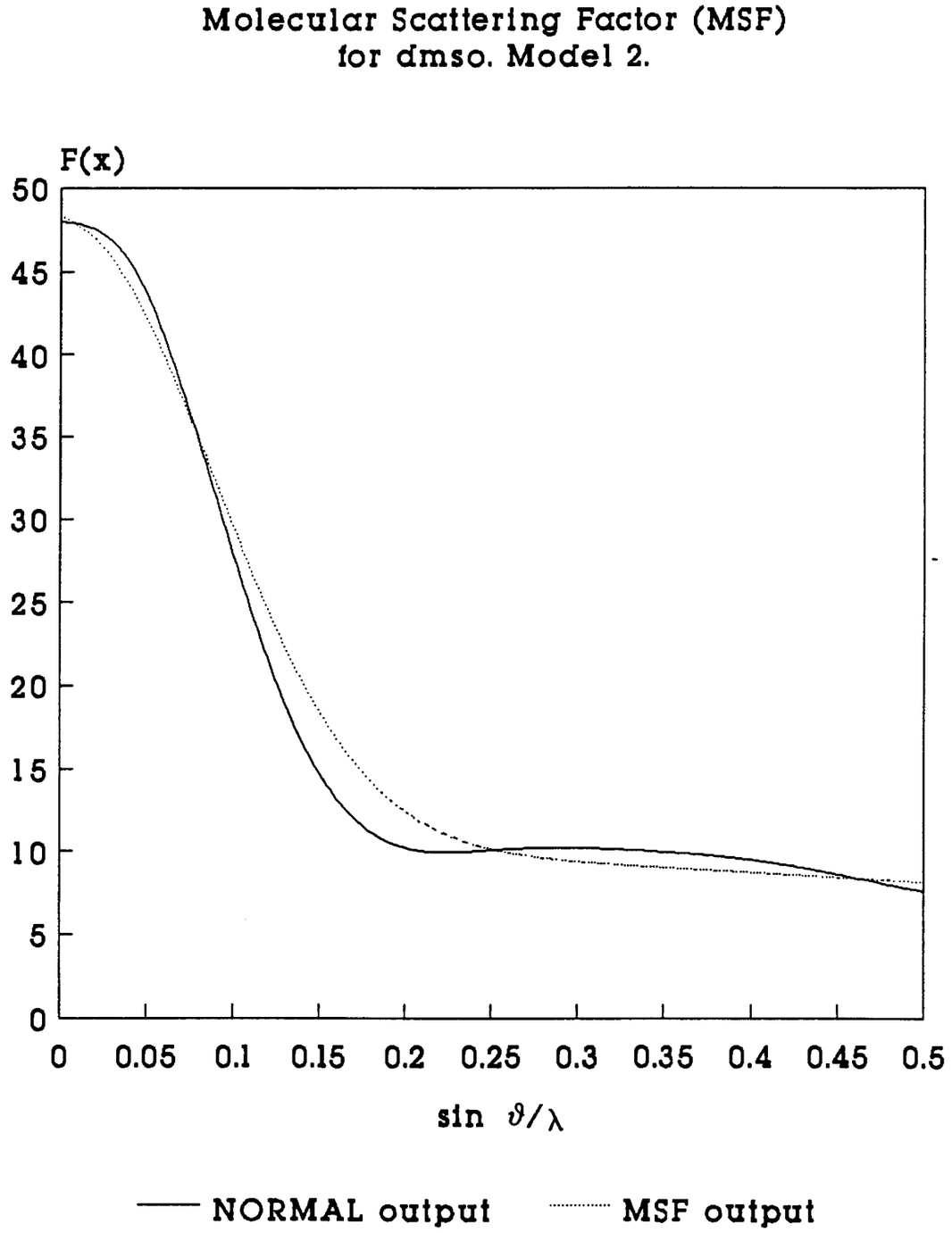

Fig 3.9 Comparison between output from NORMAL and input to SHELX for the MSF of model 2.

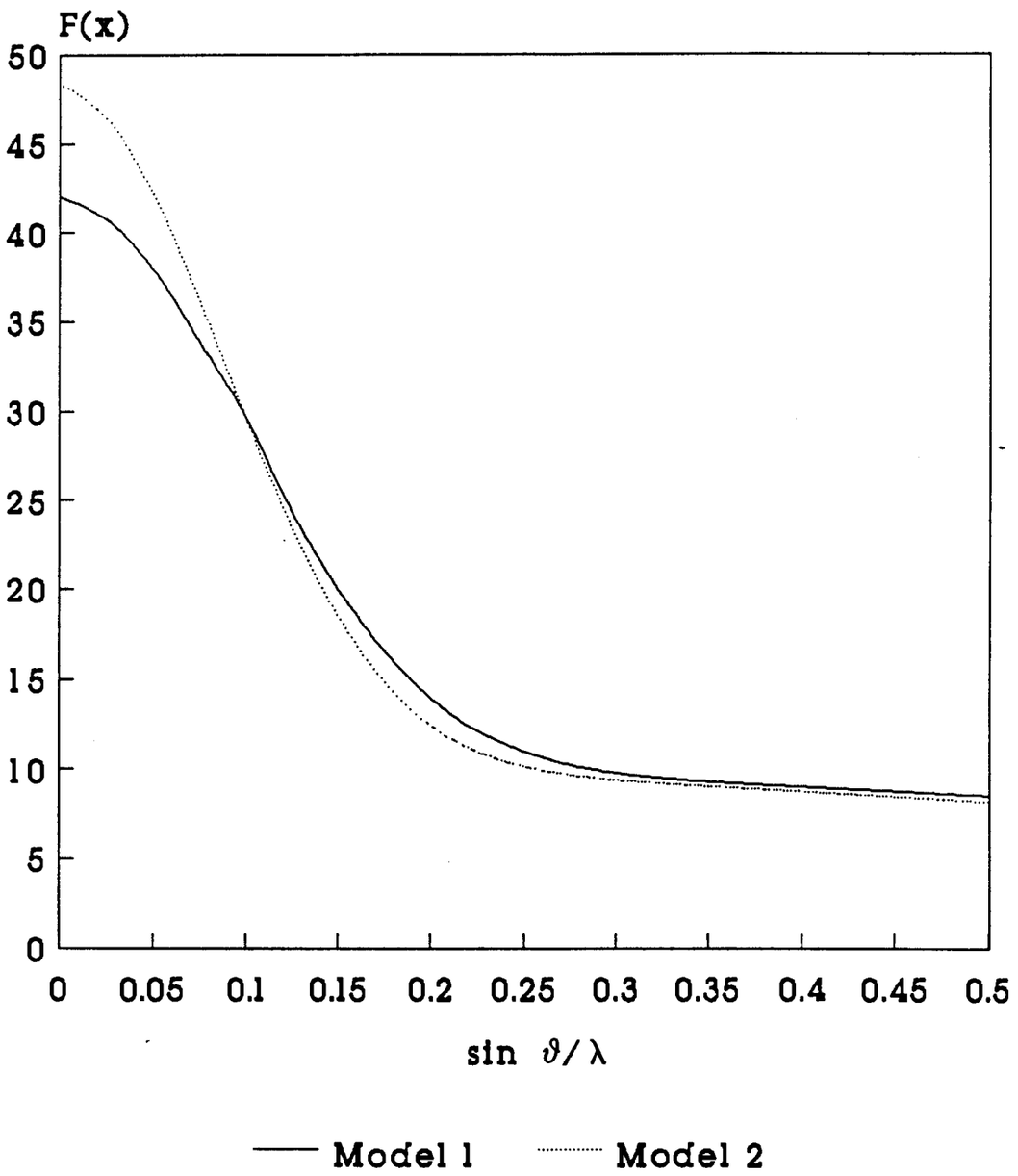

Fig 3.11 Comparison between the MSF functions obtained for model 1 and model 2.

Determination of constants for
input into SHELX.

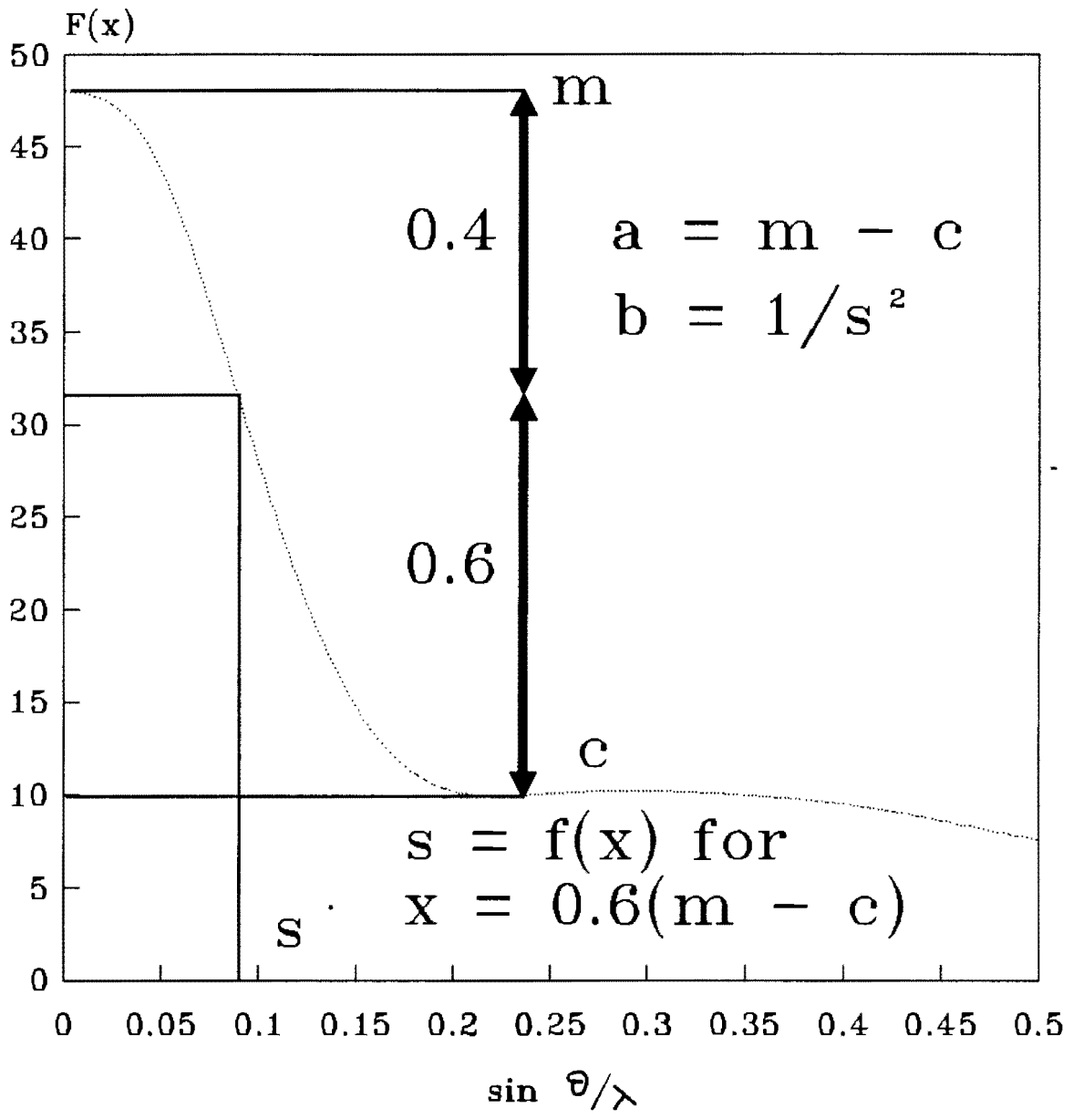

Fig 3.10 Diagram showing the determination of the constants required for the scattering factor term in SHELX.

TABLE 3.1a Fractional atomic coordinates (x 10^4)
and Thermal Parameters (A^2 x 10^3)
with e.s.d. s in parentheses for Compound (I)

Atom	x/a	y/b	z/c	U_{iso}/U_{equiv}(*)
Ni(1)	773(2)	364(1)	1352(0)	54(1) *
N(1)	1209(9)	1504(9)	1533(3)	68(4)
C(1)	1424(11)	2094(10)	1679(4)	56(5)
S(1)	1754(4)	2941(3)	1864(1)	93(2) *
N(2)	345(9)	-769(8)	1158(3)	61(4)
C(2)	-53(11)	-1359(10)	1053(3)	50(5)
S(2)	-576(4)	-2190(3)	899(1)	85(2) *
N(11)	2262(9)	219(8)	1134(3)	64(4)
C(12)	2749(12)	855(10)	975(3)	65(5)
C(13)	3713(13)	771(11)	812(4)	75(6)
C(14)	4228(13)	6(10)	827(4)	69(5)
C(15)	3722(12)	-621(10)	1014(4)	70(5)
C(16)	2760(12)	-498(10)	1157(3)	58(5)
C(111)	5280(8)	-85(8)	674(3)	76(6)
C(112)	5513(8)	334(8)	373(3)	147(8)
C(113)	6459(8)	193(8)	209(3)	176(10)
C(114)	7171(8)	-370(8)	345(3)	114(7)
C(115)	6937(8)	-790(8)	645(3)	153(9)
C(116)	5992(8)	-648(8)	809(3)	130(8)
N(21)	197(9)	943(7)	905(3)	53(4)
C(22)	-386(12)	1634(9)	948(4)	61(5)
C(23)	-992(11)	1966(9)	683(4)	57(5)
C(24)	-1041(12)	1594(9)	361(4)	58(5)
C(25)	-389(11)	886(9)	331(4)	58(5)
C(26)	172(11)	584(10)	600(4)	64(5)
C(211)	-1713(13)	1892(9)	93(4)	57(5)
C(212)	-2688(14)	2214(11)	179(4)	90(6)
C(213)	-3370(16)	2468(11)	-80(5)	98(7)
C(214)	-3106(15)	2391(11)	-421(5)	92(6)
C(215)	-2134(14)	2068(10)	-487(4)	85(6)
C(216)	-1436(13)	1821(9)	-249(4)	68(5)
N(31)	-752(10)	521(7)	1560(3)	55(3)

Table 3.1a (cont.)

C(32)	-882(13)	965(9)	1841(4)	58(5)
C(33)	-1866(12)	1167(9)	1976(4)	62(5)
C(34)	-2769(11)	933(9)	1798(4)	46(4)
C(35)	-2600(12)	452(10)	1512(3)	65(5)
C(36)	-1604(12)	257(10)	1403(4)	68(5)
C(311)	-3832(11)	1194(8)	1905(4)	44(4)
C(312)	-4006(13)	1436(9)	2243(4)	79(6)
C(313)	-4959(14)	1749(11)	2342(4)	89(7)
C(314)	-5772(15)	1796(10)	2104(4)	82(5)
C(315)	-5603(14)	1587(10)	1777(4)	81(6)
C(316)	-4615(13)	1251(10)	1674(4)	80(6)
N(41)	1257(9)	-190(8)	1809(3)	59(4)
C(42)	2116(12)	27(9)	1992(4)	58(5)
C(43)	2334(11)	-287(9)	2305(3)	52(4)
C(44)	1624(12)	-835(8)	2458(4)	46(4)
C(45)	755(12)	-1069(8)	2280(3)	56(4)
C(46)	597(12)	-740(9)	1959(4)	60(5)
C(411)	1835(9)	-1185(5)	2802(2)	51(4)
C(412)	2840(9)	-1404(5)	2903(2)	61(5)
C(413)	3002(9)	-1754(5)	3222(2)	74(6)
C(414)	2161(9)	-1885(5)	3440(2)	77(6)
C(415)	1158(9)	-1666(5)	3339(2)	81(6)
C(416)	996(9)	-1315(5)	3020(2)	70(5)

Anisotropic atoms have thermal parameters (A^2 x 10^3) of the form:

$$T=\exp(-2\pi^2(U_{11}h^2a^{*2}+U_{22}k^2b^{*2}+U_{33}l^2c^{*2}+2U_{23}klb^*c^*+ 2U_{13}hla^*c^*+2U_{12}hka^*b^*)) \times 10^3,$$

with the following parameters :

Atom	U_{11}	U_{22}	U_{33}	U_{23}	U_{13}	U_{12}
Ni(1)	57(1)	49(1)	57(1)	-5(1)	-1(2)	-2(1)
S(1)	77(4)	57(3)	145(5)	-33(3)	-16(4)	-10(3)
S(2)	84(4)	76(4)	95(4)	-35(3)	5(3)	-18(3)

TABLE 3.2a Fractional atomic coordinates (x 10^4)
and Thermal Parameters (A^2 x 10^3)
with e.s.d. s in parentheses for Compound (II)

Atom	x/a	y/b	z/c	U_{iso}/U_{equiv}(*)
Ni(1)	0(0)	0(0)	0(0)	35(1) *
N(1)	-1649(15)	-271(3)	-5(8)	47(4)
C(1)	-2375(18)	-433(4)	20(10)	42(5)
S(1)	-3522(7)	-701(1)	-26(4)	83(3) *
N(11)	-1201(14)	395(3)	-55(7)	37(4)
C(12)	-2230(20)	389(5)	-308(9)	51(6)
C(13)	-3117(19)	646(4)	-384(9)	47(5)
C(14)	-2756(18)	905(4)	-45(9)	39(4)
C(15)	-1593(22)	909(5)	223(10)	56(6)
C(16)	-834(19)	651(4)	245(9)	39(5)
C(111)	-3658(19)	1169(4)	-104(9)	47(5)
C(112)	-4138(19)	1261(4)	-629(10)	50(6)
C(113)	-4954(22)	1515(5)	-662(10)	56(6)
C(114)	-5131(24)	1689(5)	-220(10)	60(7)
C(115)	-4615(26)	1599(6)	381(12)	77(8)
C(116)	-3768(21)	1353(5)	380(10)	55(6)
N(21)	0(0)	0(0)	957(17)	85(11)
C(22)	-1139(22)	13(5)	1177(9)	57(6)
C(23)	-1169(22)	19(5)	1763(10)	58(6)
C(24)	0(0)	0(0)	2061(14)	43(8)
C(211)	0(0)	0(0)	2762(11)	27(7)
C(212)	-981(23)	119(5)	3049(11)	63(6)
C(213)	-1030(24)	132(5)	3687(11)	66(7)
C(214)	0(0)	0(0)	3968(19)	70(12)
N(41)	0(0)	0(0)	-908(8)	18(5)
C(42)	-190(16)	-254(4)	-1226(7)	28(4)
C(43)	-222(19)	-265(5)	-1826(9)	48(5)
C(44)	0(0)	0(0)	-2171(13)	35(7)
C(411)	0(0)	0(0)	-2749(17)	64(12)

Table 3.2a (cont.)

C(412)	433(20)	-259(5)	-3093(10)	48(6)
C(413)	444(24)	-245(6)	-3652(11)	73(7)
C(414)	0(0)	0(0)	-3927(25)	98(16)
C(1G)	2065(23)	873(5)	2008(12)	59(7)
C(2G)	3190(21)	1045(5)	2120(10)	56(6)
C(3G)	3713(26)	1062(5)	2650(11)	68(7)
C(4G)	3189(24)	899(5)	3086(11)	59(6)
C(5G)	2112(26)	735(6)	3038(13)	77(8)
C(6G)	1530(23)	730(5)	2473(13)	65(6)
C(11G)	1350(27)	838(6)	1453(12)	82(8)
C(21G)	3799(35)	1221(8)	1622(17)	121(12)

Anisotropic atoms have thermal parameters (A^2 x 10^3) of the form:

$$T=\exp(-2\pi^2(U_{11}h^2a^{*2}+U_{22}k^2b^{*2}+U_{33}l^2c^{*2}+2U_{23}klb^*c^*+ 2U_{13}hla^*c^*+2U_{12}hka^*b^*)) \times 10^3,$$

with the following parameters :

Atom	U_{11}	U_{22}	U_{33}	U_{23}	U_{13}	U_{12}
Ni(1)	35(2)	32(2)	39(2)	0(0)	0(0)	0(2)
S(1)	67(4)	69(4)	113(6)	10(5)	-6(5)	-22(4)

TABLE 3.3a Fractional atomic coordinates (x 10^4)
and Thermal Parameters ($Å^2$ x 10^3)
with e.s.d. s in parentheses for Compound (III)

Atom	x/a	y/b	z/c	U_{iso}/U_{equiv}(*)
Ni(1)	0(0)	2927(1)	2500(0)	50(1) *
N(1)	1856(6)	2895(3)	2934(3)	56(2)
C(1)	2778(7)	2859(3)	3273(3)	51(2)
S(1)	4078(2)	2791(1)	3742(1)	104(1) *
N(11)	663(5)	2978(3)	1667(3)	55(2)
C(12)	1846(8)	2826(3)	1596(4)	71(3)
C(13)	2328(8)	2943(4)	1084(4)	74(2)
C(14)	1600(7)	3214(3)	611(3)	54(2)
C(15)	383(8)	3385(4)	697(4)	79(3)
C(16)	-50(8)	3255(3)	1218(4)	74(3)
C(111)	2063(8)	3355(3)	59(4)	64(2)
C(112)	3348(9)	3438(4)	43(5)	95(3)
C(113)	3746(11)	3610(5)	-485(5)	119(4)
C(114)	2877(10)	3676(4)	-1001(5)	96(3)
C(115)	1624(9)	3575(4)	-992(4)	90(3)
C(116)	1215(8)	3418(4)	-468(4)	74(3)
N(21)	0(0)	2013(4)	2500(0)	54(2)
C(22)	463(7)	1714(3)	2991(4)	65(2)
C(23)	471(7)	1113(3)	3002(4)	65(2)
C(24)	0(0)	802(5)	2500(0)	57(3)
C(211)	0(0)	147(6)	2500(0)	78(4)
C(212)	161(11)	-137(5)	3005(6)	131(4)
C(213)	175(13)	-754(6)	3009(7)	167(6)
C(214)	0(0)	-997(9)	2500(0)	142(7)
N(41)	0(0)	3836(4)	2500(0)	56(2)
C(42)	1095(7)	4155(3)	2580(3)	65(2)
C(43)	1131(8)	4748(3)	2591(4)	66(2)
C(44)	0(0)	5060(5)	2500(0)	53(3)
C(411)	0(0)	5692(5)	2500(0)	55(3)
C(412)	1061(7)	6000(3)	2385(3)	60(2)

Table 3.3a (cont.)

C(413)	1069(8)	6599(4)	2385(4)	75(3)
C(414)	0(0)	6894(5)	2500(0)	75(4)
C(11G)	2498(11)	1394(5)	4615(6)	125(4)
C(12G)	3040(10)	991(5)	4268(5)	107(4)
C(13G)	3165(12)	422(6)	4395(6)	126(4)
C(14G)	2740(12)	182(6)	4899(6)	146(5)
C(15G)	2201(14)	610(8)	5235(7)	158(6)
C(16G)	2117(11)	1156(6)	5080(6)	122(4)
C(17G)	3755(13)	-16(7)	4043(7)	222(8)
C(18G)	1743(17)	370(8)	5724(9)	317(13)

Anisotropic atoms have thermal parameters ($Å^2$ x 10^3) of the form:

$$T=\exp(-2\pi^2(U_{11}h^2a^{*2}+U_{22}k^2b^{*2}+U_{33}l^2c^{*2}+2U_{23}klb^*c^*+ 2U_{13}hla^*c^*+2U_{12}hka^*b^*)) \times 10^3,$$

with the following parameters :

Atom	U_{11}	U_{22}	U_{33}	U_{23}	U_{13}	U_{12}
Ni(1)	40(1)	58(1)	49(1)	0(0)	0(1)	0(0)
S(1)	69(2)	131(3)	97(2)	-23(2)	-30(2)	24(2)

TABLE 3.4a Fractional atomic coordinates (x 10^4) and Thermal Parameters (A^2 x 10^3) with e.s.d. s in parentheses for Compound (1V)

Atom	x/a	y/b	z/c	U_{iso}/U_{equiv}(*)
Ni(1)	2119(2)	4505(1)	2328(1)	42(1) *
N(1)	605(11)	4657(9)	2765(4)	54(3)
C(1)	157(13)	4912(11)	3126(5)	49(3)
S(1)	-471(5)	5249(4)	3632(1)	80(2) *
N(2)	3663(10)	4274(8)	1906(4)	47(3)
C(2)	4228(12)	3966(10)	1602(4)	44(3)
S(2)	5025(5)	3511(4)	1164(2)	81(2) *
N(11)	3009(10)	6428(9)	2411(4)	51(3)
C(12)	3013(14)	7202(12)	2826(5)	58(4)
C(13)	3561(13)	8409(11)	2890(5)	55(4)
C(14)	4204(13)	8933(11)	2516(5)	47(3)
C(15)	4265(13)	8137(11)	2082(5)	53(3)
C(16)	3667(13)	6937(11)	2034(5)	51(3)
C(111)	4875(13)	10277(11)	2569(5)	50(3)
C(112)	5249(16)	11060(14)	3051(6)	82(5)
C(113)	5908(18)	12335(16)	3097(7)	99(6)
C(114)	6224(16)	12778(14)	2674(6)	77(5)
C(115)	5860(15)	12073(13)	2207(6)	74(4)
C(116)	5178(14)	10815(12)	2139(5)	61(4)
N(21)	774(10)	4393(8)	1647(4)	45(3)
C(22)	-51(14)	5020(12)	1673(5)	58(4)
C(23)	-897(14)	5071(12)	1243(5)	61(4)
C(24)	-921(13)	4446(10)	773(5)	46(3)
C(25)	-40(13)	3781(11)	749(5)	52(3)
C(26)	777(13)	3814(11)	1195(5)	53(3)
C(211)	-1848(13)	4455(11)	308(5)	47(3)
C(212)	-2302(16)	5398(14)	296(6)	80(5)
C(213)	-3211(17)	5424(15)	-135(6)	86(5)
C(214)	-3597(16)	4481(14)	-548(6)	78(5)
C(215)	-3104(16)	3579(14)	-556(6)	80(5)
C(216)	-2243(14)	3533(12)	-128(5)	65(4)
N(31)	1129(10)	2593(9)	2266(4)	49(3)
C(32)	-245(13)	2026(11)	2160(4)	49(3)
C(33)	-938(14)	794(12)	2147(5)	58(4)
C(34)	-157(13)	150(11)	2258(5)	47(3)
C(35)	1322(13)	756(11)	2372(5)	52(3)
C(36)	1942(14)	1975(11)	2361(5)	55(4)
C(311)	-866(14)	-1147(12)	2259(5)	55(3)
C(312)	-2078(15)	-1856(13)	1923(5)	65(4)
C(313)	-2749(18)	-3101(15)	1918(7)	91(5)
C(314)	-2175(17)	-3537(15)	2276(6)	83(5)
C(315)	-997(17)	-2857(14)	2606(6)	84(5)
C(316)	-280(17)	-1593(14)	2613(6)	77(5)
N(41)	3513(10)	4699(9)	3005(4)	48(3)
C(42)	3060(14)	4226(11)	3412(5)	58(4)
C(43)	3947(15)	4312(12)	3834(5)	65(4)
C(44)	5392(13)	4923(11)	3885(5)	51(3)
C(45)	5891(13)	5437(11)	3475(5)	52(3)
C(46)	4946(13)	5300(10)	3051(5)	48(3)
C(411)	6391(15)	5040(13)	4336(5)	64(4)
C(412)	6136(21)	4043(18)	4563(7)	109(6)
C(413)	7211(21)	4167(18)	5014(8)	115(7)
C(414)	8322(19)	5182(16)	5173(7)	95(6)
C(415)	8555(20)	6164(17)	4956(7)	103(6)
C(416)	7565(17)	6098(15)	4527(6)	82(5)
S(4G)	447(9)	9091(6)	673(3)	100(4)
S(41G)	1766(66)	9440(42)	723(18)	213(24)
O(4G)	854(16)	8809(13)	186(6)	141(5)
C(41G)	1196(21)	10627(18)	871(8)	118(7)
C(42G)	1331(23)	8642(19)	1142(8)	132(8)
S(3G)	4325(8)	424(6)	9355(3)	92(3)
S(32G)	3046(21)	257(16)	9164(7)	116(8)
O(3G)	4208(16)	780(13)	8852(6)	141(5)
C(31G)	3016(21)	-1112(18)	9228(7)	117(7)
C(32G)	3682(24)	1341(21)	9781(9)	149(9)
C(11G)	3768(24)	10891(20)	5925(8)	71(3)
C(12G)	3134(23)	11175(20)	6357(8)	71(3)
C(13G)	2103(23)	10221(20)	6498(8)	71(3)
C(14G)	1728(23)	9073(20)	6203(9)	71(3)
C(15G)	2203(24)	8716(20)	5816(9)	71(3)
C(16G)	3337(23)	9591(20)	5631(8)	71(3)
C(17G)	466(23)	8025(19)	6409(8)	71(3)
C(7G)	5385(23)	11922(23)	5784(11)	192(9)
C(24G)	7879(0)	9667(0)	5574(0)	192(9)
C(25G)	8728(0)	10896(0)	5680(0)	192(9)
C(26G)	8126(0)	11731(0)	5833(0)	192(9)
C(21G)	6675(0)	11335(0)	5878(0)	192(9)
C(22G)	5826(0)	10107(0)	5772(0)	192(9)
C(23G)	6428(0)	9271(0)	5621(0)	192(9)
C(27G)	8426(83)	8703(56)	5230(27)	192(9)

Anisotropic atoms have thermal parameters (A^2 x 10^3) of the fo

$$T=\exp(-2\pi^2(U_{11}h^2a^{*2}+U_{22}k^2b^{*2}+U_{33}l^2c^{*2}+2U_{23}klb^*c^*+ 2U_{13}hla^*c^*+2U_{12}hka^*b^*)) \times 10^3,$$

with the following parameters :

Atom	U_{11}	U_{22}	U_{33}	U_{23}	U_{13}	U_{12}
Ni(1)	43(1)	38(1)	42(1)	11(1)	11(1)	10(1)
S(1)	101(3)	108(4)	55(3)	28(2)	32(2)	60(3)
S(2)	96(3)	102(3)	71(3)	27(3)	36(2)	61(3)

TABLE 3.5a Fractional atomic coordinates (x 10^4) and Thermal Parameters (A^2 x 10^3) with e.s.d. s in parentheses for Compound (V)

Atom	x/a	y/b	z/c	U_{iso}/U_{equiv}(*)
Ni(1)	280(3)	3667(2)	2600(2)	51(1) *
N(1)	2222(23)	3667(10)	3049(10)	73(8)
C(1)	3218(27)	3755(11)	3346(11)	48(8)
S(1)	4677(9)	3803(5)	3729(4)	121(5) *
N(2)	-1710(19)	3629(9)	2169(8)	46(6)
C(2)	-2718(25)	3619(11)	1875(11)	44(7)
S(2)	-4129(8)	3586(4)	1488(5)	103(4) *
N(11)	1026(21)	3634(10)	1800(10)	71(7)
C(12)	2138(25)	3341(11)	1730(12)	57(8)
C(13)	2545(26)	3260(11)	1213(13)	60(8)
C(14)	1906(28)	3531(12)	725(13)	74(10)
C(15)	698(22)	3830(10)	788(11)	43(7)
C(16)	358(29)	3896(12)	1330(13)	75(10)
C(111)	2215(23)	3465(8)	128(8)	61(9)
C(112)	3577(23)	3381(8)	108(8)	106(12)
C(113)	4012(23)	3302(8)	-425(8)	145(15)
C(114)	3088(23)	3306(8)	-939(8)	123(14)
C(115)	1727(23)	3390(8)	-920(8)	112(12)
C(116)	1291(23)	3469(8)	-386(8)	120(14)
N(21)	296(21)	2752(8)	2595(11)	56(6)
C(22)	751(25)	2476(12)	3088(12)	62(9)
C(23)	707(22)	1890(11)	3095(11)	42(7)
C(24)	97(24)	1593(10)	2639(12)	44(7)
C(25)	-350(23)	1900(12)	2135(12)	55(9)
C(26)	-268(21)	2477(11)	2126(11)	45(8)
C(211)	5(17)	972(6)	2593(11)	75(9)
C(212)	41(17)	690(6)	3121(11)	73(9)
C(213)	-20(17)	102(6)	3132(11)	99(11)
C(214)	-115(17)	-201(6)	2613(11)	74(10)
C(215)	-150(17)	80(6)	2085(11)	92(11)
C(216)	-91(17)	668(6)	2075(11)	86(10)
N(31)	-462(19)	3689(10)	3429(9)	55(6)
C(32)	121(28)	3958(12)	3870(13)	69(9)
C(33)	-296(27)	4028(12)	4400(13)	72(9)
C(34)	-1394(26)	3680(14)	4468(13)	73(9)
C(35)	-2014(28)	3354(12)	4034(13)	69(9)
C(36)	-1537(27)	3376(12)	3497(13)	66(9)
C(311)	-1899(19)	3729(12)	5046(8)	70(8)
C(312)	-1862(19)	4228(12)	5367(8)	100(11)
C(313)	-2288(19)	4230(12)	5908(8)	181(20)
C(314)	-2752(19)	3735(12)	6129(8)	168(18)
C(315)	-2791(19)	3236(12)	5810(8)	162(18)
C(316)	-2365(19)	3233(12)	5269(8)	172(19)
N(41)	190(22)	4550(8)	2556(10)	58(6)
C(42)	1291(25)	4869(12)	2510(11)	57(8)
C(43)	1271(27)	5438(12)	2473(12)	66(9)
C(44)	67(23)	5741(10)	2435(11)	47(8)
C(45)	-1112(28)	5410(12)	2481(12)	69(9)
C(46)	-1017(30)	4820(13)	2562(13)	80(10)
C(411)	-6(18)	6362(6)	2433(8)	60(8)
C(412)	928(18)	6661(6)	2171(8)	78(10)
C(413)	859(18)	7247(6)	2138(8)	80(10)
C(414)	-148(18)	7534(6)	2366(8)	73(9)
C(415)	-1084(18)	7236(6)	2626(8)	83(10)
C(416)	-1014(18)	6648(6)	2659(8)	76(9)
C(11G)	2020(21)	6896(7)	174(11)	77(10)
C(12G)	2489(21)	6991(7)	-350(11)	123(14)
C(13G)	2582(21)	7540(7)	-556(11)	108(12)
C(14G)	2207(21)	7994(7)	-237(11)	101(12)
C(15G)	1741(21)	7899(7)	287(11)	118(13)
C(16G)	1646(21)	7352(7)	493(11)	139(15)
C(21G)	2536(34)	9667(8)	-877(12)	157(17)
C(22G)	1544(34)	9530(8)	-547(12)	192(21)
C(23G)	1436(34)	8979(8)	-350(12)	124(13)
C(24G)	2322(34)	8564(8)	-485(12)	123(14)
C(25G)	3313(34)	8703(8)	-816(12)	157(16)
C(26G)	3421(34)	9254(8)	-1013(12)	131(14)
N(1G)	2115(27)	6049(12)	1009(11)	110(10)
N(2G)	1776(34)	5464(14)	776(15)	184(16)
C(3G)	2448(36)	5273(18)	275(13)	143(15)
N(4G)	2039(34)	5288(16)	-375(13)	192(16)
N(5G)	3300(53)	5126(33)	-569(22)	428(42)

Anisotropic atoms have thermal parameters (A^2 x 10^3) of the for

$$T=\exp(-2\pi^2(U_{11}h^2a^{*2}+U_{22}k^2b^{*2}+U_{33}l^2c^{*2}+2U_{23}klb^*c^*+ 2U_{13}hla^*c^*+2U_{12}hka^*b^*)) \times 10^3,$$

with the following parameters :

Atom	U_{11}	U_{22}	U_{33}	U_{23}	U_{13}	U_{12}
Ni(1)	42(2)	53(2)	63(2)	1(3)	23(2)	5(2)
S(1)	72(6)	150(10)	126(9)	77(8)	-31(6)	-39(6)
S(2)	67(6)	97(8)	137(9)	-8(7)	-14(6)	-16(6)

TABLE 3.6a Fractional atomic coordinates (x 10^4) and Thermal Parameters ($Å^2$ x 10^3) with e.s.d. s in parentheses for Compound (VI)

Atom	x/a	y/b	z/c	U_{iso}/U_{equiv}(*)
Ni(1)	-308(2)	3487(1)	2387(1)	51(1) *
N(1)	1596(14)	3381(5)	2800(6)	57(4)
C(1)	2543(17)	3425(7)	3092(8)	58(4)
S(1)	3933(7)	3480(4)	3564(3)	135(4) *
N(2)	-2268(13)	3557(6)	1966(6)	60(4)
C(2)	-3355(16)	3590(6)	1787(7)	51(4)
S(2)	-4913(5)	3597(2)	1516(3)	93(2) *
N(11)	348(12)	3541(5)	1546(6)	52(3)
C(12)	1386(18)	3269(8)	1400(9)	69(5)
C(13)	1838(16)	3319(7)	866(8)	59(5)
C(14)	1195(16)	3680(7)	452(8)	58(5)
C(15)	135(17)	3949(8)	575(9)	69(5)
C(16)	-307(17)	3876(8)	1123(8)	70(5)
C(111)	1648(13)	3742(6)	-126(5)	71(5)
C(112)	2160(13)	3299(6)	-413(5)	116(8)
C(113)	2575(13)	3383(6)	-958(5)	102(7)
C(114)	2476(13)	3911(6)	-1213(5)	105(7)
C(115)	1962(13)	4353(6)	-926(5)	97(7)
C(116)	1549(13)	4268(6)	-383(5)	96(7)
N(21)	-457(12)	2617(5)	2310(6)	31(3)
C(22)	63(18)	2288(8)	2754(9)	71(5)
C(23)	97(18)	1725(8)	2736(9)	71(5)
C(24)	-435(15)	1435(7)	2232(7)	55(4)
C(25)	-1050(16)	1799(7)	1760(8)	61(5)
C(26)	-988(15)	2357(7)	1827(7)	55(5)
C(211)	-487(12)	824(4)	2177(6)	72(5)
C(212)	-27(12)	498(4)	2666(6)	80(6)
C(213)	-27(12)	-78(4)	2619(6)	99(7)
C(214)	-485(12)	-331(4)	2082(6)	102(7)
C(215)	-944(12)	-5(4)	1591(6)	154(11)
C(216)	-946(12)	572(4)	1640(6)	109(8)
N(31)	-996(12)	3432(6)	3209(6)	34(3)
C(32)	-350(17)	3660(7)	3700(8)	61(5)
C(33)	-740(18)	3625(7)	4239(9)	71(5)
C(34)	-1918(17)	3376(7)	4314(8)	66(5)
C(35)	-2685(18)	3126(7)	3782(8)	66(5)
C(36)	-2146(16)	3194(7)	3269(8)	63(5)
C(311)	-2389(13)	3308(6)	4877(5)	69(5)
C(312)	-1459(13)	3258(6)	5386(5)	82(6)
C(313)	-1889(13)	3211(6)	5931(5)	103(7)
C(314)	-3249(13)	3214(6)	5967(5)	101(7)
C(315)	-4178(13)	3264(6)	5459(5)	122(9)
C(316)	-3748(13)	3310(6)	4915(5)	99(7)
N(41)	-89(13)	4371(5)	2477(6)	58(4)
C(42)	1092(17)	4637(7)	2456(8)	61(5)
C(43)	1215(17)	5196(7)	2490(8)	65(5)
C(44)	100(15)	5524(7)	2525(7)	57(5)
C(45)	-1085(17)	5261(7)	2542(8)	65(5)
C(46)	-1151(17)	4681(7)	2520(8)	63(5)
C(411)	213(12)	6147(4)	2547(5)	59(5)
C(412)	1206(12)	6413(4)	2291(5)	87(6)
C(413)	1261(12)	6991(4)	2279(5)	107(8)
C(414)	323(12)	7305(4)	2520(5)	85(6)
C(415)	-668(12)	7040(4)	2776(5)	85(6)
C(416)	-723(12)	6462(4)	2789(5)	65(5)
C(11G)	3033(17)	7670(5)	-85(8)	117(8)
C(12G)	3585(17)	7238(5)	-372(8)	122(9)
C(13G)	3588(17)	6699(5)	-150(8)	97(7)
C(14G)	3040(17)	6592(5)	359(8)	91(6)
C(15G)	2489(17)	7026(5)	645(8)	121(9)
C(16G)	2486(17)	7564(5)	422(8)	158(12)
C(21G)	3009(18)	4930(5)	1009(8)	129(9)
C(22G)	1948(18)	5288(5)	1052(8)	112(8)
C(23G)	1973(18)	5832(5)	842(8)	95(7)
C(24G)	3060(18)	6015(5)	589(8)	80(6)
C(25G)	4120(18)	5658(5)	545(8)	117(8)
C(26G)	4094(18)	5115(5)	756(8)	134(10)
S(1G)	3117(17)	117(6)	301(6)	150(8) *
S(2G)	-2888(21)	1294(8)	553(8)	203(12) *

Anisotropic atoms have thermal parameters ($Å^2$ x 10^3) of the form:

$$T=\exp(-2\pi^2(U_{11}h^2a^{*2}+U_{22}k^2b^{*2}+U_{33}l^2c^{*2}+2U_{23}klb^*c^*+2U_{13}hla^*c^*+2U_{12}hka^*b^*)) \times 10^3,$$

with the following parameters :

Atom	U_{11}	U_{22}	U_{33}	U_{23}	U_{13}	U_{12}
Ni(1)	52(1)	53(1)	45(1)	0(1)	-2(1)	0(1)
S(1)	104(5)	164(7)	118(6)	23(6)	-45(4)	-20(5)
S(2)	67(3)	96(5)	106(5)	-16(4)	-20(3)	6(3)
S(1G)	229(18)	119(11)	97(11)	14(9)	6(11)	33(11)
S(2G)	275(24)	149(15)	158(17)	-12(13)	-59(15)	20(15)

TABLE 3.7a Fractional atomic coordinates (x 10^4)
and Thermal Parameters (A^2 x 10^3)
with e.s.d. s in parentheses for Compound (VII)

Atom	x/a	y/b	z/c	U_{iso}/U_{equiv}(*)
Ni(1)	0(0)	924(1)	2500(0)	49(1) *
S(1)	4336(4)	937(2)	3453(2)	94(2) *
N(1)	1954(10)	937(4)	2804(4)	62(3)
C(1)	2947(12)	932(4)	3084(5)	54(3)
N(11)	645(9)	899(4)	1704(4)	51(3)
C(12)	1793(12)	1140(5)	1569(5)	66(4)
C(13)	2223(12)	1149(5)	1036(5)	64(4)
C(14)	1457(11)	895(4)	630(5)	46(3)
C(15)	280(13)	634(6)	765(5)	71(4)
C(16)	-89(12)	656(5)	1303(5)	59(3)
C(111)	1822(11)	883(4)	55(5)	51(3)
C(112)	3174(14)	946(5)	-42(6)	75(4)
C(113)	3502(17)	930(6)	-584(7)	95(5)
C(114)	2545(17)	848(6)	-1007(7)	95(5)
C(115)	1221(14)	802(6)	-899(6)	79(4)
C(116)	883(13)	833(5)	-350(5)	69(4)
N(21)	0(0)	45(5)	2500(0)	53(4)
C(22)	1135(12)	-260(5)	2456(5)	60(3)
C(23)	1167(12)	-802(5)	2440(5)	55(3)
C(24)	0(0)	-1118(7)	2500(0)	55(4)
C(211)	0(0)	-1722(8)	2500(0)	75(5)
C(212)	1064(19)	-2016(8)	2703(7)	115(6)
C(213)	997(26)	-2613(10)	2708(9)	153(8)
C(214)	0(0)	-2857(16)	2500(0)	145(11)
N(41)	0(0)	1791(5)	2500(0)	51(4)
C(42)	617(12)	2090(5)	2897(5)	64(4)
C(43)	648(12)	2663(5)	2932(5)	63(3)
C(44)	0(0)	2976(7)	2500(0)	52(4)
C(411)	0(0)	3577(7)	2500(0)	55(4)
C(412)	68(12)	3887(5)	2974(5)	61(3)

Table 3.7a (cont.)

C(413)	38(12)	4435(5)	3002(5)	68(4)
C(414)	0(0)	4576(4)	2500(0)	134(10)
C(12G)	1502(28)	7476(13)	1153(10)	177(9)
C(11G)	1943(22)	7893(10)	924(8)	134(7)
C(1G)	2329(16)	8413(7)	689(7)	101(5)
C(2G)	2397(23)	8953(10)	955(10)	145(8)
C(3G)	2817(22)	9384(10)	670(10)	143(7)
C(4G)	3031(25)	9356(12)	121(11)	158(8)
C(5G)	2965(22)	8905(10)	-93(9)	131(7)
C(6G)	2646(17)	8410(8)	143(7)	113(6)
DM(1)	2500(0)	2500(0)	0(0)	267(52) *

Anisotropic atoms have thermal parameters (A^2 x 10^3) of the form :

$$T=\exp(-2\pi^2(U_{11}h^2a^{*2}+U_{22}k^2b^{*2}+U_{33}l^2c^{*2}+2U_{23}klb^*c^*+ 2U_{13}hla^*c^*+2U_{12}hka^*b^*)) \times 10^3,$$

with the following parameters :

Atom	U_{11}	U_{22}	U_{33}	U_{23}	U_{13}	U_{12}
Ni(1)	49(2)	47(2)	52(2)	0(0)	3(1)	0(0)
S(1)	71(3)	105(4)	100(3)	-21(2)	-31(2)	0(2)
DM(1)	285(82)	265(31)	222(85)	130(87)	191(89)	124(78)

TABLE 3.8a Fractional atomic coordinates (x 10^4)
and Thermal Parameters (A^2 x 10^3)
with e.s.d. s in parentheses for Compound (VIII)

Atom	x/a	y/b	z/c	U_{iso}/U_{equiv}(*)
Ni(1)	0(0)	0(0)	0(0)	38(1) *
N(1)	1854(8)	-372(7)	-536(6)	43(2)
C(1)	2822(10)	-698(8)	-877(7)	44(3)
S(1)	4140(3)	-1201(3)	-1341(2)	71(2) *
N(11)	1200(8)	1831(7)	367(6)	46(2)
C(12)	506(12)	2633(10)	540(8)	57(3)
C(13)	1194(12)	3852(10)	778(8)	65(3)
C(14)	2712(10)	4197(9)	849(7)	46(3)
C(15)	3478(12)	3365(10)	658(8)	59(3)
C(16)	2661(11)	2183(9)	421(7)	51(3)
C(111)	3528(11)	5495(9)	1118(8)	51(3)
C(112)	4748(13)	5813(11)	1758(9)	71(4)
C(113)	5494(14)	7057(11)	2002(10)	80(4)
C(114)	4963(12)	7820(11)	1632(9)	68(3)
C(115)	3768(13)	7488(11)	1013(9)	73(4)
C(116)	2983(12)	6264(10)	740(8)	64(3)
N(21)	553(9)	-272(7)	1414(6)	53(2)
C(22)	1941(11)	-65(9)	1754(8)	53(3)
C(23)	2381(11)	-171(9)	2701(8)	54(3)
C(24)	1307(11)	-487(9)	3372(8)	53(3)
C(25)	-117(11)	-724(9)	3022(8)	53(3)
C(26)	-460(11)	-573(9)	2063(8)	55(3)
C(211)	1693(12)	-610(10)	4371(9)	66(3)
C(212)	3011(14)	165(11)	4858(10)	81(4)
C(213)	3438(16)	16(13)	5844(11)	101(5)
C(214)	2518(17)	-837(14)	6237(12)	107(5)
C(215)	1303(16)	-1513(13)	5785(12)	104(5)
C(216)	809(13)	-1466(11)	4807(10)	77(4)
C(11G)	3724(22)	3649(16)	5393(15)	139(3)
C(12G)	2697(20)	3649(16)	4677(15)	139(3)

Table 3.8a (cont.)

C(13G)	3033(21)	3264(16)	3597(15)	139(3)
C(14G)	4255(22)	2932(16)	3471(15)	139(3)
C(15G)	5269(19)	3002(15)	4226(15)	139(3)
C(16G)	4978(21)	3383(16)	5289(15)	139(3)
C(21G)	-145(21)	6335(16)	2170(14)	132(3)
C(22G)	-1409(21)	5601(17)	1877(14)	132(3)
C(23G)	-1884(19)	4578(16)	2284(14)	132(3)
C(24G)	-1004(20)	4433(16)	3068(14)	132(3)
C(25G)	405(19)	5298(16)	3372(14)	132(3)
C(26G)	799(19)	6231(16)	2864(14)	132(3)

Anisotropic atoms have thermal parameters (A^2 x 10^3) of the form:

$$T=\exp(-2\pi^2(U_{11}h^2a^{*2}+U_{22}k^2b^{*2}+U_{33}l^2c^{*2}+2U_{23}klb^*c^*+ 2U_{13}hla^*c^*+2U_{12}hka^*b^*)) \times 10^3,$$

with the following parameters :

Atom	U_{11}	U_{22}	U_{33}	U_{23}	U_{13}	U_{12}
Ni(1)	27(1)	48(1)	36(1)	0(1)	4(1)	8(1)
S(1)	56(2)	110(3)	56(2)	5(2)	14(2)	44(2)

TABLE 3.9a Fractional atomic coordinates (x 10^4) and Thermal Parameters (A^2 x 10^3) with e.s.d. s in parentheses for Compound (IX)

Atom	x/a	y/b	z/c	U_{iso}/U_{equiv}(*)
Ni(1)	4393(1)	4659(1)	305(0)	41(0) *
Cl(1)	5031(1)	3385(1)	-137(1)	51(1) *
Cl(2)	3766(1)	5996(1)	716(1)	50(1) *
N(11)	2822(4)	4453(3)	-97(2)	41(1)
C(12)	2333(5)	3731(4)	-84(3)	44(2)
C(13)	1316(5)	3594(4)	-320(3)	42(2)
C(14)	740(5)	4224(4)	-621(3)	41(2)
C(15)	1264(5)	4968(4)	-635(3)	52(2)
C(16)	2282(5)	5062(4)	-389(3)	49(2)
C(111)	-362(5)	4123(4)	-880(3)	40(2)
C(112)	-993(5)	3478(4)	-721(4)	58(2)
C(113)	-2038(6)	3387(5)	-960(4)	68(2)
C(114)	-2503(7)	3957(5)	-1357(4)	71(2)
C(115)	-1912(6)	4611(5)	-1514(4)	78(3)
C(116)	-851(6)	4726(5)	-1297(4)	68(2)
N(21)	4844(4)	5209(3)	-641(3)	44(1)
C(22)	5388(5)	5908(4)	-657(3)	47(2)
C(23)	5749(5)	6256(4)	-1253(3)	50(2)
C(24)	5503(5)	5886(4)	-1882(3)	41(2)
C(25)	4924(5)	5177(4)	-1865(3)	45(2)
C(26)	4611(5)	4866(4)	-1250(3)	44(2)
C(211)	5885(5)	6242(4)	-2540(3)	46(2)
C(212)	6881(6)	6594(4)	-2586(4)	58(2)
C(213)	7232(7)	6956(5)	-3205(4)	75(3)
C(214)	6524(7)	6947(5)	-3742(5)	84(3)
C(215)	5522(8)	6604(5)	-3713(5)	85(3)
C(216)	5213(6)	6247(4)	-3110(3)	60(2)
N(31)	5932(4)	4928(3)	713(3)	45(1)
C(32)	6055(6)	5368(5)	1293(4)	59(2)
C(33)	7036(6)	5667(4)	1519(4)	61(2)
C(34)	7946(5)	5525(4)	1155(3)	44(2)
C(35)	7832(5)	5069(4)	565(3)	53(2)
C(36)	6828(5)	4774(4)	367(4)	54(2)
C(311)	9006(5)	5870(4)	1363(3)	44(2)
C(312)	9079(6)	6340(5)	1960(4)	64(2)
C(313)	10062(7)	6648(5)	2164(4)	73(2)
C(314)	10927(6)	6525(5)	1766(4)	72(3)
C(315)	10876(7)	6081(5)	1193(5)	91(3)
C(316)	9905(7)	5733(5)	974(4)	75(3)
N(41)	3960(4)	4111(3)	1246(3)	47(2)
C(42)	4596(6)	3575(4)	1526(4)	61(2)
C(43)	4446(6)	3242(4)	2184(3)	61(2)
C(44)	3559(6)	3465(4)	2549(3)	47(2)
C(45)	2868(6)	4021(4)	2256(3)	56(2)
C(46)	3092(6)	4338(4)	1610(3)	50(2)
C(411)	3339(6)	3139(4)	3264(3)	50(2)
C(412)	4235(7)	2917(4)	3665(4)	68(2)
C(413)	4043(7)	2642(5)	4343(5)	81(3)
C(414)	2994(7)	2600(5)	4565(5)	83(3)
C(415)	2117(7)	2804(5)	4177(4)	74(2)
C(416)	2313(6)	3092(4)	3524(4)	63(2)
O(1G)	1269(5)	3159(4)	7135(3)	99(2)
C(1G)	1313(8)	3771(7)	7628(5)	109(3)

Anisotropic atoms have thermal parameters (A^2 x 10^3) of the form:

$$T=\exp(-2\pi^2(U_{11}h^2a^{*2}+U_{22}k^2b^{*2}+U_{33}l^2c^{*2}+2U_{23}klb^*c^*+2U_{13}hla^*c^*+2U_{12}hka^*b^*)) \times 10^3,$$

with the following parameters :

Atom	U_{11}	U_{22}	U_{33}	U_{23}	U_{13}	U_{12}
Ni(1)	42(0)	42(0)	39(0)	2(0)	0(0)	-1(1)
Cl(1)	58(1)	38(1)	58(1)	0(1)	0(1)	3(1)
Cl(2)	55(1)	48(1)	48(1)	-2(1)	1(1)	0(1)

TABLE 3.10a Fractional atomic coordinates (x 10^4) and Thermal Parameters ($Å^2$ x 10^3) with e.s.d. s in parentheses for Compound (X)

Atom	x/a	y/b	z/c	U_{iso}/U_{equiv}(*)
Ni(1)	624(1)	994(1)	2688(1)	39(0) *
Cl(1)	-342(1)	1480(1)	1250(1)	51(1) *
Cl(2)	1493(1)	562(1)	4118(1)	51(1) *
N(11)	-859(4)	392(4)	2919(3)	43(1)
C(12)	-1546(5)	-190(5)	2335(4)	45(2)
C(13)	-2505(6)	-603(5)	2455(5)	48(2)
C(14)	-2855(5)	-384(5)	3207(4)	44(2)
C(15)	-2145(6)	212(5)	3801(5)	50(2)
C(16)	-1174(6)	575(5)	3643(4)	47(2)
C(111)	-3920(6)	-762(5)	3339(5)	49(2)
C(112)	-4739(7)	-1041(7)	2655(6)	68(2)
C(113)	-5756(9)	-1349(8)	2798(7)	83(3)
C(114)	-5926(9)	-1374(8)	3594(7)	89(3)
C(115)	-5119(9)	-1145(9)	4276(8)	96(3)
C(116)	-4125(8)	-831(7)	4140(6)	75(3)
N(21)	326(4)	2497(4)	3110(4)	46(1)
C(22)	-629(6)	2919(6)	2855(5)	55(2)
C(23)	-849(6)	3905(6)	3079(5)	58(2)
C(24)	-65(6)	4525(6)	3586(5)	50(2)
C(25)	910(6)	4068(6)	3872(5)	58(2)
C(26)	1063(6)	3077(6)	3630(5)	53(2)
C(211)	-253(6)	5609(6)	3823(5)	55(2)
C(212)	-1178(10)	6074(9)	3429(8)	99(3)
C(213)	-1342(12)	7111(11)	3685(9)	120(4)
C(214)	-575(9)	7647(9)	4268(7)	95(3)
C(215)	336(9)	7202(9)	4616(7)	93(3)
C(216)	491(8)	6173(7)	4391(6)	76(3)
N(31)	2127(4)	1564(4)	2445(4)	45(1)
C(32)	2184(6)	2303(6)	1878(5)	51(2)
C(33)	3128(6)	2648(6)	1658(5)	53(2)
C(34)	4081(6)	2232(5)	2036(4)	47(2)
C(35)	4026(6)	1458(6)	2642(5)	55(2)

Table 3.10a (cont.)

C(36)	3046(6)	1138(6)	2822(5)	53(2)
C(311)	5085(6)	2520(5)	1779(5)	48(2)
C(312)	5289(7)	3537(7)	1521(5)	65(2)
C(313)	6253(8)	3781(8)	1267(6)	76(3)
C(314)	6992(7)	3049(7)	1233(6)	71(2)
C(315)	6809(7)	2070(7)	1480(6)	69(2)
C(316)	5878(6)	1798(6)	1761(5)	59(2)
N(41)	904(4)	-507(4)	2229(4)	45(1)
C(42)	1018(5)	-654(5)	1429(4)	47(2)
C(43)	1096(6)	-1649(6)	1102(5)	50(2)
C(44)	1101(5)	-2512(5)	1621(4)	42(2)
C(45)	1004(6)	-2331(6)	2446(5)	51(2)
C(46)	931(5)	-1338(5)	2732(4)	46(2)
C(411)	1150(6)	-3575(5)	1293(4)	45(2)
C(412)	1752(6)	-3759(6)	681(5)	61(2)
C(413)	1796(8)	-4759(7)	350(6)	71(2)
C(414)	1184(7)	-5574(7)	630(6)	68(2)
C(415)	597(7)	-5389(7)	1223(6)	66(2)
C(416)	583(6)	-4404(6)	1567(5)	58(2)
C(11G)	6062(9)	7295(9)	835(7)	90(3)
C(12G)	5970(9)	8202(8)	394(7)	83(3)
C(13G)	6859(9)	8742(9)	187(7)	88(3)
C(14G)	7851(11)	8350(10)	452(8)	109(4)
C(15G)	7959(11)	7494(11)	899(9)	113(4)
C(16G)	7119(10)	6931(10)	1119(8)	108(4)
C(17G)	5073(13)	6770(12)	1034(11)	140(5)
C(18G)	6745(14)	9733(14)	-260(11)	150(6)
C(21G)	3570(18)	4902(18)	3953(16)	183(8)
C(22G)	3431(12)	5846(13)	4528(11)	135(5)
C(23G)	3464(19)	5738(22)	5411(17)	196(9)
C(24G)	3601(22)	4979(25)	5896(21)	245(12)
C(25G)	3684(17)	4109(19)	5425(16)	192(8)
C(26G)	3682(16)	4052(17)	4594(14)	174(7)
C(27G)	3559(24)	5178(23)	3128(19)	265(13)
C(28G)	3392(21)	6711(21)	5820(16)	234(11)

Table 3.10a (cont.)

Anisotropic atoms have thermal parameters ($Å^2$ x 10^3) of the for

$T=\exp(-2\pi^2(U_{11}h^2a^{*2}+U_{22}k^2b^{*2}+U_{33}l^2c^{*2}+2U_{23}klb^*c^*+2U_{13}hla^*c^*+2U_{12}hka^*b^*))$ x 10^3,

with the following parameters :

Atom	U_{11}	U_{22}	U_{33}	U_{23}	U_{13}	U_{12}
Ni(1)	43(1)	37(1)	37(1)	0(0)	10(0)	2(0)
Cl(1)	54(1)	58(1)	42(1)	5(1)	7(1)	7(1)
Cl(2)	56(1)	56(1)	39(1)	2(1)	6(1)	5(1)

TABLE 3.11a Fractional atomic coordinates (x 10^4)
and Thermal Parameters ($Å^2$ x 10^3)
with e.s.d. s in parentheses for Compound (XI)

Atom	x/a	y/b	z/c	U_{iso}/U_{equiv}(*)
Ni(1)	0(0)	1898(1)	2500(0)	40(1) *
Cl(1)	-2118(3)	1875(1)	1940(1)	55(1) *
N(11)	0(0)	2787(5)	2500(0)	44(3)
C(12)	-1172(10)	3075(4)	2493(4)	46(2)
C(13)	-1233(11)	3654(4)	2493(4)	49(3)
C(14)	0(0)	3979(6)	2500(0)	42(3)
C(111)	0(0)	4583(6)	2500(0)	41(3)
C(112)	-1034(11)	4882(4)	2685(4)	48(3)
C(113)	-1041(12)	5451(5)	2685(4)	61(3)
C(114)	0(0)	5755(7)	2500(0)	58(4)
N(21)	1233(8)	1953(3)	1918(3)	44(2)
C(22)	795(11)	2268(4)	1547(4)	53(3)
C(23)	1667(11)	2401(5)	1198(4)	55(3)
C(24)	3018(11)	2205(4)	1232(4)	52(3)
C(25)	3429(12)	1872(5)	1618(4)	61(3)
C(26)	2505(12)	1740(5)	1943(4)	56(3)
C(211)	3990(12)	2358(5)	886(4)	58(3)
C(212)	3579(16)	2705(6)	509(6)	83(4)
C(213)	4435(21)	2859(8)	172(7)	116(6)
C(214)	5750(21)	2628(8)	201(8)	114(6)
C(215)	6204(25)	2342(9)	603(8)	138(7)
C(216)	5327(19)	2164(7)	935(7)	105(5)
N(31)	0(0)	1019(5)	2500(0)	46(3)
C(32)	-154(11)	730(4)	2097(4)	49(3)
C(33)	-150(11)	152(4)	2074(4)	51(3)
C(34)	0(0)	-150(6)	2500(0)	44(3)
C(311)	0(0)	-773(5)	2500(0)	41(3)
C(312)	-93(14)	-1059(5)	2079(5)	73(4)
C(313)	-98(13)	-1655(5)	2072(5)	68(3)
C(314)	0(0)	-1920(9)	2500(0)	72(5)

Table 3.11a (cont.)

C(11G)	8885(16)	479(6)	10788(5)	85(2)
C(12G)	9438(16)	-22(6)	10688(6)	85(2)
C(13G)	8770(16)	-507(6)	10794(5)	85(2)
C(14G)	7546(16)	-487(6)	10991(5)	85(2)
C(15G)	6938(16)	2(6)	11087(5)	85(2)
C(16G)	7653(16)	504(6)	10991(5)	85(2)
C(17G)	9588(15)	1052(6)	10673(5)	85(2)
C(18G)	6802(16)	-1041(6)	11093(5)	85(2)
C(21G)	3315(21)	-279(9)	5644(8)	124(2)
C(22G)	3299(21)	160(9)	5335(8)	124(2)
C(23G)	3097(21)	658(9)	5481(8)	124(2)
C(24G)	2879(22)	790(9)	5978(8)	124(2)
C(25G)	2956(21)	364(9)	6270(8)	124(2)
C(26G)	3123(22)	-148(9)	6121(8)	124(2)
C(27G)	3612(22)	-824(9)	5429(7)	124(2)
C(28G)	2630(21)	1360(8)	6152(8)	124(2)

Anisotropic atoms have thermal parameters ($Å^2$ x 10^3) of the form:

$$T=\exp(-2\pi^2(U_{11}h^2a^{*2}+U_{22}k^2b^{*2}+U_{33}l^2c^{*2}+2U_{23}klb^*c^*+ 2U_{13}hla^*c^*+2U_{12}hka^*b^*)) \times 10^3,$$

with the following parameters :

Atom	U_{11}	U_{22}	U_{33}	U_{23}	U_{13}	U_{12}
Ni(1)	35(1)	29(1)	59(1)	0(0)	18(1)	0(0)
Cl(1)	48(2)	53(2)	63(2)	1(1)	2(1)	0(1)

TABLE 3.12a Fractional atomic coordinates (x 10^4) and Thermal Parameters ($Å^2$ x 10^3) with e.s.d. s in parentheses for Compound (XII)

Atom	x/a	y/b	z/c	U_{iso}/U_{equiv}(*)
Ni(1)	0(0)	1355(1)	2500(0)	42(1) *
Cl(1)	2256(2)	1307(1)	3227(1)	56(1) *
N(11)	0(0)	2232(4)	2500(0)	47(2)
C(12)	1200(9)	2540(3)	2600(4)	50(2)
C(13)	1262(9)	3117(3)	2613(4)	49(2)
C(14)	0(0)	3427(5)	2500(0)	47(2)
C(111)	0(0)	4037(4)	2500(0)	44(2)
C(112)	1103(9)	4334(3)	2279(4)	55(2)
C(113)	1091(10)	4917(4)	2280(4)	61(2)
C(114)	0(0)	5197(6)	2500(0)	70(4)
N(31)	0(0)	466(4)	2500(0)	38(2)
C(32)	157(10)	182(4)	3029(4)	61(2)
C(33)	157(10)	-402(4)	3053(4)	64(2)
C(34)	0(0)	-707(5)	2500(0)	52(3)
C(311)	0(0)	-1335(5)	2500(0)	62(3)
C(312)	233(12)	-1632(5)	3060(5)	80(3)
C(313)	235(14)	-2227(5)	3031(7)	97(4)
C(314)	0(0)	-2500(7)	2500(0)	87(4)
N(41)	1166(7)	1401(2)	1711(3)	47(2)
C(42)	2493(11)	1209(4)	1746(5)	72(3)
C(43)	3350(11)	1284(4)	1298(5)	70(3)
C(44)	2817(9)	1570(4)	746(4)	55(2)
C(45)	1447(11)	1772(4)	705(5)	67(2)
C(46)	674(10)	1682(4)	1184(4)	64(2)
C(411)	3704(9)	1663(4)	242(4)	58(2)
C(412)	5155(13)	1745(5)	388(6)	90(3)
C(413)	6018(17)	1835(6)	-82(7)	109(4)
C(414)	5353(16)	1829(6)	-685(8)	113(4)
C(415)	3962(16)	1768(6)	-849(7)	108(4)
C(416)	3097(13)	1692(5)	-389(6)	86(3)

Table 3.12a (cont.)

C(11G)	2947(22)	4701(11)	4593(13)	143(5)
C(12G)	2793(22)	4712(11)	5226(13)	143(5)
C(13G)	1477(22)	4853(11)	5405(13)	143(5)
C(14G)	315(22)	4983(11)	4950(13)	143(5)
C(15G)	469(22)	4970(11)	4318(13)	143(5)
C(16G)	1786(22)	4829(11)	4138(13)	143(5)
C(21G)	3645(21)	4360(10)	4501(12)	136(5)
C(22G)	3471(21)	4378(10)	5133(12)	136(5)
C(23G)	2180(21)	4561(10)	5304(12)	136(5)
C(24G)	1062(21)	4726(10)	4844(12)	136(5)
C(25G)	1235(21)	4708(10)	4215(12)	136(5)
C(26G)	2527(21)	4525(10)	4043(12)	136(5)

Anisotropic atoms have thermal parameters ($Å^2$ x 10^3) of the form:

$$T=\exp(-2\pi^2(U_{11}h^2a^{*2}+U_{22}k^2b^{*2}+U_{33}l^2c^{*2}+2U_{23}klb^*c^*+ 2U_{13}hla^*c^*+2U_{12}hka^*b^*)) \times 10^3,$$

with the following parameters :

Atom	U_{11}	U_{22}	U_{33}	U_{23}	U_{13}	U_{12}
Ni(1)	40(1)	42(1)	43(1)	0(0)	6(1)	0(0)
Cl(1)	48(1)	60(1)	56(1)	1(1)	-2(1)	4(1)

TABLE 3.13a Fractional atomic coordinates (x 10^4)
and Thermal Parameters (A^2 x 10^3)
with e.s.d. s in parentheses for Compound (XIII)

Atom	x/a	y/b	z/c	U_{iso}/U_{equiv}(*)
Ni(1)	0(0)	1699(1)	2500(0)	46(1) *
N(1)	1778(6)	1699(3)	3234(4)	53(2)
C(1)	2613(7)	1701(4)	3755(5)	53(2)
S(1)	3799(3)	1718(2)	4517(2)	105(1) *
N(11)	910(6)	1699(3)	1449(4)	53(2)
C(12)	298(13)	1591(5)	724(8)	117(4)
C(13)	870(12)	1580(5)	26(8)	122(5)
C(14)	2155(9)	1653(4)	84(6)	70(3)
C(15)	2787(10)	1758(4)	843(7)	90(3)
C(16)	2147(9)	1787(4)	1487(6)	81(3)
C(17)	2793(9)	1615(4)	-646(6)	91(3)
N(21)	0(0)	767(4)	2500(0)	61(3)
C(22)	1101(8)	463(4)	2536(5)	59(2)
C(23)	1140(8)	-139(4)	2534(5)	60(2)
C(24)	0(0)	-466(5)	2500(0)	60(3)
C(211)	0(0)	-1111(5)	2500(0)	65(4)
C(212)	-894(9)	-1407(4)	2857(6)	75(3)
C(213)	-867(10)	-2022(5)	2864(6)	89(3)
C(214)	0(0)	-2303(7)	2500(0)	104(6)
N(31)	0(0)	2626(4)	2500(0)	51(3)
C(32)	504(8)	2934(3)	3161(5)	56(2)
C(33)	518(7)	3539(3)	3190(5)	55(2)
C(34)	0(0)	3854(5)	2500(0)	58(3)
C(311)	0(0)	4505(6)	2500(0)	71(4)
C(312)	161(10)	4809(5)	1818(7)	94(3)
C(313)	178(12)	5439(5)	1804(8)	119(4)
C(314)	0(0)	5680(8)	2500(0)	107(6)
C(1G)	2352(15)	4897(12)	5230(14)	140(10)
C(2G)	3605(14)	4794(12)	4908(12)	128(10)
C(3G)	4800(14)	4956(13)	5353(10)	142(11)

Table 3.13a (cont).

C(4G)	5895(14)	4952(13)	4985(13)	124(10)
C(5G)	7220(15)	5128(15)	5464(16)	183(14)
O(1G)	3564(16)	4554(10)	4208(11)	212(11)
O(2G)	5843(16)	4728(11)	4277(13)	221(11)

Anisotropic atoms have thermal parameters (A^2 x 10^3) of the form:

$$T=\exp\{-2\pi^2(U_{11}h^2a^{*2}+U_{22}k^2b^{*2}+U_{33}l^2c^{*2}+2U_{23}klb^*c^*+ 2U_{13}hla^*c^*+2U_{12}hka^*b^*)\} \times 10^3,$$

with the following parameters :

Atom	U_{11}	U_{22}	U_{33}	U_{23}	U_{13}	U_{12}
Ni(1)	42(1)	47(1)	48(1)	0(0)	1(1)	0(0)
S(1)	77(2)	156(3)	70(2)	-4(2)	-16(2)	2(2)

TABLE 3.14a Fractional atomic coordinates (x 10^4)
and Thermal Parameters ($Å^2$ x 10^3)
with e.s.d. s in parentheses for Compound (XIV)

Atom	x/a	y/b	z/c	U_{iso}/U_{equiv}(*)
Ni(1)	0(0)	1793(1)	2500(0)	42(1) *
N(1)	1699(7)	1787(4)	3260(4)	51(3) *
C(1)	2543(9)	1805(5)	3771(6)	52(3)
S(1)	3773(3)	1828(2)	4490(2)	98(2) *
N(11)	942(7)	1787(4)	1446(4)	43(2)
C(12)	395(10)	1741(6)	673(7)	74(4)
C(13)	970(10)	1717(5)	-28(7)	76(4)
C(14)	2266(9)	1691(5)	72(6)	54(3)
C(15)	2837(10)	1760(6)	861(7)	76(4)
C(16)	2179(10)	1810(5)	1502(7)	70(3)
C(17)	2928(10)	1644(5)	-661(6)	76(4)
N(21)	0(0)	867(5)	2500(0)	54(4)
C(22)	1074(10)	565(5)	2558(6)	61(3)
C(23)	1116(10)	-46(5)	2565(6)	60(3)
C(24)	0(0)	-378(8)	2500(0)	62(5)
C(211)	0(0)	-1019(8)	2500(0)	62(5)
C(212)	-915(11)	-1322(5)	2835(7)	74(4)
C(213)	-924(12)	-1945(6)	2839(8)	90(5)
C(214)	0(0)	-2194(9)	2500(0)	96(7)
N(31)	0(0)	2723(5)	2500(0)	48(4)
C(32)	520(10)	3005(5)	3179(6)	55(3)
C(33)	515(9)	3621(5)	3198(7)	57(3)
C(34)	0(0)	3920(7)	2500(0)	51(4)
C(311)	0(0)	4600(9)	2500(0)	77(6)
C(312)	216(12)	4866(6)	1794(8)	102(5)
C(313)	222(14)	5521(7)	1800(9)	124(6)
C(314)	0(0)	5747(10)	2500(0)	111(8)

Table 3.14a (cont.)

Na(1)	2714(33)	4802(25)	4536(18)	450(25) *
C(2G)	3918(34)	5125(20)	5041(38)	312(36)
C(3G)	5081(32)	4941(19)	4679(22)	190(17)
C(4G)	6014(37)	5442(16)	4829(45)	328(36)
Na(2)	7410(33)	5192(20)	4866(17)	449(24) *

Anisotropic atoms have thermal parameters ($Å^2$ x 10^3) of the form:

$$T=\exp(-2\pi^2(U_{11}h^2a^{*2}+U_{22}k^2b^{*2}+U_{33}l^2c^{*2}+2U_{23}klb^*c^*+ 2U_{13}hla^*c^*+2U_{12}hka^*b^*)) \times 10^3,$$

with the following parameters :

Atom	U_{11}	U_{22}	U_{33}	U_{23}	U_{13}	U_{12}
Ni(1)	38(1)	38(1)	47(1)	0(0)	-1(1)	0(0)
N(1)	54(6)	52(5)	43(5)	-3(5)	-7(4)	-3(5)
S(1)	64(2)	138(4)	80(3)	-13(3)	-23(2)	3(3)
Na(1)	357(31)	623(55)	349(42)	-72(44)	-12(31)	-88(35)
Na(2)	527(45)	484(42)	278(33)	-2(31)	110(29)	128(36)

TABLE 3.15a Fractional atomic coordinates (x 10^4)
and Thermal Parameters ($Å^2$ x 10^3)
with e.s.d. s in parentheses for Compound (XV)

Atom	x/a	y/b	z/c	U_{iso}/U_{equiv}(*)
Ni(1)	0(0)	1035(0)	2500(0)	39(0) *
N(1)	-1655(4)	1020(2)	3260(3)	51(1)
C(1)	-2328(5)	1030(2)	3896(4)	43(1)
S(1)	-3282(2)	1042(1)	4796(1)	75(1) *
O(2)	1130(3)	1032(2)	3935(3)	54(1) *
S(2)	2659(1)	1068(1)	4074(1)	57(1) *
C(2)	3172(7)	581(3)	5050(5)	78(2)
C(3)	3009(9)	1698(3)	4772(7)	118(3)
N(21)	0(0)	1947(2)	2500(0)	45(1)
C(22)	-616(5)	2247(2)	3168(4)	55(1)
C(23)	-641(5)	2833(2)	3178(4)	54(1)
C(24)	0(0)	3156(3)	2500(0)	42(2)
C(211)	0(0)	3779(3)	2500(0)	42(2)
C(212)	-1134(5)	4083(2)	2710(4)	48(1)
C(213)	-1131(5)	4679(2)	2701(4)	56(1)
C(214)	0(0)	4970(4)	2500(0)	61(2)
N(41)	0(0)	137(2)	2500(0)	47(2)
C(42)	26(5)	-157(2)	1645(4)	52(1)
C(43)	13(5)	-747(2)	1610(4)	54(1)
C(44)	0(0)	-1053(3)	2500(0)	58(2)
C(411)	0(0)	-1696(4)	2500(0)	69(2)
C(412)	-606(7)	-1984(3)	1648(6)	86(2)
C(413)	-600(8)	-2591(4)	1666(7)	112(3)
C(414)	0(0)	-2844(6)	2500(0)	115(4)

Table 3.15a (cont.)

Anisotropic atoms have thermal parameters ($Å^2$ x 10^3) of the form:

$$T=\exp(-2\pi^2(U_{11}h^2a^{*2}+U_{22}k^2b^{*2}+U_{33}l^2c^{*2}+2U_{23}klb^*c^*+ 2U_{13}hla^*c^*+2U_{12}hka^*b^*)) \times 10^3,$$

with the following parameters :

Atom	U_{11}	U_{22}	U_{33}	U_{23}	U_{13}	U_{12}
Ni(1)	37(1)	42(1)	37(1)	0(0)	5(0)	0(0)
S(1)	82(1)	84(1)	65(1)	6(1)	38(1)	5(1)
O(2)	47(2)	68(2)	44(2)	2(2)	-1(2)	-3(2)
S(2)	51(1)	71(1)	48(1)	3(1)	0(1)	-5(1)

TABLE 3.16a Fractional atomic coordinates (x 10^4)
and Thermal Parameters (A^2 x 10^3)
with e.s.d. s in parentheses for Compound (XVI)

Atom	x/a	y/b	z/c	U_{iso}/U_{equiv}(*)
Ni(1)	0(0)	0(0)	0(0)	32(0) *
Cl(1)	1199(1)	-2131(1)	-581(1)	46(0) *
S(1)	1413(1)	3460(1)	-447(1)	38(0) *
O(1)	1600(3)	1623(3)	-424(1)	40(1) *
C(1)	2818(6)	4034(6)	-1009(2)	55(1)
C(2)	2657(6)	4221(6)	198(2)	55(1)
N(11)	-1941(4)	351(4)	-703(1)	37(1)
C(12)	-1648(6)	740(6)	-1276(2)	47(1)
C(13)	-2941(6)	875(6)	-1738(2)	50(1)
C(14)	-4653(5)	575(5)	-1634(2)	38(1)
C(15)	-4946(5)	164(6)	-1040(2)	43(1)
C(16)	-3586(5)	80(5)	-602(2)	41(1)
C(111)	-6080(5)	632(5)	-2124(2)	42(1)
C(112)	-5951(7)	1567(7)	-2635(2)	64(1)
C(113)	-7308(7)	1619(7)	-3095(3)	74(2)
C(114)	-8765(7)	745(7)	-3046(3)	69(2)
C(115)	-8896(6)	-216(6)	-2540(2)	60(1)
C(116)	-7572(6)	-263(5)	-2076(2)	49(1)

Anisotropic atoms have thermal parameters (A^2 x 10^3) of the form:

$$T=\exp\{-2\pi^2(U_{11}h^2a^{*2}+U_{22}k^2b^{*2}+U_{33}l^2c^{*2}+2U_{23}klb^*c^*+ 2U_{13}hla^*c^*+2U_{12}hka^*b^*)\} \times 10^3,$$

with the following parameters :

Atom	U_{11}	U_{22}	U_{33}	U_{23}	U_{13}	U_{12}
Ni(1)	31(0)	30(0)	37(0)	0(0)	6(0)	0(0)
Cl(1)	52(1)	35(1)	52(1)	-4(1)	18(1)	2(1)
S(1)	35(1)	33(1)	47(1)	2(1)	6(1)	2(1)
O(1)	38(2)	28(2)	55(2)	4(1)	12(1)	0(1)

TABLE 3.17a Fractional atomic coordinates (x 10^4)
and Thermal Parameters ($Å^2$ x 10^3)
with e.s.d. s in parentheses for Compound (XVII)

Atom	x/a	y/b	z/c	U_{iso}/U_{equiv}(*)
Ni(1)	0(0)	2500(0)	3533(1)	66(1) *
N(1)	849(3)	2947(3)	3570(3)	76(2)
C(1)	1328(4)	3104(3)	3718(3)	66(2)
S(1)	2000(1)	3361(2)	3962(2)	128(1) *
N(11)	326(2)	1882(2)	2692(3)	67(2)
C(12)	767(4)	2065(4)	2201(4)	84(2)
C(13)	1039(4)	1673(4)	1708(5)	84(2)
C(14)	884(3)	1052(3)	1674(3)	60(2)
C(15)	417(3)	881(3)	2152(4)	70(2)
C(16)	168(3)	1285(3)	2644(4)	70(2)
C(17)	1211(4)	589(4)	1161(4)	85(2)
C(171)	1512(4)	926(5)	495(5)	103(4) *
C(172)	778(7)	126(6)	860(9)	149(6) *
C(173)	1743(5)	305(6)	1630(7)	142(6) *
N(21)	309(3)	1866(3)	4371(3)	71(2)
C(22)	870(4)	1603(4)	4334(5)	86(2)
C(23)	1064(4)	1155(4)	4844(5)	96(3)
C(24)	703(4)	965(3)	5405(4)	79(2)
C(25)	126(4)	1245(4)	5452(5)	93(2)
C(26)	-59(4)	1690(4)	4934(4)	82(2)
C(27)	921(4)	463(5)	5945(6)	100(3)
C(271)	1465(8)	707(8)	6398(8)	162(7) *
C(272)	425(9)	304(9)	6480(10)	226(11) *
C(273)	1124(16)	-67(6)	5491(10)	287(16) *

Anisotropic atoms have thermal parameters ($Å^2$ x 10^3) of the form:

$$T=\exp\{-2\pi^2(U_{11}h^2a^{*2}+U_{22}k^2b^{*2}+U_{33}l^2c^{*2}+2U_{23}klb^*c^*+2U_{13}hla^*c^*+2U_{12}hka^*b^*)\} \times 10^3,$$

with the following parameters :

Atom	U_{11}	U_{22}	U_{33}	U_{23}	U_{13}	U_{12}
Ni(1)	60(1)	62(1)	75(1)	0(0)	-17(6)	0(0)
S(1)	84(2)	141(3)	158(3)	-23(2)	-38(2)	-9(2)
C(171)	106(7)	106(7)	97(6)	-21(5)	15(5)	1(5)
C(172)	145(11)	105(8)	198(12)	-63(8)	62(9)	-37(7)
C(173)	139(10)	130(9)	157(10)	3(8)	31(8)	71(8)
C(271)	144(11)	189(14)	154(11)	71(10)	-61(9)	-36(10)
C(272)	190(17)	286(24)	201(16)	161(17)	-38(13)	-21(15)
C(273)	565(44)	118(11)	177(15)	0(11)	103(22)	102(19)

TABLE 3.18a Fractional atomic coordinates (x 10^4)
and Thermal Parameters (A^2 x 10^3)
with e.s.d. s in parentheses for Compound (XVIII)

Atom	x/a	y/b	z/c	U_{iso}/U_{equiv}(*)
Ni(1)	0(0)	3737(0)	0(0)	36(0) *
N(1)	1831(9)	3799(3)	608(5)	44(2)
C(1)	2908(10)	3779(3)	871(6)	37(3)
S(1)	4448(4)	3760(1)	1232(2)	70(1) *
N(2)	-1844(9)	3676(3)	-570(5)	42(2)
C(2)	-2908(10)	3687(3)	-861(6)	37(3)
S(2)	-4384(4)	3706(1)	-1298(2)	62(1) *
N(11)	-822(8)	4395(3)	646(4)	41(2)
C(12)	-2139(10)	4417(4)	833(5)	40(2)
C(13)	-2690(10)	4824(4)	1271(5)	42(2)
C(14)	-1879(11)	5231(4)	1481(6)	46(3)
C(15)	-468(11)	5219(4)	1313(6)	54(3)
C(16)	-6(10)	4794(3)	880(5)	44(2)
C(17)	-2404(11)	5692(4)	1982(6)	50(3)
C(111)	-2013(11)	6242(4)	1741(6)	50(3)
C(112)	-2459(11)	6424(4)	1042(6)	63(3)
C(113)	-2102(13)	6952(5)	823(7)	77(4)
C(114)	-1347(12)	7267(4)	1290(6)	62(3)
C(115)	-943(13)	7084(5)	1976(7)	76(3)
C(116)	-1270(12)	6569(4)	2215(7)	66(3)
N(21)	745(8)	4325(3)	-790(4)	38(2)
C(22)	-171(10)	4613(3)	-1193(5)	45(2)
C(23)	186(10)	5056(4)	-1612(6)	52(3)
C(24)	1509(10)	5232(4)	-1651(6)	42(2)
C(25)	2478(12)	4935(4)	-1251(6)	57(3)
C(26)	2081(11)	4490(4)	-839(6)	51(3)
C(27)	1876(13)	5728(4)	-2071(7)	61(3)
C(211)	1702(11)	6239(4)	-1610(6)	49(3)
C(212)	1292(10)	6239(5)	-838(6)	62(3)
C(213)	1072(13)	6721(5)	-451(8)	76(4)
C(214)	1284(12)	7195(5)	-843(7)	68(3)
C(215)	1701(12)	7202(4)	-1596(7)	61(3)
C(216)	1909(12)	6726(4)	-1961(7)	65(3)
N(31)	816(8)	3075(3)	-619(4)	36(2)

Table 3.18a (cont.)

C(32)	2157(10)	3051(4)	-823(5)	47(3)
C(33)	2714(11)	2635(4)	-1224(5)	52(3)
C(34)	1887(11)	2207(4)	-1471(6)	44(3)
C(35)	543(11)	2227(4)	-1215(6)	55(3)
C(36)	10(11)	2659(4)	-818(6)	51(3)
C(37)	2509(13)	1749(4)	-1907(7)	65(3)
C(311)	2126(9)	1202(4)	-1600(5)	43(2)
C(312)	2600(11)	1043(4)	-899(6)	59(3)
C(313)	2314(11)	551(4)	-617(7)	67(3)
C(314)	1557(11)	190(4)	-1036(6)	55(3)
C(315)	1092(11)	328(4)	-1725(6)	56(3)
C(316)	1348(12)	839(4)	-2010(7)	64(3)
N(41)	-773(8)	3150(3)	815(5)	43(2)
C(42)	157(11)	2862(4)	1216(6)	54(3)
C(43)	-194(11)	2402(4)	1623(6)	57(3)
C(44)	-1523(12)	2237(4)	1611(6)	52(3)
C(45)	-2496(11)	2531(4)	1227(5)	47(3)
C(46)	-2063(10)	2987(4)	827(5)	44(3)
C(47)	-1959(11)	1710(4)	2003(6)	53(3)
C(411)	-1638(10)	1213(4)	1542(5)	47(3)
C(412)	-1269(10)	1235(5)	800(6)	57(2)
C(413)	-1008(13)	772(4)	394(7)	71(3)
C(414)	-1131(12)	285(4)	744(7)	68(3)
C(415)	-1445(13)	259(5)	1436(7)	70(4)
C(416)	-1747(12)	722(4)	1883(7)	62(3)

Anisotropic atoms have thermal parameters (A^2 x 10^3) of the form:

$$T=\exp\{-2\pi^2(U_{11}h^2a^{*2}+U_{22}k^2b^{*2}+U_{33}l^2c^{*2}+2U_{23}klb^*c^*+ 2U_{13}hla^*c^*+2U_{12}hka^*b^*)\} \times 10^3,$$

with the following parameters :

Atom	U_{11}	U_{22}	U_{33}	U_{23}	U_{13}	U_{12}
Ni(1)	30(0)	27(0)	50(1)	-1(1)	-4(0)	1(1)
S(1)	43(2)	61(2)	107(3)	-2(2)	-32(2)	-4(1)
S(2)	45(2)	58(2)	83(2)	4(2)	-22(2)	-5(1)

REFERENCES

3.1 W.C. Hamilton, *Acta. Cryst.*, **18**, 502 (1965).

3.2 A.I. Kitaigorodskii in 'Organic Chemical Crystallography', Chapter 1, Academic Press, New York (1973).

3.3 J.G. Jones, S. Schwarzbaum ,L. Lessinger and B.W. Low, *Acta. Cryst.*, **B38**, 1207 (1982).

3.4 R. Thomas, C.B. Shoemaker and K. Eriks, *Acta. Cryst.*, **21**, 12 (1966).

3.5 L.R. Nassimbeni, S. Papanicolaou and M.H. Moore, *J. Incl. Phenom.*, **4**, 31 (1986).

3.6 M.H. Moore, L.R. Nassimbeni and M.L. Niven, *J. Chem. Soc., Dalton Trans.*, 2125 (1987).

3.7 P. Main, S.E. Hull, L. Lessinger, G. Germain, J-P. Declercq and M.M. Woolfson in ' MULTAN 78. A System of Computer Programs for the Automatic Solution of Crystal Structures form X-Ray Diffraction Data', Universities of York, England and Louvain, Belgium (1978).

3.8 G.M. Sheldrick in 'Computing in Crystallography', Eds. H. Schenk, R. Olthof-Hazekamp, H. van Koningvelt and G.C. Bassi, Delft University Press, pp. 34-42 (1978).

3.9 G.M. Sheldrick in 'Crystallographioc Computing 3', Eds. G.M. Sheldrick, C. Kruger and R. Goddard, Oxford University Press, pp. 175-189 (1985)

CHAPTER FOUR

DISCUSSION OF STRUCTURES

4.1 HOST CONFORMATION

For all compounds mentioned in this work, the host molecule comprises a central nickel atom displaying irregular octahedral coordination. For the Class A, Class C compounds and Compounds (XVII) and (XVIII) the nickel is surrounded by 6 nitrogen atoms. For the Class B compounds coordination is to 4N and 2Cl atoms whilst Compounds (XV) and (XVI) have the nickel atom surrounded by 4 Nitrogen atoms and 2 oxygen atoms. The anionic ligands are always *trans* to each other as are like ligands in mixed ligand complexes.

For those structures containing the isothiocyanate anion, the ligand is always bent at the N atom, *i.e.* Ni-N-C angle < 180° (ranging from 173.9 to 163.9° with an average angle of 168(5)°), and the N-C-S angle is almost linear (179.4 to 172.6°, average 177(2)°). The Ni-N_{CS} bond (2.10 to 2.04Å, average 2.07(2)Å)is always significantly shorter than the Ni-N_{py} bond (2.24 to 2.10, average 2.14(3)Å). Fig 4a shows the average bond distances with e.s.d.'s in parentheses for all reported complexes containing the isothiocyanate anion, whilst Fig 4b shows the average bond angles, (e.s.d.'s in parentheses) for the same compounds.

For the Class B compounds, the Ni-N_{py} bond is comparable to that of the Class A compounds (2.14 to 2.09, average 2.13(2)Å), whilst the Ni-Cl bond is much longer (2.49 to 2.41, average 2.45(3)Å). The average environment about the Ni atom for all four compounds in Class B is shown

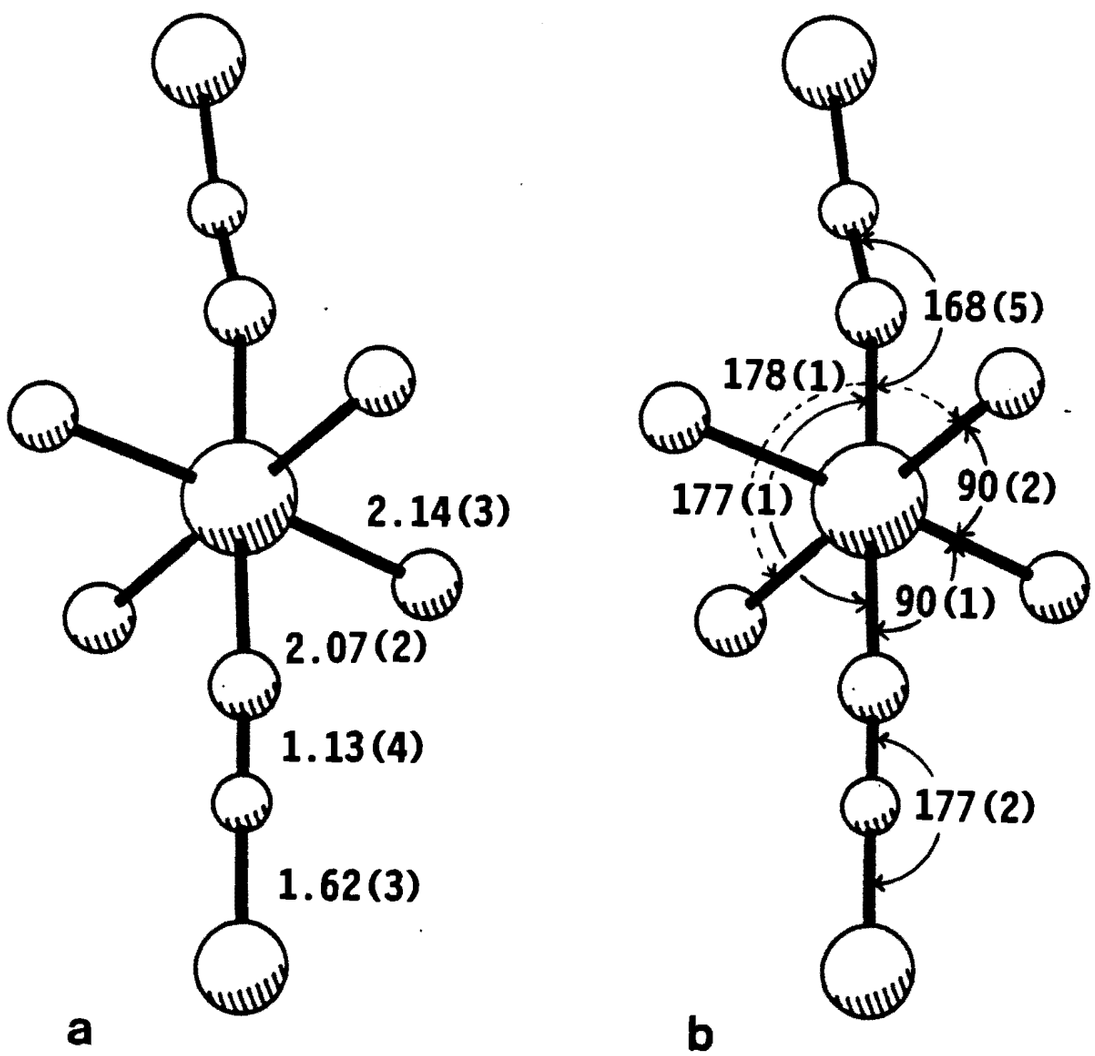

Fig 4a & b Average environment of the nickel atom for the eight compounds in Class A with:
a) displaying bond lengths (Å) and
b) displaying bond angles (°) with esd.'s in parentheses

in Figs 4c and 4d.

The average N-C bond distance of the pyridine base is 1.34(3)Å (ranging from 1.38 to 1.27Å) for all 18 complexes whilst the average C-C bond distance for both pyridine and phenyl groups is 1.38(4)Å (1.51 to 1.25Å). The average bond angles for these groups is 120(3)° (123.4 to 117.8°). The single bond character of the C_{Py}-C_{Ph} bond is displayed in its increased length (max 1.54, min 1.45, average 1.48(2)Å) when compared with the aromatic bonds.

The structure of each compound is discussed individually and with the aid of packing diagrams, attempts will be made to describe the size, shape and orientation of the cavities in which the guest molecules are situated.

One of the possible reasons to explain the success of inorganic complexes of this type to form clathrates[4.1] is the rotational freedom about the Ni-N bonds. This supposedly allows adjustment of substituted pyridines to accommodate the various guest molecules. In the case of the 4-PhPy compounds, there are the added parameters of the four torsion angles describing the conformation of the phenyl rings with respect to their parent pyridines.

Possible correlations between torsion angles and guest molecules are examined in detail after the discussion of the individual compounds.

Packing diagrams for many of the structures do not give a clear picture

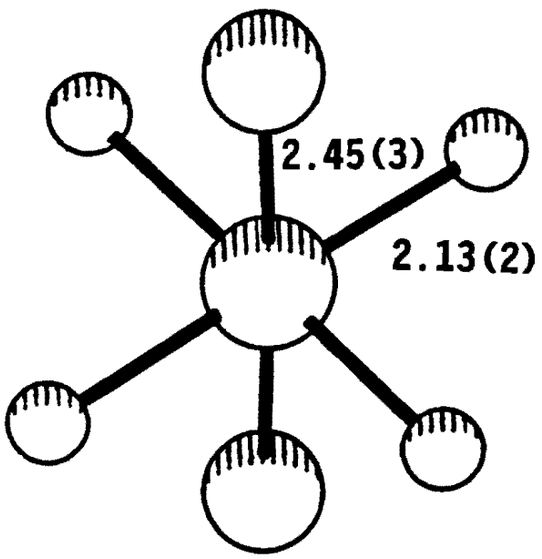

C

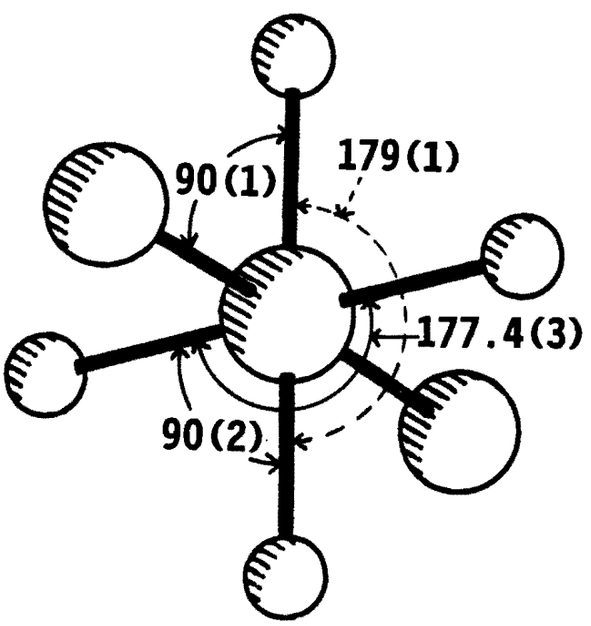

D

Fig 4c & d Average environment of the nickel atom for the four compounds in Class B with:
c) displaying bond lengths (Å) and
d) displaying bond angles (°) with esd.'s in parentheses

of the cavity extent owing to the necessity of a two dimensional representation of a three dimensional structure. Thus extensive use has been made of the program OPEC[4.2.], using the facility which undertakes packing and volume analyses, to determine the environment around the guest molecules. The program was modified to include improvements suggested by Gavezzotti (December, 1984) and also to include full physical parameters for the nickel atom. Output from this program shows clearly the direction and size of the cavities within the host structure but unfortunately this information is displayed on many sheets(layers). Use of transparencies (as for Compound (IX)) although extremely informative, is too bulky to be repeated for each structure in this work and is also unsuitable for publication in Journals.

For each of the Class A compounds, the volume/non H atom for the α-phase compound or residual volume (Res Vol) available for the guest atom for the β-phase compounds and its residual volume per guest atom (Res Vol/G-atom) is indicated.

The residual volume mentioned above is defined as :

1) $(\text{Vol.cell/Z(host)})_{clath} - (\text{Vol.cell/Z(host)})_{\alpha\text{-phase}}$

and it makes the assumption that the α-phase complex packs in the most efficient manner possible (*i.e.* the interstitial space is a minimum). The Res Vol/G-atom is the above volume divided by the total number of non-H guest atoms in the asymmetric unit. For a well ordered compound, this Res Vol/G-atom is about $18A^3$, which can therefore be considered as

the baseline; thus the larger this figure the greater the severity of the disorder.

For the Class B and C compounds, no α-phase compound has yet been characterized and thus determining the minimum volume required for each host presents problems. The following approach has been taken in order to determine an approximate figure for the Res Vol/G-atom. For Class B: the average volume for a non-hydrogen atom for the α-phase of the 4-PhPy derivative (Compound (I)) has been calculated (19.28$Å^3$). The volume of the α-phase [$NiCl_2$(4-PhPy)$_4$] is then assumed to be the product of this figure and the number of non-H atoms in the complex (51), which gives a volume of 983$Å^3$. This volume is then inserted in to Equation 1) above, to calculate the Res Vol/G-atom. The same approach has been taken for the Class C α-phase, with the number of atoms in the host being 45, giving a value of 868$Å^3$.

Although these figures obtained from the previous calculations might not be directly comparable among classes, they certainly are within a class and the trend that they display is qualitatively correct both within and among the different classes.

4.2 CLASS A (Atomic nomenclature - Fig 4.1a).

Compound (I) $[Ni(NCS)_2(4\text{-}PhPy)_4]$. Pbca, Z = 8,
a = 12.846, b = 16.160, c = 39.377Å.
Packing efficiency = 18.2Å^3/atom.

As expected, this compound has no space between atoms large enough to accommodate guest molecules. The host molecules are stacked in rows parallel to [100] such that the NCS moieties in neighbouring stacks are approximately 45° to each other as illustrated in Fig 4.1b. The packing of this α-phase structure is similar, with respect to the Ni,NCS and pyridine rings, to the 4-ViPy α-phase structure[4.3] which also crystallizes in the Pbca space group. The phenyl group of Compound (I) has a similar orientation to that of the vinyl group but extends further out of the row. A coloured space filling diagram of Compound (I) is displayed in Fig 4.1c to indicate the volume occupied by the molecule which is not always obvious from a stick diagram.

Compound (II) $[Ni(NCS)_2(4\text{-}PhPy)_4]$.2*o*-xylene. Fdd2, Z = 8,
a = 10.376, b = 44.414, c = 23.436Å.
Res. vol = 328Å^3, Res Vol/G-atom = 20.5Å^3.

The *o*-xylene molecules are situated in channels running alternately in the [101] and [10$\bar{1}$] directions in the planes of the diamond glides perpendicular to **b**. The packing is shown in Fig 4.2a which displays the structure along [100] with guest molecules shaded for clarity. The low Res Vol/G atom indicates a well ordered guest molecule and this is

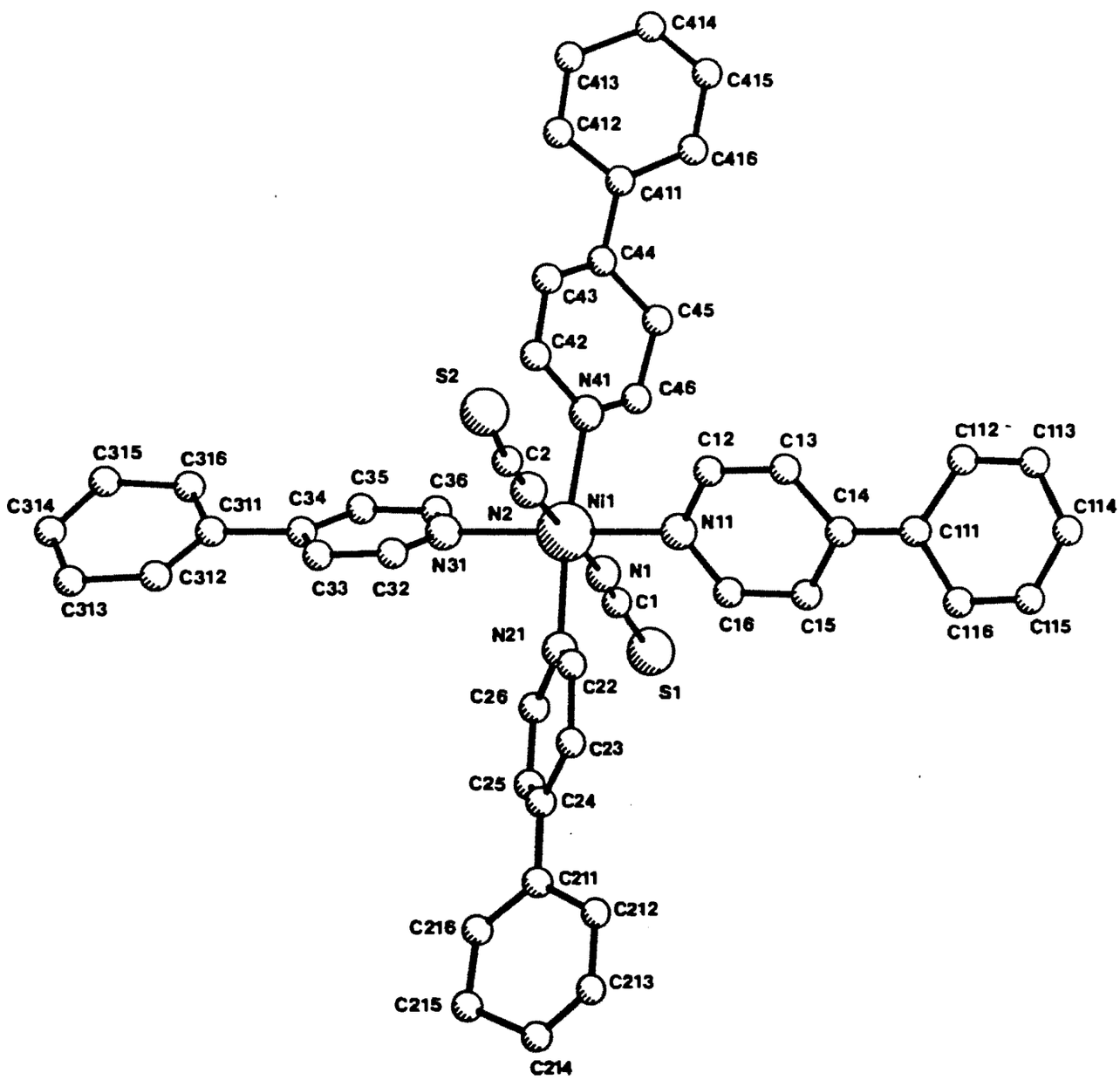

Fig 4.1a Perspective view of Compound (I) with atomic nomenclature applicable to all Class A compounds.

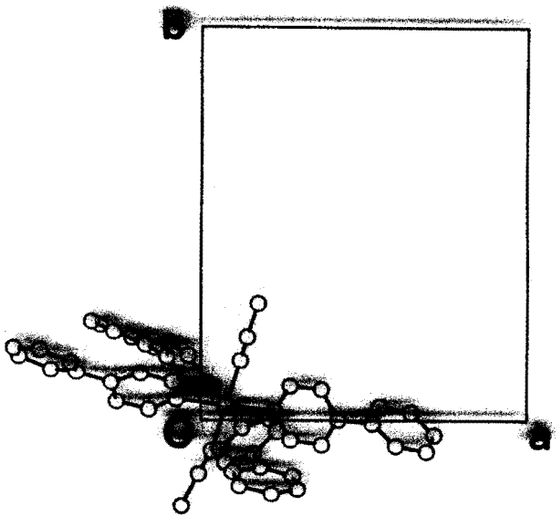

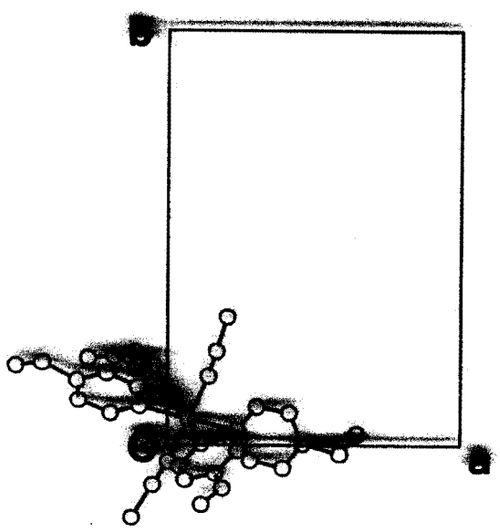

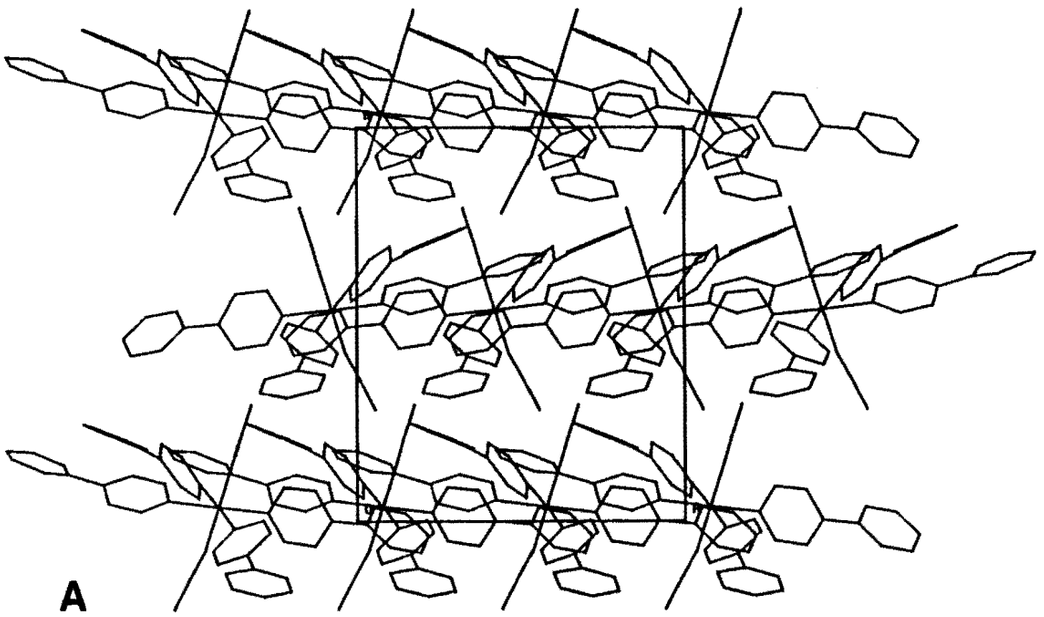

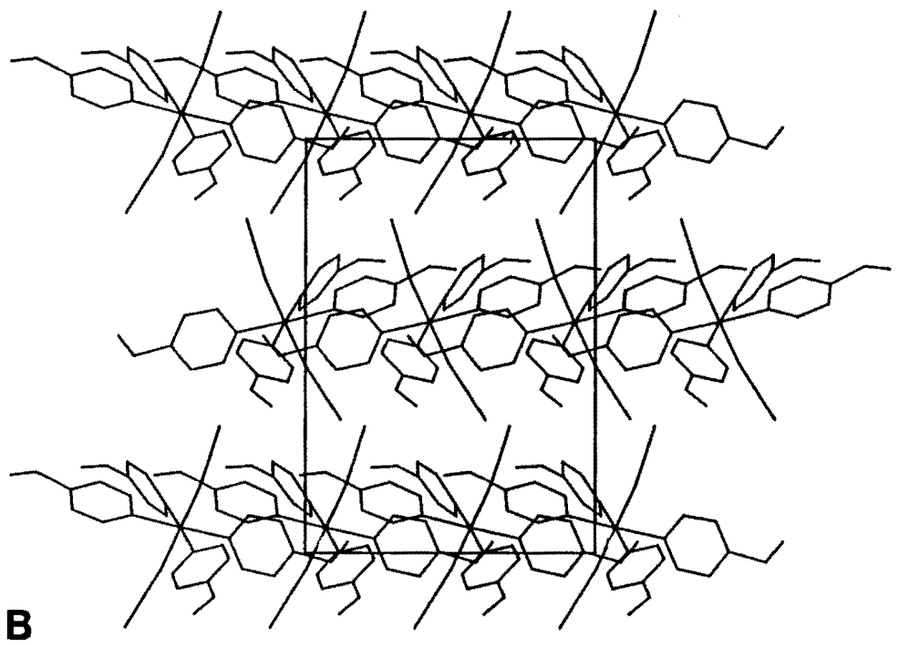

Fig 4.1b Packing diagram of **a)** Compound (I) and **b)** the 4-ViPy analogue both viewed along [001] with a ball and stick representation of a single molecule on the transparency.

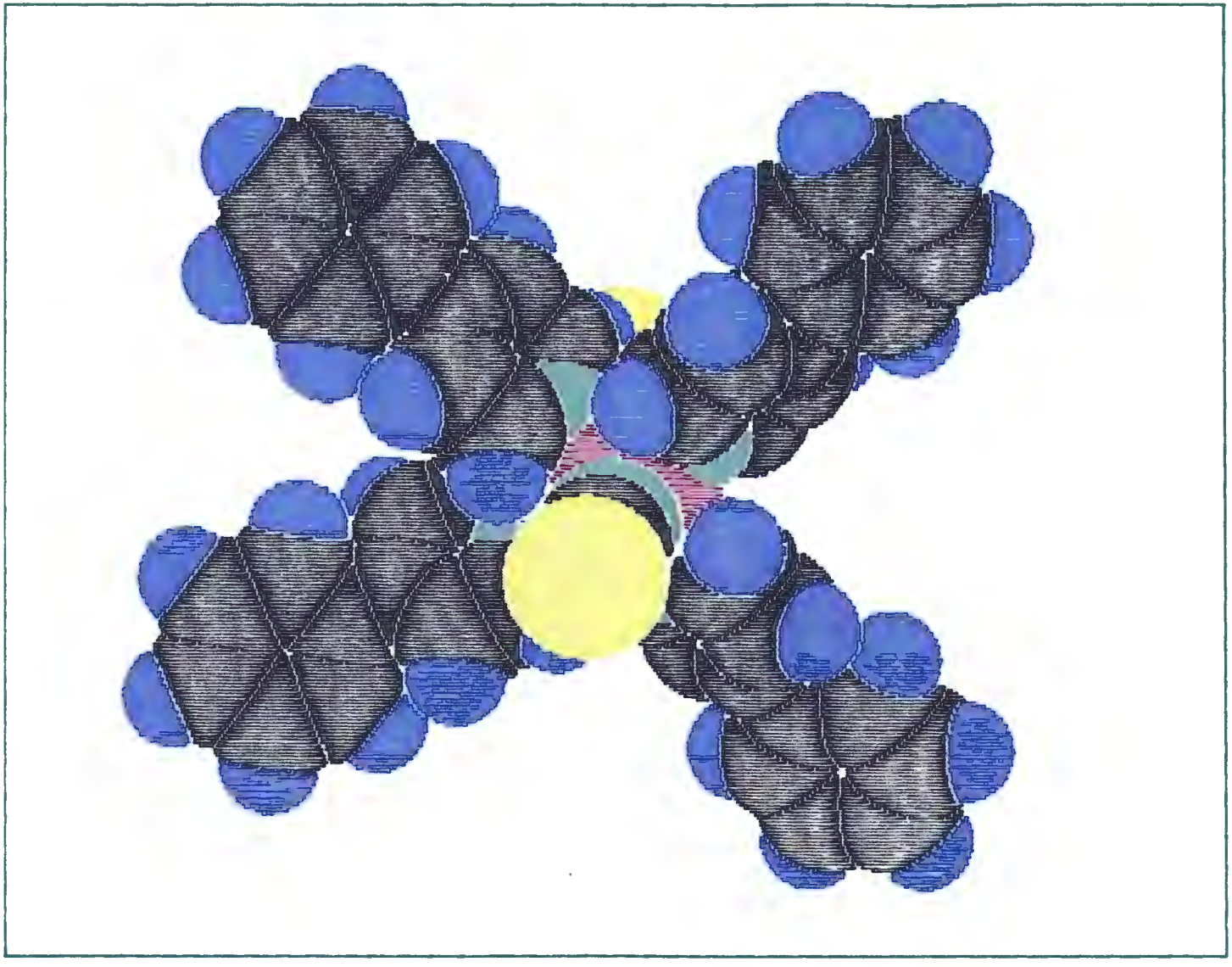

Alchemy

TRIPOS Associates

St. Louis, Mo.

Fig 4.1c Space filling diagram of Compound (I).

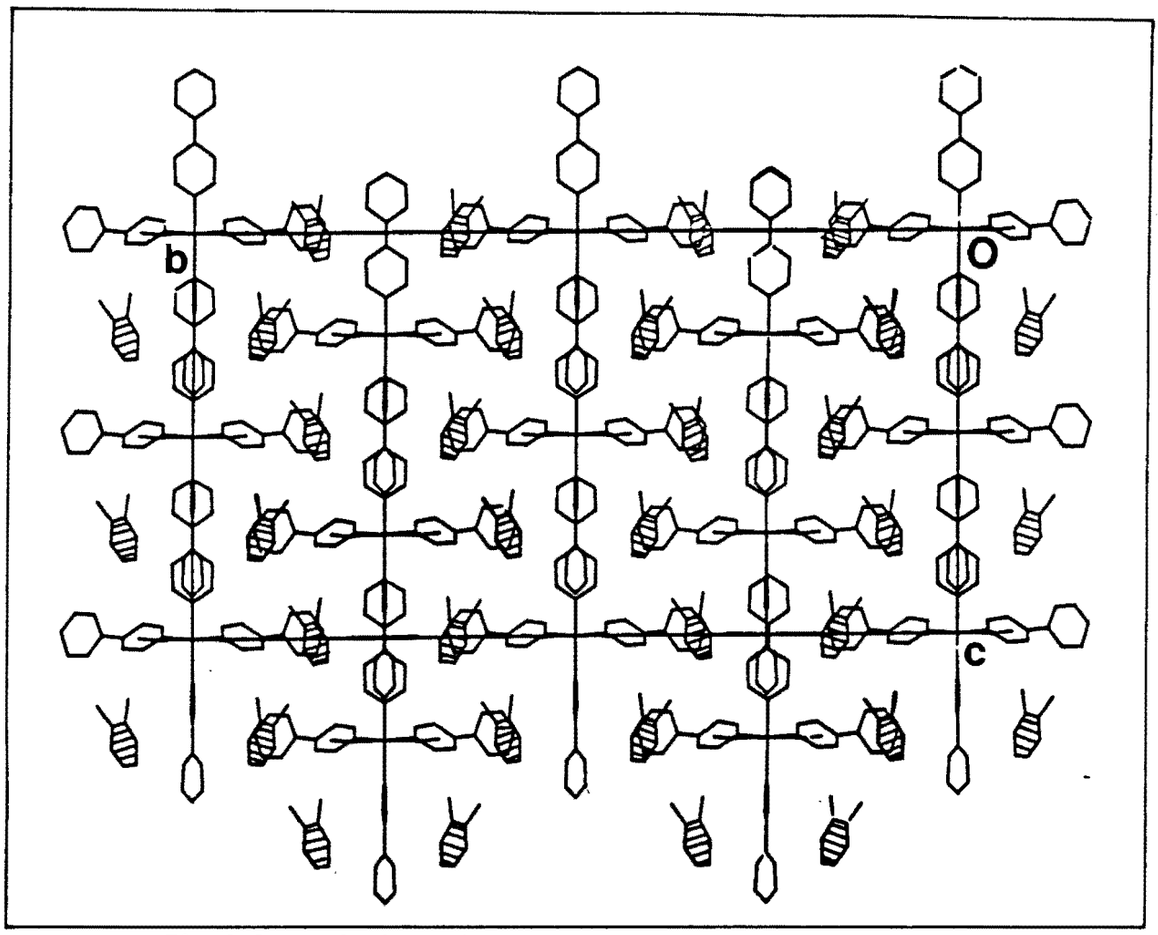

Fig 4.2a Packing diagram of Compound (II) viewed along [100] with the guest *o*-xylene molecules shaded.

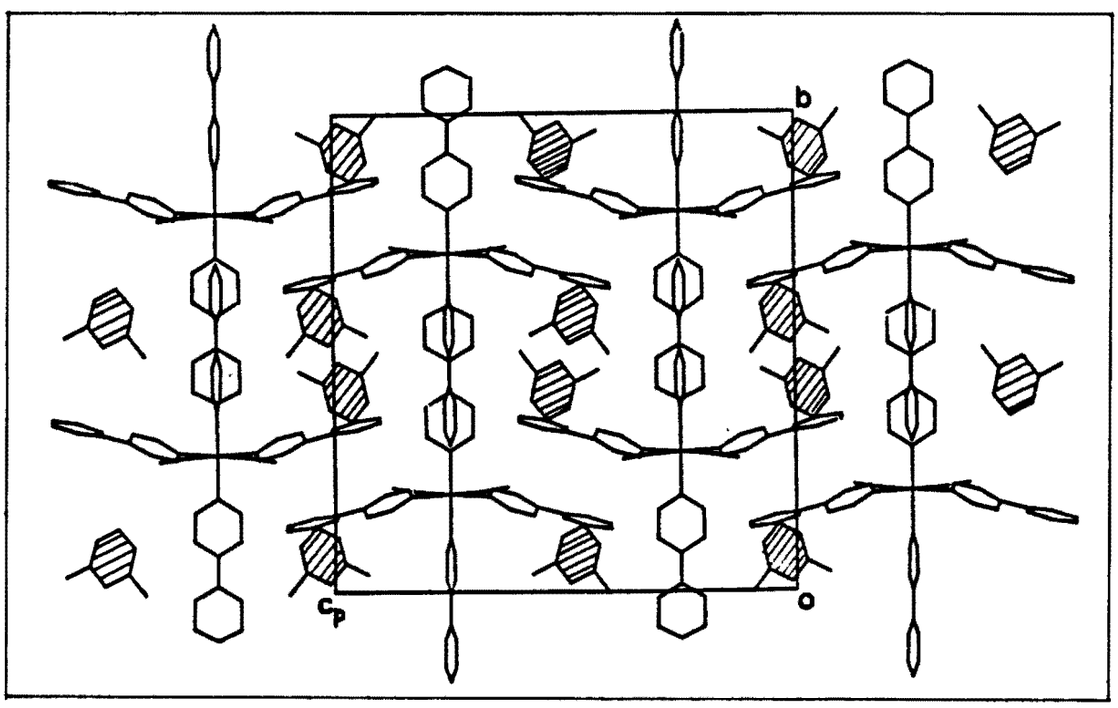

Fig 4.3a Packing diagram of Compound (III) viewed along [100] with the guest *m*-xylene molecules shaded.

confirmed by the low thermal parameters for the guest atoms.

Compound (III) $[Ni(NCS)_2(4\text{-}PhPy)_4]$.2 m-xylene. C2/c, Z = 4,
a = 16.610, b = 23.181, c = 22,950Å, β = 99.63°.
Res Vol = 369Å^3, Res Vol/G atom = 23.1Å^3/atom

The *m*-xylene molecules are situated in channels running parallel to a at b = 1/2, c = 0 and in the equivalent channel at b, c = 1/2. Packing of host molecules in this compound causes a considerable overlap of pyridine ligands when viewed along [010]. Close contacts between these ligands, on average 3.7Å, cause distortion of the N(21) - Ni(1) - N(11) bond angle from the ideal 90° to 93.3°. This is shown in Fig 4.3a which displays the packing of the structure viewed along [100], with the *m*-xylene guest molecules shaded. The moderately high Res.Vol/G-atom is in agreement with the thermal parameters of the guest atoms in indicating that the guest molecule, although not disordered, has a considerable thermal motion.

Compound (IV) $[Ni(NCS)_2(4\text{-}PhPy)]$.*p*-xylene.2dmso. $P\bar{1}$, Z = 2,
a = 10.149, b = 12.234, c = 27.014Å,
α = 99.60, β = 95.27, γ = 111.55°.
Res Vol = 495Å^3, Res Vol/G-atom = 31Å^3/atom.

This compound has two independent channels, one containing disordered dmso molecules whilst the other contains the disordered *p*-xylene molecules. A space filling diagram of the host molecules only, viewed along [100] is shown in Fig 4.4a which highlights the differences

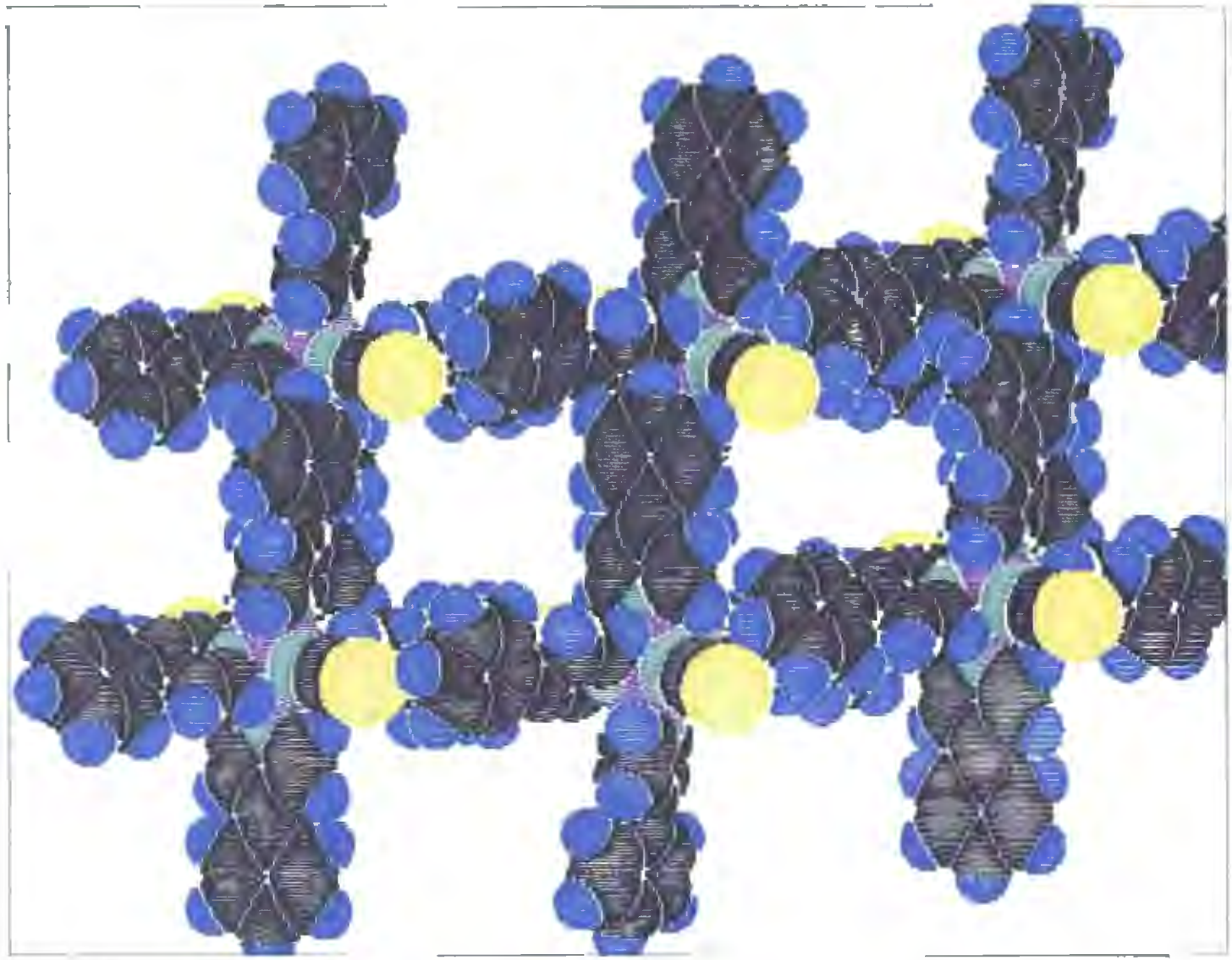

Alchemy

TRIPOS Associates

St. Louis, Mo.

Fig 4.4a Space filled packing diagram of Compound (IV), viewed along [100].

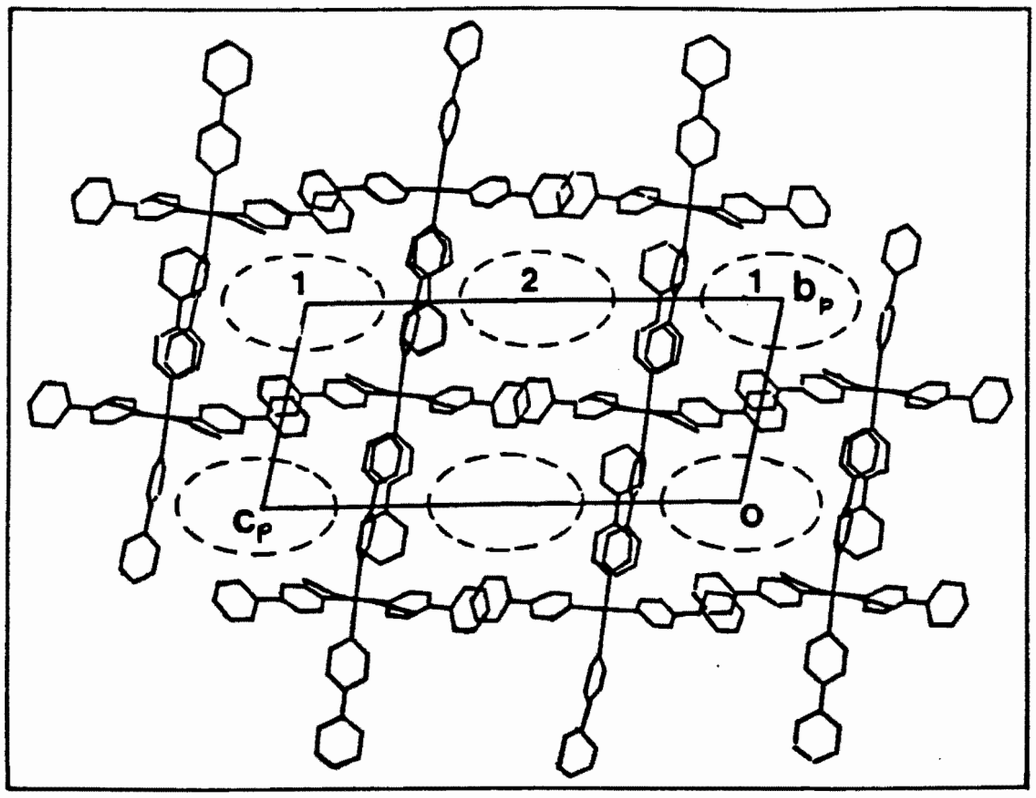

Fig 4.4b Packing diagram of Compound (IV) viewed along [100] with guest molecules omitted.

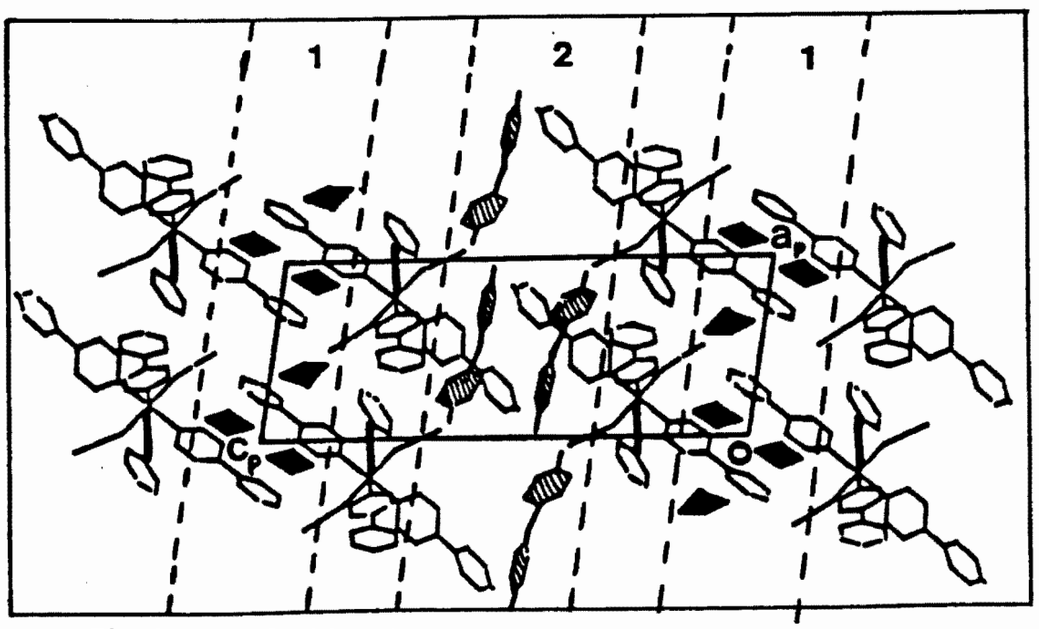

Fig 4.4c Packing diagram of Compound (IV) viewed along [010] with the disordered dmso molecules solid and the disordered *p*-xylene molecules shaded.

between the cross sections of the channels. The same view, also with guest molecules omitted is displayed as a packing diagram in Fig 4.4b. The view along [010] is shown in Fig 4.4c with the disordered dmso molecules (solid) located in the channel at y = 0 and 1 while the disordered *p*-xylene (shaded) lie in the central channel at y = 1/2. The high Res Vol/G-atom indicates the severity of the disorder in this complex.

Compound (V) $[Ni(NCS)_2(4\text{-}PhPy)_4].4\text{-}PhPy.2\text{-}methoxy\ EtOH.$
$P2_1/n$, Z = 4, a = 10.085, b = 23.723,
c = 23.266Å, β = 99.19°.
Res Vol = 352Å^3, Res Vol/G-atom = 20.7Å^3/atom,

and

Compound (VI) $[Ni(NCS)_2(4\text{-}PhPy)_4].4\text{-}PhPy.dmso.$
$P2_1/n$, Z = 4, a = 10.150, b = 24.073,
c = 23.049Å, β = 98.62°.

Res Vol = 370Å^3, Res Vol/G-atom = 23.1Å^3/atom,

These two compounds are isomorphous with respect to the structures of host and aromatic guest molecules. The aliphatic guests occupy similar regions in the lattice. Both types of guests are located in channels running parallel to a. The 4-PhPy guests occupy one set of channels at y, z = 0 while the aliphatic guests occupy the second set at y = 0, z = 1/2. For Compound (V) the packing viewed along [010] and [100] are

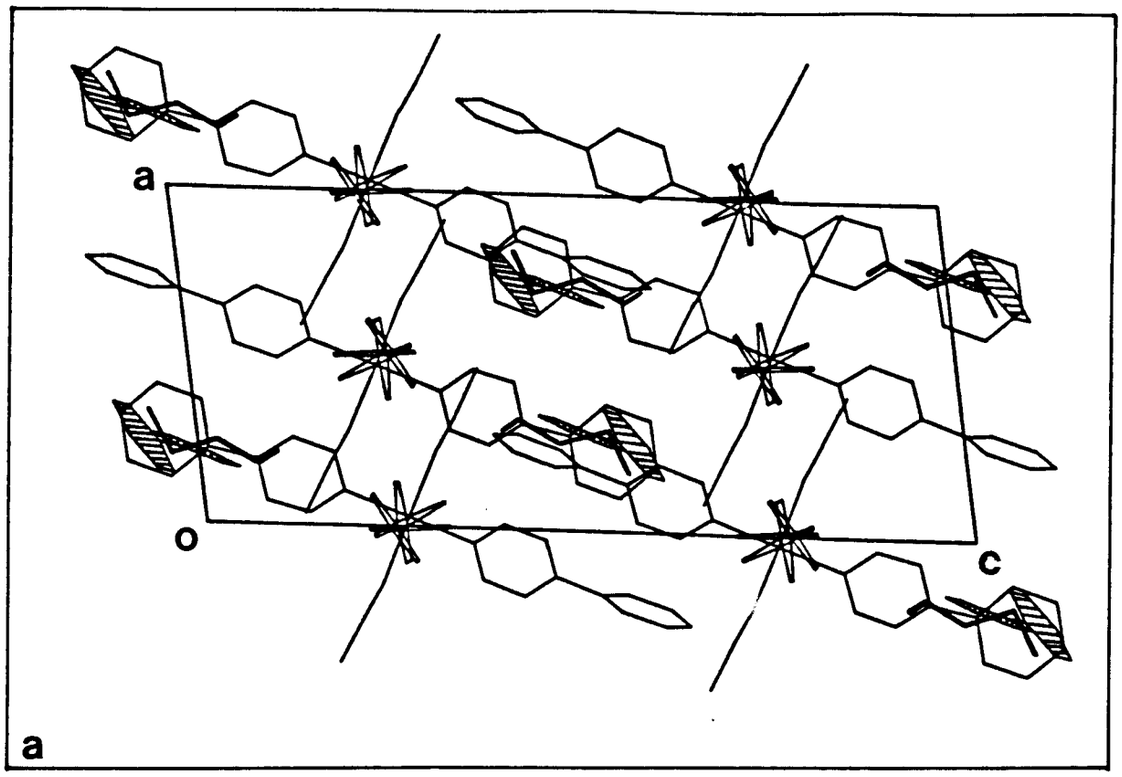

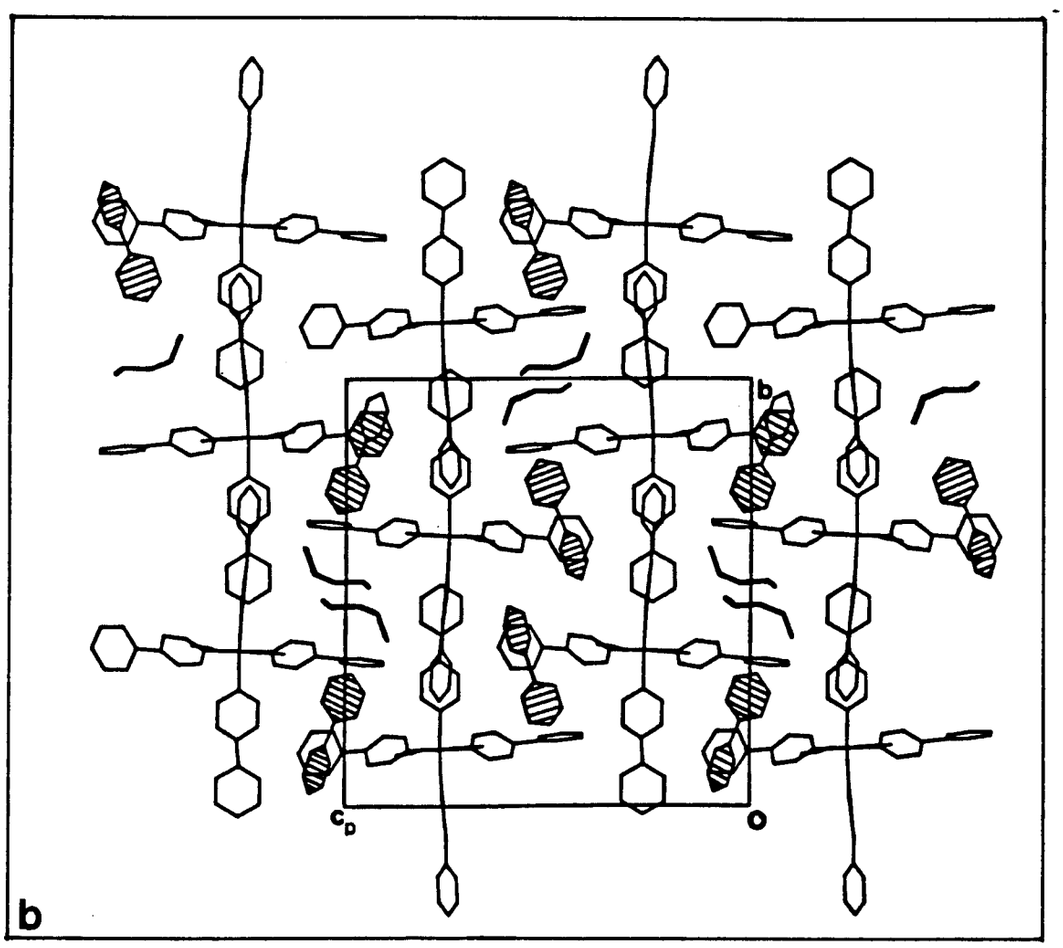

Fig 4.5 Packing diagram of Compound (V) viewed along: a) [010] and b) [100] with the 4-PhPy guest molecules shaded.

shown in Figs 4.5a and 4.5b respectively. The high degree of disorder of the dmso molecule in Compound (VI) is shown in the res vol/G atom which is 2.5Å^3 larger than that for the 2-methoxyethanol derivative.

Compound (VII) $[Ni(NCS)_2(4\text{-}PhPy)_4]$.2phenylacetylene.1dmso

C2/c, Z = 4, a = 10.065, b = 24.147,

c = 24.743Å, β = 94.00°.

Res Vol = 478Å^3, Res Vol/G-atom = 23.9Å^3/atom

The packing of the host compound in this structure is very similar to that in the previous two complexes. The phenylacetylene molecules lie on either side of the centre of inversion located at Wyckoff position *a*,. while the disordered dmso molecules lie at Wyckoff position *c*. Together they form an undulating channel running parallel to b at z = 1/2. This is shown in Fig 4.7a which views the packing along [100] and in Fig 4.7b which views along [010].

The space group $P2_1/n$ is a subset of C2/c with the diads, some of the centres of inversion and the glide plane removed in the primitive space group. This is illustrated in Fig 4.7c. It is this additional symmetry in the latter space group that causes the major differences in the packing between Compounds (V), (VI) and Compound (VII). The centre of symmetry at Wyckoff position *c* in the latter structure restricts the ligands lying around it to pack parallel to each other. When this centre is absent, the individual ligands gain some conformational freedom. This difference is highlighted in Fig 4.7d which shows this region, with guest absent for clarity, for Compounds (V) and (VII).

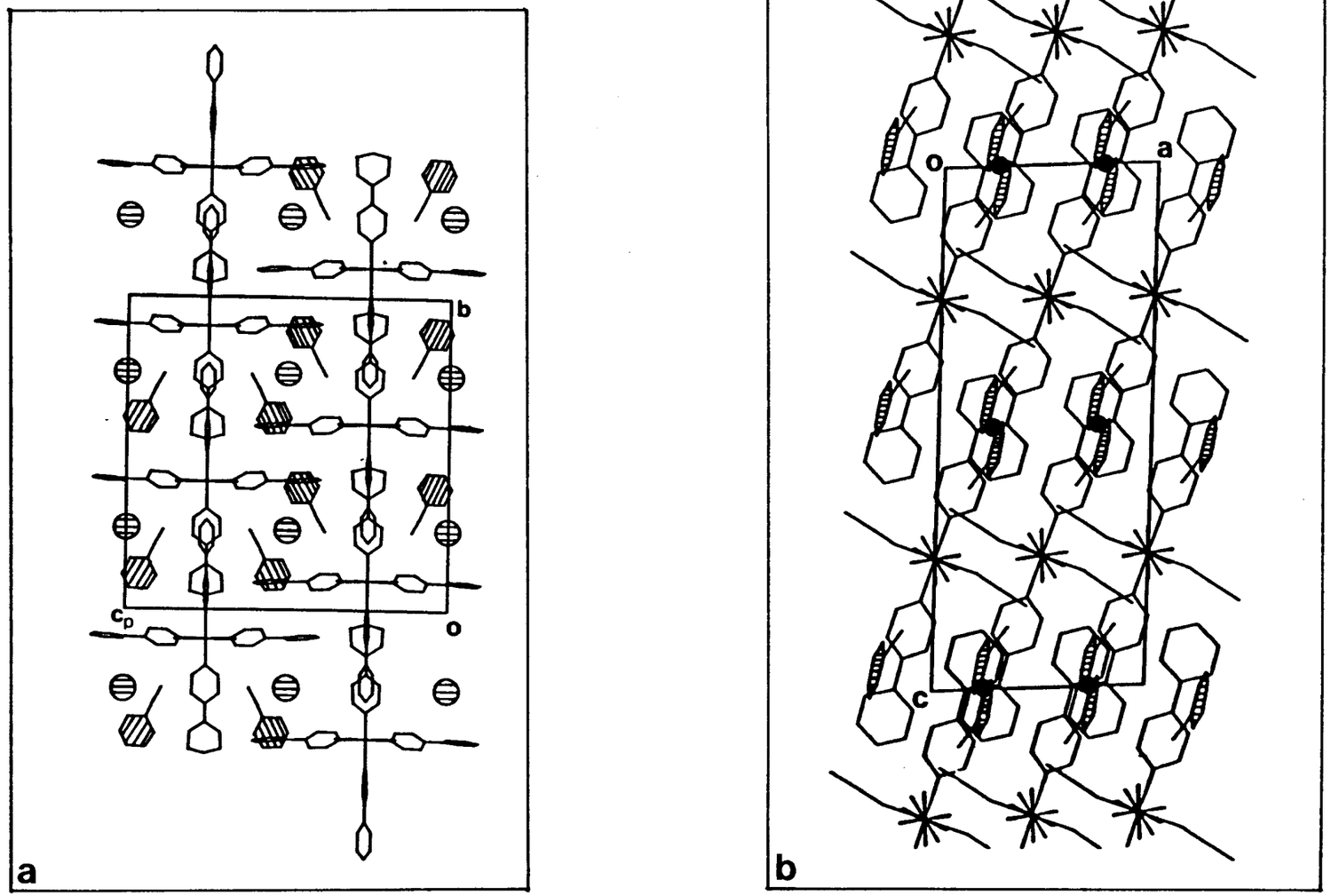

Fig 4.7a & b Packing diagram of Compound (VII) viewed along:
a) [100] and **b)** [010]. The phenylacetylene guest molecules are shaded whilst the disordered dmso is equated to a circle.

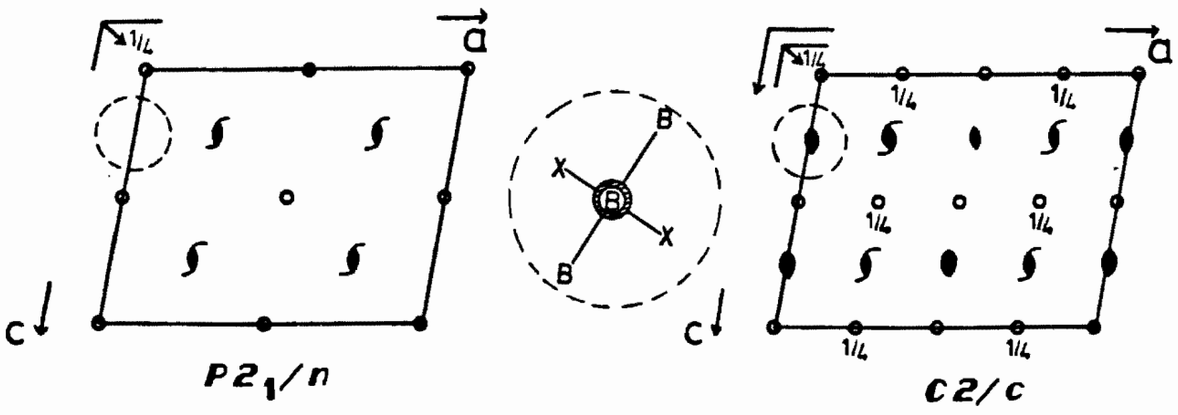

Fig 4.7c The [010] projection of the space group C2/c and its subgroup $P2_1/n$ illustrating the symmetry elements with the orientation and position of a host molecule shown schematically.

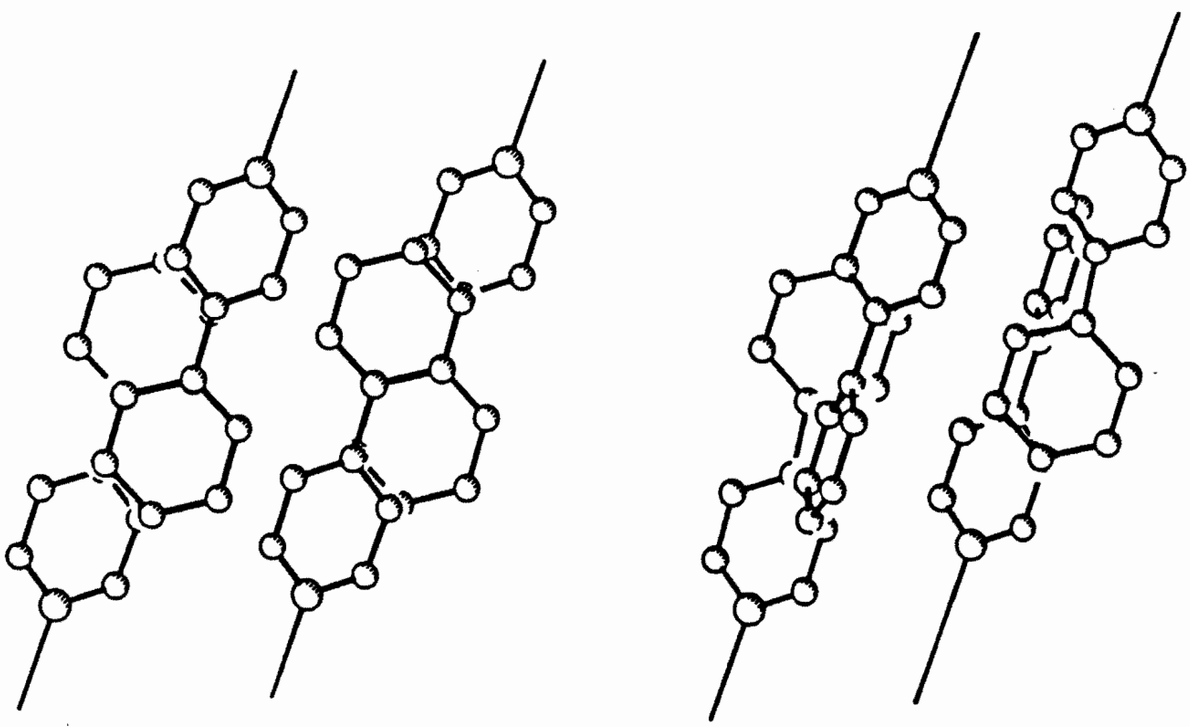

Fig 4.7d Packing of the 4-PhPy ligands around Wyckoff position *c* in the C2/c space group for Compound (VII) and the analogous region for the $P2_1/n$ space group of Compound (V).

Compound (VIII) $[Ni(NCS)_2(4\text{-}PhPy)_4].4C_6H_6$, $P\bar{1}$, Z = 1,

a = 9.52, b = 12.19, c = 13.72Å

α = 100.3, β = 90.3, γ = 105.9°

Res Vol = 482Å^3, Res Vol/G-atom = 20.0Å^3/atom.

This structure has one large channel running parallel to a, centred around y, z = 1/2 containing all four of the guest molecules and bounded by the host molecules at each corner of the unit cell. This is illustrated in Fig 4.8a which is viewed down [100] with guest molecules shaded for clarity, whilst Fig 4.8b is the same view of a space filling diagram, with all atoms shaded in black for ease of reproduction of the host alone.

Figs 4.8c and 4.8d show the extent of the cavity, calculated from van der Waals radii, and sectioned at x = 0.05 and x = 0.4 respectively, which are the regions of two of the guest molecules. Passage between channels in the c direction is prevented by one set of 4-PhPy ligands which run 15° off parallel to the b axis and are tilted 30° to the yz plane. The other pair of 4-PhPy ligands is 7° off parallel to the c axis, tilted -15° to the yz plane and prevents interconnection in the b direction. The low Res Vol/G-atom indicates the order of the guest atoms and is reflected in the low value of the thermal parameters of the guest atoms.

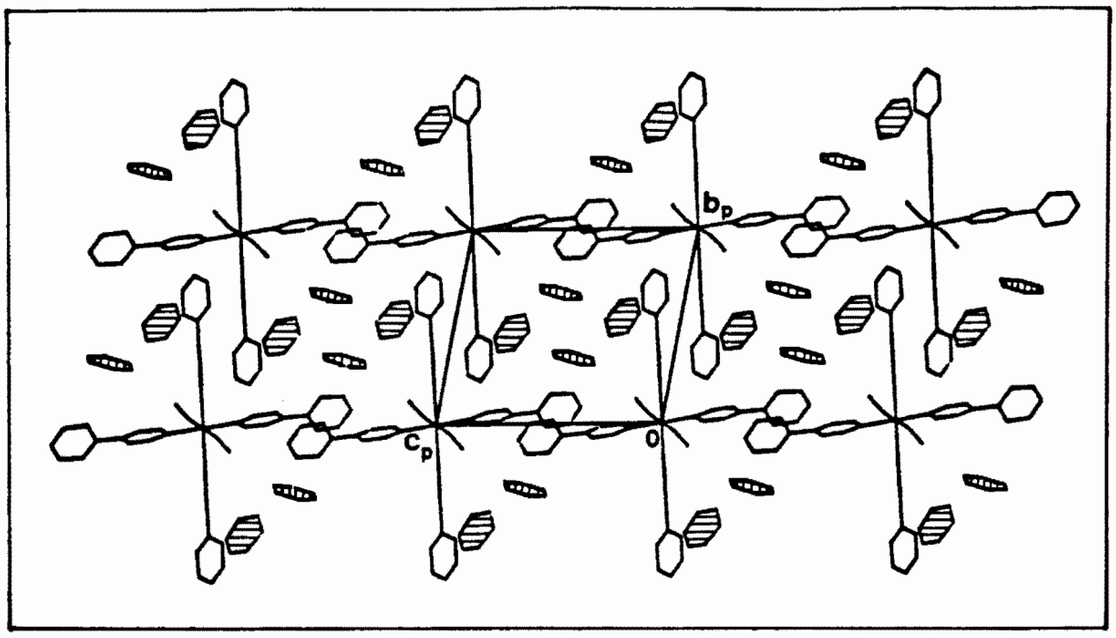

Fig 4.8a Packing diagram of Compound (VIII) viewed along [100] with the benzene guest molecules shaded.

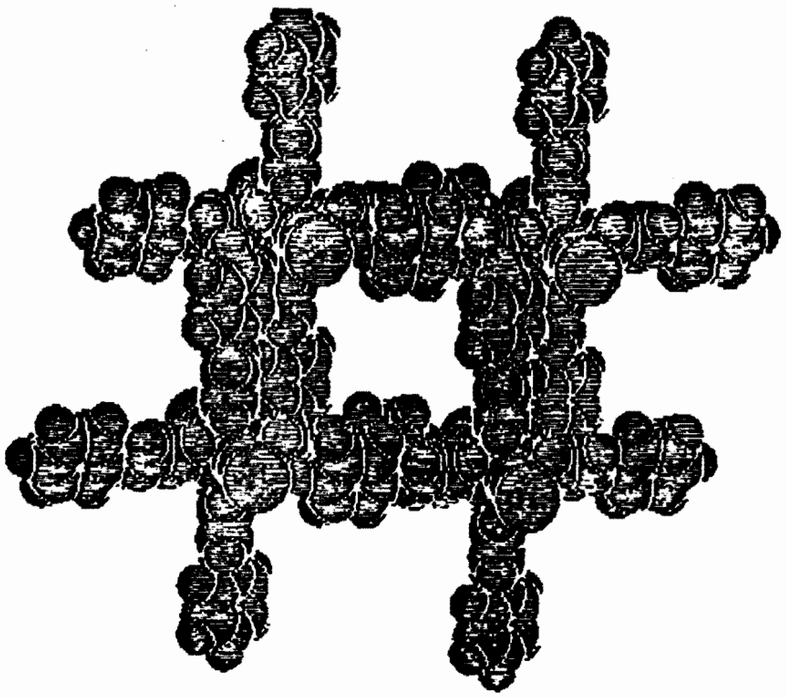

Fig 4.8b Space filling diagram of Compound (VIII) with guest molecules omitted to illustrate the extent of the cavity.

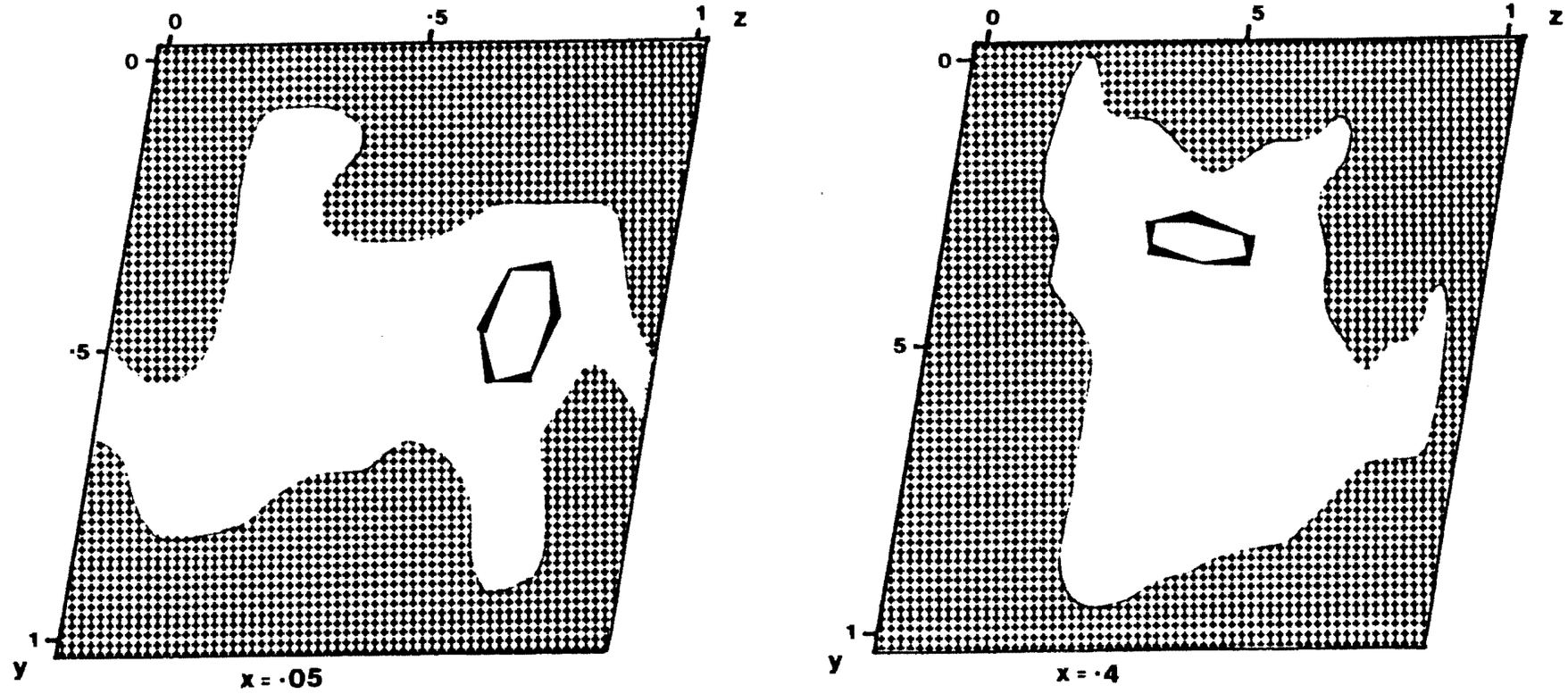

Fig 4.8c Illustrations of the extent of the cavity of Compound (VIII) viewed along [100] and sectioned at x = 0.05 and x = 0.40 with the position of a benzene molecule indicated.

4.3 CLASS B (Atomic nomenclature Fig 4.9a)

Compound (IX) $[NiCl_2(4\text{-}PhPy)_4].MeOH$, $P2_12_12_1$, Z = 4,
a = 12.470, b = 16.550, c = 19.525Å

The packing of this compound which is illustrated in Fig 4.9b is remarkably similar to that of Compound (I) (Fig 4.1b) which is the α-phase complex for the isothiocyanate derivative. The methanol occupies a region in space near (3.1Å) to the Cl(2) atom of the host molecule and its orientation is such that the three atoms: Cl of the host and the two atoms of the guest, can be compared with one of the NCS groups of Compound (I). The cell parameters for the two compounds are comparable except the cell length in the c-direction for Compound (I) is twice that of Compound (IX). The space group $P2_12_12_1$ is a subset of Pbca (Fig 4.9c) with the glides and centres of inversion missing in the former space group. Thus it is not surprising that the molecular packing of these two compounds is so similar especially when the number of non-H atoms are compared: 51 for (IX) and 55 for (I). Attempts to synthesize the α-phase of the chloride derivative have proved to be unsuccessful. The enclathration process is believed to require the α-phase structure to change to a β_0-phase, in which the host molecules have realigned to form interstices. The guest molecules then act as a template so that as they enter these cavities, the β_0-phase structure rearranges to form the true β-phase. The β_0-phase, being an intermediate, is not stable and thus will not form crystals. If, however, only slight rearrangement is required when small molecules (*e.g.* MeOH) enter the host lattice, then we can consider this compound as being very close to the structure of

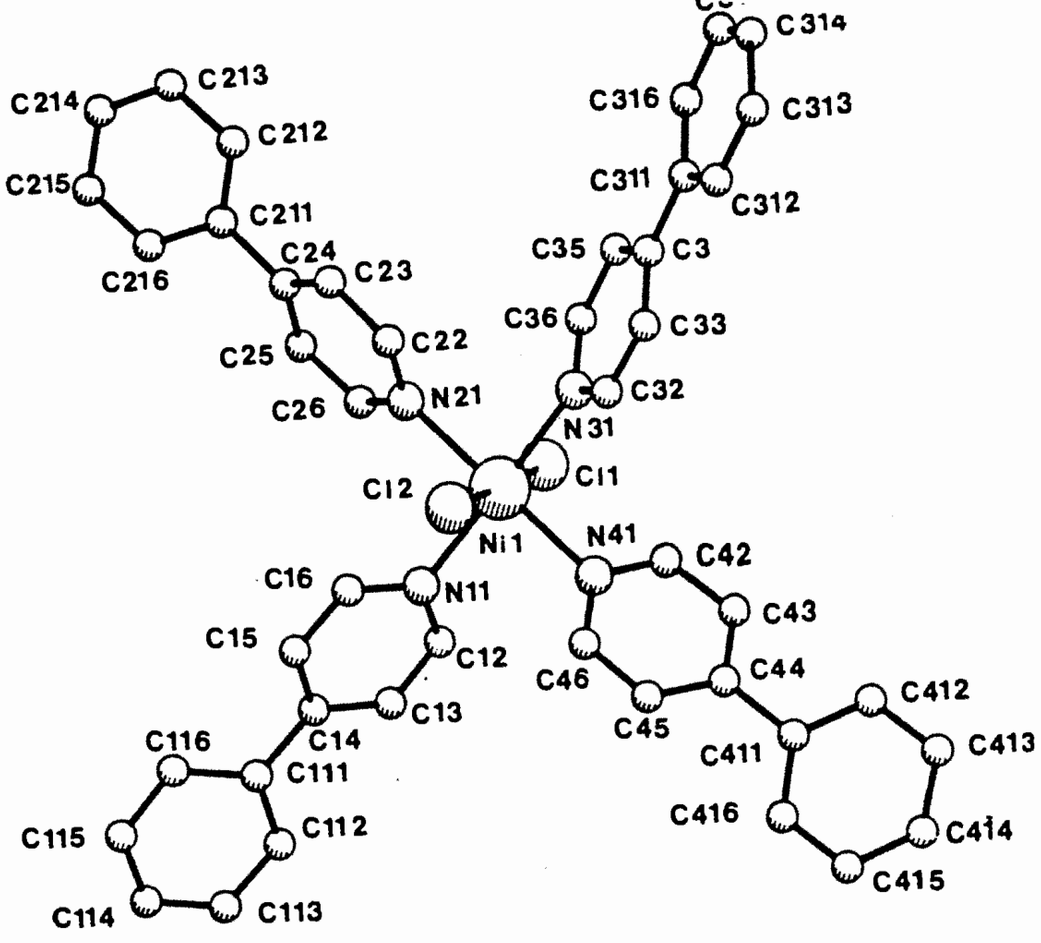

Fig 4.9a Perspective view of the host molecule of Compound (IX) with atomic nomenclature applicable to all Class B compounds.

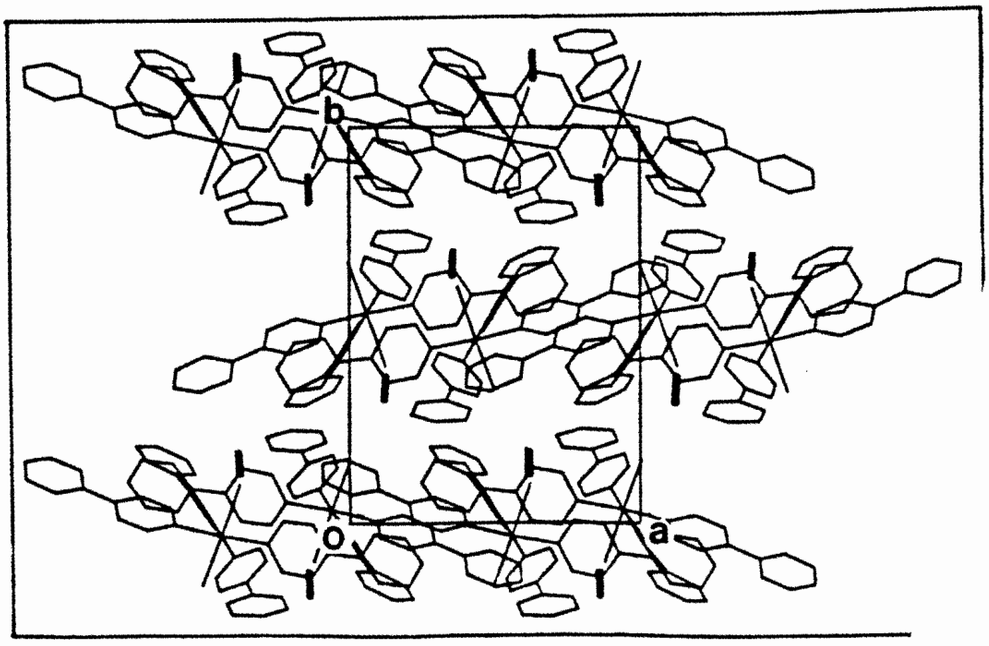

Fig 4.9b Packing diagram of Compound (IX) viewed alo [001] with the methanol guests highlighted

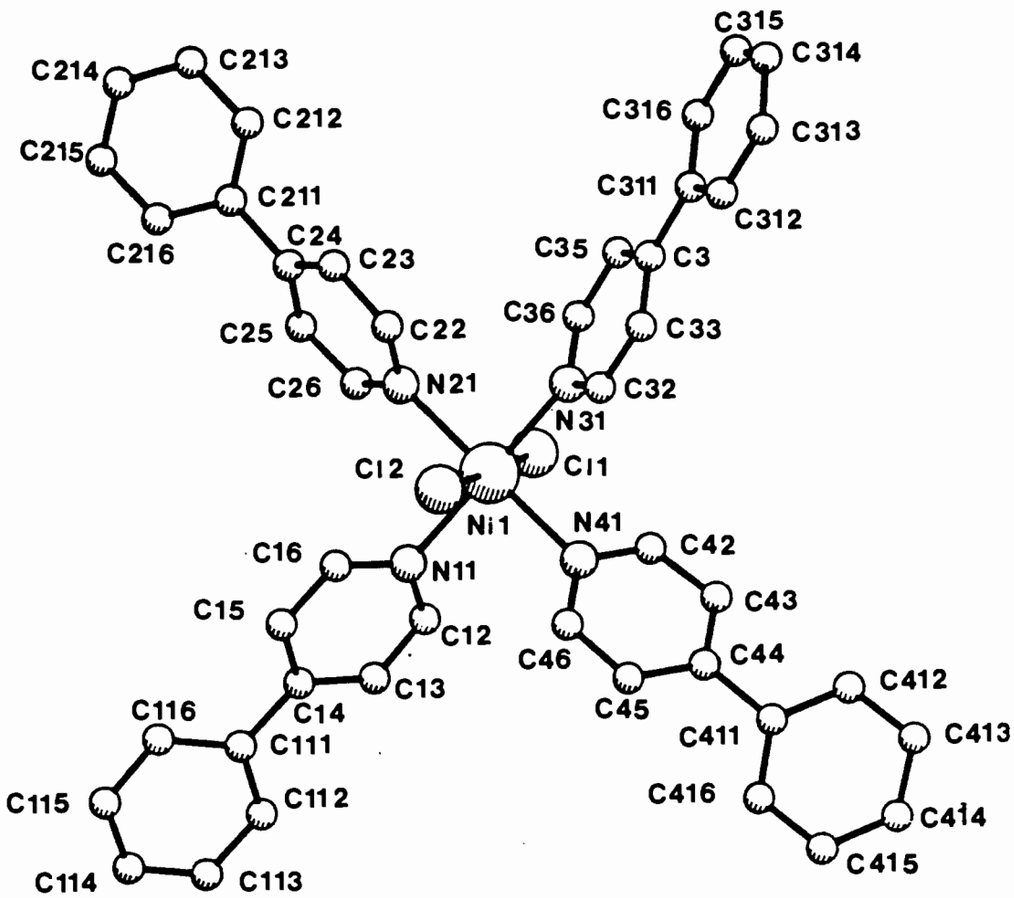

Fig 4.9a Perspective view of the host molecule of Compound (IX) with atomic nomenclature applicable to all Class B compounds.

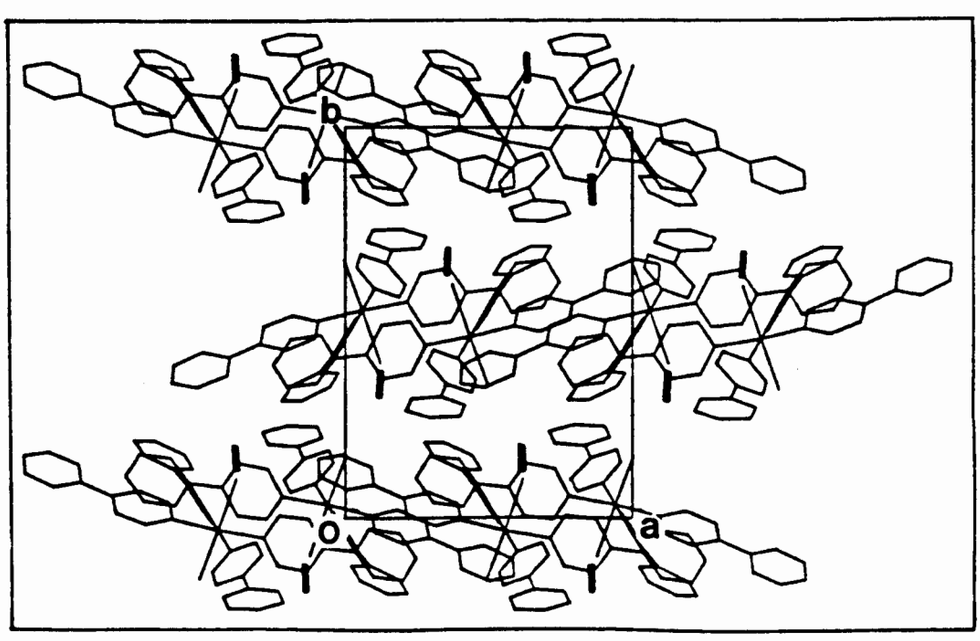

Fig 4.9b Packing diagram of Compound (IX) viewed along [001] with the methanol guests highlighted.

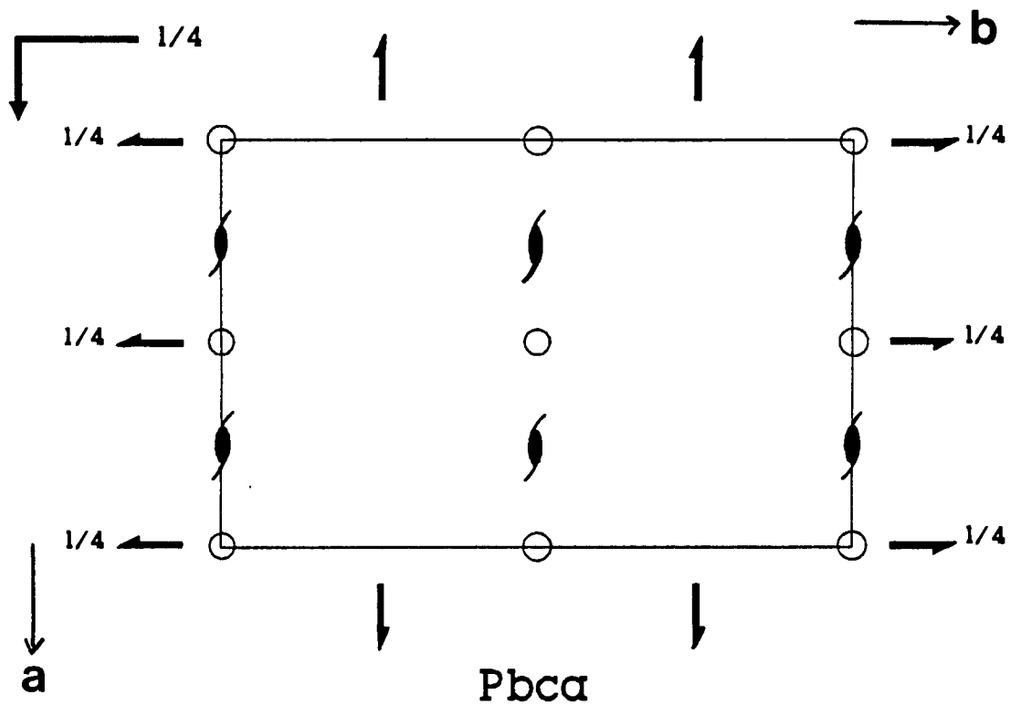

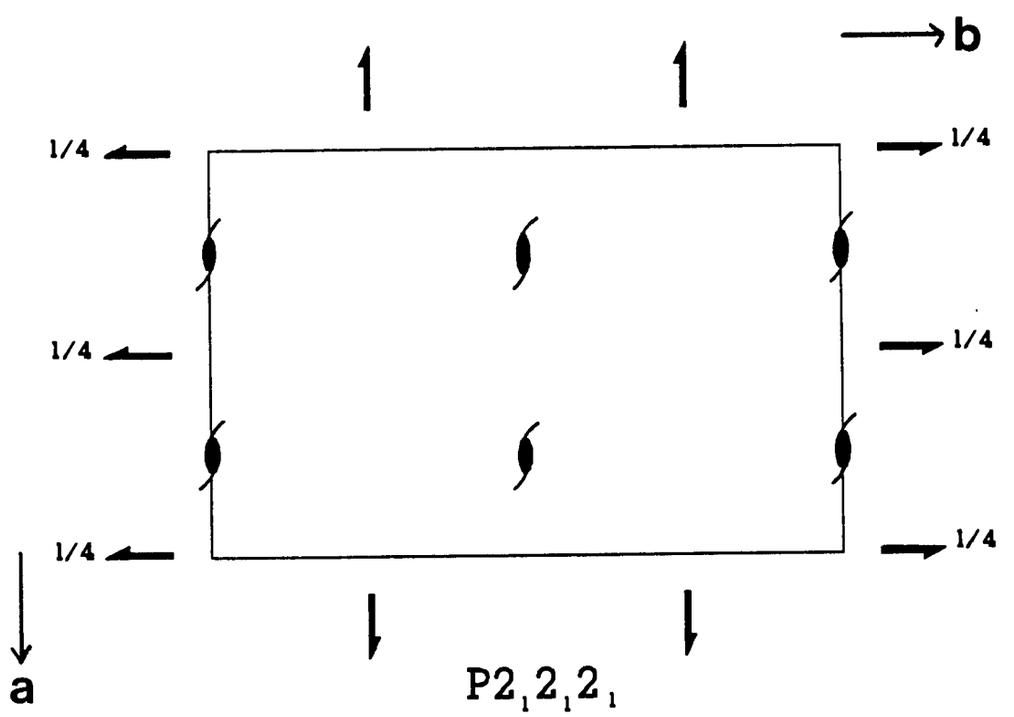

Fig 4.9c The [001] projection of the space group Pbca and its subgroup $P2_12_12_1$ illustrating the common symmetry elements.

COMPOUND (IX)

z = 0.5

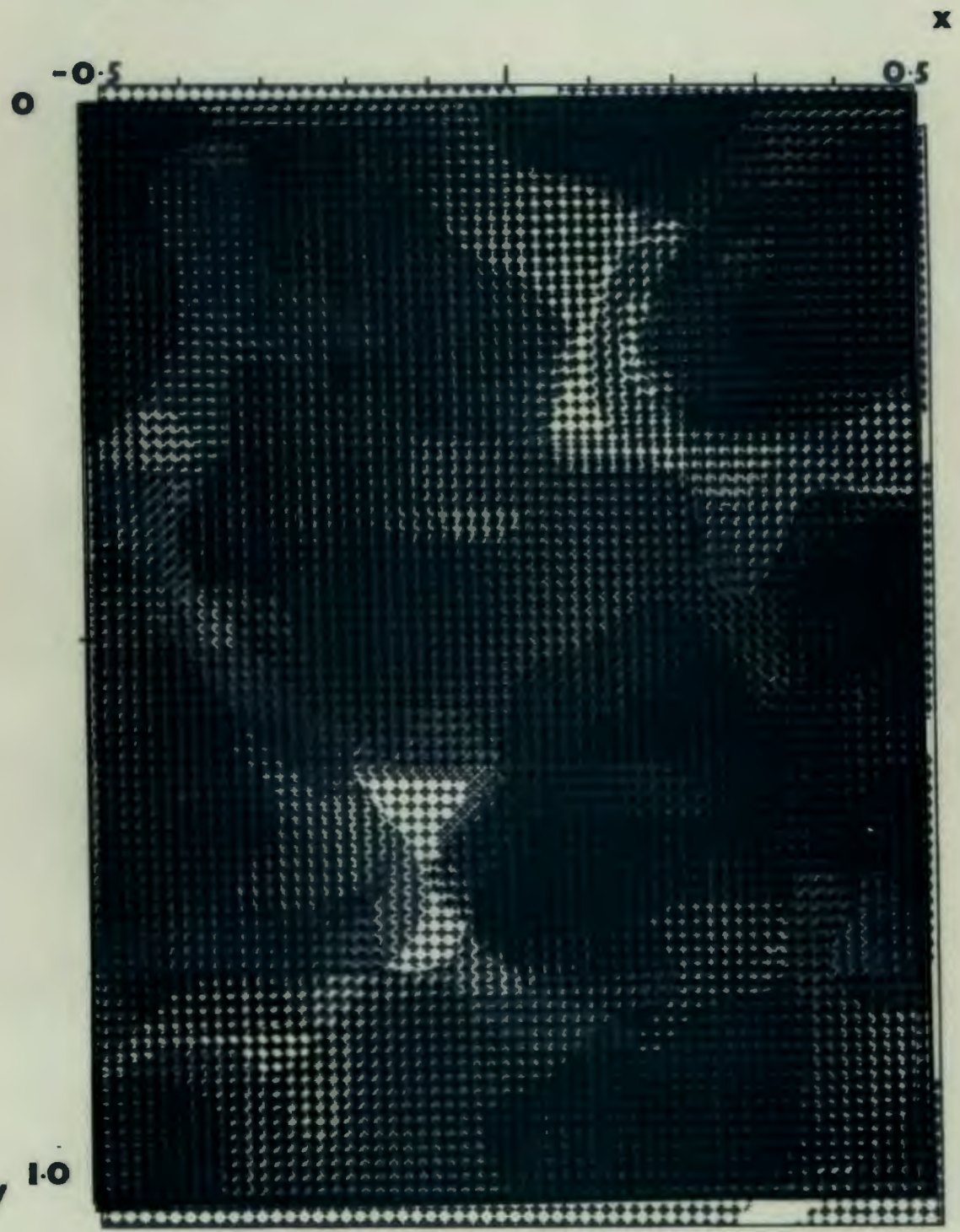

Fig 4.9d Sections of the unit cell of Compound (IX) indicating the regions occuppied by the host molecules and the channels remaining in which the guest molecules are located.

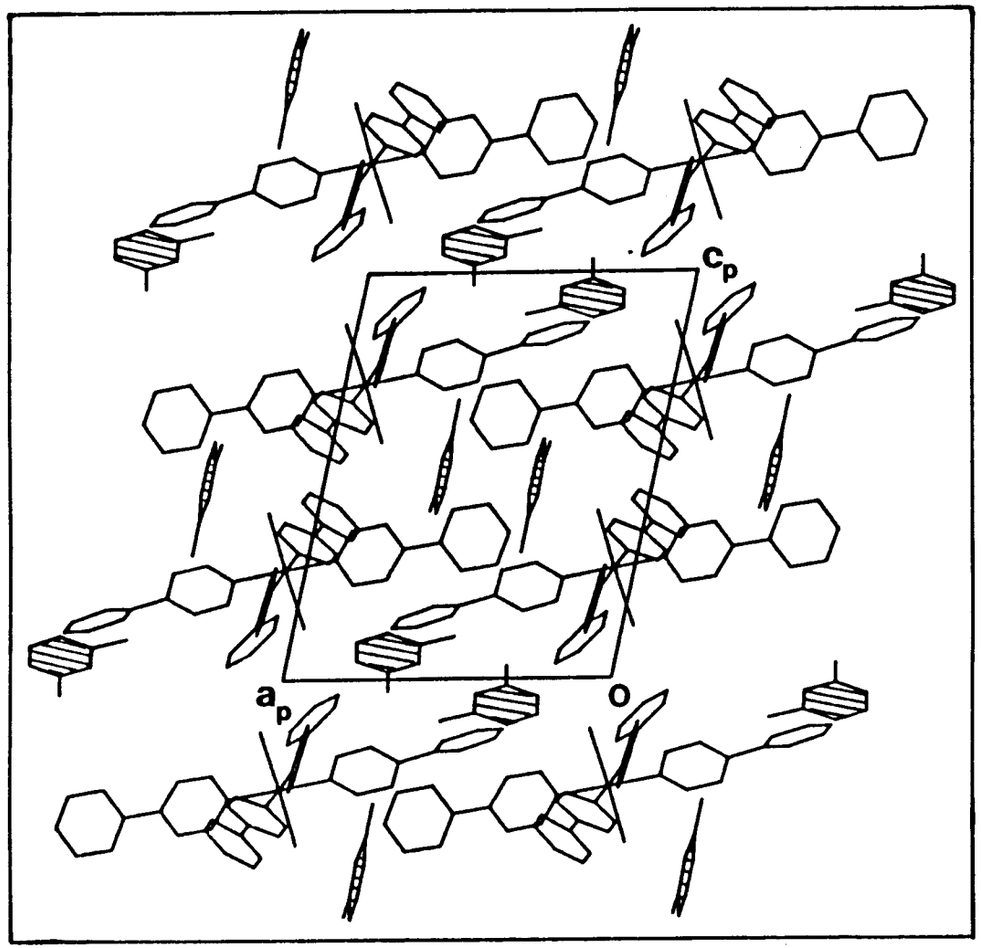

Fig 4.10a Packing diagram of Compound (X) viewed along [010] with the guest *m*-xylene molecules shaded.

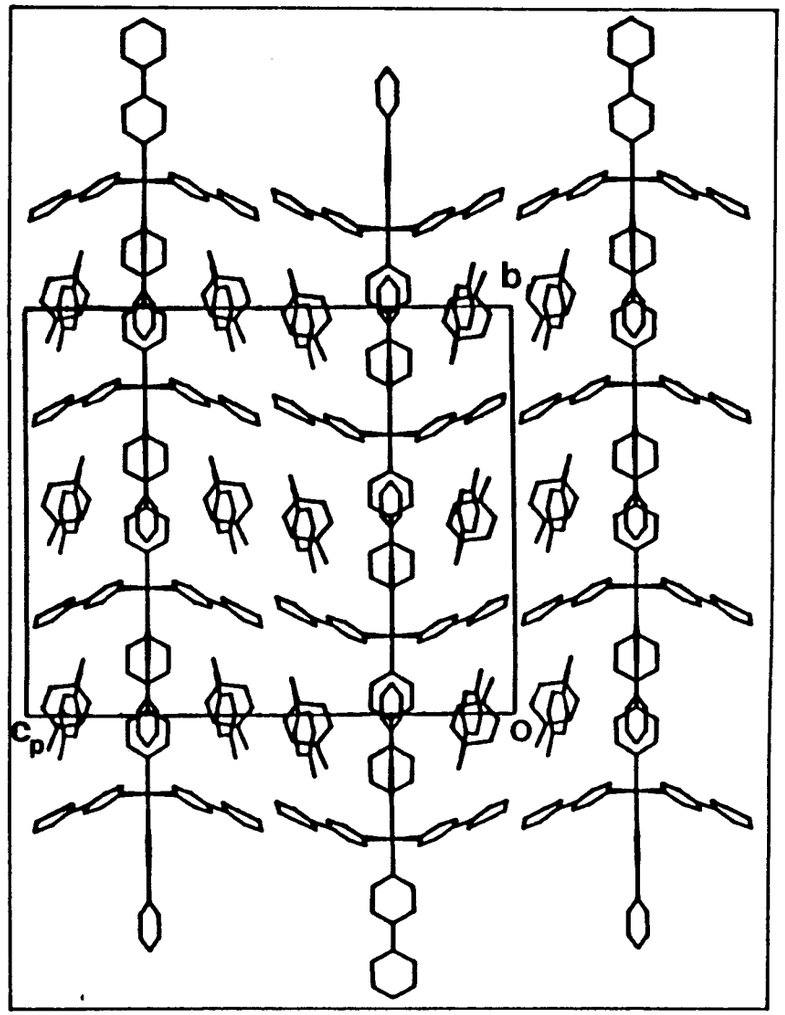

Fig 4.11a Packing diagram of Compound (XI) viewed along [100].

direction of the channel. Fig 4.10a illustrates the packing of this complex with the guest xylene molecules shaded for clarity.

The agreement between the figure obtained for the Res Vol/G-atom and that of the 'baseline' figure of 18Å^3 is contradictory to the thermal parameters of the guest atoms which range from .090 to .265Å^2. The former value indicates well ordered guest molecules, whilst the latter shows the movement that these molecules possess about their optimum position. Thus the figure of 18Å^3 is probably too low an estimate for the Res Vol/G-atom when this is calculated in the manner that it has been for these compounds.

Compound (XI) $[NiCl_2(4\text{-}PhPy)_4].4p$-xylene, C2/c, Z = 4,
a = 9.692, b = 23.955, c = 28.385Å, β = 96.4°.
Res Vol = 654Å^3, Res Vol/G-atom = 20.4Å^3.

This clathrate packs in a similar manner to all the other compounds which crystallize in the C2/c space group *e.g.* Compounds (III) and (VII). Comparing Fig 4.11a which shows the packing of this compound viewed along [100] and Fig 4.3a which is the same view for the *m*-xylene clathrate of the NCS^- derivative, it is apparent that the degree of overlap of the 4-PhPy ligands running in the c-axis, is considerably less in the Cl^- derivative complex. This is owing to the increased length of the c-axis (22.950 - 28.385Å) which enables the host atoms to move 2.7Å further apart in that direction. This results in an increase of nearly 24% in the cross sectional area of the cavity in the yz plane (the b axes for both compounds are approximately equal). This dilation

enables twice the number of guest molecules to be located in the channel with their methyl substituents orientated in the b direction. Close interactions between the pyridine ligands an adjacent host molecules, on average about 3Å, cause distortion of the N(21) - Ni(1) - N(31) bond angle by 3.5° off the ideal 90°.

Compound (XII) $[NiCl_2(4\text{-PhPy})_4].4\text{-PhPy}$, C2/c, Z = 4,
a = 9.436, b = 23.841, c = 21.577Å, β = 98.4°.
Res Vol = 1200Å^3, Res Vol/G-atom = 18.1Å^3.

As for the previous compound, this clathrate packs in what can be termed as the typical C2/c structure when referring to the 4-PhPy derivative of Werner Clathrates. Overlap between ligands on adjacent host molecules is increased, but interactions between these ligands has decreased as their close contacts are now of the order of 3.5Å. Thus the bond angle, N(31)-Ni(1)-N(41), is slightly less distorted at 92.9°, compared to the 93.5° of the previous compound, from the ideal angle of 90°. The atoms C(11G), C(14G), C(24G) and C(21G) are not collinear with the angle (≈5°) defined by the vector between the former two atoms and that between the latter two atoms indicating that packing forces have caused this molecule to become arched. A packing diagram, viewed along [100] is illustrated in Fig 4.12a whilst the bow-shape of the guest molecule is shown in Fig 4.12b.

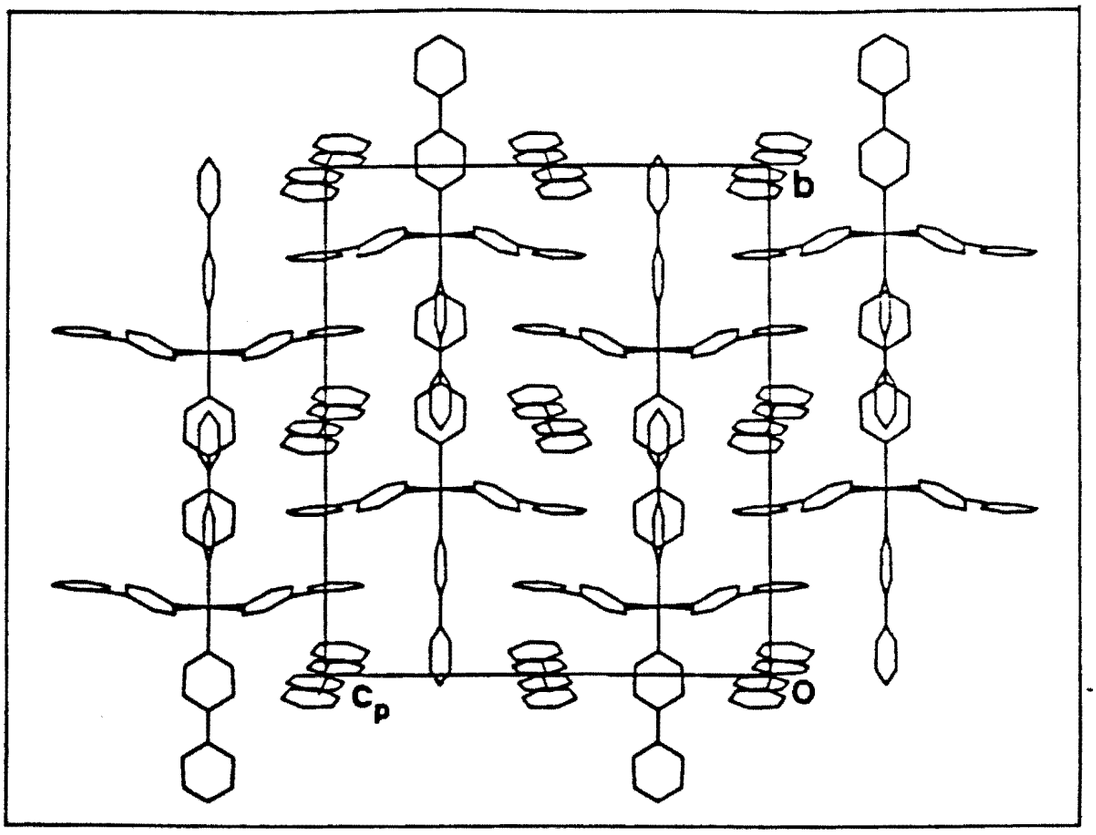

Fig 4.12a Packing diagram of Compound (XII) viewed along [100] illustrating the disorder of the 4-PhPy guest molecules.

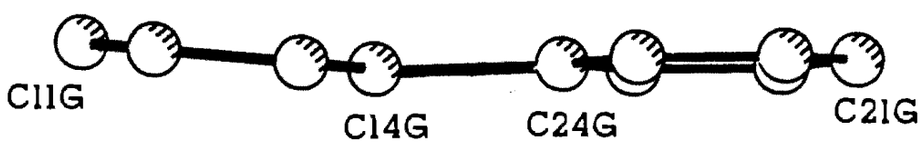

Fig 4.12b Perspective view of the guest 4-phenyl pyridine of Compound (XII) illustrating the bow-shape adopted by the molecule.

4.4 CLASS C (Atomic nomenclature Fig 4.13a)

Compound (XIII) $[Ni(NCS)_2(4\text{-}MePy)_2(4\text{-}PhPy)_2]$.acac

C2/c, Z = 4, a = 10.541, b = 22.879, c = 16.814Å,

β = 99.85°.

Res Vol = 999Å^3, Res Vol/G-atom = 18.8Å^3.

and

Compound (XIV) $[Ni(NCS)_2(4\text{-}MePy)_2(4\text{-}PhPy)_2]$.1-chlorobutane

C2/c, Z = 4, a = 10.771, b = 23.027, c = 16.405Å,

β = 99.1°.

Res Vol = 1004Å^3, Res Vol/G-atom = 27.3Å^3.

These two compounds are isomorphous with respect to the host molecules, and the guest molecules occupy similar regions within the host lattice. The guest molecules in both complexes are located in undulating channels running parallel to a at y, z = 1/2. The isothiocyanate moiety and the 4-MePy ligands form the roof and floor of this channel, if viewed parallel to the xz plane, whilst the 4-PhPy ligands form the walls. The packing of Compound (XIII) viewed along [100] and that of Compound (XIV) viewed down [010] is shown in Fig 4.13b and 4.14a respectively. Fig 4.14b is a coloured space filling diagram of Compound (XIV).

Over 15 different attempts were made to form clathrates of this host with aromatic guest molecules, aliphatic molecules containing $CH_3(CH_2)_2Cl$ with n = 2-9, and aliphatic molecules containing potential H-bond donors. Gross variations were made to the crystallization procedure: ranging from wide deviations in the concentration of the host

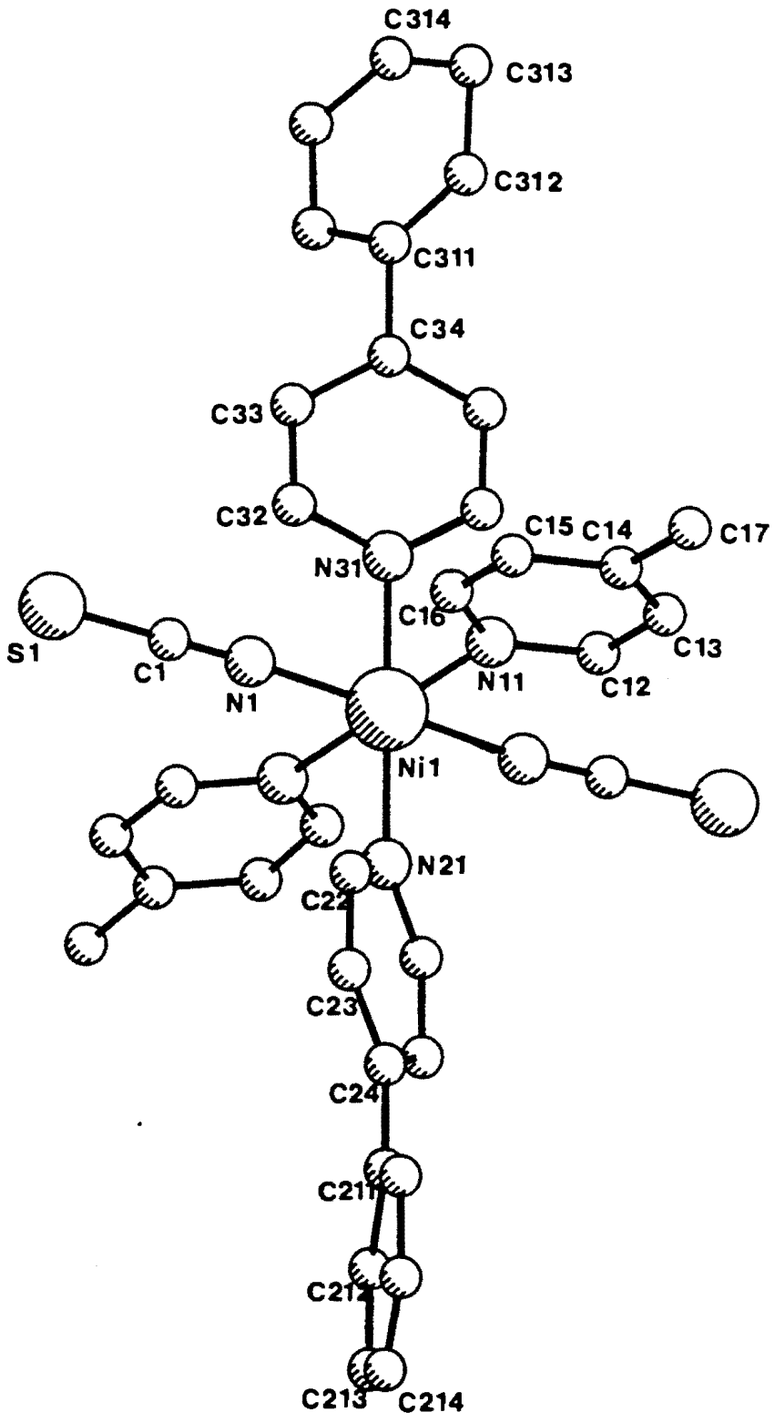

Fig 4.13a Perspective view of Compound (XIII) showing atomic nomenclature applicable to all Class C compounds.

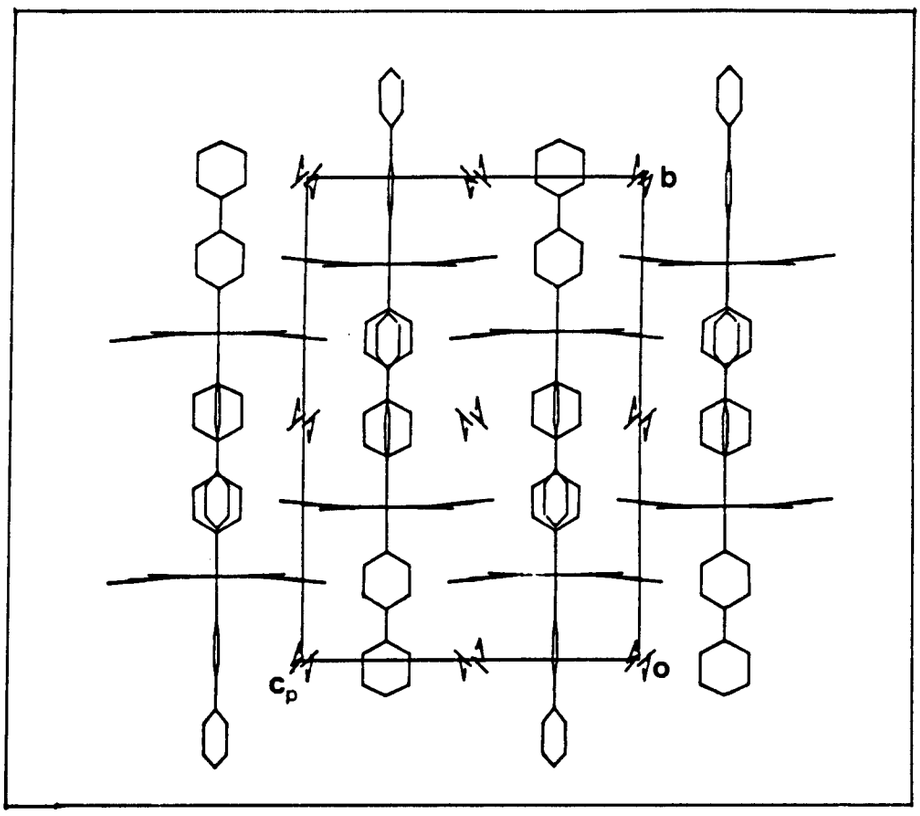

Fig 4.13b Packing diagram of Compound (XIII) viewed along [100] illustrating the two-fold statistically disordered acetylacetone in the channel.

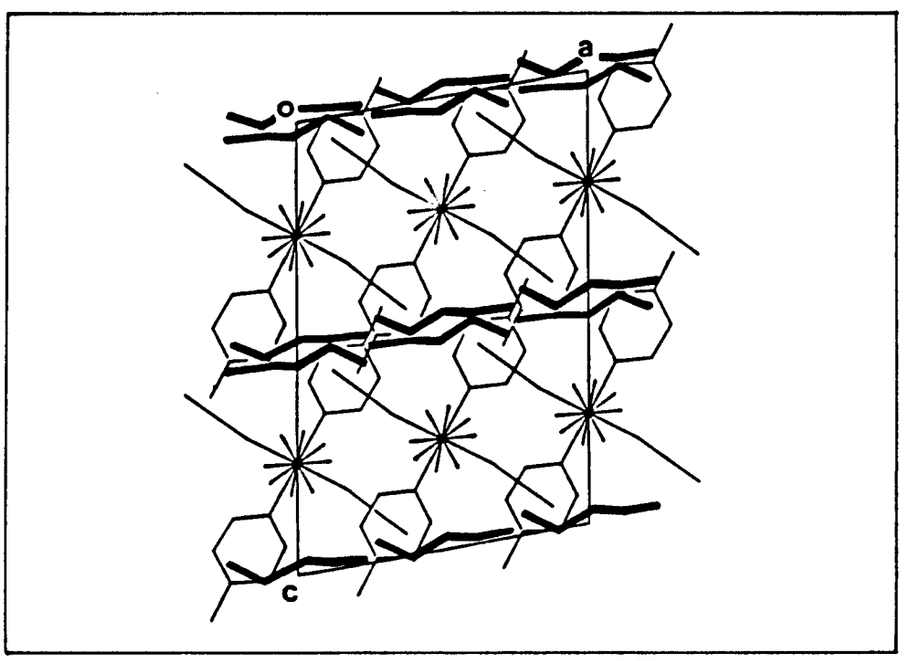

Fig 4.14a Packing diagram of Compound (XIV) viewed along [010] with the guest 1-chlorobutane molecule highlighted

the β_o-phase for $[NiCl_2(4\text{-}PhPy)_4]$. Cross-sections of the xy plane are shown in Fig 4.9d which illustrates the extent of the cavity in which the guest molecules are located. The drawings result from calculations performed by OPEC on the host structure alone.

The extremely low Res Vol/G-atom of 12.5Å^3 is obviously unrealistic in an absolute sense, but it still indicates the high degree of order of the methanol molecule which is surprising. Methanol has a high vapour pressure and therefore it would be expected to fit very loosely within the cavity and thus have a high degree of disorder. The thermal parameters of the two non-hydrogen guest atoms (approximately 0.10Å^2) is indicative of the lack of vibration that this molecule has within the host lattice.

Compound (X) $[NiCl_2(4\text{-}PhPy)_4].2m$-xylene, $P\bar{1}$, Z = 2,
a = 12.747, b = 12.888, c = 16.187Å
α = 90.05, β = 102.21, γ = 92.38°.
Res Vol = 316Å^3, Res Vol/G-atom = 19.7Å^3.

The two independent guest molecules occupy different channels within the host framework of this compound. Both channels run parallel to the a axis; one is centred around this axis at y = 1/2, whilst the other is centred around y, z = 1/2. One pair of guests, located about the centre of inversion at Wyckoff position *h*, has the guests not only parallel to each other, but also separated by less than 3.9Å thus having considerable π-π interaction. Passage between channels is prevented by the 4-PhPy ligands of the host which are orientated parallel to the

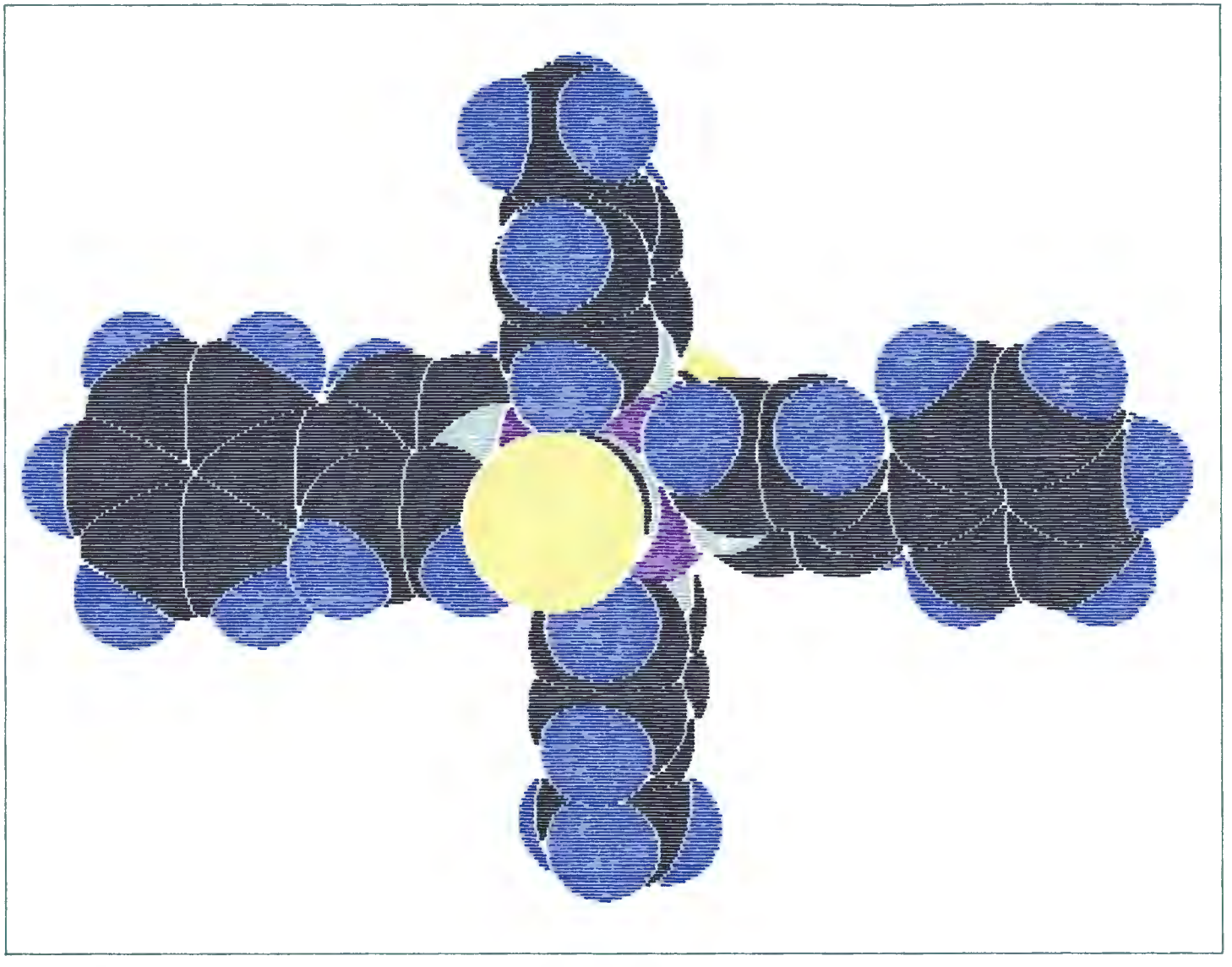

Alchemy

TRIPOS Associates

St. Louis, Mo.

Fig 4.14b Space filling diagram of Compound (XIV).

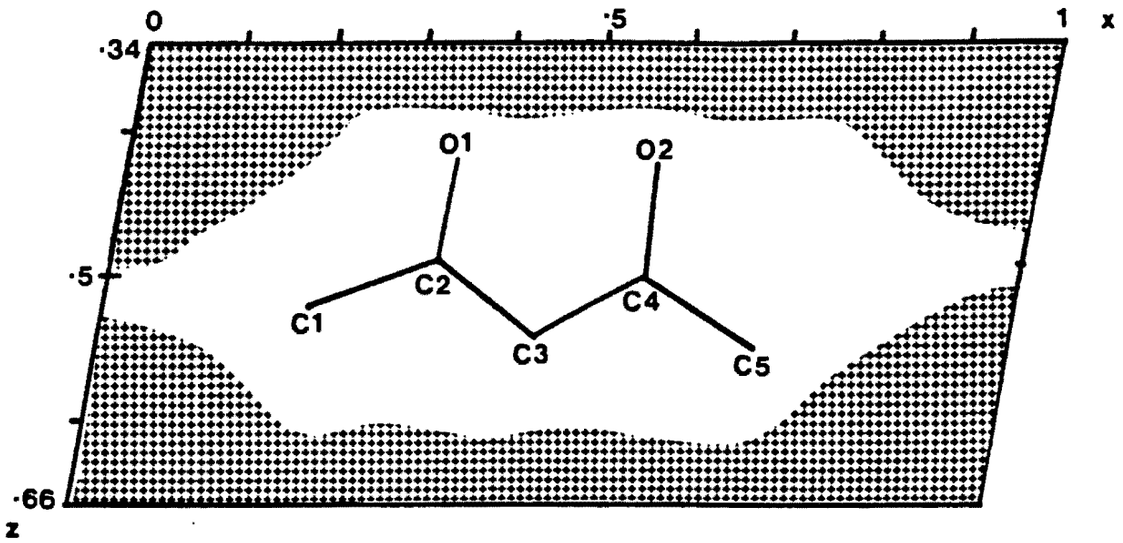

Fig 4.13c Section of the channel of Compound (XIII) viewed along [010] and sectioned at y = 1/2 showing the position of the guest acetylacetone molecule as located and minimized by EENY.

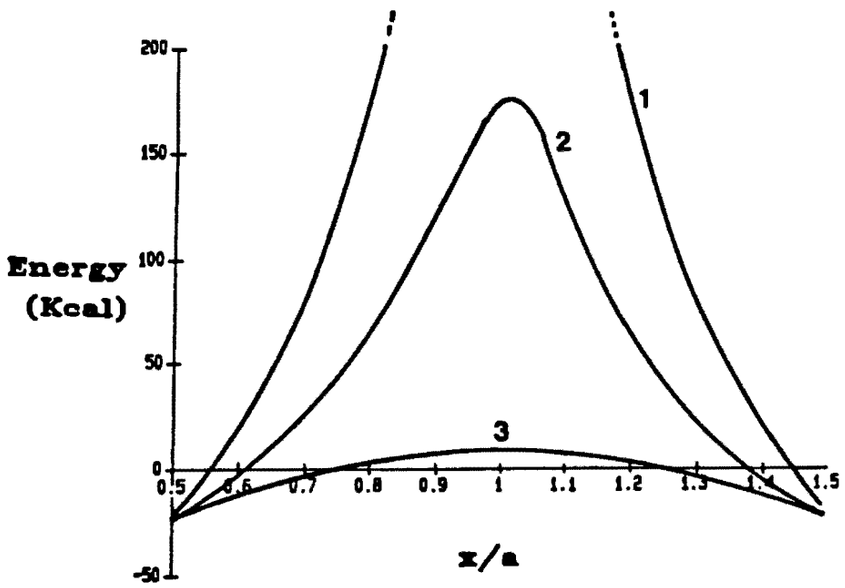

Fig 4.13d Potential energy plot of Compound (XIII) as the guest molecule is systematically moved through the channel with:

1) No host or guest freedom,
2) Guest allowed restricted freedom, and
3) Host and guest allowed partial freedom.

solution through to large differences in the temperature of the solutions. Hot solutions, at various temperatures, were cooled in a variety of manners: quickly, slowly and some retained isothermally for several days. The technique of producing crystals with anything but the guest molecules mentioned below, however, has thus far proved to be elusive. The cross-sectional area of the channels (≈3.6Å, determined by volume calculations) is too small to accommodate aromatic guests and it appears that there is a strong preference for aliphatic molecules which contain a skeleton of five atoms. Thus, to date, the only three clathrates reported containing this host complex are these two compounds and that reported by Bond *et al*[4.4] which included methyl cellosolve (2-methoxyethanol) as the guest molecule.

This preference for molecules which have 5 atom linear chains has been used to selectively retain butanol from a mixture of alcohols when passed through a gas chromatograph. This is discussed in more detail in Chapter 5.

The potential energy of the guest molecules in their crystal lattices has been studied in order to determine possible dynamic conformation changes in the host lattice, and to ascertain the nature and strength of the forces which retain the guest molecule in the clathrate.

Using the program EENY, attempts were first made to place the guest molecule in the channel of the clathrate. The shape of the channel was obtained by calculating the potential energy environment of a "probe molecule". A hydrogen atom was systematically moved throughout the

region of the channel. This region was sliced into eleven sections along the y-direction and at each interval two-dimensional energy maps were evaluated and contoured at the zero kcal level. Movement within EENY is along the orthogonal axes. Thus for a monoclinic structure, movement in the xz plane is parallel to $\underline{c}$ for a z-translation but the x-translation is in the direction of a^*. Therefore movement in the true x direction required both a translation in the direction of $\underline{a}$ and one in the direction of $\underline{c}$, both translations involving a trigonometric function of beta. A model of the guest molecule, consisting of spheres representing van der Waals radii, was positioned so as to give minimal protrusion beyond the zero energy surface. The approximate guest coordinates were then refined by energy minimization. The refined atomic positions were essentially an intermediate between the two "half" molecules found in the crystal structure. The energy minimization places the guest molecule such that interactions between host and guest are at a minimum. No attempts were made to apply all the space group symmetry to the guest molecule and thus no guest-guest interactions were applied. Fig 4.13c shows the position of the guest molecule for Compound (XIII) in the channel which is bounded by the zero kcal energy contour.

For Compound (XIII), in order to ascertain the forces retaining the guest molecules within the clathrate, one of the two possible orientations of the acetylacetone was arbitrarily chosen. This molecule was then translated through the channel in steps of 1Å and the energy calculated on the assumption that both host and guest molecules remain rigid (Graph 1, Fig 4.13d). This model was then refined by allowing the guest molecule small variations in its rotational parameters, so that it

could twist about its centre, and undergo translation in the y-direction to overcome the undulations in the channel, in order to find a local minimum in the energy profile after each 1Å translation (Graph 2, Fig 4.13d). Partial conformational freedom of the host molecule was then permitted by allowing all six rings and the isothiocyanate ligands to twist about their Ni-N or pyridine-phenyl bonds (Graph 3, Fig 4.13d). After each host minimization, the guest was allowed small variations in its rotational parameters and its translation in the y-direction before host minimization was performed again. This cyclic host/guest energy minimization was repeated until a local minimum in potential energy was achieved. The guest was then translated a further 1Å along the channel and the procedure repeated. No account was taken of partial atomic charges nor of dipole interactions, and the energy values derived mean little in an absolute sense. No parameters could be found for the constants applying to a nickel atom and thus the nickel atom was omitted from the host structure. Parallel runs with a methyl group, a sulphur atom, an oxygen atom and a hydrogen atom as the central atom indicated that this atom is at a distance which is too great to contribute significantly to any intermolecular interactions. Thus all host/guest interactions are constant (within 0.3kcal) regardless of the central atom.

To ensure that all host/guest interactions were calculated by EENY, all host molecules inside a box defining the extremities of the channel were located using the PACKAN subroutine of OPEC.

The energy profiles displayed in Fig 4.13d represent the extremes for

modelling the movement of guest molecules through the channel. On one side, the guest is forced as a rigid body past the obstructions offered by the host ligands which are not allowed to adjust themselves to enable easier passage of the guest. This model results in energy values which are completely unrealistic and is obviously incorrect. The other extreme is when both host and guest can freely adjust themselves to allow passage of the guest molecule through the channel. This results in an energy barrier which is extremely low, suggesting that there is no restriction on the guests' movements. This is clearly unreasonable because if this were the case, then the stability of the clathrate crystal would be very low owing to the guest being able to diffuse out of the host lattice very rapidly. Although the crystals are not indefinitely stable when removed from their mother liquor, they do not decompose as rapidly as the solvent evaporates, indicating that the guest is partially restricted in its movements. Thus a more realistic clathrate energy model should include a guest with rotational freedom, and partial conformational freedom of the host molecule. Experimentally, an activation energy for the diffusion of *p*-xylene through a host lattice of $[Ni(NCS)_2(4\text{-}MePy)_4]$ has been established as *ca* 15.8 kcal mol^{-1} [4.5]. This is consistent with a clathration model which involves the host adopting a specific conformation in order to entrap guest molecules, thus preventing totally free diffusion of these molecules.

The large difference in the figures for the Res Vol/G-atom between Compounds (XIII) and (XIV) (18.8 *vs* 27.3$Å^3$) indicates the rigidity of the host framework. Acetylacetone has two oxygen atoms on the side of a linear skeleton whilst 1-chlorobutane consists solely of a straight

chain. Thus the width of the latter molecule is far less than that of the former but even with this narrow molecule in the host lattice, there is no reduction in the size of the cavity. Thus the host structure is unaffected by the width of the guest atom: as long as the length is correct, and provided the molecule is less than a certain width, the host framework will most likely always be the same.

4.5 CLASS D

The last four compounds reported in the work are all α-phase compounds and thus there is no cavity to describe. However it is still informative to study packing diagrams to observe how these host molecules can pack so that no large spaces result. Thus a brief description and a packing diagram from a suitable view will be given for each of these compounds.

Compound (XV) $[Ni(NCS)_2(dmso)_2(4\text{-}PhPy)_2]$, C2/c, Z = 4,
a = 10.016, b = 23.430, c = 13.290Å, β = 96.94°.

Although this compound packs in the C2/c space group which has been observed in six previous compounds reported in this work, the packing here is very different. The 4-PhPy ligands are orientated parallel to the b axis with the NCS^- moiety parallel to the xz plane, and the reduced length and increased depth of the dmso molecule, when compared with either a 4-MePy or 4-PhPy ligand, result in a 'spider-web' pattern as illustrated in Fig 4.15a. This view indicates the lack of suitable space to accommodate a guest molecule which is also prevented from lying in between the layers of dmso/NCS^- ligands by the second carbon of dmso

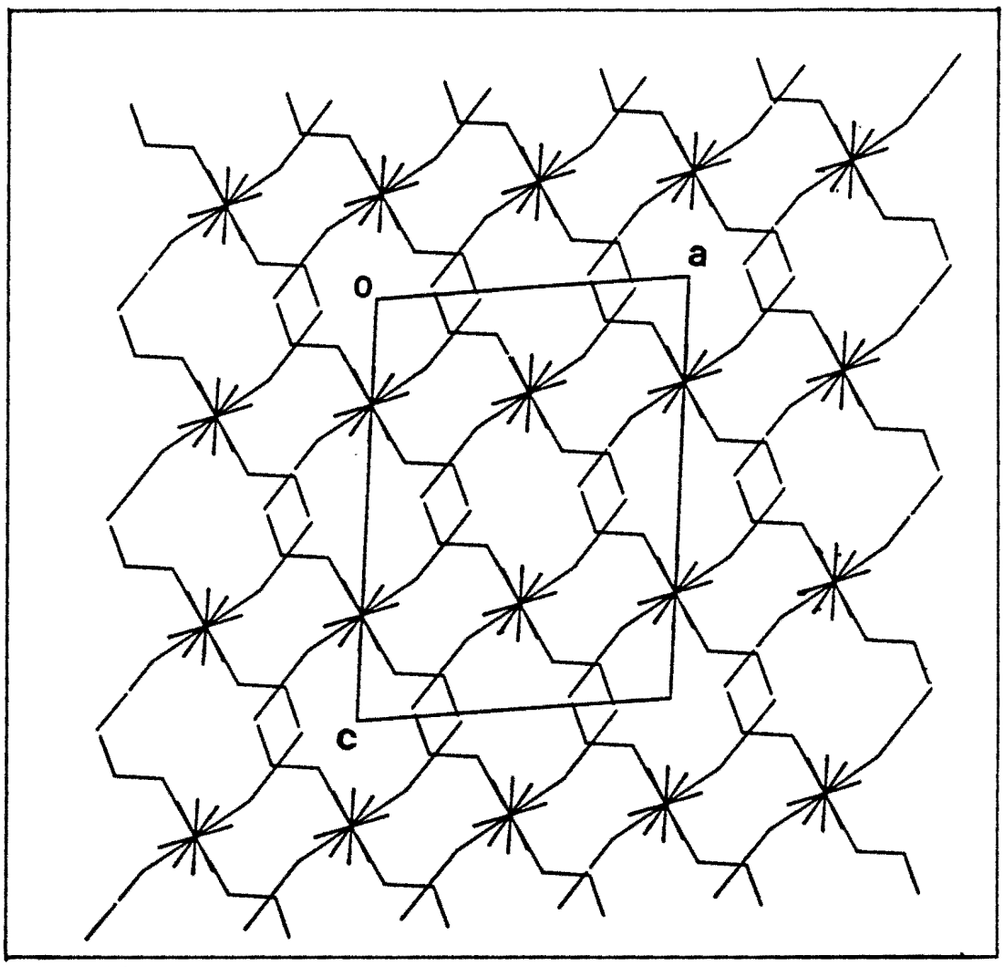

Fig 4.15a Packing diagram of Compound (XV) viewed along [010].

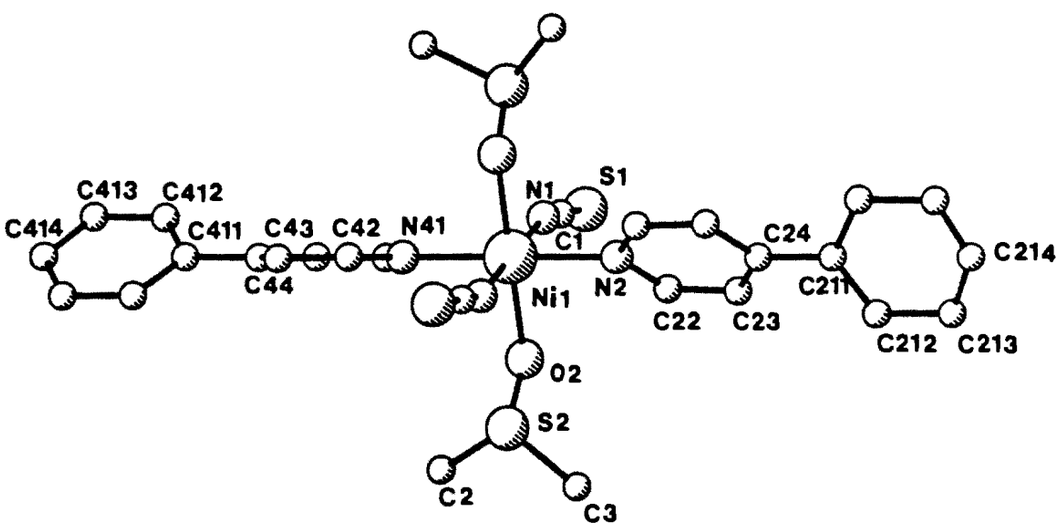

Fig 4.15b Perspective view of Compound (XV) with atomic nomenclature.

Fig 4.15c Space filling diagram of Compound (XV).

which is underneath the first when viewed from this direction. The Ni atom, NCS^- moieties and the S and O atoms of the dmso ligand are all in a plane parallel to the xz plane with the two 4-PhPy ligands perpendicular to this plane. The packing is similar to that of the mixed pyridine Werner clathrate $[Ni(NCS)_2(4\text{-}MePy)_2(4\text{-}PhPy)_2]$ (*e.g.* Compound (XIV)) but the channel present in that structure has been closed owing to the Ni atoms packing closer together. Fig 4.15b shows a perspective view of the molecule with atomic nomenclature whilst Fig 4.15c is a coloured space filling diagram of this complex.

Compound (XVI) $[NiCl_2(dmso)_2(4\text{-}PhPy)_2]$, $P2_1/c$, $Z = 2$,
$a = 7.800$, $b = 8.250$, $c = 22.138$Å, $\beta = 95.15°$

With the nickel atom located on the centre of symmetry at Wyckoff position *a*, the molecules of this compound run in parallel 'ribbons' in the direction of the b axis at $z = 0$ and $z = 1/2$. The 4-PhPy ligands are a few degrees off parallel to the c axis and the gap between these ligands on adjacent molecules is filled by the methyl groups of the dmso ligands. The packing diagram illustrated in Fig 4.16a shows how the host molecules (atomic nomenclature illustrated in Fig 4.16b) pack closer together than in the complex where all four neutral ligands are substituted pyridines *e.g.* Compound (IX).

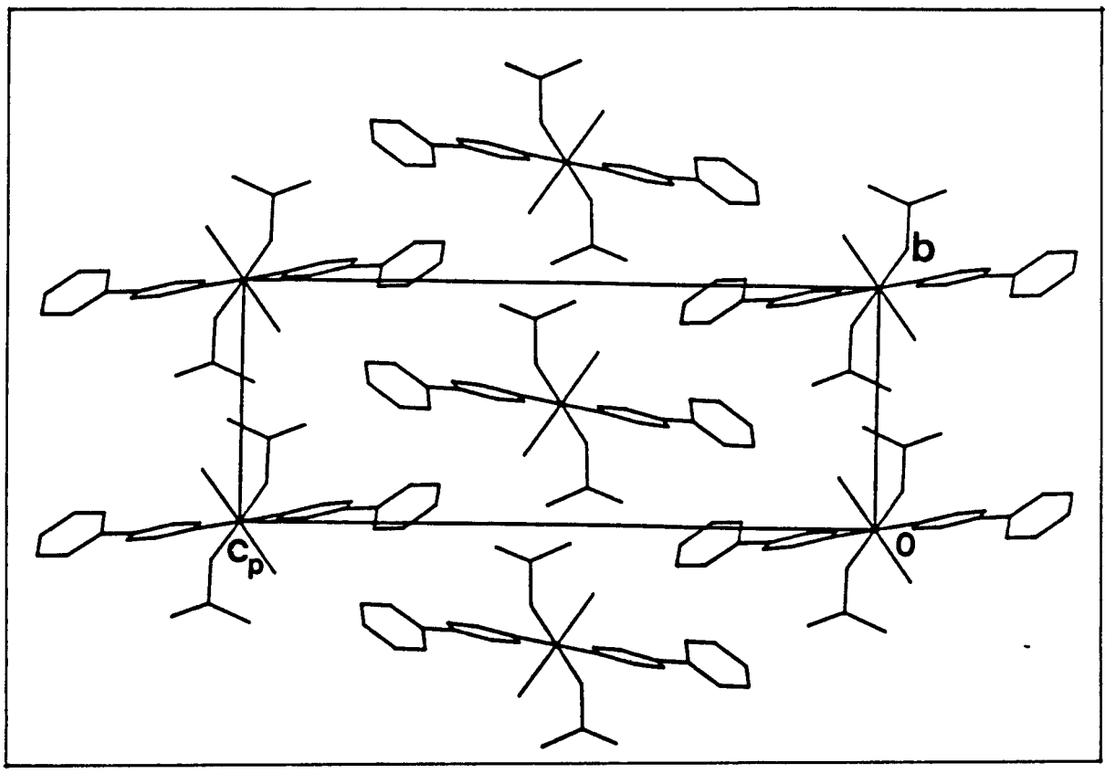

Fig 4.16a Packing diagram of Compound (XVI) viewed along [100].

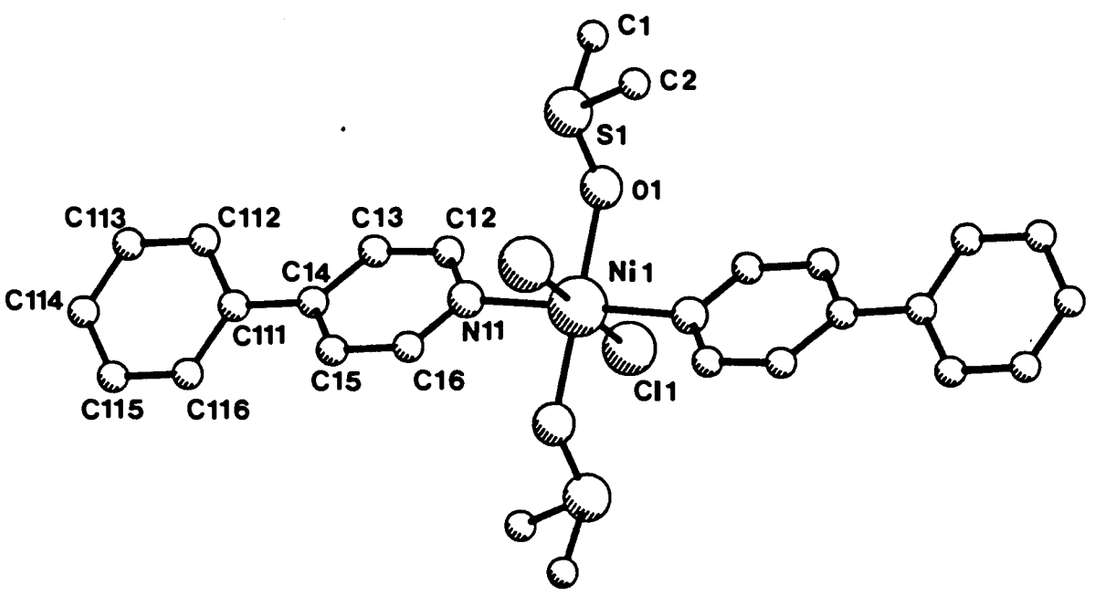

Fig 4.16b Perspective view of Compound (XVI) with atomic nomenclature.

Compound (XVII) $[Ni(NCS)_2(4\text{-}t\text{-}BuPy)_4]$, $I4_1/a$, Z = 8,
a = 21.501, c = 18.003Å

The packing of this compound is very similar to the typical 'β-phase' of the $[Ni(NCS)_2(4\text{-}EtPy)_4]$ complex[4.6] although the cell parameters are somewhat different (a = 16.738, c = 25.172Å). The packing, viewed along [001] is shown in Fig 4.17a whilst Fig 4.17b shows a perspective view of an individual molecule with atomic nomenclature. A coloured space filling diagram of this complex is displayed in Fig 4.17c which illustrates the 'bulkiness' of the *t*-butyl group of the substituted pyridine.

Compound (XVIII) $[Ni(NCS)_2(4\text{-}BzPy)_4]$, Cc, Z = 4,
a = 9.686, b = 25.015, c = 17.728Å, β = 90.29°

This compound packs in 'ribbons' running parallel to b with the nickel atom alternating between x = 0 and x = 1/2. The pyridine groups are all nearly perpendicular to the xy plane whilst the phenyl moieties are parallel to the same plane. Fig 4.18a shows a perspective view of the molecule with atomic nomenclature whilst Fig 4.18b illustrates the packing as viewed along [100]. Fig 4.18c is a coloured space filling diagram of the molecule.

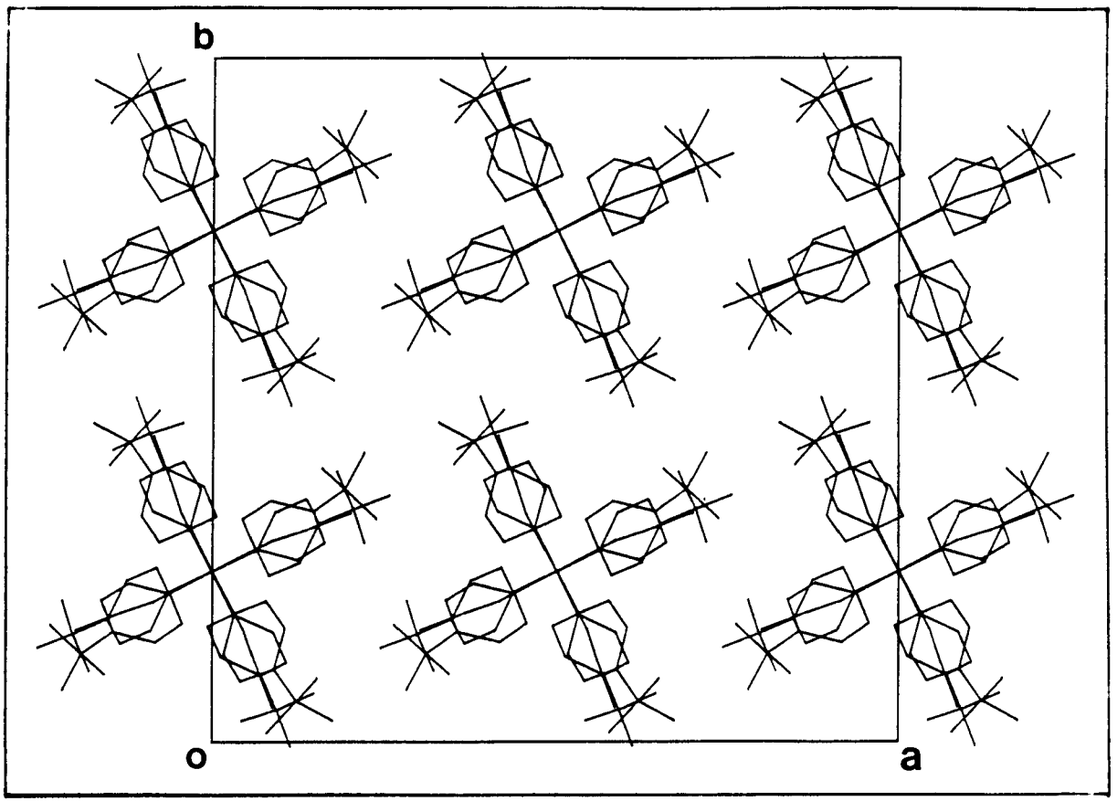

Fig 4.17a Packing diagram of Compound (XVII) viewed along [001].

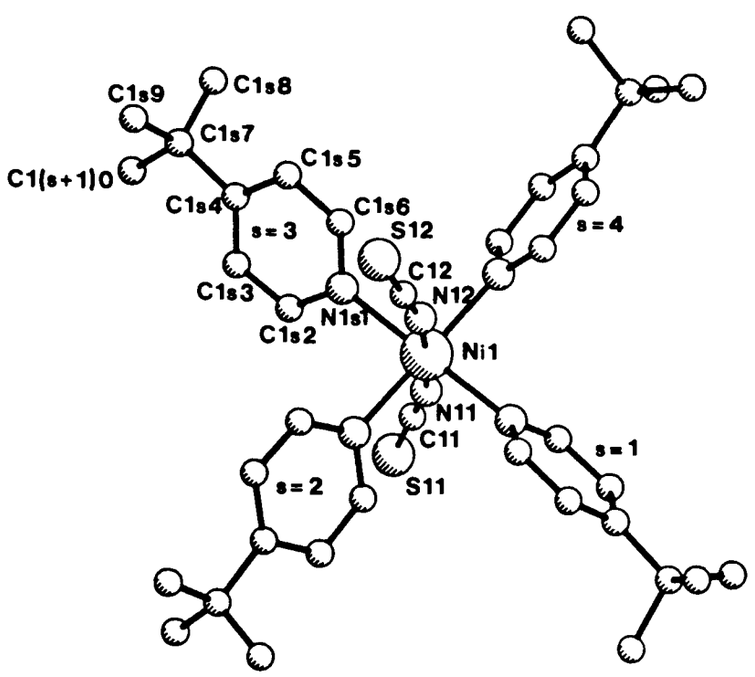

Fig 4.17b Perspective view of Compound (XVII) showing atomic nomenclature of one of the host molecules.

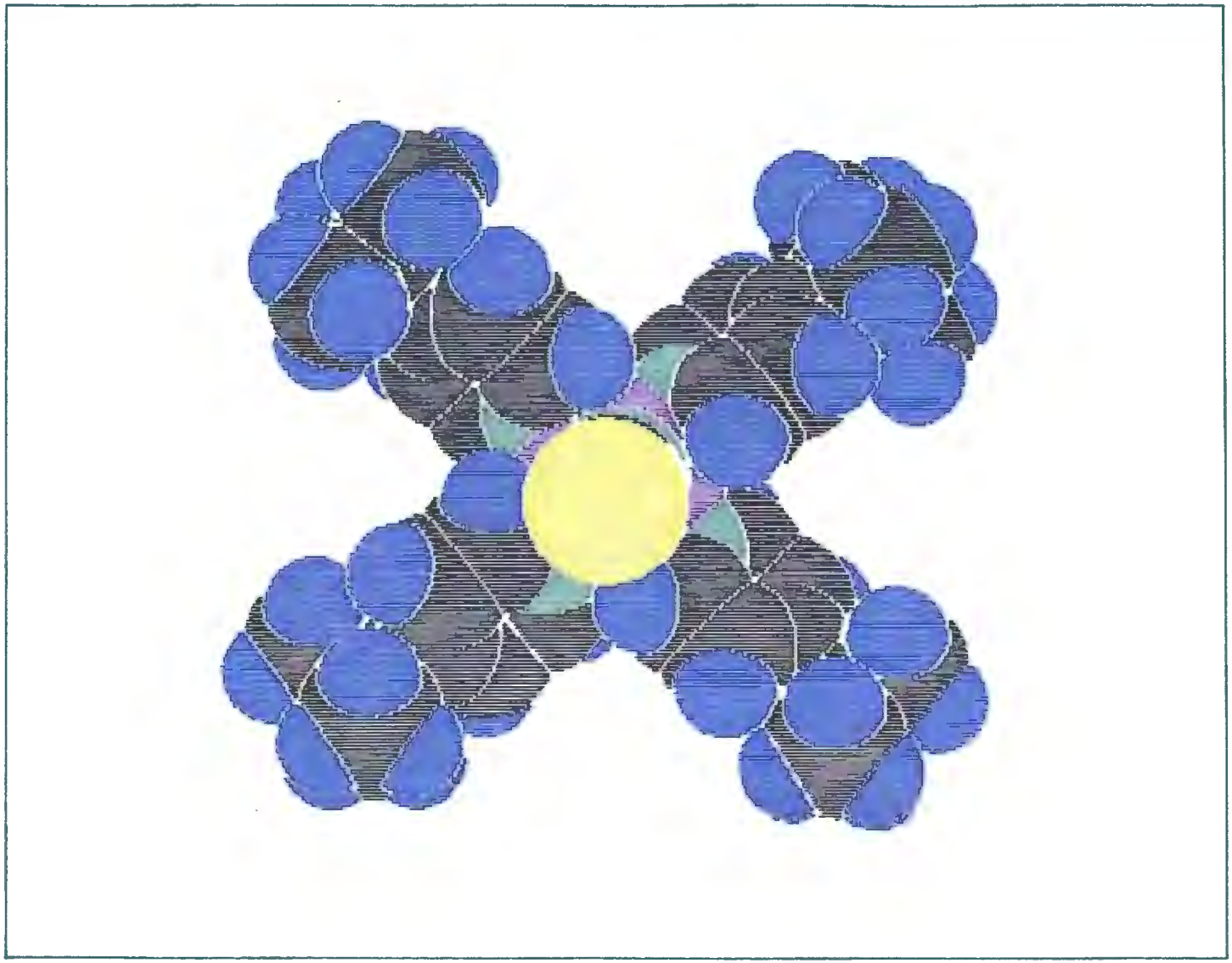

Alchemy

TRIPOS Associates

St. Louis, Mo.

Fig 4.17c Space filling diagram of Compound (XVII).

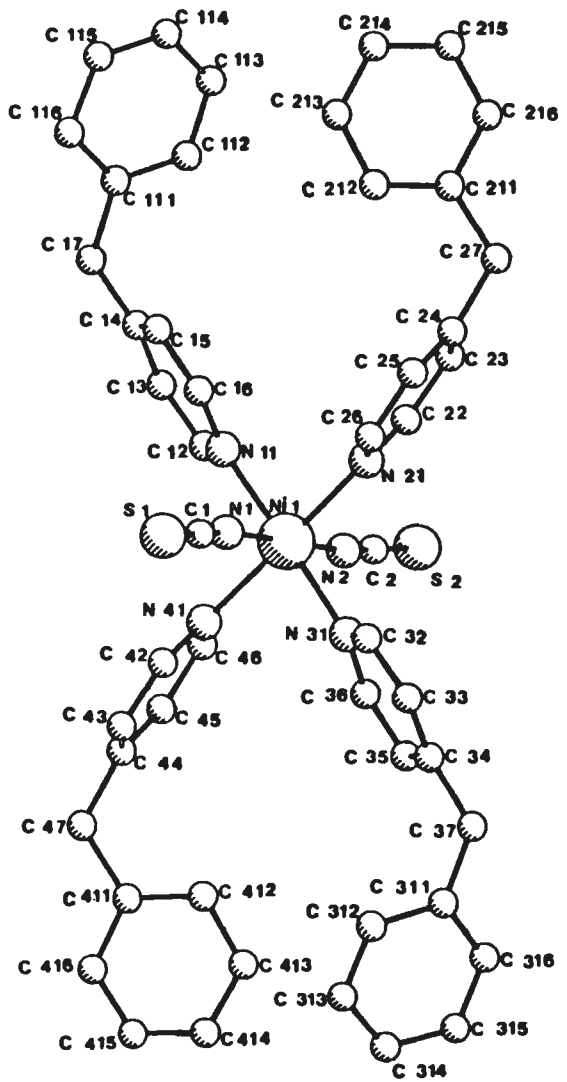

Fig 4.18a Perspective view of Compound (XVIII) with atomic nomenclature.

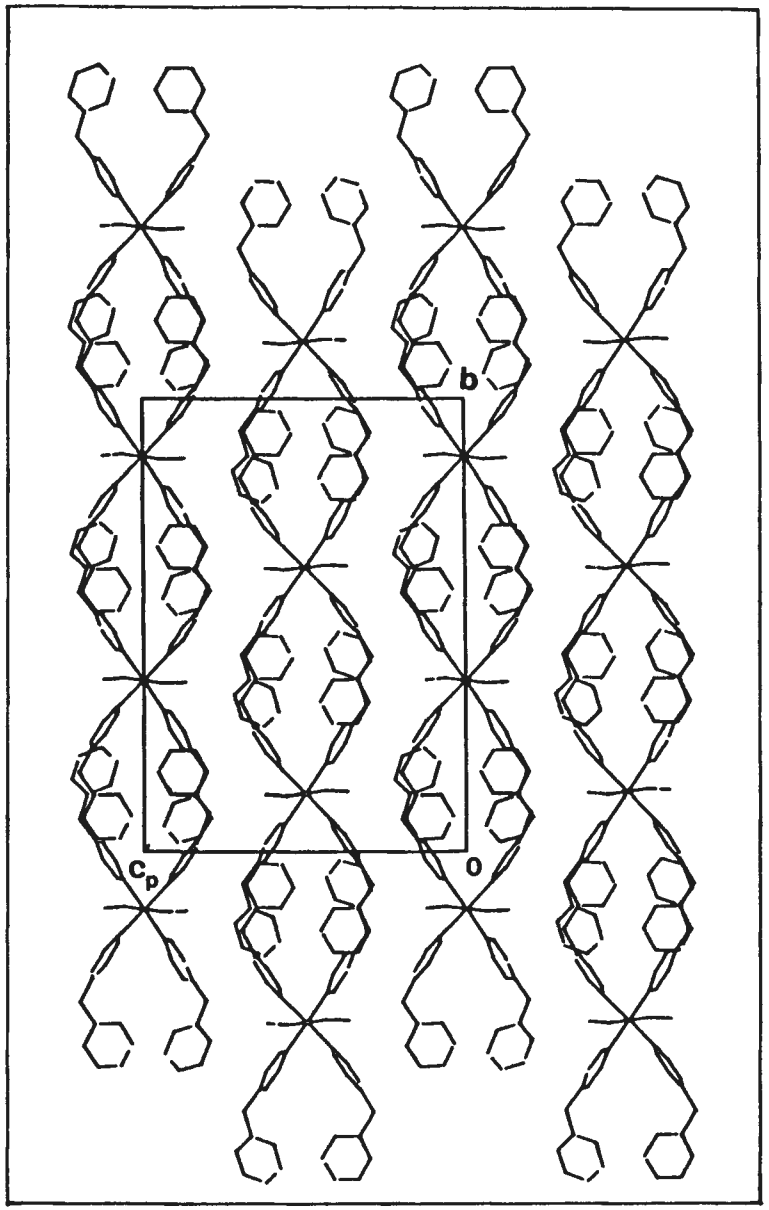

Fig 4.18b Packing diagram of Compound (XVIII) viewed along [100].

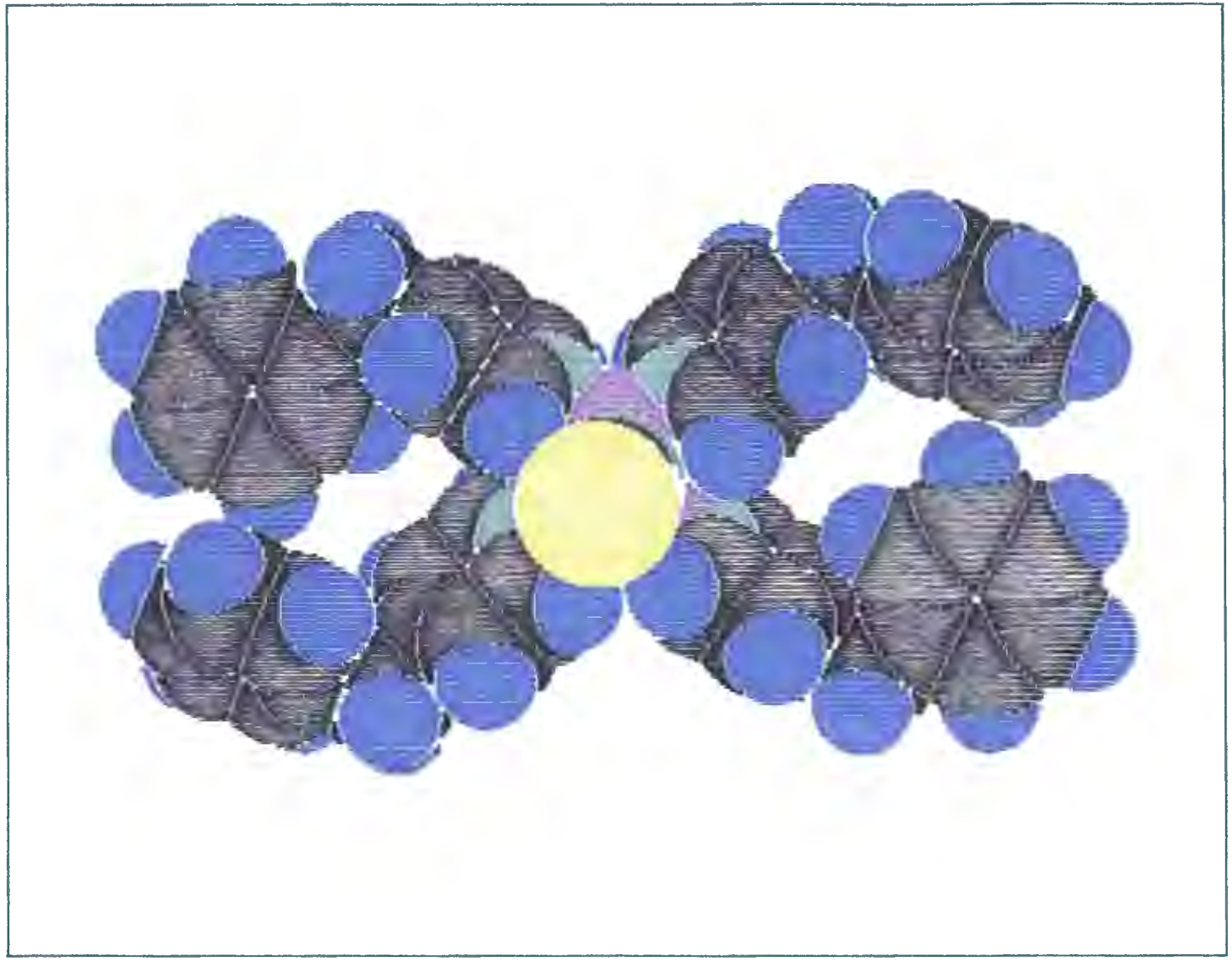

Alchemy

TRIPOS Associates

St. Louis, Mo.

Fig 4.18c Space filling diagram of Compound (XVIII).

4.6 TRENDS IN PACKING BETWEEN MOLECULES

Two of the most pertinent questions regarding Werner clathrates are:

i) why do some host molecules form clathrates with a particular guest solvent but not with others and

ii) with the same guest molecule, why does variation of the pyridine substituent affect the complex's ability to form a clathrate?

For the 4-PhPy host, even if we consider the NCS^- moiety as a rigid group, there are ten fragments (4 pyridine rings, 4 phenyl rings and two anion ligands) that can rotate and thus the number of possible conformations that the molecule can adopt is infinite! It is the rotation about the Ni-N bonds that has been suggested[4.5] as one of the possible reasons to explain the formation of clathrates by these kinds of inorganic complexes. This freedom supposedly allows adjustment of the host molecules' to accommodate a variety of guests, differing in size and shape. It has been shown[4.7] that it is the *ortho* hydrogens on the pyridine ring that govern the extent to which the substituted pyridines may turn, while the variation of substituents at the *meta* and *para* positions makes only a secondary contribution. Thus by changing the pyridine substituent from a phenyl to a benzyl group (*i.e.* adding an extra bridging methylene group), the molecule's ability to allow rotation about the $Ni\text{-}N_{py}$ bond should be unaffected and therefore there must be another factor to explain the failure of Compound (XVIII) to form a clathrate.

In order to try and ascertain trends in clathrate formation, it is probably easier to approach this complicated process by asking the negative question: is there any trend among molecules which points at

non-clathrate formation? To answer this question, it is necessary to look at several α-phase compounds.

4.7 ALPHA-PHASE COMPOUNDS

With the exception of the five α-phase clathrates described in this work (Compounds (I), and (XV) - (XVIII)), there are 4 other complexes mentioned in the literature that are non-clathrating $[Ni(NCS)_2(RPy)_4]$ complexes. These are, with codenames in square parentheses:

R = 4-H *i.e.* unsubstituted pyridine [Py][4.8],

R = 4-methyl [Me][4.9],

R = 4-ethyl[4.6], with two different conformations, [Et1] and [Et2],

and R = 4-vinyl [Vi][4.10].

The 3,5-dimethylpyridine (3,5-lutidene)[4.7] [Lut] complex could also possibly be included in this group, but the variation in the substituents' position makes direct comparison difficult.

It is interesting to compare the torsion angles of these α-phase complexes. It is reasonable to assume that four pyridines are required in order for the host to gain the required degrees of freedom and thus Compounds (XV) and (XVI) have been excluded from this comparison. The inner, or pyridine, torsion angles are defined as:

$$\tau_x = \min |N(1) - Ni(1) - N(x1) - C(xy)|$$

where y = 2 or 6 for x = 1-4. For the ethyl substituted pyridines ([Et1&2] there are two independent host molecules in the asymmetric unit designated a and b. Thus the above formula for each host becomes:

$$\tau_x = \min |N(11) - Ni(1) - N(1x1) - C(1xy)|$$

or $$= \min |N(21) - Ni(2) - N(2x1) - C(2xy)|.$$

If a molecule crystallizes in a centrosymmetric space group, the different enantiomers will have opposite signs for the same torsion angle. Thus, although some of the molecules give negative torsion angles if the supplied coordinates are used, the angles quoted in Table 4.1 are such that the majority within a structure are positive. When a molecule is located on a centre of symmetry however, there are restrictions placed on the values of the torsion angles that the molecule can display. Because of the position of the pseudo two-fold axis in Compound (XVIII) , and because of the C_i symmetry of the host molecule in [Py], both have $\tau_1 \approx -\tau_3$ and $\tau_2 \approx -\tau_4$.

Labelling of the ligands in each structure, although carried out cyclically, was initially done arbitrarily and thus it is not feasible to compare the various τ_i angles directly. A systematic search for the combination of torsion angles (τ_1 to τ_4) which yielded a minimum in the sum of the squares of the differences was performed in order to make more meaningful comparisons. This search was performed with the negative angles both included and also set temporarily to the equal positive number and also with the two compounds (XVIII) and [Py] excluded altogether to try and detect any trends in the packing with respect to their ligand arrangements. The reason for the setting of the negative angles to the equal positive value is because although the energy might be higher for the ++-- configuration, the positioning of the guest molecule might be independent of the orientation of the ring. However the search would be biased by these negative angles and if the similarity is in the magnitude and not the direction of the rotation about the Ni-N bond, then this trend might be missed if they were to be included.

Table 4.1 Inner Torsion angles for the 10 tetra substituted-pyridine α-phase host molecules.

Compound	τ_1	τ_2	τ_3	τ_4
I	41	46	32	38
XVII	30	46	36	42
XVIII	34	14	-37	-25
Py	25	36	-25	-36
Me	34	38	29	34
Et1a	39	45	38	38
Et1b	36	33	41	36
Et2a	44	35	33	41
Et2b	33	47	35	37
Vi	36	40	38	43

Table 4.2 Comparison of packing efficiency and carbon/hydrogen ratio for the 8 different α-phase complexes.

Compound	Packing effic. ($Å^3$/non-H atom)	No. H/No. C ratio (ring atoms)
I	18.6	0.82
XVII	22.1	1.44
XVIII	18.2	0.92
Py	18.7	1.00
Me	20.6	1.17
Et1 & 2	20.8	1.29
Vi	19.9	1.00
Lut	21.2	1.29
XV	19.8	
XVI	20.3	

The results of these searches are displayed as histograms in Figs 4.19 - 4.21. The four groups of torsion angles which yielded the minimum in the search are now labelled τ_A, τ_B, τ_C and τ_D as the search has rearranged the angles so that for the minimized case, τ(1,2,3 & 4) are not necessarily the same as τ(A,B,C and D). Excluding [Py] and Compound (XVIII), the range of angles that the remaining compounds adopt is small (29-47°). They all have the ++++ propeller configuration common to many Werner clathrates[4.11] which is the configuration that has the lowest potential energy.

Looking at Fig 4.19 which displays the results of the search of the 10 α-phase compounds, the following can be observed:

i) there is no trend of incremental variation in the new groups of torsion angles *e.g.* $\tau_A < \tau_B < \tau_C < \tau_D$.

ii) the *trans* torsion angles (τ_A/τ_C and τ_B/τ_D) do not have any obvious relationship to each other.

iii) the range of torsion angles displayed is extremely narrow (25 to 47° if we exclude the 14° of Compound (XVIII) and take the absolute value of all the angles). This variation of torsion angles is displayed in Fig 4.22a which shows the distribution of the 39 angles whilst Fig 4.22b illustrates the comparable histogram of the β-phase complexes.

Another factor which could govern clathrate formation is the ability of the complex to pack efficiently. The better the packing, the less the free space within the host framework and therefore the smaller the likelihood of guest's being included. The packing efficiency of a

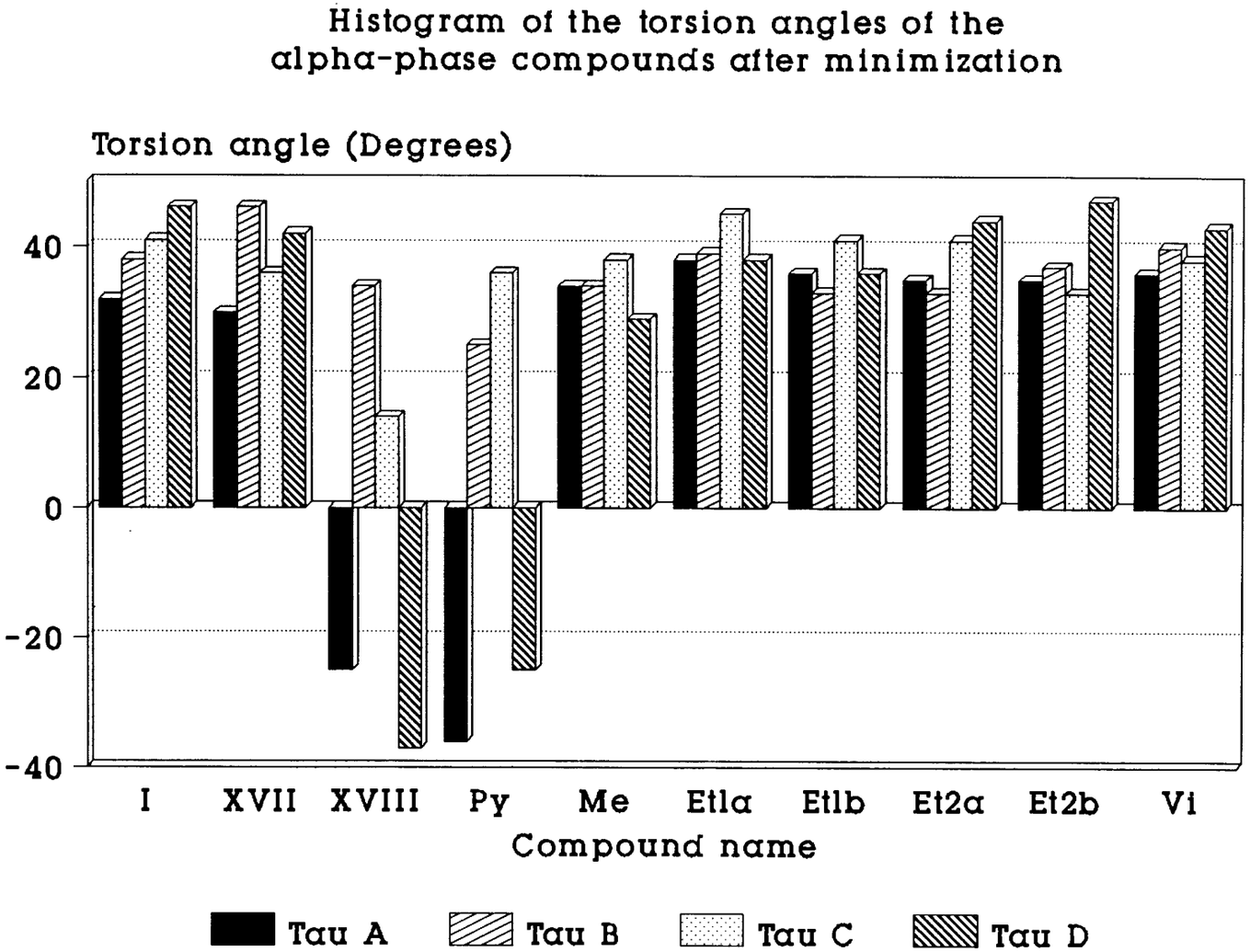

Fig 4.19 Results of a minimization of the torsion angles for all 10 α-phase complexes.

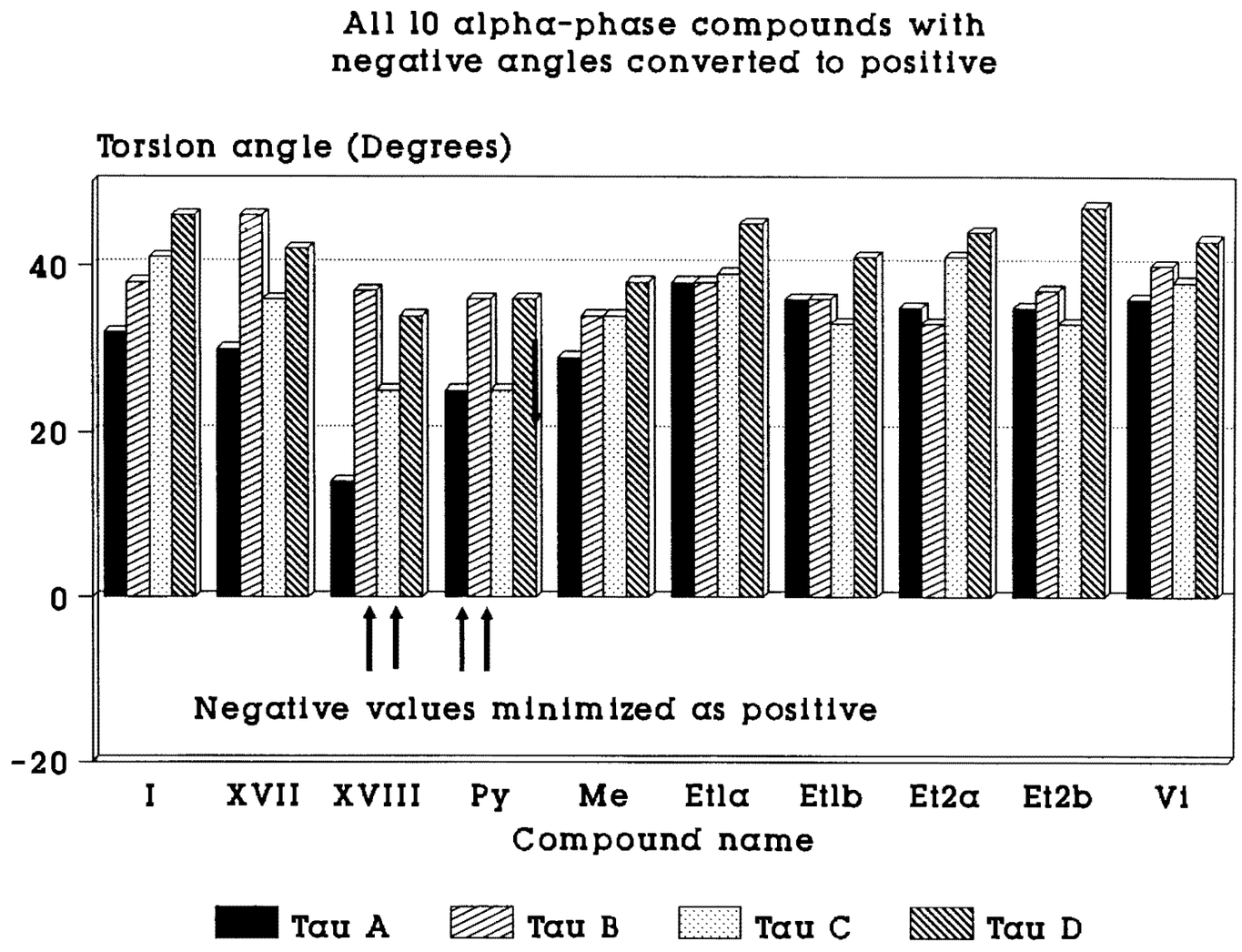

Fig 4.20 Results of a minimization of the torsion angles for all 10 α-phase complexes with negative values converted to equivalent positive values.

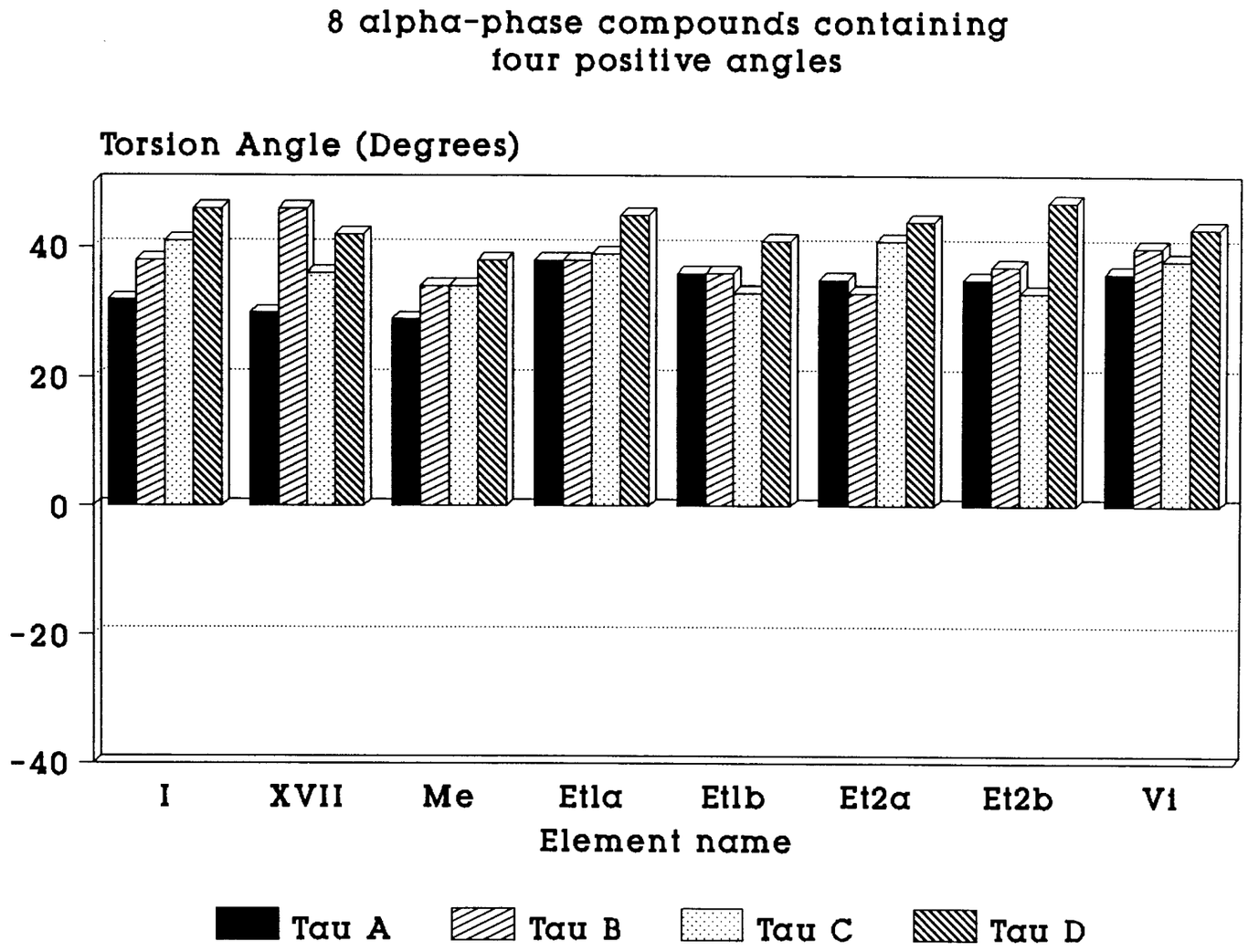

Fig 4.21 Results of a minimization of the torsion angles for all those α-phase complexes having all four angles as positive values.

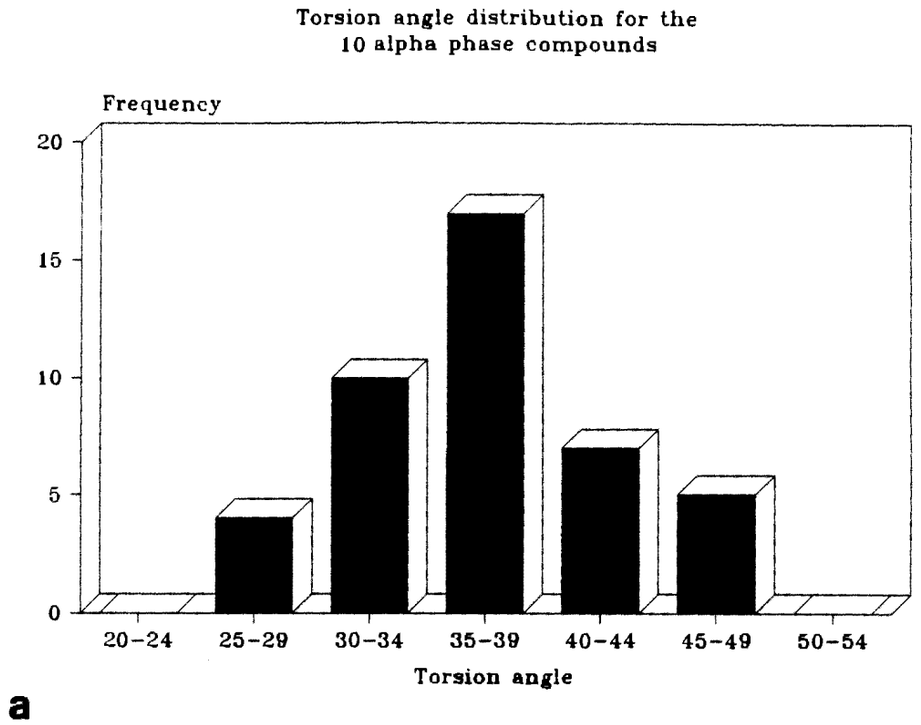

a

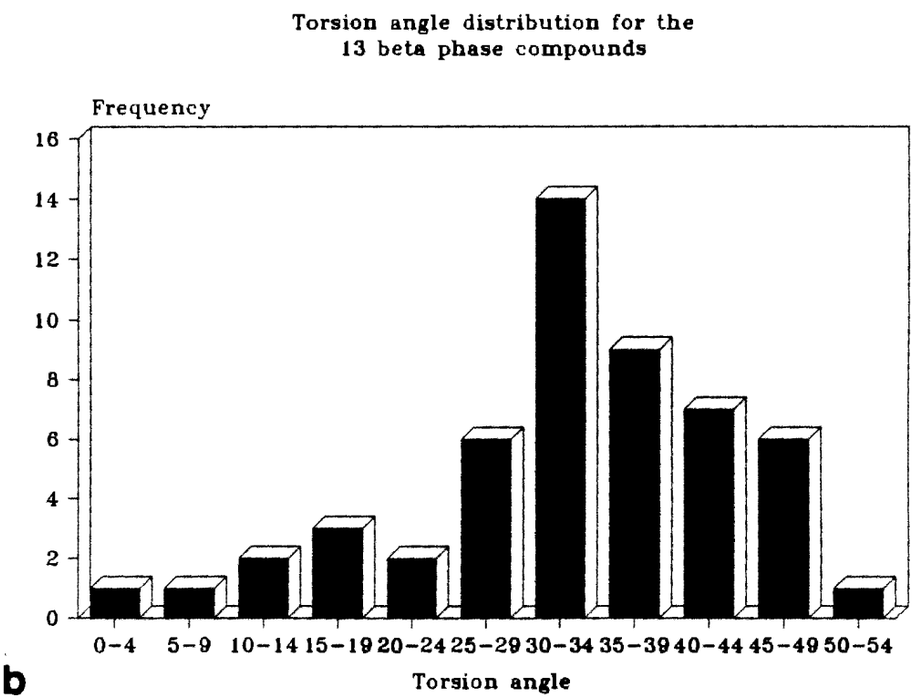

b

Fig 4.22 Histogram illustrating the frequency distribution of torsion angles for the a) α-phase and b) β-phase complexes.

complex is defined as: [volume cell/(total number of non-H atoms in the cell)] and the packing efficiency for all the α-phase complexes (including Compounds (XV), (XVI) and [Lut]) are listed in Table 4.2.

The order of decreasing packing efficiency is:
XVIII > I > [Py] > XV > [Vi] > XVI > [Me] > [Et] > [Lut] > XVII.
For the following progression of ligands, the H/C ratio of the pyridine rings and the packing efficiency of their respective host compounds is reported.

	Py	Me	Et	XVII
	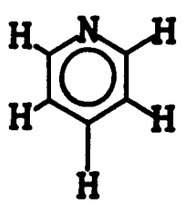	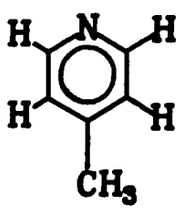	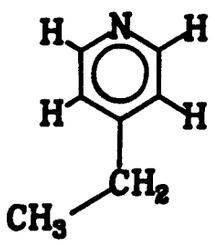	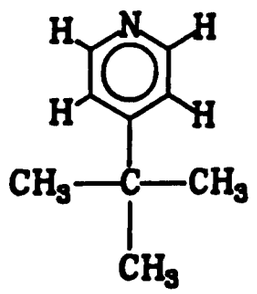
H/C ratio	1.00	1.17	1.29	1.44
Pack. eff. (A^3/atom)	18.7	20.6	20.8	22.1

It can be observed that there is a direct relationship between the degree of aromaticity of the ligand and the ability of the complex to pack efficiently: the more aliphatic character the ligand possesses, the greater the volume required for packing. Thus, for a Werner Clathrate containing a new ligand, knowing the H/C ratio of the substituted pyridine ligand, it would be possible to predict the volume that the complex would require to pack in an α-phase form. If we plot a graph of packing efficiency *vs* H/C ratio for all the α-phase complexes

(Fig 4.23), the 'goodness of fit' for the straight line drawn through the points is reasonable ($r \approx 0.95$). In fact, with the exception of Compound (XVIII) which is misplaced by one position, the order of H/C ratio is the same as that for the packing efficiency ratio for these complexes.

The following negative statement is true; if a host molecule cannot pack efficiently enough, it can only form a β-phase clathrate *i.e.* guest molecules will always be included, however the converse is not true. All of these α-phase complexes can pack efficiently but this does not tell us if they can form a host-guest complex.

A third factor to consider is that of solubility of the host complex powder in the prospective guest solvent. Previous studies[4.3] have indicated that there is a possible relationship between solubility and clathrate formation. With the 4-ViPy and 4-EtPy derivatives, there appears to be a range of solubilities from which the formation of clathrates is possible. Below this range, too little host powder can dissolve to form crystals *i.e.* K_{sp} is too small, whilst above it, the host is too soluble and will not crystallize.

These observations can be understood in terms of simple thermodynamic considerations, as previously undertaken by Lipkowski[4.12] whereby the equilibrium constant of the reaction:

$$H(\text{solution}) + nG(l) = HG_n(\text{solid})$$

where: H = host complex,

G = guest solvent

HG_n = clathrate,

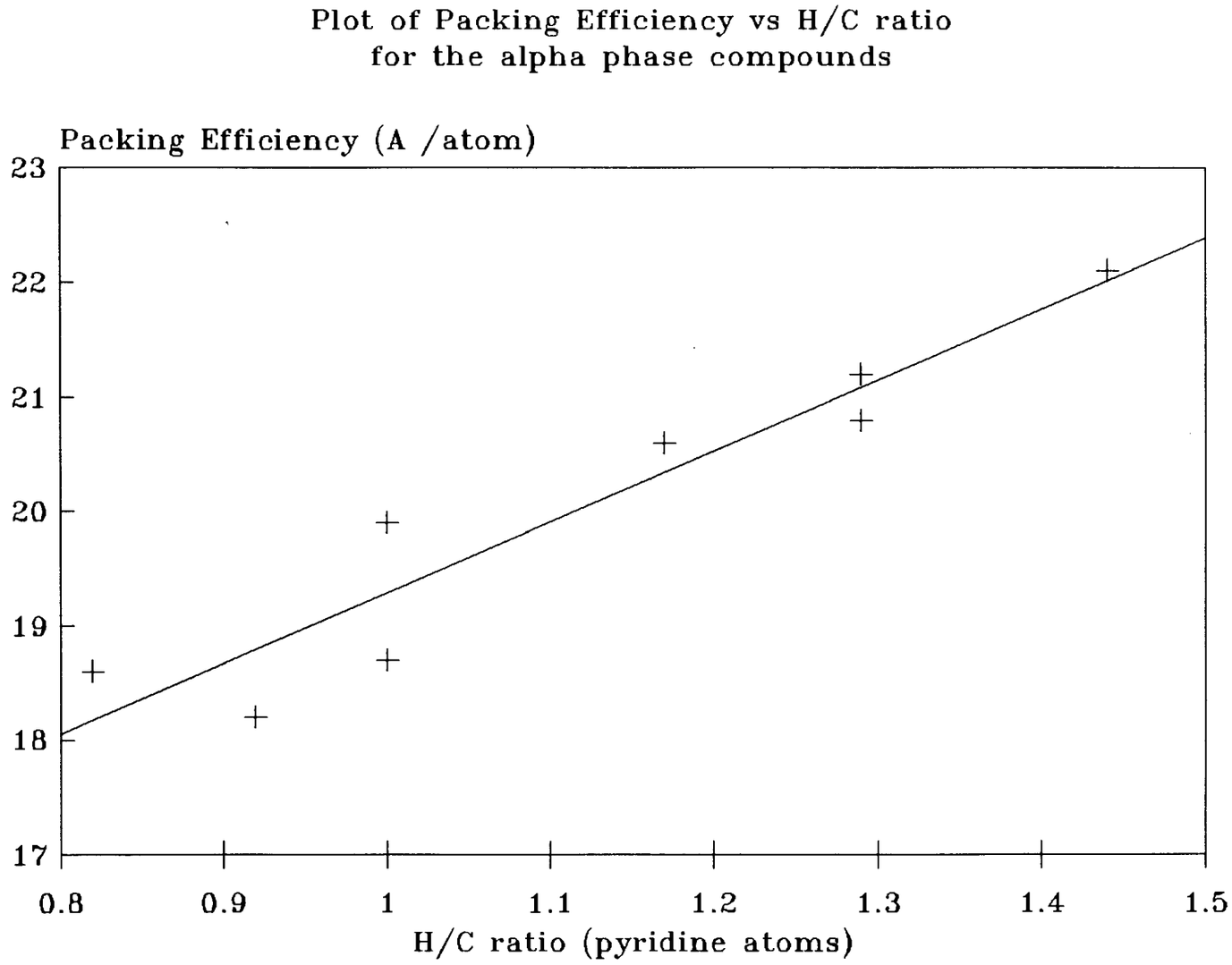

Fig 4.23 Best-line plot of packing efficiency *vs* pyridine ring C/H ratio for the α-phase complexes.

is approximated by:

$$K = \frac{[HG_n]}{[H][G]^n}$$

Since the clathrate is a solid, and the guest solvent is in such excess so as to be considered as a constant, the equation reduces to:

$$K \propto 1 / [H]$$

i.e. the less soluble the host complex is in a given solvent, the larger the value of K, and the greater the likelihood of clathrate formation. Obviously, the validity of the proportionality is dependent on the attainment of equilibrium, otherwise, if something were to be completely insoluble, it would imply that clathrate formation would be assured -. wishful thinking unfortunately !

The solubilities of the two host Compounds (XVII) and (XVIII) have been measured in various potential guest solvents, and these are reported in Table 4.3. The solubilities, expressed as mole fraction of host at saturation at 56°C, show that the tertiary-butyl host (XVII) is only sparingly soluble, but that the benzyl host (XVIII) can reach solubilities of $X_{host} = 35.5 \times 10^{-3}$. These values are similar to those found for the 4-vinyl host in chloroform, which yielded an inclusion compound[4.13]. Thus solubility is not the decisive factor which dictates clathrate formation, but it must be a contributing factor.

Table 4.3 Solubilities of Host Compounds (XVII) and (XVIII) at 56°C expressed as 10^3 X_{host}.

Guest	(XVII)	(XVIII)
dmso	35.3	8.6
thf	23.3	5.2
$CHCl_3$	17.6	3.7
EtOH	2.7	1.7

4.8 BETA-PHASE STRUCTURES

For the 13 β-phase structures reported in this work, the range of space groups in which the complexes crystallize is extremely varied even within the individual classes. In Class A, the symmetry of the space group decreases from the orthorhombic Fdd2 (Compound (II)) through monoclinic C2/c (Compounds (III) and (VII)) to $P2_1/n$ (Compounds (V) and (VI)) down to triclinic P1 (Compounds (IV) and (VIII)). The variation in the Class B compounds is equally dramatic: from $P2_12_12_1$ (Compound (IX)) to monoclinic C2/c (Compounds (XI) and (XII)) down to triclinic P1 (Compound (X)). It is interesting to note that unlike in the 4-ViPy derivative host complex[4.10], the variation in the substituents positions on the guest xylene molecules causes a major rearrangement of the host molecules resulting in the compounds packing in different space groups *c.f.* Compounds (II) and (III), each with two guest molecules, crystallize in Fdd2 for the *ortho*- and C2/c for the *meta*-xylene. Variation of the anionic ligand causes a similar variation even with the same guest molecule *c.f.* Compound (III) (C2/c) with NCS^- *vs* Compound (X) (P1) with Cl^- both with *m*-xylene as the guest molecule. There is however

a predominance of structures crystallizing in the C2/c, or its subset $P2_1/n$, space group. These complexes all pack with two pyridine ligands and the nickel atom lying on the diad at Wyckoff position *e* if C2/c, or in an equivalent position but without the symmetry restriction if $P2_1/n$.

The most significant question regarding the β-phase clathrates is: what causes these dramatic alterations in packing when small variations (compared to the overall shape and size of the complexes) are made to either the guest or anionic ligand of the host ? Perhaps if we could establish what causes these variations, it might be possible to predict what will happen when the host is crystallized in the presence of a particular guest !

With the 4-phenylpyridine ligand, there is not only rotational freedom about the Ni-N bonds, but also free rotation about the C_{Py}-C_{Ph} bond. Thus for this host complex there are 8 torsion angles that can adjust in order to accomodate the guest molecules. These angles are displayed in Table 4.4 below with τ_1-τ_4 the inner or pyridine and τ_5-τ_8 the outer or phenyl torsion angles. These angles are defined as follows:

Pyridine: $\tau_x = \min|$ N(1) - Ni(1) - N(x1) - C(xy) $|$
with y = 2 or 6 for x = 1-4.

Phenyl: $\tau_{(x+4)} = \min|$ C(xy) - C(x4) - C(x11) - C(x1z) $|$
with y = 3 or 5, z = 2 or 6 for x = 1-4.

Considering the pyridine torsion angles initially, Fig 4.22b shows the wide range that are adopted by these β-phase complexes. Interestingly, all compounds, with the exception of Compound (VIII), adopt the ++++ configuration following Lipkowski's definition[4.12], *i.e.* all angles are

Table 4.4 Inner or pyridine (τ_1-τ_4) and outer or phenyl (τ_5-τ_8) torsion angles (°) for the β-phase structures.

Compound	τ_1	τ_2	τ_3	τ_4	τ_5	τ_6	τ_7	τ_8
II	32	38	38	45	43	23	40	32
III	19	46	29	20	-26	16	-29	23
IV	32	34	46	37	19	23	34	39
V	36	47	36	33	-35	28	32	33
VI	33	41	39	34	35	3	-29	27
VII	31	27	29	39	-24	-33	-26	30
VIII	-17	30	17	-25	-38	35	40	-36
IX	40	45	42	41	15	38	2	29
X	44	42	26	30	-21	-10	35	35
XI	39	40	49	31	27	0	3	1
XII	28	32	52	23	35	-32	-3	-34
XIII	10	33	13	36				
XIV	4	32	6	34				

positive indicating that the ligands are all rotated in the same direction. Compound (VIII) adopts the energetically higher +--+ configuration necessitated by the nickel being located on a centre of inversion.

The phenyl torsion angles do not adopt any particular conformation with respect to their parent pyridine ligand nor to each other. Presumably each moiety twists in order to best accomodate its particular guest. Thus their range is considerable, varying from -38° to 43° with no discernable pattern emerging.

If we consider the 8 "C2/c" structures (Compounds (III), (V)-(VII) and (XI)-(XIV)) and perform a search as conducted for the α-phase complexes, we obtain a result as displayed in Fig 4.24. It is interesting to note that for eight compounds, the torsion angles grouped together and labelled as τ_D are always the largest and correspond to the ligands lying on the diad (or in an equivalent position for the $P2_1/n$ structures). This indicates that the pyridine ligands forming the "walls" of the cavity (if viewed perpendicular to the xz plane) are twisted away from the Ni-NCS vector more than for those forming the "floor" and "roof" of the cavity. This effect results in the cavity being narrower in the z-direction (wall to wall) than in the y-direction (floor to roof).

This difference between the torsion angles lying along the diad compared to those perpendicular to it is dramatically illustrated for the two Class C compounds (Compounds (XIII) and (XIV)). The two pyridine ligands forming the "floor" of the cavity are, on average, 22° less than their

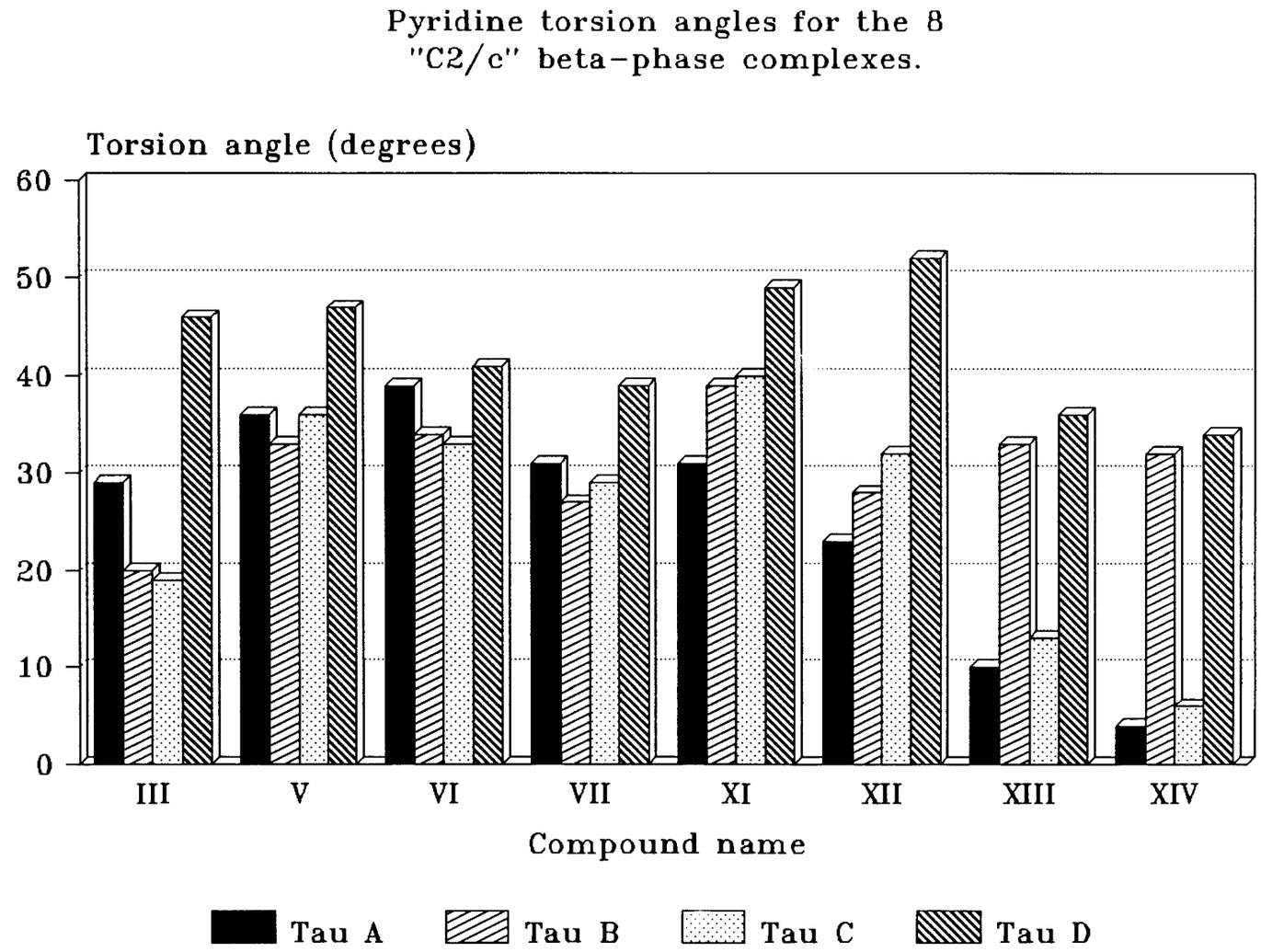

Fig 4.24 Results of a minimization of the torsion angles of the 8 β-phase complexes crystallizing in the C2/c or $P2_1/n$ space groups.

counterparts forming the "walls". The low values of τ_1 and τ_3 for both these structures arises from the 4-methylpyridine ring being nearly parallel to the NCS moiety. This results in close interactions between these two ligands (for Compound (XIV) there are 8 contacts less than 3.5Å), which in turn causes an increase in the total energy of the system. If however, the 4-MePy ligand is allowed to rotate to a torsion angle of 30°, the number of close contacts (less than 3.5Å) between this ligand and the guest molecule increases dramatically from 2, to over twenty. Thus in order to accomodate the guest molecule, the host complex is required to adjust so that although intermolecular host-host interactions increase, the number of host-guest interactions decreases. The overall energy of the system is therefore lower with these torsion angles near unity.

Unfortunately it is not possible to establish any connection between solubility of the host powder complex in a particular potential guest solvent and its ability to form a clathrate. This is owing to the use of a co-solvent in order to form crystals. For all Class A and B compounds, the solubilty of the host complex (expressed as a mole fraction X_{host}) is less than 10^{-6} in any solvent other than those used as the co-solvent *i.e.* dmso and methanol respectively. Solubilities of this order prevent sufficient host powder from dissolving which precludes crystal formation.

REFERENCES

4.1 J.Lipkowski, 'Structure and Physico-Chemical behaviour of clathrates formed of the $Ni(NCS)_2(4\text{-}MePy)_4$ complex', Polskiej Akademii Nauk, Wroclaw/Warsaw/Krakow/Gdansk, 1980.

4.2 A. Gavezzotti, 'OPEC Organic Packing Energy Calculation Program', *J. Am. Chem. Soc.*, **105**, No. 16, 5220 (1983).

4.3 M.H. Moore, 'Structure-Activity Relationships in Werner Clathrates', Ph.D. thesis, University of Cape Town, (1987).

4.4 D.R. Bond, G.E. Jackson and L.R. Nassimbeni, *S. Af. J. Chem.*, **36(1)**, 19 (1983).

4.5 J. Lipkowski, Accademia Polacca Delle Scienze, Biblioteca Centro di Studi a Roma, 'Conferenze 81', (1980).

4.6 M.H. Moore, L.R. Nassimbeni and M.L. Niven, *J. Chem. Soc., Dalton Trans.*, 2125 (1987).

4.7 L.R. Nassimbeni, S. Papanicolaou and M.H. Moore, *J. Incl. Phenom.*, **4**, 31 (1986).

4.8 F. Valach, P. Sivy and B. Koren, *Acta. Cryst.*, **C40**, 957 (1984).

4.9 I.S. Kerr and D.J. Williams, *Acta. Cryst.*, **B33**, 3589 (1977).

4.10 M.H. Moore, L.R. Nassimbeni, M.L. Niven and M.W. Taylor, *Inorg. Chim. Acta.*, 115, 211 (1986)

4.11 J. Lipkowski, *J. Mol. Struct.*, 75, 132 (1981).

4.12 J. Lipkowski in 'Inclusion Compounds', eds. J.L. Atwood, J.E.D. Davies and D.D. MacNicol, Academic Press, New York, Vol 1, Chap 3 (1984).

4.13 M.H. Moore, L.R. Nassimbeni and M.L. Niven, *Inorg. Chim. Acta.*, 131, 45 (1987)

CHAPTER FIVE

PHYSICAL TECHNIQUES

5.1 COMPETITION EXPERIMENTS

The rationale behind these experiments has been described in Chapter 1. The aim is to determine whether a particular host will preferentially include a particular guest molecule when offered a choice of two. The experimental procedure, described in Section 2.6, was employed firstly with $[Ni(NCS)_2(4\text{-}MePy)_4]$ as the host and *p*-xylene/benzene, *p*-xylene/ethylbenzene and *p*-xylene/toluene as guest combinations to check the validity of the modified technique. This was repeated secondly with the 4-ViPy derivative as the host complex with the same guest combinations.

All quantities used and the intermediate results are given in Tables 5.1a - 5.6a in **Appendix A**. By definition, R_L = mole ratio of guest solvents in the liquid phase and R_S = mole ratio in the solid phase with *p*-xylene always being the numerator for all guest combinations in both R ratios. The results R_L and R_S for each combination of guests are given below in Table 5.1. For each guest combination, in the range of R values studied, R_S changes continuously with the R_L so that there are no invariant liquids. A plot of ln R_S vs ln R_L gives, within experimental error, a straight line for all combinations with both host complexes. All results for the equation $\ln R_S = a + b \ln R_L$ are given in Table 5.2 and the graphs displayed in Fig 5.1 - 5.6. The calibration graphs for the three guest combinations are displayed in Fig 5.7 - 5.9 in **Appendix A**.

Table 5.1 Guest distribution (mole ratios) with the 4-MePy and 4-ViPy derivative host complexes.

Host	4-MePy		4-ViPy	
Guests:	*p*-Xylene / Benzene		*p*-Xylene / Benzene	
Run	R_L	R_S	R_L	R_S
1	0.185	7.491	0.193	4.560
2	0.237	7.855	0.254	5.446
3	0.313	8.834	0.333	6.057
4	0.458	10.053	0.467	6.930
5	0.899	13.092	0.925	9.082
6	1.838	15.585	1.908	10.139
7	2.805	18.662	2.873	11.059
8	3.661	19.656	3.724	11.504
9	4.500	21.188	4.489	13.874
Guests:	*p*-Xylene / Toluene		*p*-Xylene / Toluene	
Run	R_L	R_S	R_L	R_S
1	0.182	1.809	0.176	1.620
2	0.360	2.808	0.365	2.479
3	0.595	4.093	0.613	3.418
4	0.734	4.677	0.743	4.262
5	0.945	5.232	0.916	4.314
6	1.876	9.787	1.799	10.376
7	2.937	11.757	2.945	7.100
8	4.083	13.187	3.985	8.938
9	5.078	14.813	4.894	10.909
Guests:	*p*-Xylene / Ethylbenzene		*p*-Xylene / Ethylbenzene	
Run	R_L	R_S	R_L	R_S
1	0.172	1.284	0.153	0.757
2	0.405	3.679	0.327	1.798
3	0.583	5.597	0.512	3.288
4	0.771	7.929	0.726	4.563
5	0.968	8.575	0.885	5.624
6	1.979	24.211	1.906	11.937
7	3.052	36.717	2.763	16.061
8	4.000	48.335	3.728	26.810
9	5.057	79.802	4.616	33.779

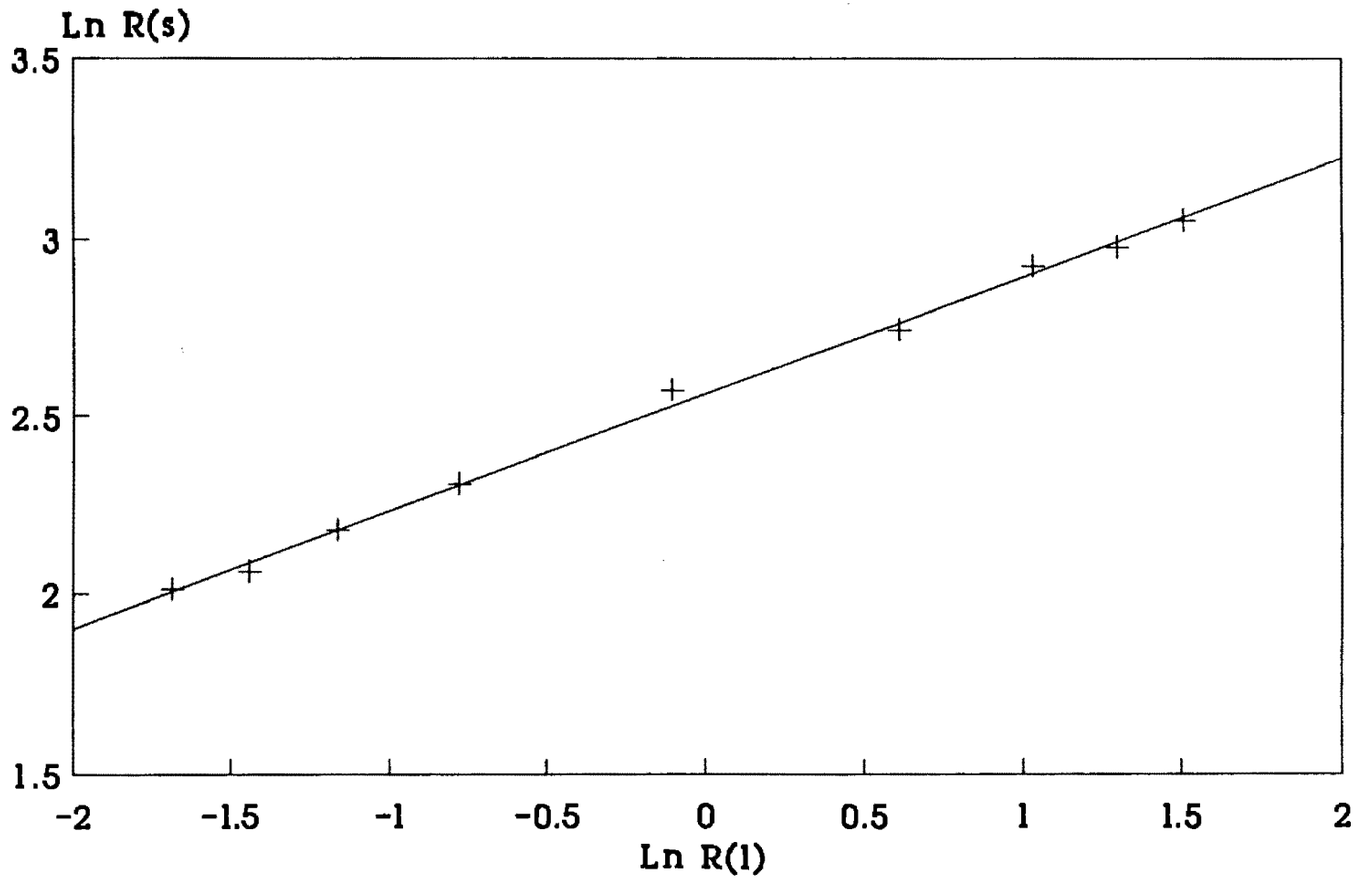

R(l) = mole ratio in liquid phase
R(s) = mole ratio in solid phase

Fig 5.1 Distribution between liquid and solid phases for *p*-xylene/benzene with the 4-MePy host.

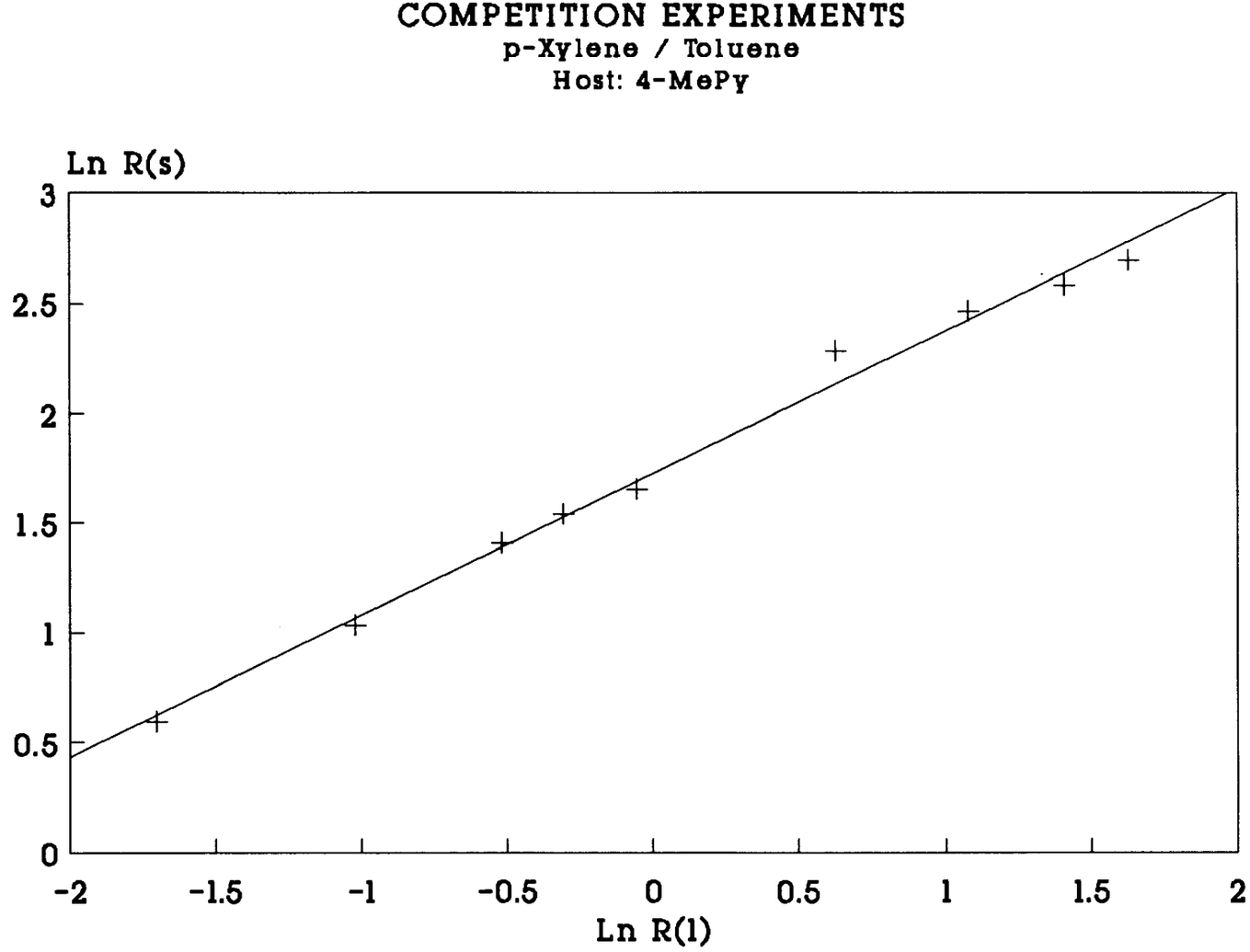

R(l) = mole ratio in liquid phase
R(s) = mole ratio in solid phase

Fig 5.2 Distribution between liquid and solid phases for *p*-xylene/toluene with the 4-MePy host.

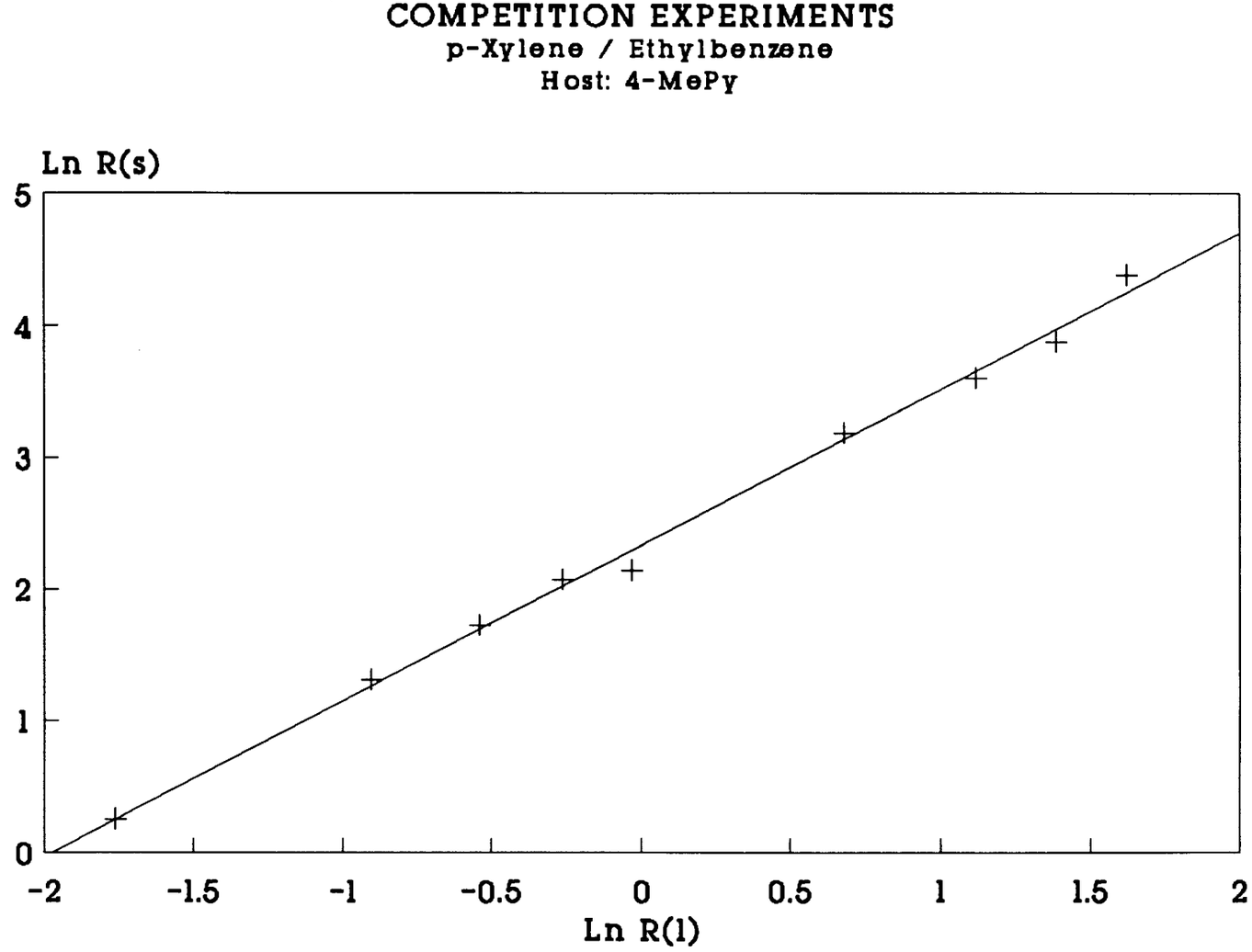

R(l) = mole ratio in liquid phase
R(s) = mole ratio in solid phase

Fig 5.3 Distribution between liquid and solid phases for *p*-xylene/ethylbenzene with the 4-MePy host.

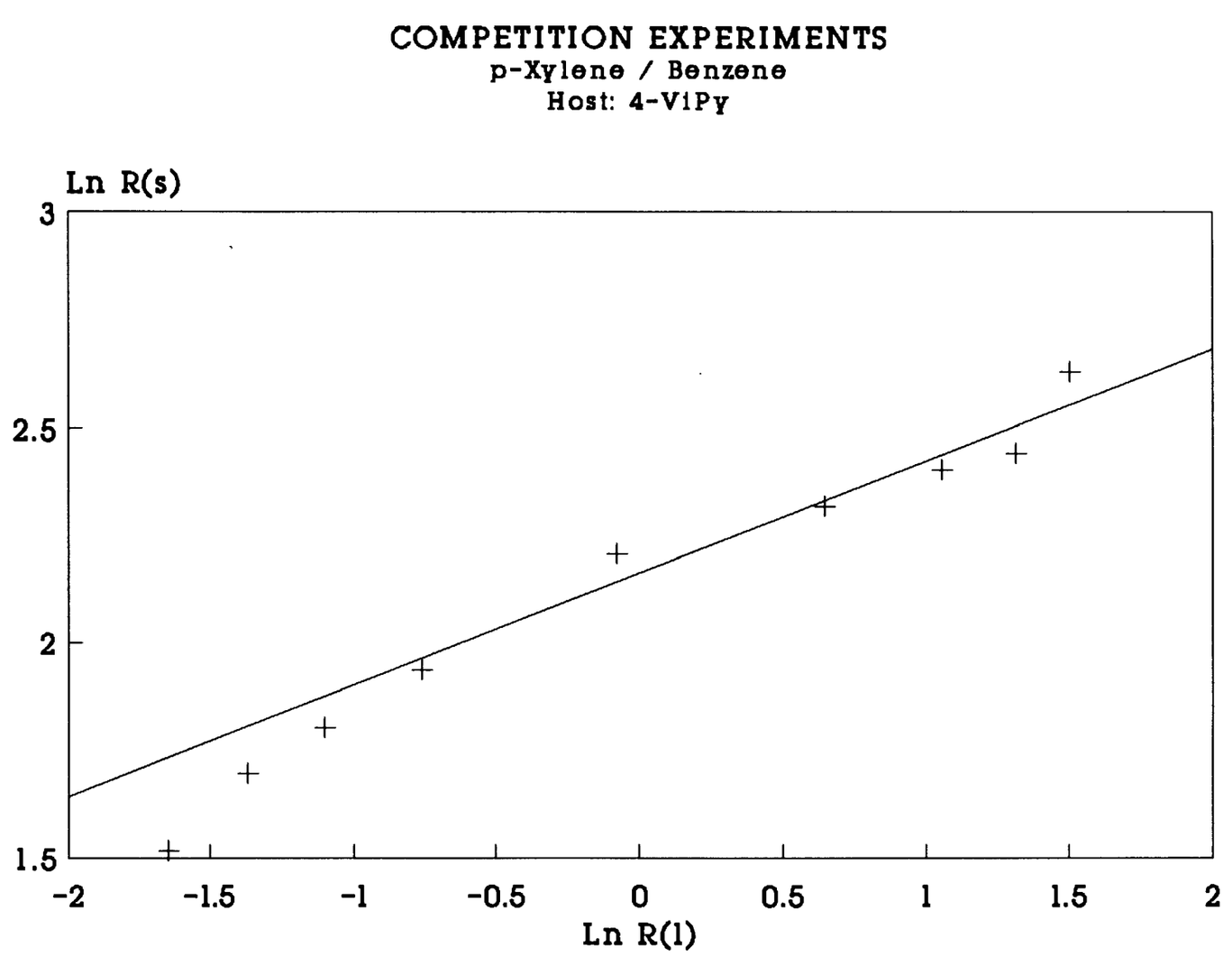

R(l) = mole ratio in liquid phase
R(s) = mole ratio in solid phase

Fig 5.4 Distribution between liquid and solid phases for *p*-xylene/benzene with the 4-ViPy host.

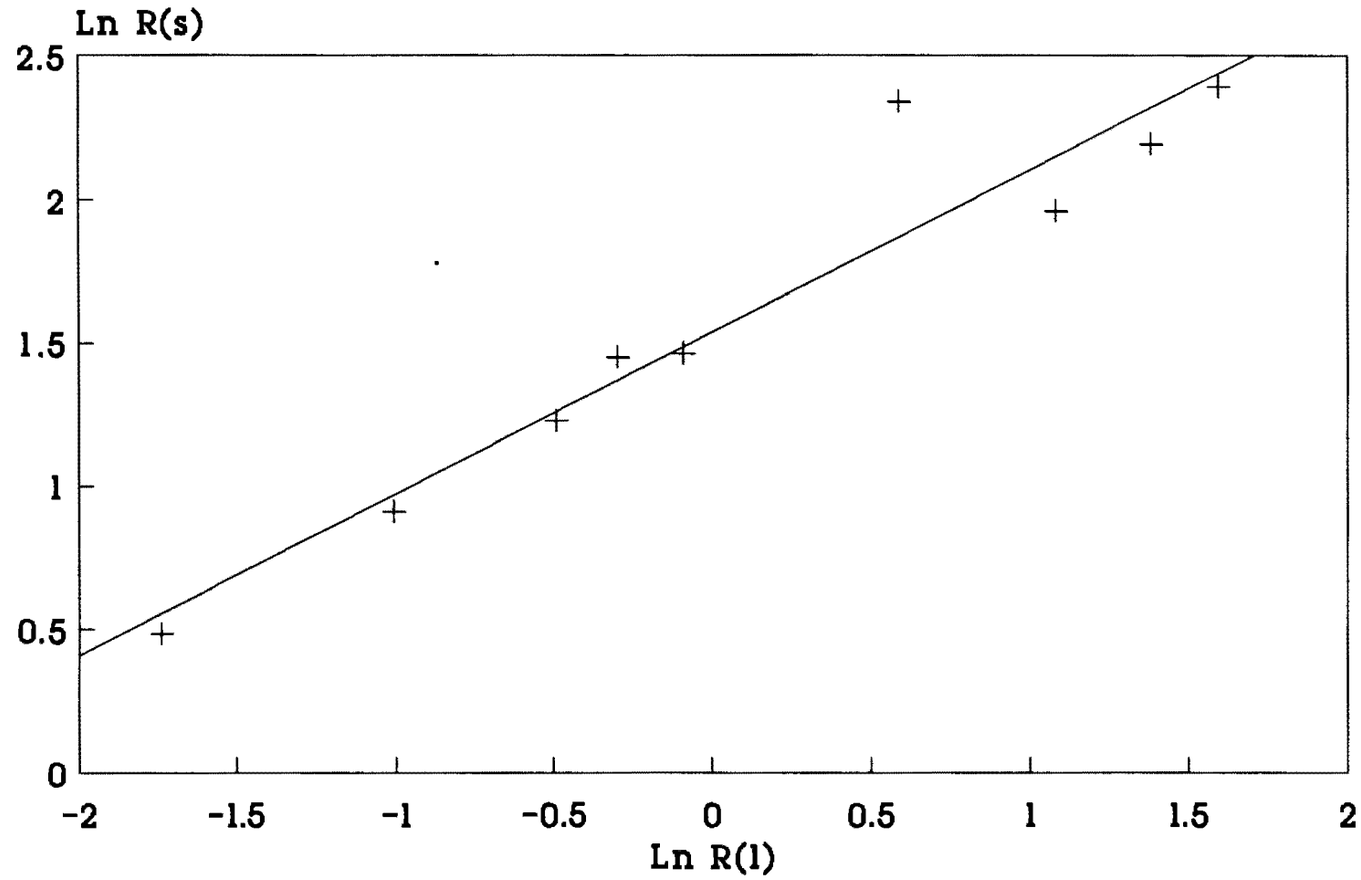

R(l) = mole ratio in liquid phase
R(s) = mole ratio in solid phase

Fig 5.5 Distribution between liquid and solid phases for *p*-xylene/toluene with the 4-ViPy host.

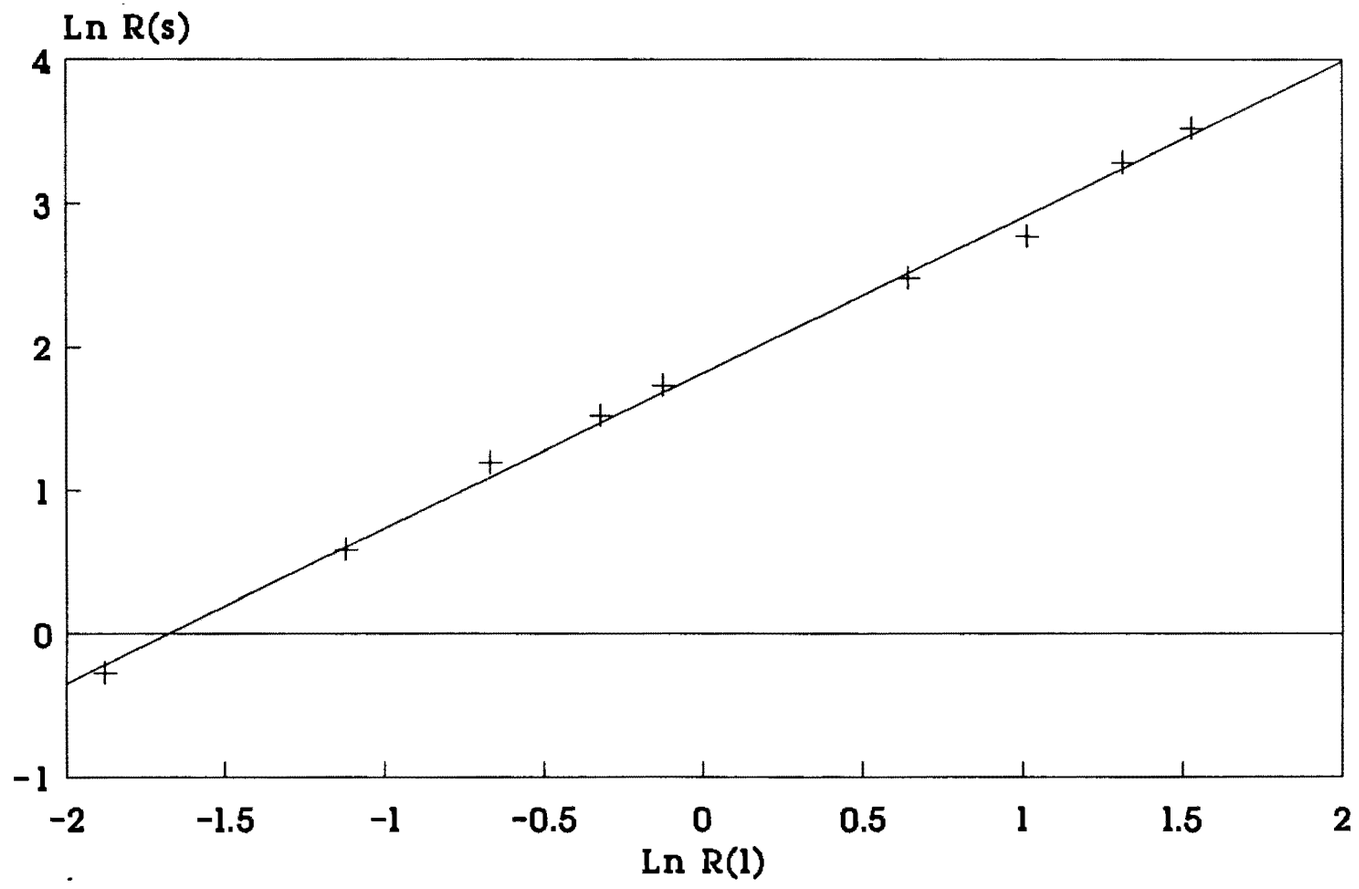

R(l) = mole ratio in liquid phase
R(s) = mole ratio in solid phase

Fig 5.6 Distribution between liquid and solid phases for *p*-xylene/ethylbenzene with the 4-ViPy host.

Table 5.2 Parameters for $\ln R_S = a + b \ln R_L$

Host	Guest Pair	a	b	R_S/R_L (R_S=1)
4-MePy	*p*-Xylene/Benzene	2.565	0.331	2320
	p-Xylene/Toluene	1.725	0.647	14.4
	p-Xylene/Ethylbenzene	2.330	1.180	7.2
4-ViPy	*p*-Xylene/Benzene	2.162	0.261	3958
	p-Xylene/Toluene	1.480	0.540	15.5
	p-Xylene/Ethylbenzene	1.819	1.085	5.3

The results for the runs with the 4-MePy host complex agree favourably with those obtained by Smith and coworkers[5.7], indicating the validity of the technique employed in this work. For the host $[Ni(NCS)_2(4\text{-ViPy})_4]$, as with the 4-MePy derivative, $b \neq 1$ indicating that one of the guests has been preferentially enclathrated. If we arbitrarily set R_S equal to unity then $R_S/R_L = e^{b/m}$ and this value gives a relative indication of preference of a host for a particular guest. Thus the order of preference with respect to *p*-xylene for the 4-ViPy complex is the same as that for the 4-MePy : ethylbenzene > toluene > benzene. However, the preference for *p*-xylene over benzene is almost twice as great for the 4-ViPy host when compared to the 4-MePy host.

During the course of this work, the crystal structure of the complex $[Ni(NCS)_2(4\text{-ViPy})_4]$ has been solved with benzene as a guest[5.1] and the

host : guest ratio has been established as 1:3. Thus the assumptions made to derive the equation to calculate R_S are not strictly valid. However, *p*-xylene is enclathrated in the 4-ViPy host complex nearly 4000 times more readily than benzene and thus the equation is valid except in solutions of low mole ratios of *p*-xylene/benzene. Thus in Fig 5.4, at high benzene concentrations (low R_L values) the points differ significantly from the least-squares line which has been calculated for the remaining seven points.

Table 5.2 reveals that the selectivity of enclathration for toluene is approximately equal for both host complexes studied, although the deviations from the least-squares line for the 4-ViPy host are large especially at higher *p*-xylene concentrations. The point relating to the 6th run in Fig 5.5 is obviously an outlier and has been excluded in the least-squares calculation. No explanation can be offered for this discrepancy although the run was duplicated and the error involved between runs was small (<5%). The crystal structure for toluene in the host $[Ni(NCS)_2(4\text{-ViPy})_4]$ has not yet been elucidated and it is possible that the clathrate containing *p*-xylene is not isomorphous with that containing toluene. A phase change at high *p*-xylene concentrations is a possibility.

Uptake of ethylbenzene is greater in the 4-ViPy host than in the 4-MePy host, but still fewer than 1 in 5 sites in the host lattice are occupied by this guest when competing with *p*-xylene.

Although the trend of selectivity for guests of the 4-ViPy host is the

same as that of the 4-MePy host for the three guest combinations studied, it would be imprudent to try and suggest a reason for this selectivity with a sample size of only three. This method, however, has proved that it is possible to determine both R_L and R_S with one analysis. Thus for systems where the clathrate is highly unstable when exposed to the atmosphere, which is typically the case when a host other than the 4-MePy derivative is employed, it is still possible to determine R_S without having to separate the two phases. The disadvantages are, unfortunately, numerous. Firstly great care must be taken to ensure no solvent is lost in either the sealing or the opening stages of the tubes containing the mixtures. The tubes must be sufficiently long to ensure that the frozen mixture is not thawed when the tubes are sealed. The tubes were refrozen before opening as a significant vapour pressure was present within the tubes when thawed, and opening them in this state produces a fountain of solvent which can (and did) result in a spectacular fire erupting from the mouth of the tube.

The biggest drawback with this technique lies in the fact that any error in obtaining A (the ratio of the peak areas) results in an erroneous R_L which inversely affects the value of R_S. Thus when the ratio R_S/R_L is calculated the error propagation is dramatic. However in systems where guest desorption to the atmosphere is significant, the errors resulting from this technique are probably smaller than those that would be obtained if analysis on the solid phase were to be attempted.

5.2 MOLECULAR SIEVE EXPERIMENTS

Attempts have been made to produce crystals of the mixed base complex $[Ni(NCS)_2(4\text{-}MePy)_2(4\text{-}PhPy)_2]$ from a wide variety of potential guest solvents. However, thus far, the only three combinations that have produced crystals are those containing acetylacetone (Compound (XIII)), 1-chlorobutane (Compound (XIV)) and 2-methoxyethanol[5.2] as the guest molecules. All three of these guests are molecules containing a five atom straight chain skeleton. The size and shape of the channel present within the host lattice of Compound (XIII) was determined using the program OPEC. The cross-sections of this channel, viewed along each axis, are displayed in Figs 5.10 - 5.12 which are sections at the midpoint of the axis of viewing. The view of the xz plane clearly shows the restrictions present within the channel, and it appears that the distance between restrictions (≈ 8Å) is the governing factor which determines the length of the guest molecule that can be located within the channel.

It was decided to see if this apparent specificity for a 5 atom long molecule by this host, could be used to selectively enclathrate a particular guest (*e.g.* butanol) from a mixture of guest solvents (*e.g.* $CH_3(CH_2)_nOH$ for n = 2-5). Crystals of the complex $[Ni(NCS)_2(4\text{-}MePy)_2(4\text{-}PhPy)_2.acac]$ (Compound (XIII)) grow rapidly (±5 days) but not with a particularly high yield (<35% as determined by the moles of 4-MePy derivative host complex *vs* moles crystals formed). Density measurements of these crystals taken after 24 hours in a vacuum oven at 60°C (D_m = 1.10gcm^{-3}) indicate that all the guest has been

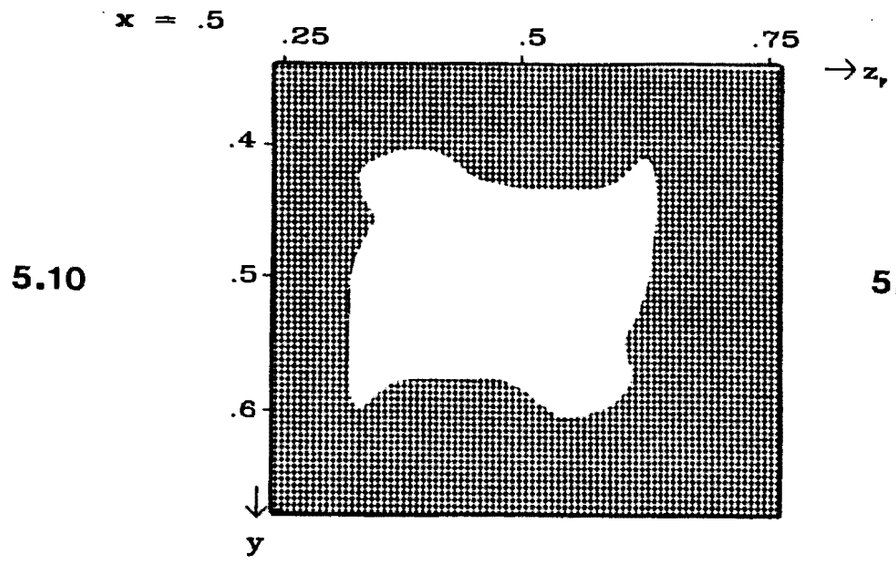

5.10

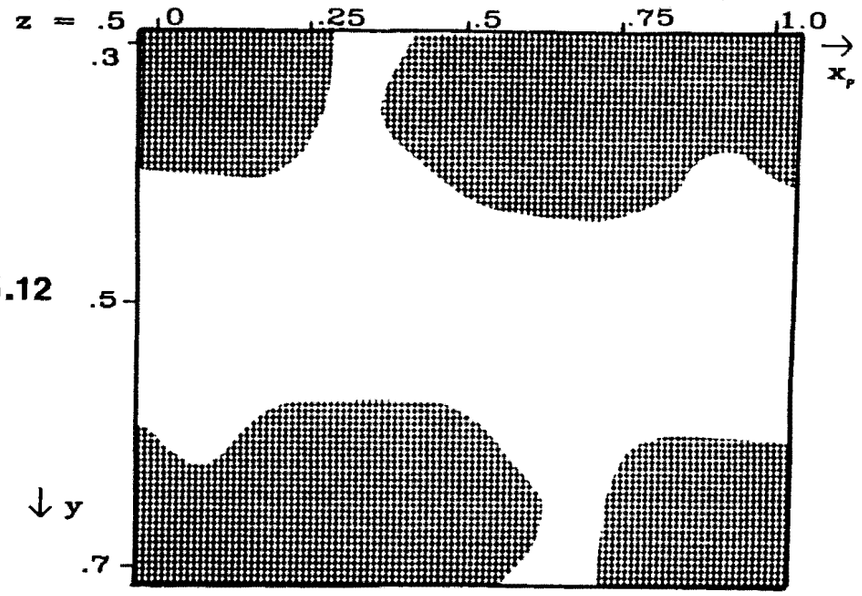

5.12

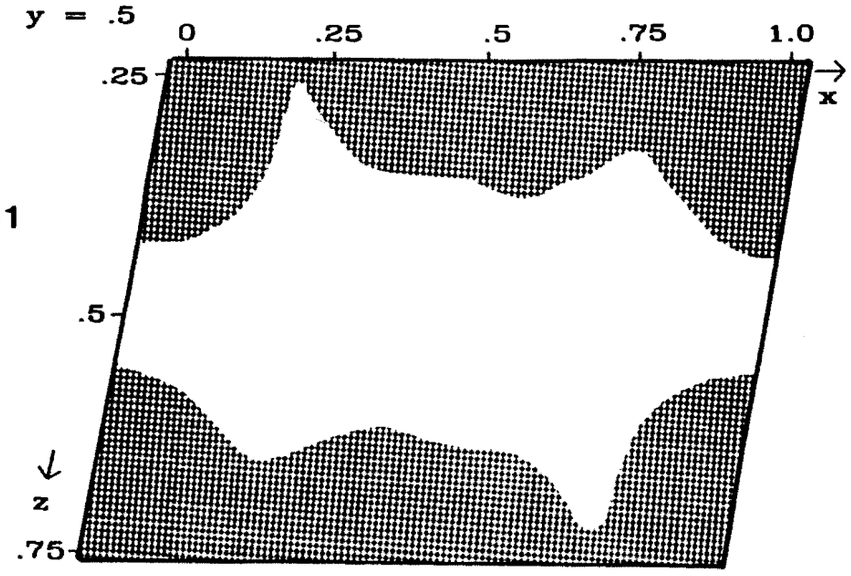

5.11

Fig 5.10, 5.11 and 5.12
Cross-sections of the channel present in Compound (XIII) viewed along [100], [010] and [001] respectively. Each layer is sectioned at the midpoint of the axis of viewing.

driven out of the clathrate, but that the host molecule has not decomposed (D_c = 1.12gcm^{-3} for [Ni(NCS)$_2$(4-MePy)$_2$(4-PhPy)$_2$]). Powder diffractograms were collected for the host-guest complex of Compound (XIII) and for the complex after 24 hours in a vacuum oven at 60°C. These are displayed in Fig 5.13 and the interplanar distances of the more prominent reflections are tabulated below in Table 5.3

Table 5.3 Interplanar distances for the more prominent reflections from X-ray Powder Diffraction.

Before evac.		After evac.	
d_{exp}	**% Int**	**d_{exp}**	**% Int**
9.51	58	9.31	30
8.19	80	7.97	100
7.83	70	7.69	48
5.22	54	5.10	40
4.80	100	4.65	85
4.13	35	4.08	58
3.92	77	3.77	60
3.49	17	3.40	15
3.16	19	3.10	13

The interplanar distances, both before and after guest desorption, were similar enough to confirm that the rigid molecular framework of the host is retained. Slight variations of the most prominent reflections can be attributed to small contractions of the host framework once the guest molecule had departed.

Powder diffractogram of Compound (XIII)
before evacuation.

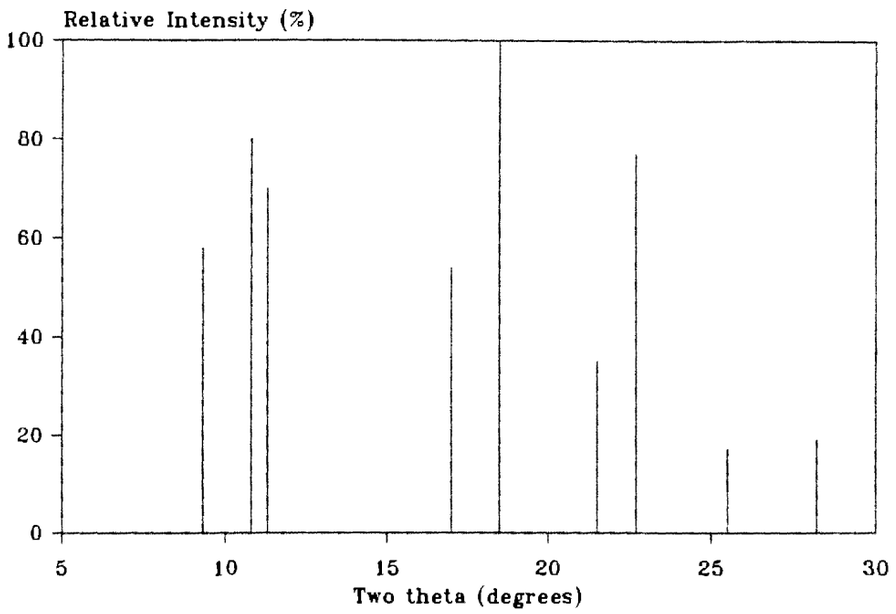

Powder Diffractogram of Compound (XIII)
after evacuation.

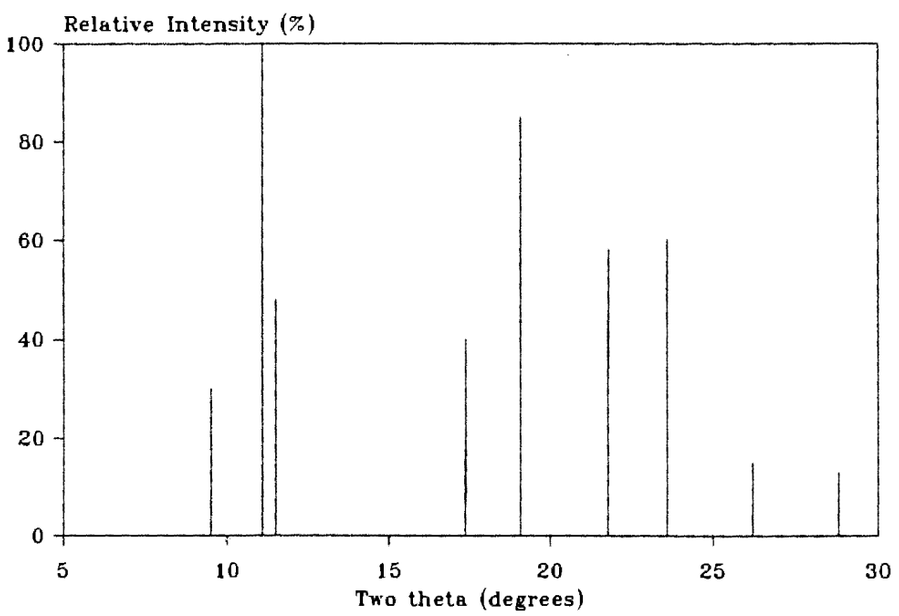

Fig 5.13 Powder diffractograms of Compound (XIII)
a) before evacuation and
b) after evacuation of the guest molecules.

The dried crystals (which were white and non-transparent) were then placed in an evacuated desiccator containing a separate beaker of acetylacetone. The density of the crystals was determined periodically to monitor the uptake of the solvent. The results of this analysis are displayed in Fig 5.14. Thus it can be seen that the uptake of the guest is rapid at the beginning, but this uptake decreases with time and even after 3 days of exposure, the number of guest molecules included within the host framework never reaches that present in the original clathrate.

This trend can be ascribed to the rate of diffusion of the guest into the channels of the complex. Initially, there is a rapid uptake of guest as all the sites near the surface of the crystal are filled. To fill sites further away from the surface, the acetylacetone has to diffuse through the channels. Apparently, there reaches a point of equilibrium where the energy released by occupation of a site is equal to that required to move the guest molecule. Thus no net additional diffusion takes place and therefore not all sites become reoccupied.

A better percentage of reoccupation could possibly have been obtained if smaller crystals were used. Crystals grown from a solution of acetylacetone are typically rectangular in longitudinal cross-section with the longest dimension being of the order of 5mm in length. Crushing of the crystals might have increased the uptake of guest, but it then becomes extremely difficult to accurately determine the density of the resulting powder.

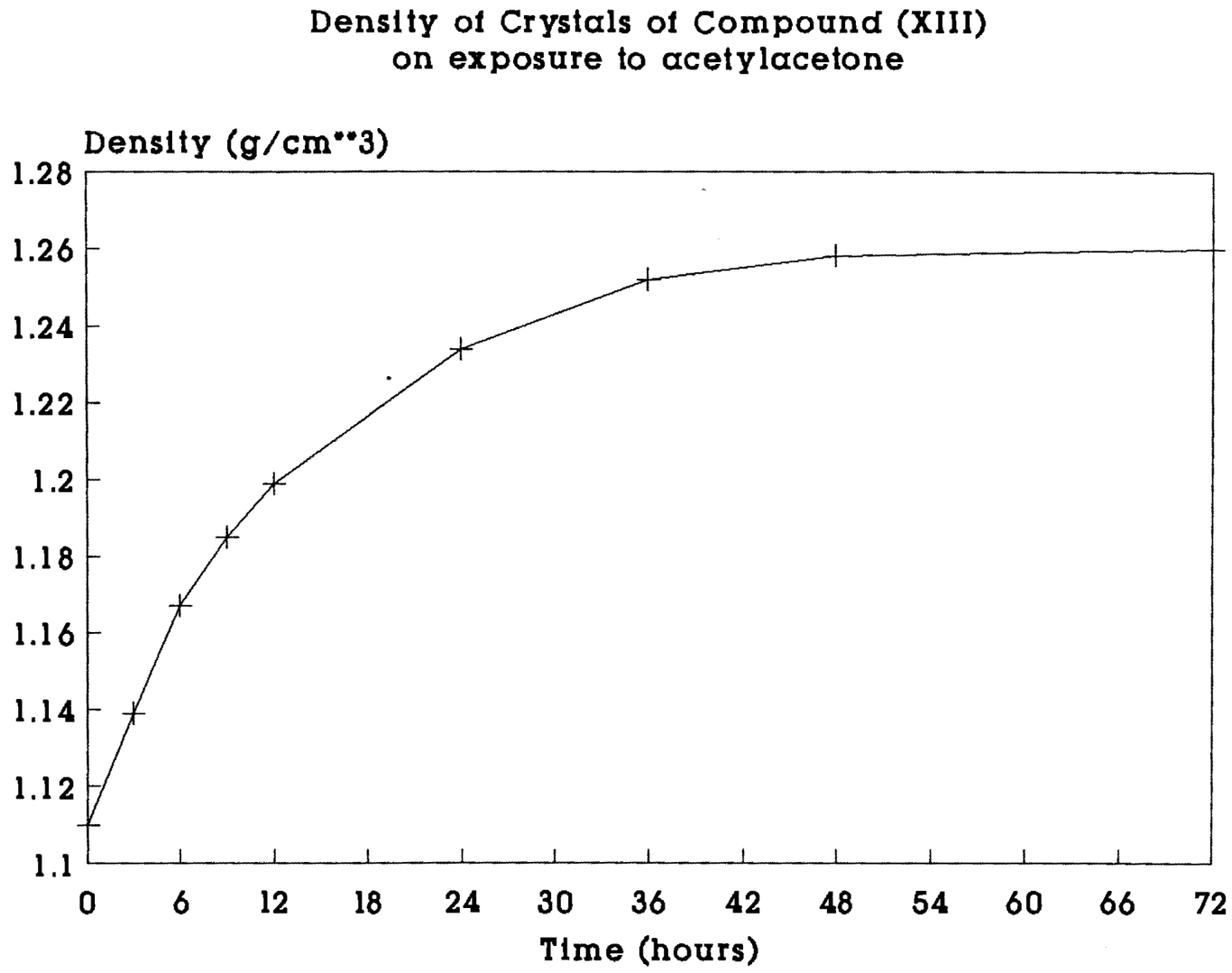

Fig 5.14 Variation of density of dried crystals of Compound (XIII) on exposure to acetylacetone.

This cycle of evacuation/occupation of the void spaces within the host lattice was repeated consistently 3 or 4 times before the host began to turn a pale yellow and the uptake of solvent began to deteriorate. This is indicative of the host decomposing when continually exposed to elevated temperatures of 60°C. Thus for a few cycles at least, this complex can be considered zeolitic in nature in that it has the ability to re-absorb guest solvent after complete desorption has occurred.

Theoretical calculations were first performed using the program EENY to ascertain the potential energy of the system as a series of alcohols are systematically translated through the channel. Molecules of the alcohols ($CH_3(CH_2)_nOH$ with n = 2-5) were constructed and minimized as isolated molecules using ALCHEMY. The coordinates thus obtained were then placed in EENY and the molecule translated, in 1Å steps, through the channel present in the host framework. At each step, the guest molecule was allowed small variations in its rotational parameters as well as in its translation in the y direction, in order to find a local minimum in the energy profile. No variation was allowed in the host framework. The results of this guest translation are displayed for all four alcohols in Fig 5.15.

This graph shows that the alcohol which causes the system to have the lowest potential energy is butanol. Propanol has a wide valley for its minimum profile but it is always greater than 10kcal/mol higher in energy that the minimum for butanol. Pentanol is the next lowest alcohol in terms of potential energy whilst hexanol results in the system having a minimum energy of about 40kcal/mol. Both these latter two alcohols

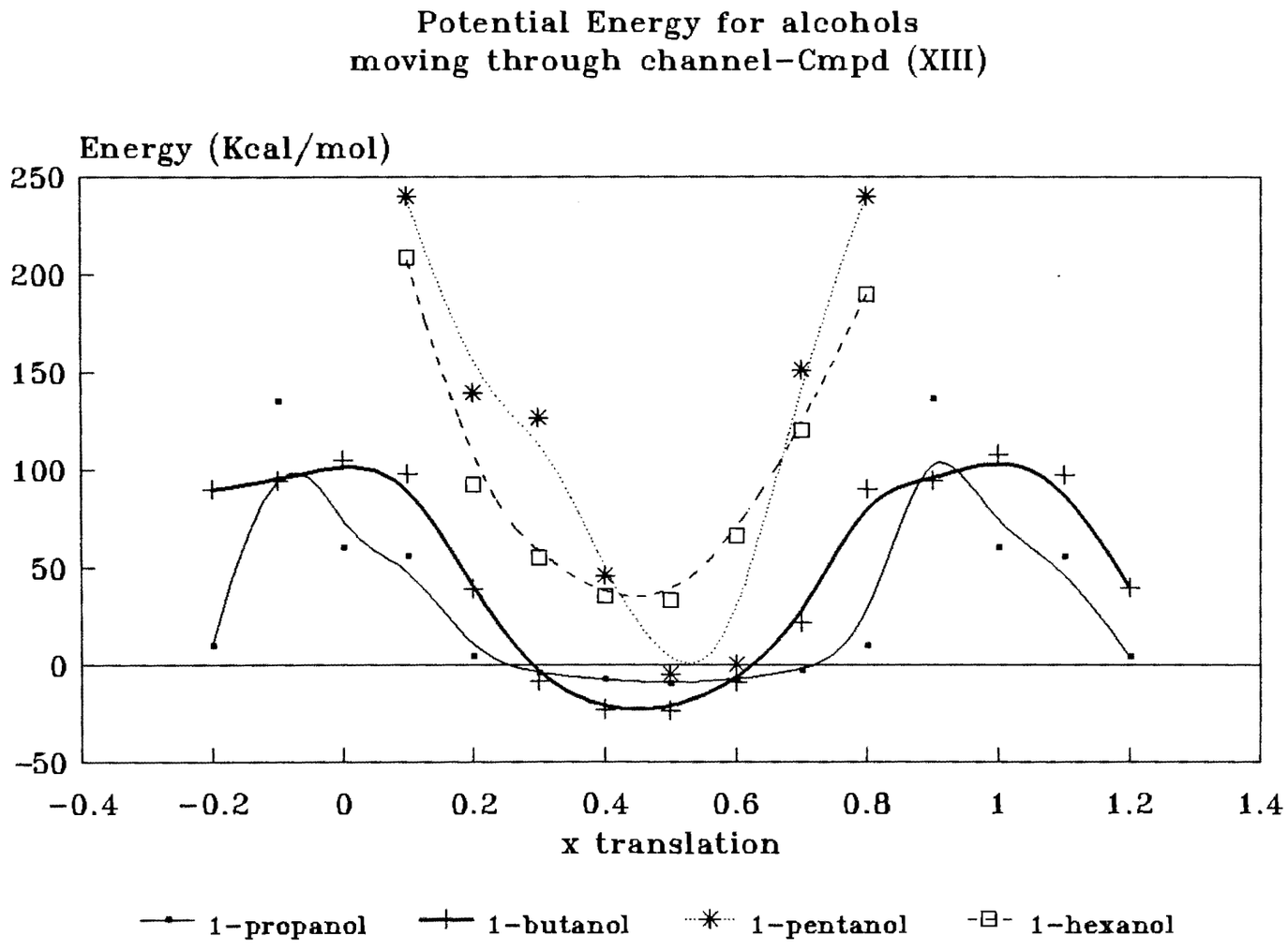

Fig 5.15 Potential Energy diagram for the alcohols systematically translated through the channel of Compound (XIII).

have energy barriers rising up into the thousands of kcal/mol and thus their curves have been truncated to allow a suitable scale for the graph to be used. The energy barrier for propanol is significantly higher than that for butanol and thus the variation between maximum and minimum energies is also higher.

The distance between the hydroxyl hydrogen and the methyl hydrogen for the alcohols is: 5.28Å (propanol), 6.52Å (butanol), 7.78Å (pentanol) and 9.06Å (hexanol). If the 'usable' length of the channel in the host framework is of the order of 8Å, and if the van der Waals radii for the hydrogens are added to the above distances, it can be seen that only the two smaller alcohols can fit in the cavity without interference from the host molecules. Propanol however is much smaller than the cavity and thus it can move about without undue interference; hence the valley. This looseness of fit however, causes the potential energy to be higher than if the molecule is located without excess freedom of movement. Butanol fits into the cavity securely, and thus the host/guest interactions cause this system to have the lowest potential energy.

Thus potential energy calculations indicate that if a mixture of alcohols were to be offered to this host complex, the order of preference for retention would be:

butanol > propanol > pentanol > hexanol.

To test the validity of this prediction experimentally, a column for the gas chromatograph was prepared, as described in Section 2.5, containing a 30% w/w mixture of $[Ni(NCS)_2(4\text{-}MePy)_2(4\text{-}PhPy)_2]$ on an inert support.

The chromatograph was operated isothermally at 80°C, with a flow rate of nitrogen carrier gas of 30ml/min and an injection aliquot of 5μl. Each alcohol was run through the column individually to ascertain its retention time before an equimolar mixture of all four alcohols was introduced. The resulting chromatogram is shown in Fig 5.16a whilst Fig 5.16b shows the order of elution of the same mixture when introduced into a commercially packed column (10% silicone SE-30). The commercial column retains the alcohols in the expected order of increasing size, and thus hexanol having the longest chain length and being the most viscous is retained the longest.

The order of elution for the clathrate column is however very different. Hexanol and pentanol are first eluted almost simultaneously; propanol follows shortly afterwards and then there is a delay of several minutes before the butanol emerges off the column.

If the potential energy diagram displayed in Fig 5.15 is considered, it is extremely unlikely that the two larger alcohols will enter the cavities at all because this will involve an increase in energy to unrealistically high values. Thus the time taken for pentanol and hexanol to pass through the column must be due to the steric interferences within the column. The dependence of height equivalent to a theoretical peak (HETP) on the average carrier gas velocity v, is expressed by the van Deemter equation:

$$HETP = A + B/v + Cv.$$

The A term, attributed to eddy diffusion, represents the multiple path effects of gas flow through the packed column. It incorporates the

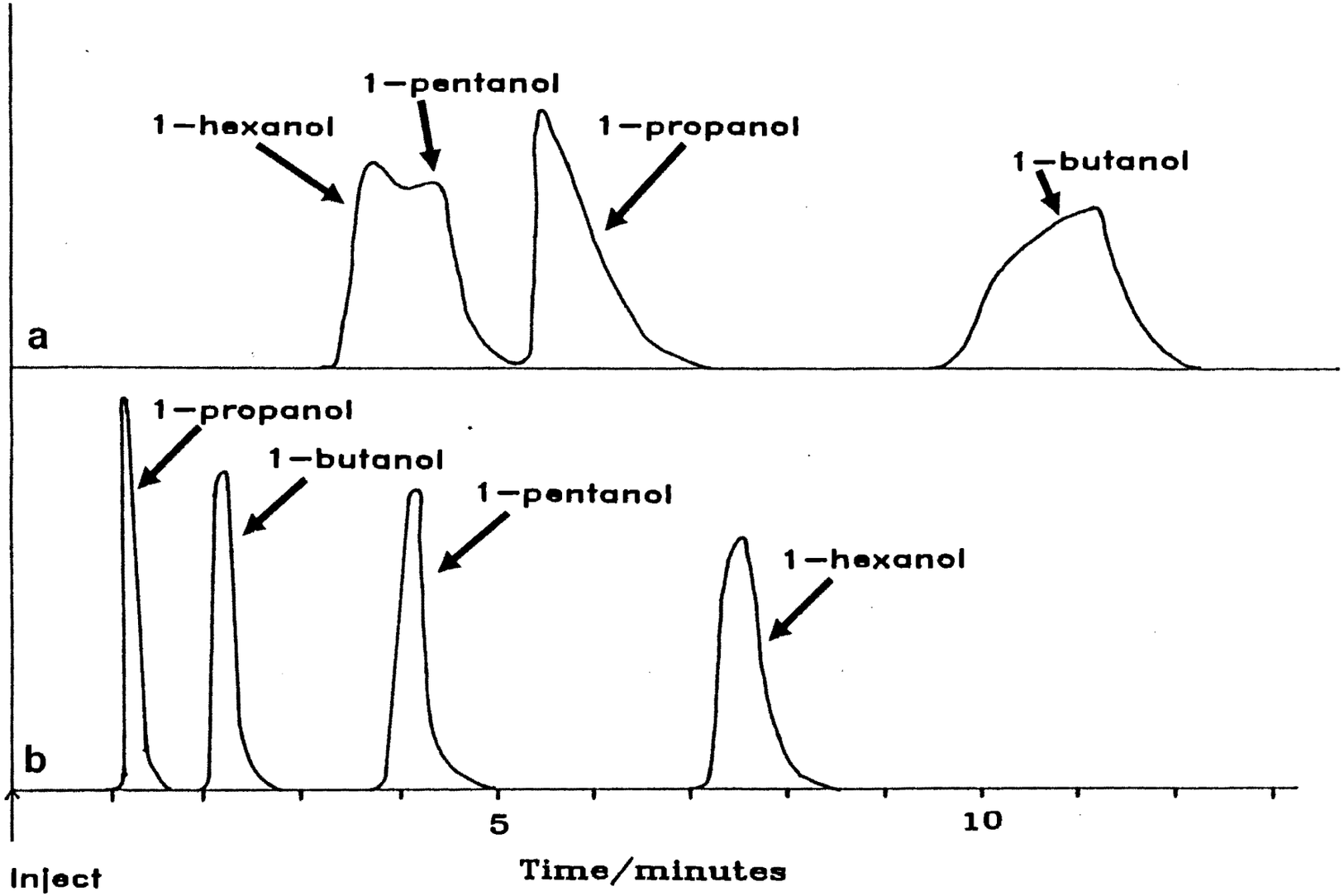

Fig 5.16a & b Chromatograms of the alcohols separated using gas chromatography employing a column of:
a) crushed, dried crystals of Compound (XIII) on an inert support and
b) a commercial packing (10% silicone SE-30).

packing density and average particle diameter of the stationary support. The B term, expresses the tortuosity of the channels in the packed column and the molecular diffusion coefficient of the solute in the gas phase. The C term reflects the resistance to mass transfer between the gaseous and liquid phase, and within the liquid phase.

Terms A and B are related to the physical properties of the column and its packing and for a particular column, under the same conditions of temperature and flow rate, these are constant for solutes which do not differ significantly in their molecular diffusion coefficients. Thus, among the alcohols, the only significant variable in the van Deemter equation is the C term.

Comparing butanol and hexanol, it can be seen that the latter alcohol spends the majority of its time in the gaseous phase and very little time in the solid phase within the column. Thus its resistance to mass transfer is very high resulting in a large HETP value. HETP is inversely proportional to N, the number of theoretical plates, which in turn is directly proportional to the square of the retention volume (directly related to retention time). Thus an increase in C causes a large decrease in the retention time. Butanol however, has a lower resistance to mass transfer and thus its retention time is much longer. The length of retention within a column is therefore directly related to its ability to enter the cavities of the solid phase.

The broadening of all these peaks (especially that of butanol) can be ascribed to the variation in particle size of the solid phase. Although

the host powder was sieved before being mixed with the support, in its dried state it is very brittle and the mixing and packing process could have caused it to fragment further. This fragmentation would have caused variation in the particle size and hence in the packing density within the column which, with reference to the van Deemter equation again, would have given rise to a variation in the A term and hence the HETP value. HETP is basically a measure of the extent of the band broadening during the transit time of the solute. Thus any variation in HETP would cause a concomitant variation in retention volume (time) and cause the eluted peak to broaden.

Unfortunately, constant exposure to the elevated temperatures caused the host complex to decompose and the magnitude of this decomposition could be observed by the column becoming pale yellow, especially at the ends which were attached to the injector (200°C) and detector (250°C). After about three hours of continuous running, the column had completely lost its ability to separate the alcohols and therefore it had to be discarded.

The zeolitic nature of the $[Ni(NCS)_2(4\text{-}MePy)_2(4\text{-}PhPy)_2]$ complex allows it to be used to selectively retain molecules of a specific length. The size of the channel as determined by X-ray crystallography indicates that the length is suitable for a linear chain containing 5 atoms. Potential energy calculations predict an order of retention which is substantiated experimentally as: butanol > propanol > pentanol > hexanol

5.3 THERMAL ANALYSIS

Thermal analysis is the measurement of changes in physical properties of a substance as a function of *temperature* whilst the substance is subjected to a controlled temperature programme. Although the study of the effect of heat on materials can be traced back to man's earliest attempts at extracting metals (≈8000BC), it was the advent of the analytical balance which allowed experiments to become more controlled and more quantitative. Although there are over ten different types of thermal analysis techniques, they all have a basic common feature: a physical property of a sample is measured (usually continuously) under a particular heating programme (often linear) and the variation in this property is converted into an electrical signal - the thermal analysis curve ('thermogram' is not an approved term by the International Confederation of Thermal Analysis (ICTA)).

The two techniques studied in this work are: Thermogravimetry (TG) which measures mass variations and Differential Thermal Analysis (DTA) which monitors temperature variations. Thermogravimetry is used to monitor the decomposition pathway of the breakdown of the clathrate. The percentage mass loss is measured continuously and because the starting compound is known, the intermediates involved as the host-guest complex decays can be described. All the Werner clathrates studied using TG involve multi-stage decompositions with relatively stable intermediates and the mass loss after each stage can be determined accurately. All samples were single crystals, cut to the required mass (approx. 10mg), and thus sample preparation is constant from run to run. Although samples for

thermal analysis are usually ground to a uniform size for consistent and accurate results, Werner Clathrates obviously cannot be prepared in this manner. Thus it was decided to use a single crystal of a clathrate for analysis. Although guest loss would be partly governed by its rate of diffusion through the host lattice, this factor would prevent premature decomposition of the compound. By using a single crystal the surface area/ volume ratio is kept to a minimum and thus evaporation is reduced. A crystal was cut to an appropriate size whilst still in its mother liquor. This crystal was then quickly removed from the solvent, patted dry in a tissue and weighed before being placed in its crucible, the furnace positioned and the analysis started.

In Differential Thermal Analysis, the difference in temperature, ΔT, between the sample and a reference material is recorded while both are subjected to the same heating programme. During an endothermic thermal event (positive ΔH), the sample temperature, T_s, will lag behind the temperature of the reference, T_r, which follows the heating programme, whilst for an exothermic reaction (negative ΔH), the response will be in the opposite direction. The difference, $\Delta T = T_s - T_r$, when plotted against T_r results in a DTA curve as illustrated in Fig 5.17. Endo- and exotherms are characterized by their onset temperature, T_{onset}, which is the quoted temperature for an event. The temperature at which the recorder response is at its maximum distance from the baseline, ΔT_{max}, is not used because it is very dependent on the heating rate, sample size and thermocouple position. An important aspect of DTA is that the area under the peak is proportional to the amount of material present and the enthalpy of the reaction.

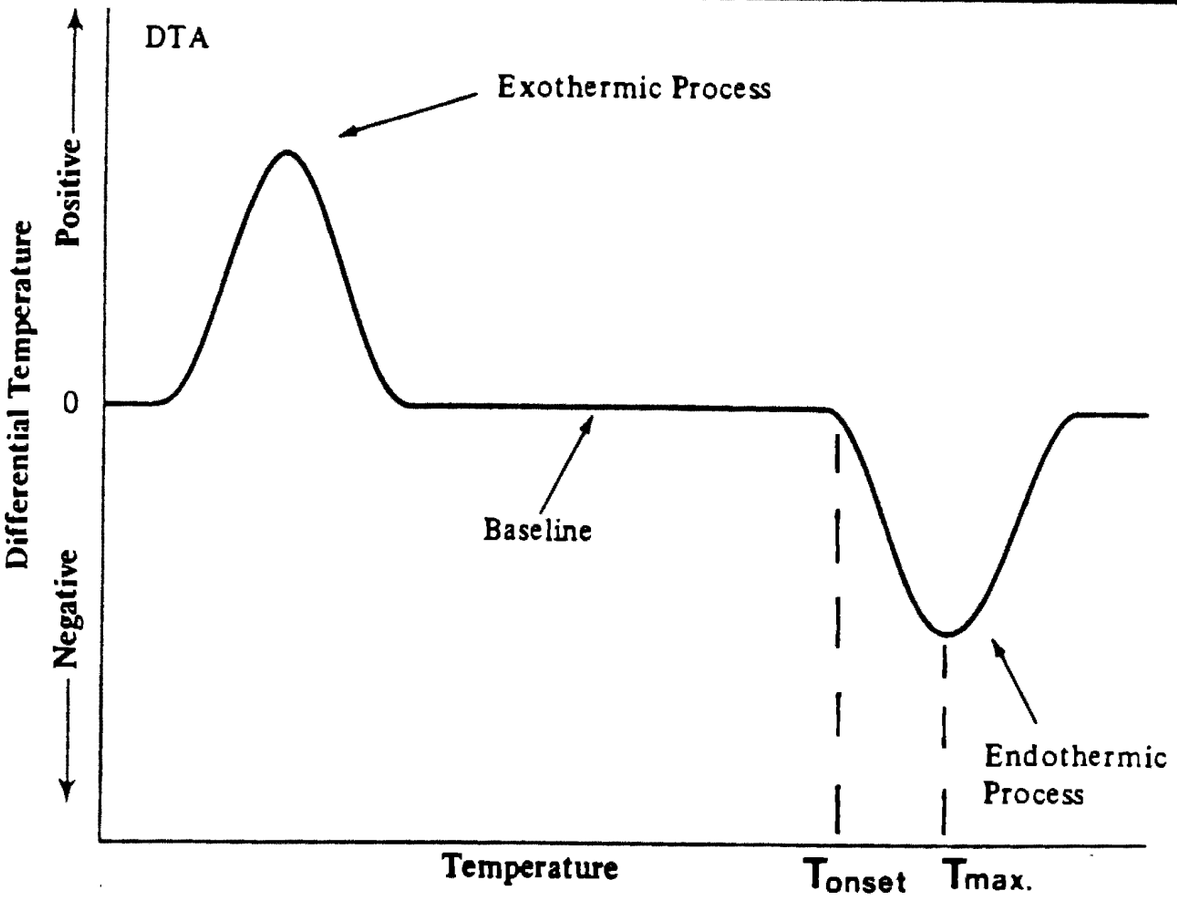

Fig 5.17 Schematic diagram of a Differential Thermal Analysis curve.

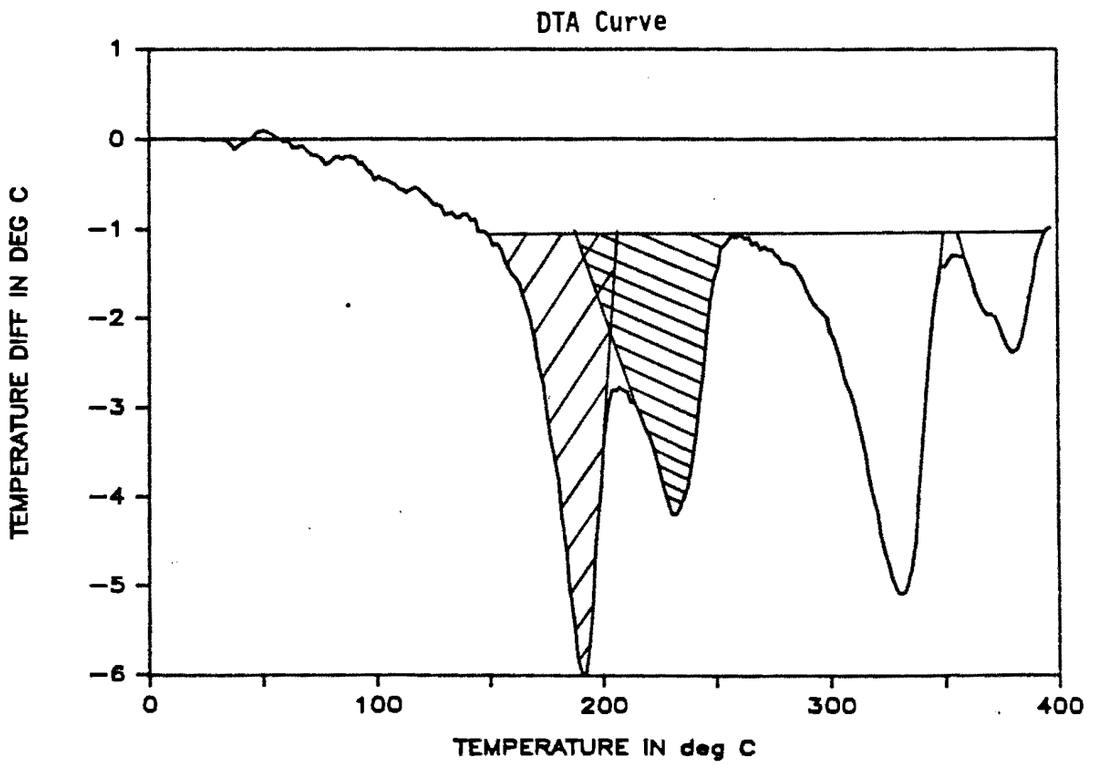

Fig 5.18 Diagram to illustrate the method of peak separation for overlapping DTA peaks.

Thus $A_s \propto \Delta H \times m_s$

or $A_s \times K = \Delta H \times m_s$

where A_s = measured peak area, m_s = sample mass and K = calibration factor. This factor has to be determined by relating a known enthalpy change to a measured peak area. The value of K is markedly dependent upon temperature so calibrations should be performed throughout the temperature range of the analysis. The standards used should be matched, as far as possible, with the samples and therefore inorganic standards (*e.g.* metals), which are easily obtainable and well characterized, are not suitable for Werner clathrates which are predominantly organic in character. Although several organic standards of know ΔH values were used, all except one were either impure, and hence gave more than one peak, or gave additional peaks of phase changes which overlapped with the melting point peaks. The only reliable standard was naphthalene which, melting at 80°C, is a suitable median temperature associated with guest release in Werner clathrates. It is this guest release which is of greater interest than the subsequent breakdown of the host complex. The ΔH values quoted for the host decay are calculated using the calibration factor of naphthalene even though these thermal events occur at higher temperatures.

For naphthalene:

$$K = \Delta H_{melt} \times \text{mass} / \text{Area} = 0.319 \text{ J/cm}^2$$

with the recorder's ordinate scale and the sensitivity of the instrument kept constant.

Thus for Werner clathrates:

$$\Delta H = A_S \times 0.319 / m_S$$

where m_S(g) is the mass of the sample associated with the particular event giving rise to the peak of area A_S (cm^2) which is scaled so as to be consistent with the scale used for the naphthalene standard. In multi-stage decompositions, this mass is therefore different at the beginning of each event and the enathlpy values (J/g) quoted in this work are calculated using this adjusted mass. The molar enthalpy values however can be calculated directly using the starting mass because as the mass decreases at each step, there is a concomitant decrease in molar mass.

Unfortunately, this method of calculating enthalpy values is somewhat inaccurate because of the inherent difficulties in calculating the peak area. Initial displacements of the baseline itself from zero result from a mismatching of the thermal properties of the sample and the reference material (alumina, Al_2O_3) and asymmetry in the construction of sample and reference holders (constructed from platinum). Determination of the baseline was sometimes difficult and other feasible corrections could have been made. It was endeavoured, however, to be consistent in the baseline construction, so the results are at least comparable with each other. When peaks overlapped *i.e.* a second thermal event started before the first one had finished, the shape of the individual peaks was determined by extrapolation of the steepest slope of each peak to the baseline. Fig 5.18 illustrates this procedure for the determination of the peaks of Compound (IX). Areas were determined by the 'cutting and weighing' method.

Results of both the thermogravimetric and differential thermal analyses are given in Table 5.4 whilst the relevant thermal analysis curves for the naphthalene standard are shown in Fig 5.19 whilst those for the samples are shown in Figs 5.20 - 5.31. The table and Figures are displayed at the end of this chapter.

The calibration curve used to calculate the temperature lag of the sample behind the furnace (Fig 5.32) was constructed by observing the displayed furnace temperature of melting and plotting this against the known melting point for six standards in the range 100-350°C. The resulting straight line was assumed to be valid over the whole analysis range of 20-400°C.

The steps discussed in Table 5.4 are as follows:

1) $NiX_2L_4.nG \rightarrow NiX_2L_4 + nG$ (Guest release)

2) $NiX_2L_4 \rightarrow NiX_2L_2 + 2L$ (Initial host breakdown)

3) $NiX_2L_2 \rightarrow NiX_2 + 2L$ (Final host breakdown)

where X = NCS^- or Cl^- and L = substituted pyridine.

For all compounds, with the exception of Compound (IX), the final product is $Ni(NCS)_2$. The breakdown mechanism for Compounds (II), (IV) and (IX) differs from that displayed above as follows:

For Compound (II) the breakdown is:

1) $[Ni(NCS)_2(4\text{-}PhPy)_4].2C_8H_{10} \rightarrow [Ni(NCS)_2(4\text{-}PhPy)_4].C_8H_{10} + C_8H_{10}$

1[a]) $[Ni(NCS)_2(4\text{-}PhPy)_4].C_8H_{10} \rightarrow [Ni(NCS)_2(4\text{-}PhPy)_4] + C_8H_{10}$

Steps 2 and 3 are the same as mentioned previously in the general

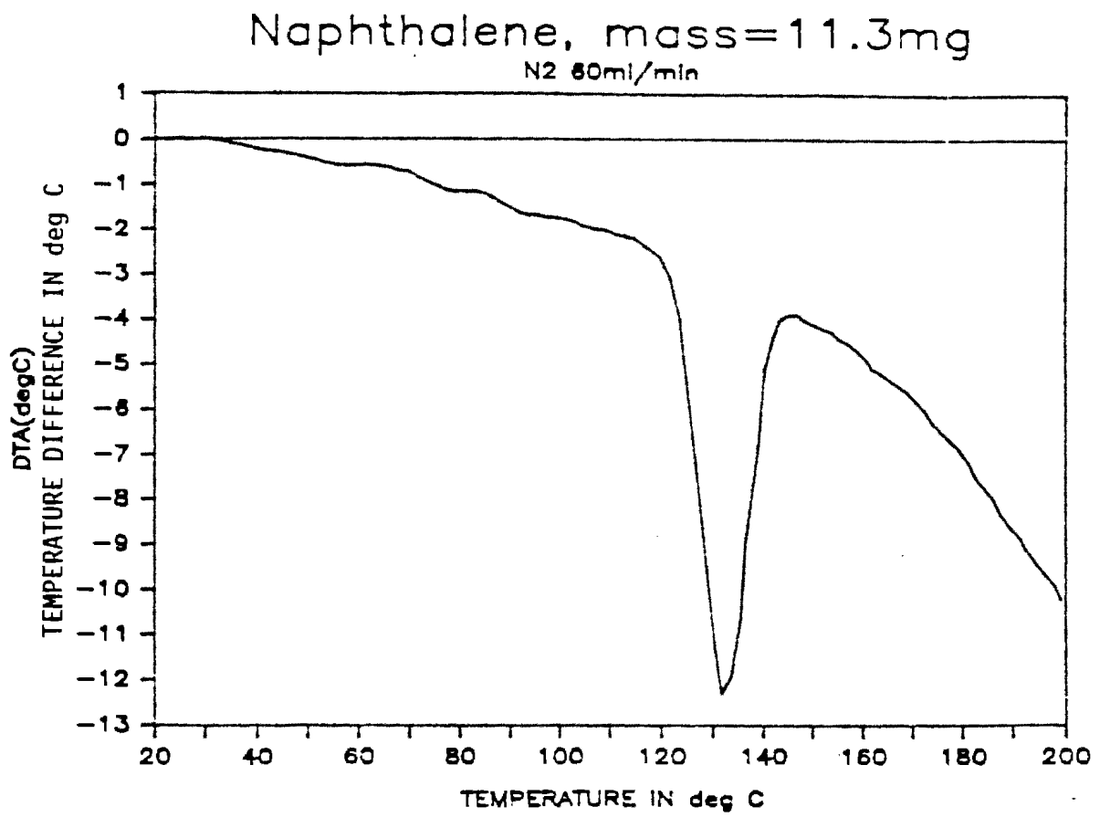

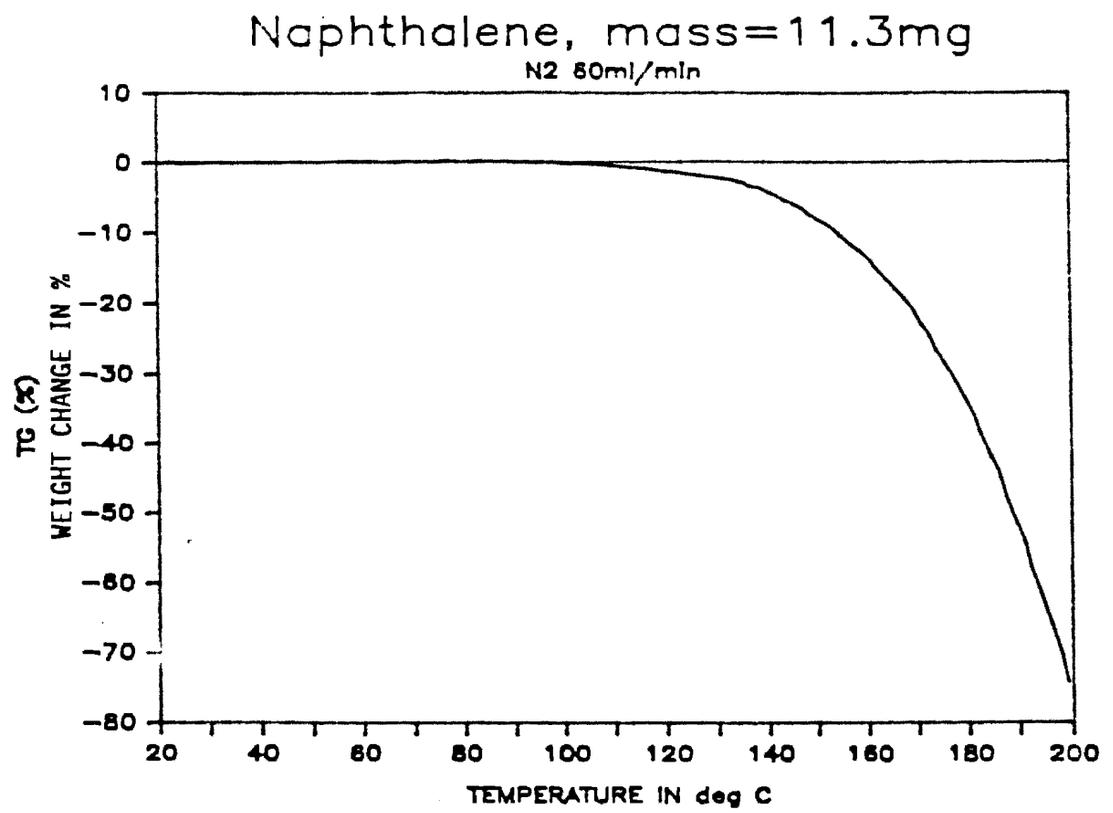

Fig 5.19 Thermogravimetric (TG) and Differential Thermal Analysis (DTA) curves for Naphthalene.

scheme. For Compound (IV), the following occurs:

1) $[Ni(NCS)_2(4\text{-}PhPy)_4].C_8H_{10}.2dmso \rightarrow [Ni(NCS)_2(4\text{-}PhPy)_4].2dmso + C_8H_{10}$

1[a]) $[Ni(NCS)_2(4\text{-}PhPy)_4].2dmso \rightarrow [Ni(NCS)_2(4\text{-}PhPy)_4].dmso + dmso$

2) $[Ni(NCS)_2(4\text{-}PhPy)_4].dmso \rightarrow [Ni(NCS)_2(4\text{-}PhPy)_2] + dmso + 2(4\text{-}PhPy)$

3) $[Ni(NCS)_2(4\text{-}PhPy)_2] \rightarrow [Ni(NCS)_2] + 2(4\text{-}PhPy)$

The decomposition pattern of Compound (IX), unfortunately the only one obtained for a chloride derivative, has several features which cannot be explained by a "normal" breakdown. With methanol as the guest molecule, it is not surprising that there is no clear plateau after guest loss in the TG curve. However a point of inflection at about 4% weight loss is in good agreement with the theoretical value. The next step:

$$[NiCl_2(4\text{-}PhPy)_4] \rightarrow [NiCl_2(4\text{-}PhPy)_2] + 2(4\text{-}PhPy)$$

gives good agreement between theoretical and measured weight loss. However, the 3rd and 4th steps give problems. If the breakdown of the host is similar to that followed by the 4-EtPy derivative[5.3], then step 3 should be:

$$[NiCl_2(4\text{-}PhPy)_4] \rightarrow [NiCl_2(4\text{-}PhPy)_3] + (4\text{-}PhPy)$$

with a calculated weight loss of 63.5%. However, the measured percentage of 68 agrees more favourably with a complex of formula NiClPy, which could be formed by loss of an anion and a base (68% weight loss). For this complex to be possible, a polymer such as that displayed below must form

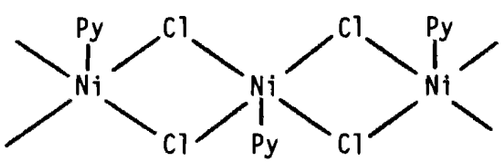

The final step, involving a weight loss of 70amu (9%) appears to leave

NiPy which is clearly unacceptable but no other sensible suggestion can be made. This structure has been omitted from the following discussion as its breakdown pattern is uncertain and its ΔH values are much lower than those for any other complex.

For the other compounds, comparison of the ΔH values reveals some interesting trends. The two α-phase complexes (Compounds (I) and (XVII)) have the lowest total enthalpy values for their breakdown (152 and 167 $kJmol^{-1}$ respectively), whilst the mixed base complexes (Compounds (XIII) and (XIV)) require less energy, in general, to enable their complete breakdown (190 and 172 $kJmol^{-1}$ respectively) than their tetra (4-phenylpyridine) analogues. The % weight loss from the TG curves indicates that the 4-PhPy ligand is lost before the 4-MePy ligand. As these complexes are synthesized from the 4-MePy host powder complex, it indicates why the large excess (6 fold) of the 4-PhPy ligand is required in order to displace two of the bases. It would also explain why attempts to prepare these complexes in the reverse direction, *i.e.* by addition of 4-MePy to $[Ni(NCS)_2(4\text{-}PhPy)_4]$ only produced crystals of the 4-MePy analogue.[5.4]. It is surprising to note that the average $Ni\text{-}N_{py}$ bond in the eight tetra (4-PhPy) complexes (2.14(3)Å) is the same as that in 10 tetra (4-MePy) complexes (2.13(2)Å) that are reported in the literature. It would be expected that because the Ni-N bond of the 4-PhPy ligand is broken before that of its methyl analogue, the bond of the former compound would be longer than that of the latter.

The range of ΔH_{tot} values for the $[Ni(NCS)_2(4\text{-}PhPy)_4]$ complexes is narrow: from 179 (Compound (IV)) to 248 $kJmol^{-1}$ (Compound (III)). It

must be emphasized again however, that the uncertainty in determining peak areas makes evaluation of totals somewhat precarious.

For all β-phase clathrates, the trend in magnitudes of ΔH values for the various steps is the same. The first step (or steps) involving guest release is always the smallest: in agreement with there being no formal covalent bonds between host and guest molecules. Thus this energy is required to manipulate host and guest moieties so as to allow the guest to escape but not to break any bonds. The second step is also the second largest in terms of enthalpy. The comparatively weak Ni-N bonds (when compared with C-C or N-C bonds) are broken to allow the substituted pyridine ligands to depart: there are no electrostatic forces involved as the base is a neutral ligand and thus the ΔH values are relatively small (*ca.* 90 compared to 413kJmol^{-1} for C-H). The removal of the remaining bases to form a divalent nickel complex is the step requiring the most energy. Although the departing moieties are the same for steps 2 and 3, the starting complexes are very different. When one considers that the total 'bond energy' of the Ni is spread over 6 ligands at the start of step 2 compared to 4 at the beginning of step 3, it makes sense that the last step has the highest ΔH value.

The low ΔH values for the guest release is in agreement with our experience in handling crystals of these complexes. The total ΔH values indicate why these complexes do not melt but instead sublime on heating. By the definition of Casellato and Casu[5.5], complexes which allow guest release to occur before the host breaks down are thermally 'unstable'. Thus all of these β-phase clathrates are unstable in the

thermogravimetric sense. This is in agreement with the crystal structure results which indicate that hydrogen bonding host-guest and host-host does not play a role in keeping the structure intact, unlike complexes such as the choleic acids[5,6].

Table 5.4 Thermal Analysis Data for Various Compounds.

Cmpd (Fig)	Step	%Weight Loss Calc	Meas	Temp (°C) T_f	T_s	Mass (mg)	Area (cm^2)	ΔH J/g	ΔH kJ/mol	ΔH Tot kJ/mol
I	2	38.9	39	234	194	11.0	6.0	87	69	
(5.20)	3	77.9	78	311	275	6.71	7.2	171	83	152
II	1	10.5	11	126	81	10.9	1.95	37	38	
(5.21)	1[a]	21.0	20	204	163	9.70	1.18	25	23	
	2	51.8	52	242	203	8.72	3.75	89	71	
	3	82.5	81	315	279	5.23	3.78	150	73	205
III	1	21.0	19	78	30	9.30	1.99	49	50	
(5.22)	2	51.8	52	215	174	7.53	4.30	131	104	
	3	82.5	81	306	270	4.46	3.74	193	94	248
IV	1	10.0	10	130	85	10.9	1.61	31	33	
(5.23)	1[a]	17.4	16	195	153	9.81	0.44	9	9	
	2	54.0	56	240	200	9.16	2.92	66	58	
	3	83.4	83	311	275	4.80	3.77	163	79	179
V	1	22.5	23	94	47	10.7	3.9	58	60	
(5.24)	2	52.7	53	193	151	8.24	4.7	91	72	
	3	82.9	82	262	224	5.03	5.4	171	83	215
VI	1	22.6	23	90	43	10.1	3.9	62	64	
(5.25)	2	52.8	53	170	127	7.78	4.9	100	80	
	3	82.9	82	278	240	4.75	4.8	161	78	222

Table 5.4 (cont)

Cmpd (Fig)	Step	%Weight Loss Calc	Meas	Temp (°C) T_f	T_s	Mass (mg)	Area (cm^2)	ΔH J/g	ΔH kJ/mol	ΔH Tot kJ/mol
VII	1	24.5	23	84	37	10.6	3.8	57	61	
(5.26)	2	53.9	53	187	145	8.06	4.5	89	71	
	3	83.3	82	257	218	4.88	4.4	144	70	202
VIII	1	28.1	28	81	34	10.9	6.1	60	66	
(5.27)	2	56.1	56	201	160	7.85	5.9	80	64	
	3	84.1	84	279	242	4.80	7.5	166	81	211
IX	1	4.1	5.0							
(5.28)	2	43.7	42	135	90	11.4	2.56	72	28	
	3		68	194	153	6.61	2.06	99	23	
	4		77	261	223	3.65	2.93	256	32	83
XIII	1	13.0	13	113	67	10.5	2.9	44	34	
(5.29)	2	53.2	52	214	173	9.14	6.1	106	71	
	3	77.3	77	289	250	5.04	7.3	231	85	190
XIV	1	12.1	12	121	76	11.2	3.1	44	34	
(5.30)	2	52.7	53	220	180	9.86	5.1	83	63	
	3	77.1	78	295	258	5.26	6.7	203	75	172
XVII	2	37.4	34	210	169	9.90	5.04	117	84	
(5.31)	3	74.8	75	287	250	6.53	5.02	177	83	167

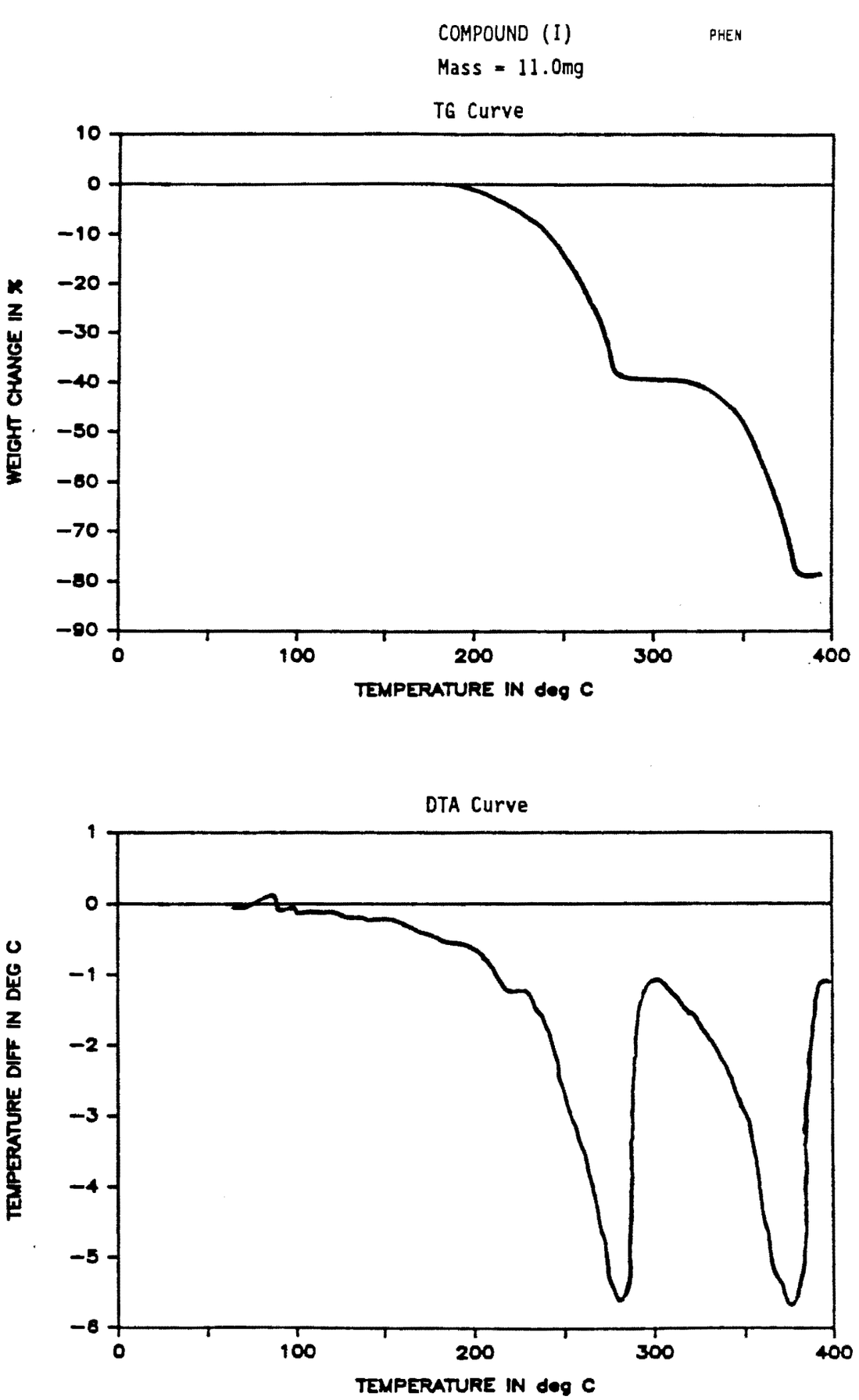

Fig 5.20 Thermogravimetric (TG) and Differential Thermal Analysis (DTA) curves for Compound (I).

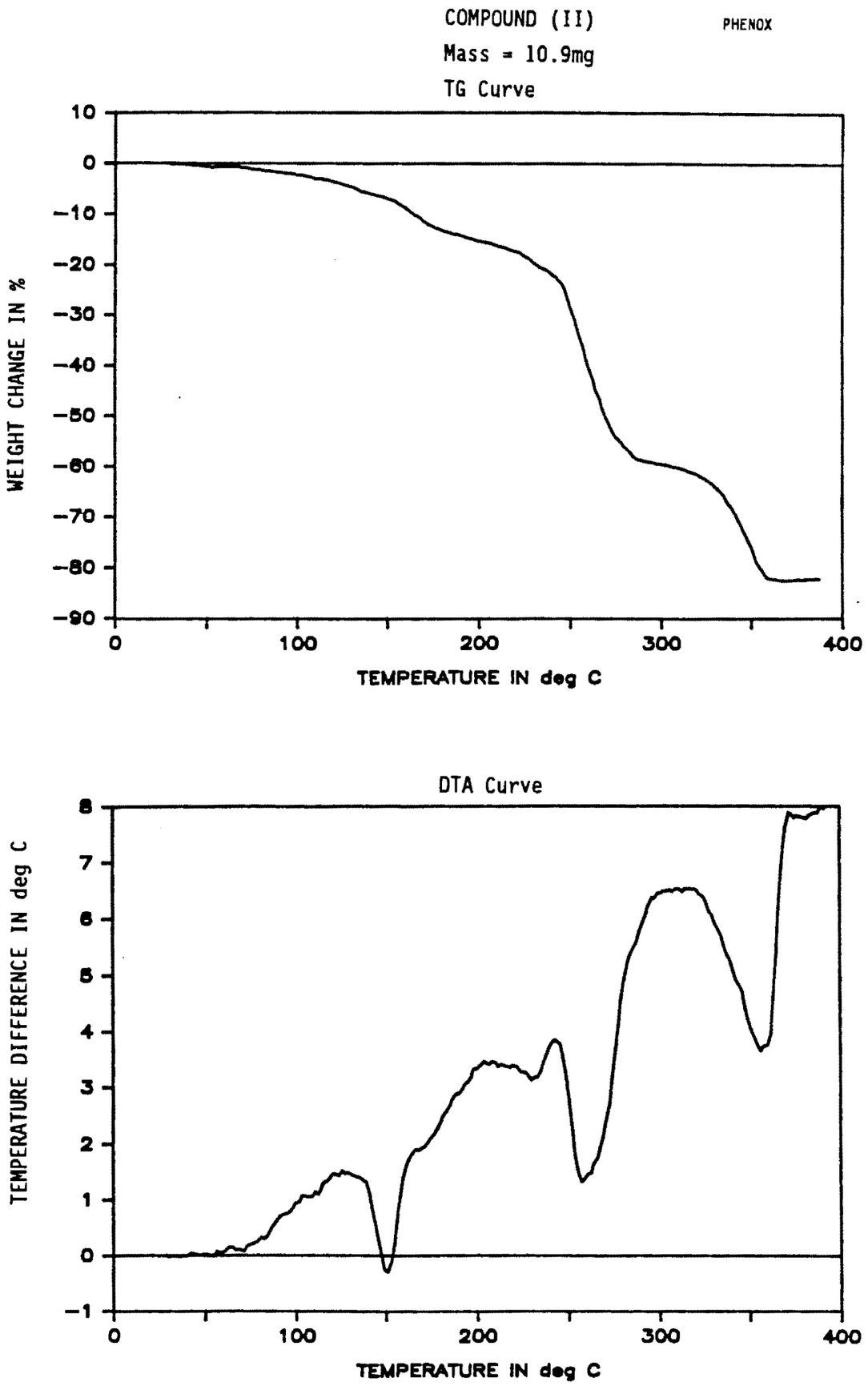

Fig 5.21 Thermogravimetric (TG) and Differential Thermal Analysis (DTA) curves for Compound (II).

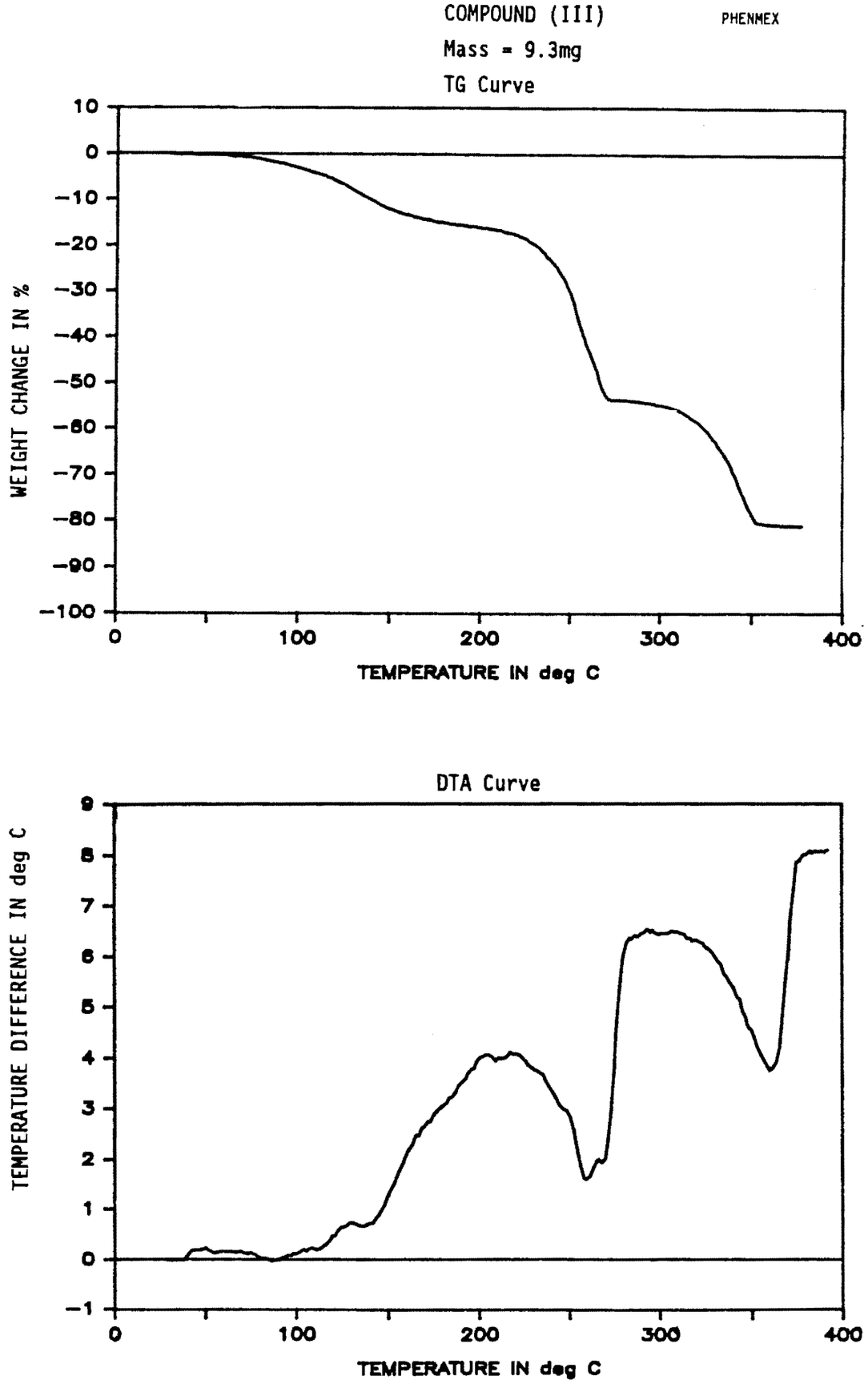

Fig 5.22 Thermogravimetric (TG) and Differential Thermal Analysis (DTA) curves for Compound (III).

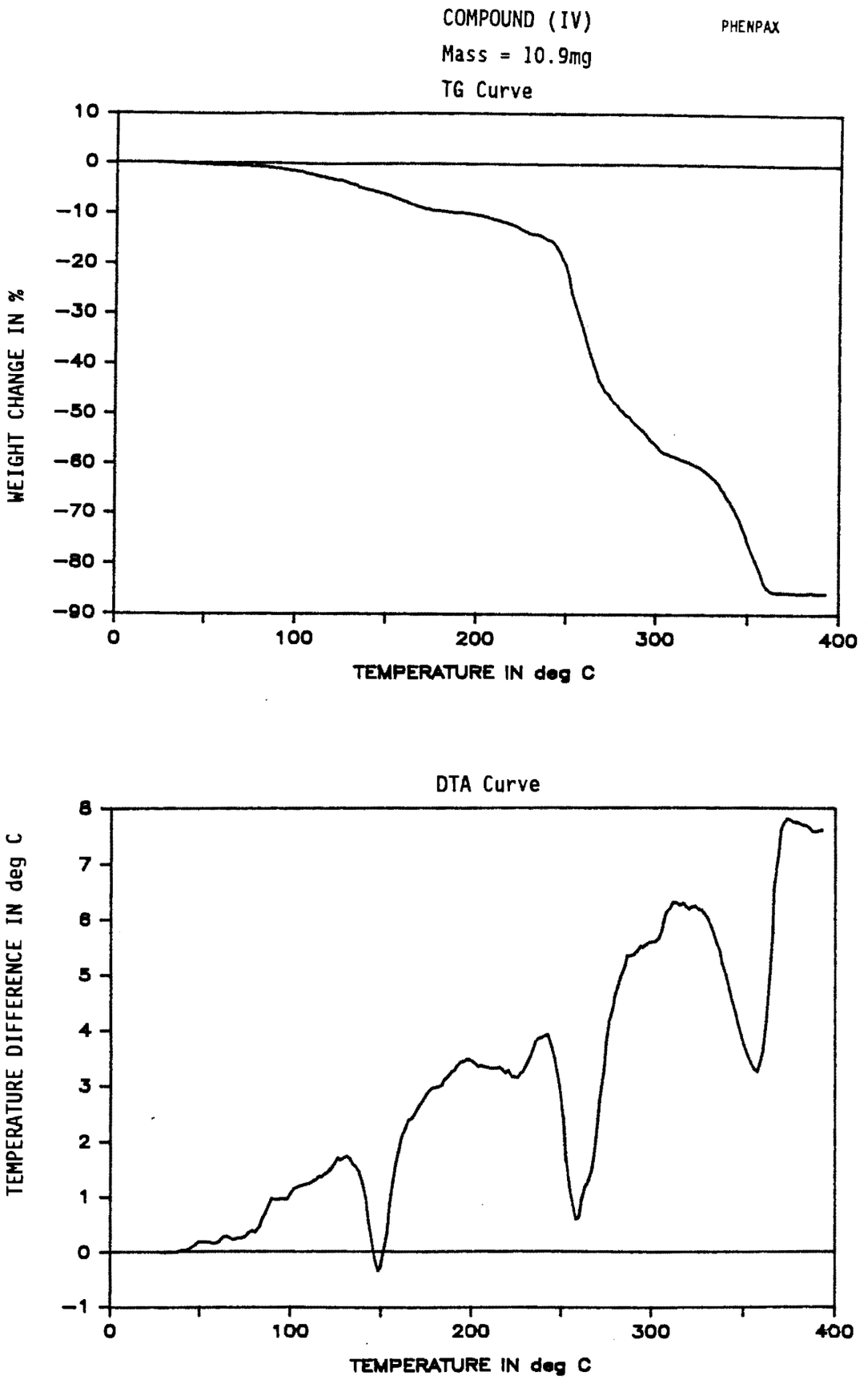

Fig 5.23 Thermogravimetric (TG) and Differential Thermal Analysis (DTA) curves for Compound (IV).

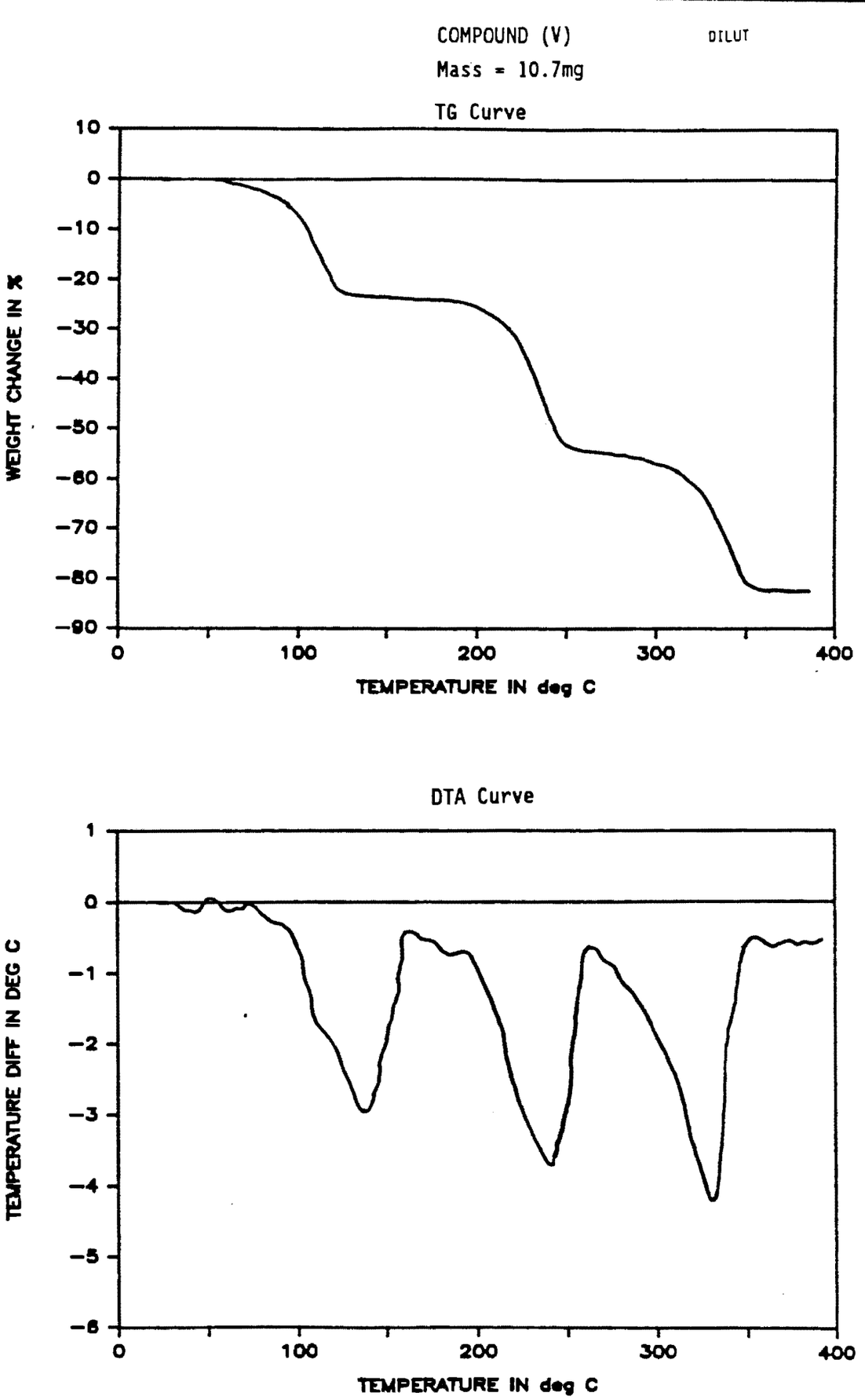

Fig 5.24 Thermogravimetric (TG) and Differential Thermal Analysis (DTA) curves for Compound (V).

COMPOUND (VI) PHENALC

Mass = 10.1mg

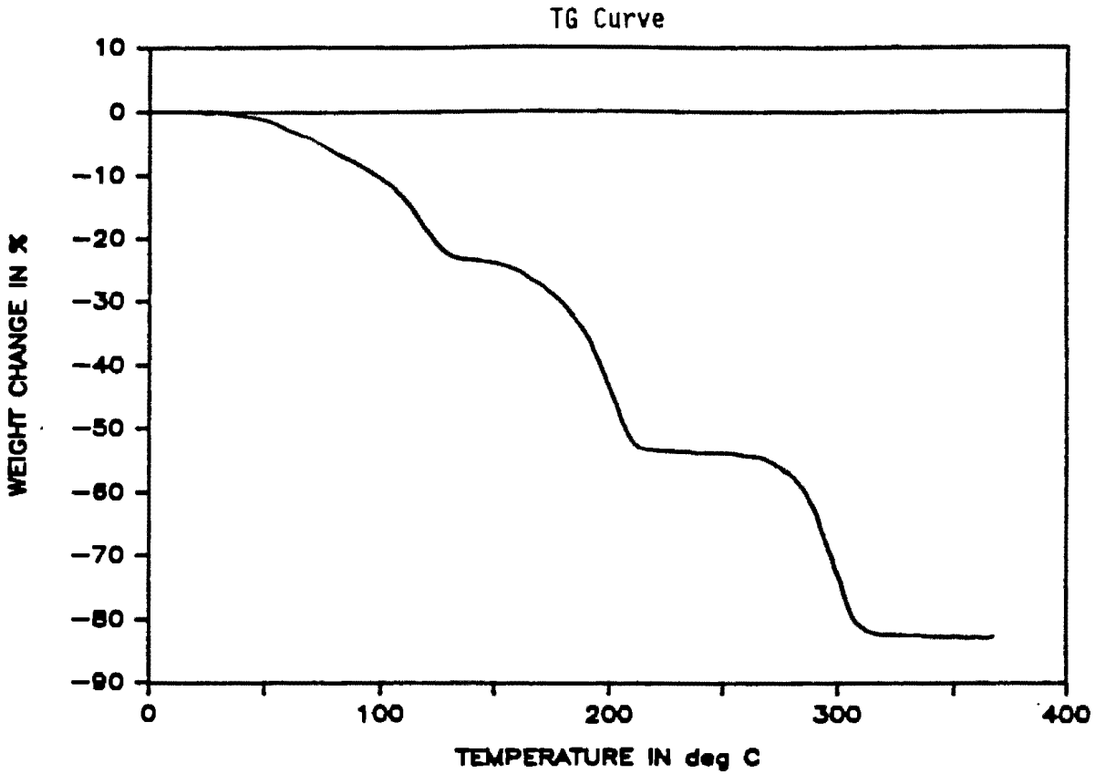

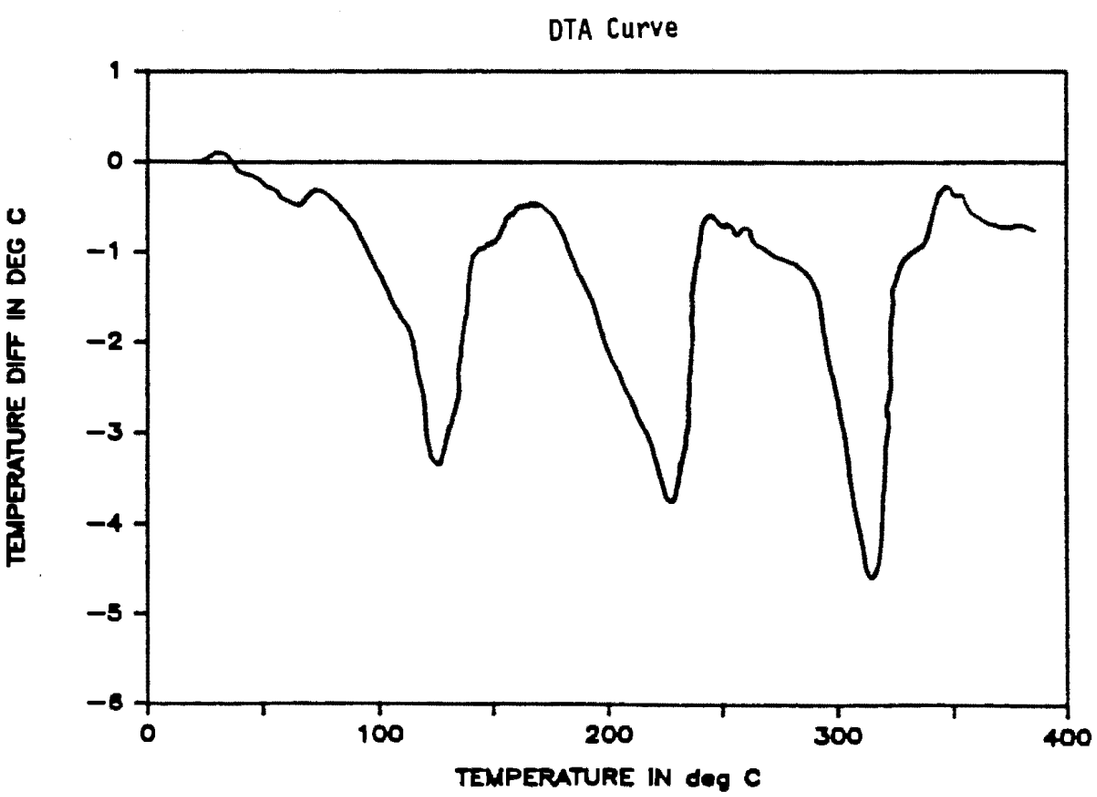

Fig 5.25 Thermogravimetric (TG) and Differential Thermal Analysis (DTA) curves for Compound (VI).

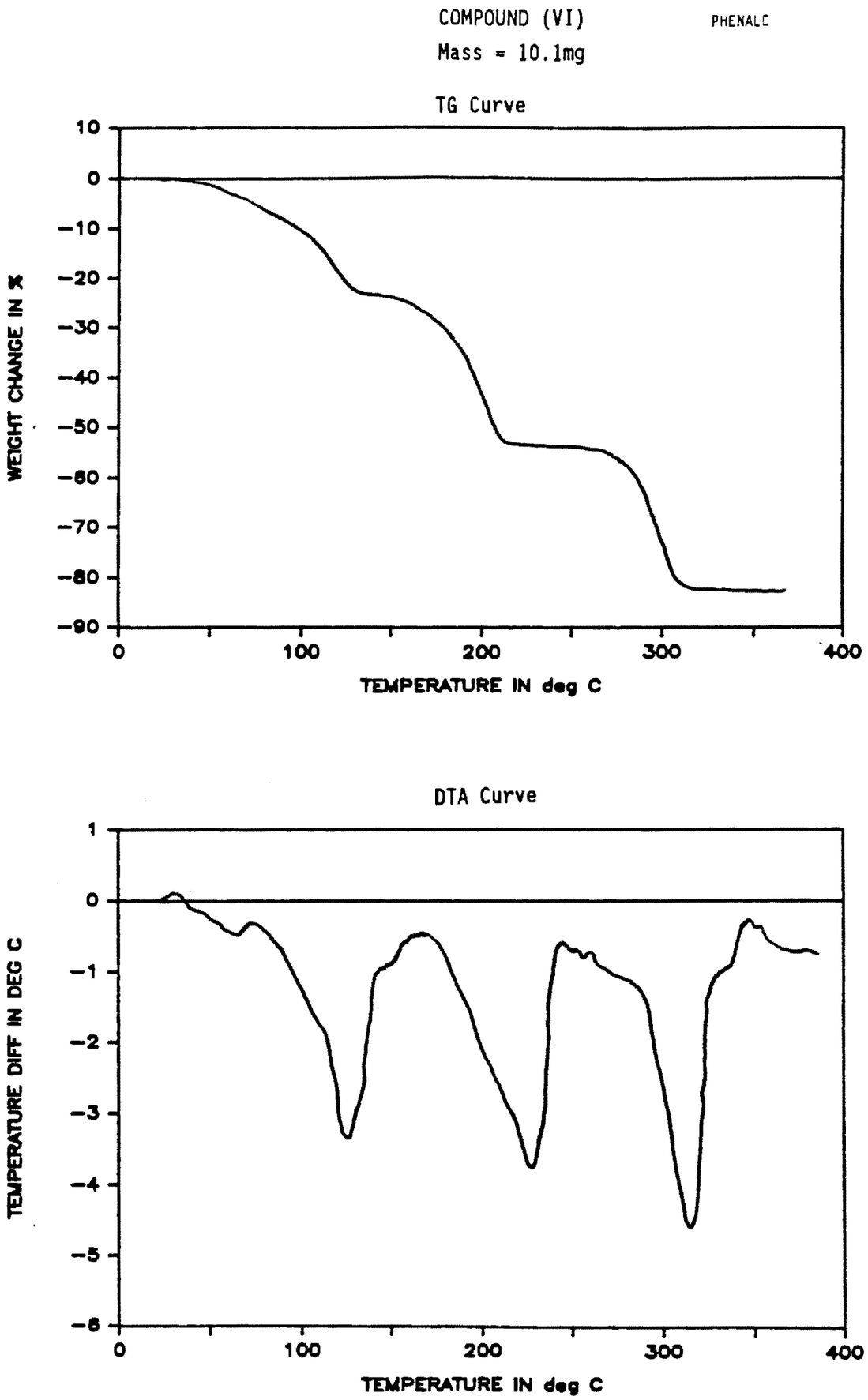

Fig 5.25 Thermogravimetric (TG) and Differential Thermal Analysis (DTA) curves for Compound (VI).

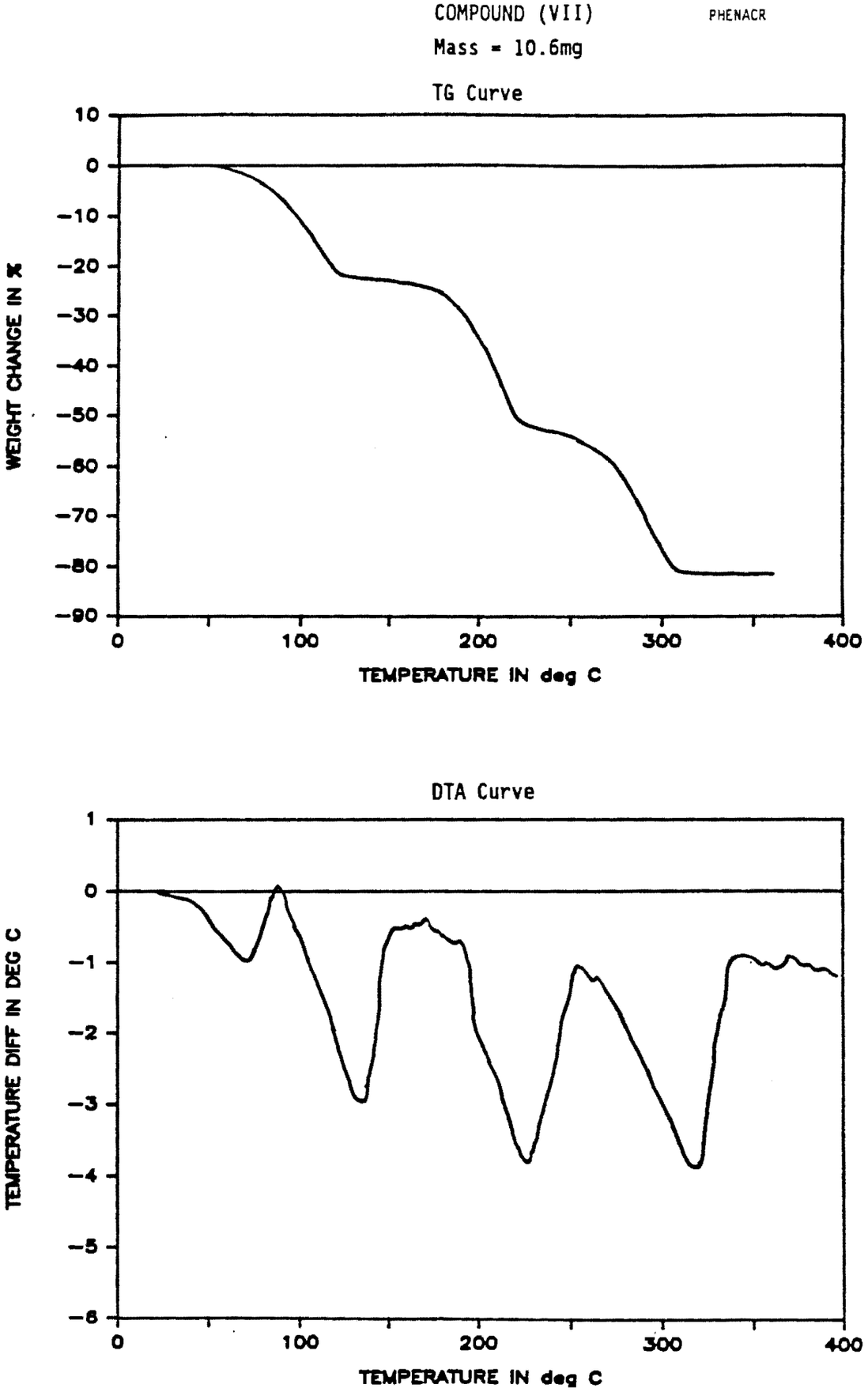

Fig 5.26 Thermogravimetric (TG) and Differential Thermal Analysis (DTA) curves for Compound (VII).

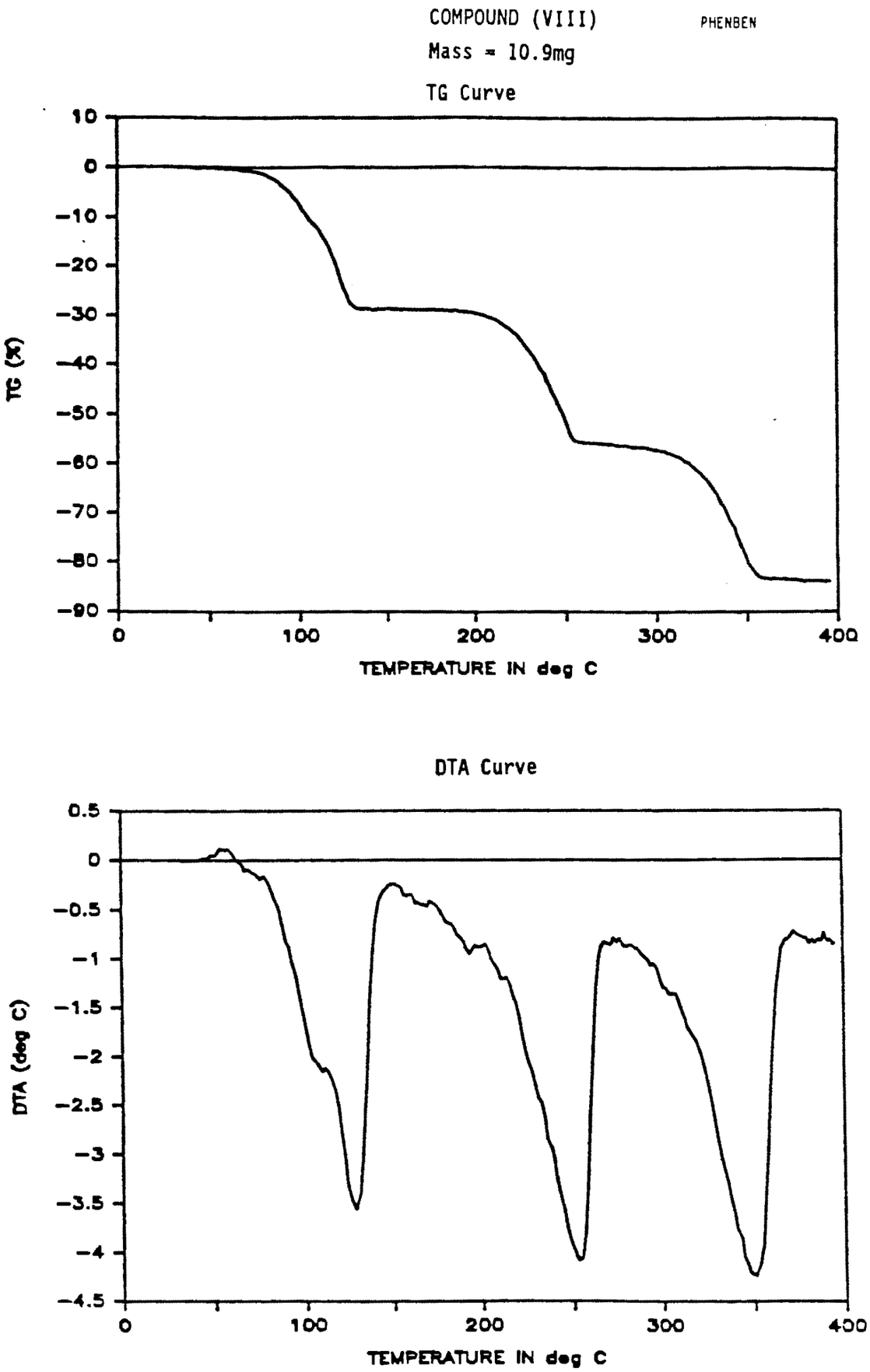

Fig 5.27 Thermogravimetric (TG) and Differential Thermal Analysis (DTA) curves for Compound (VIII).

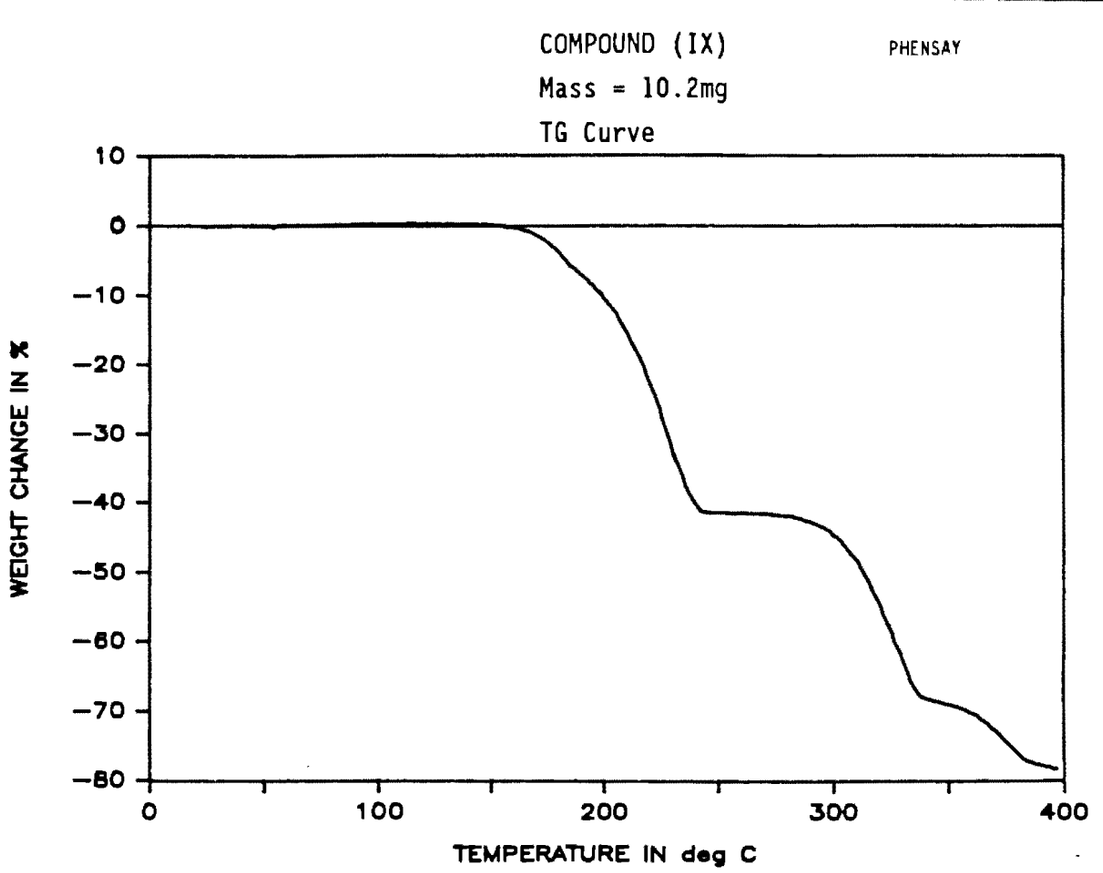

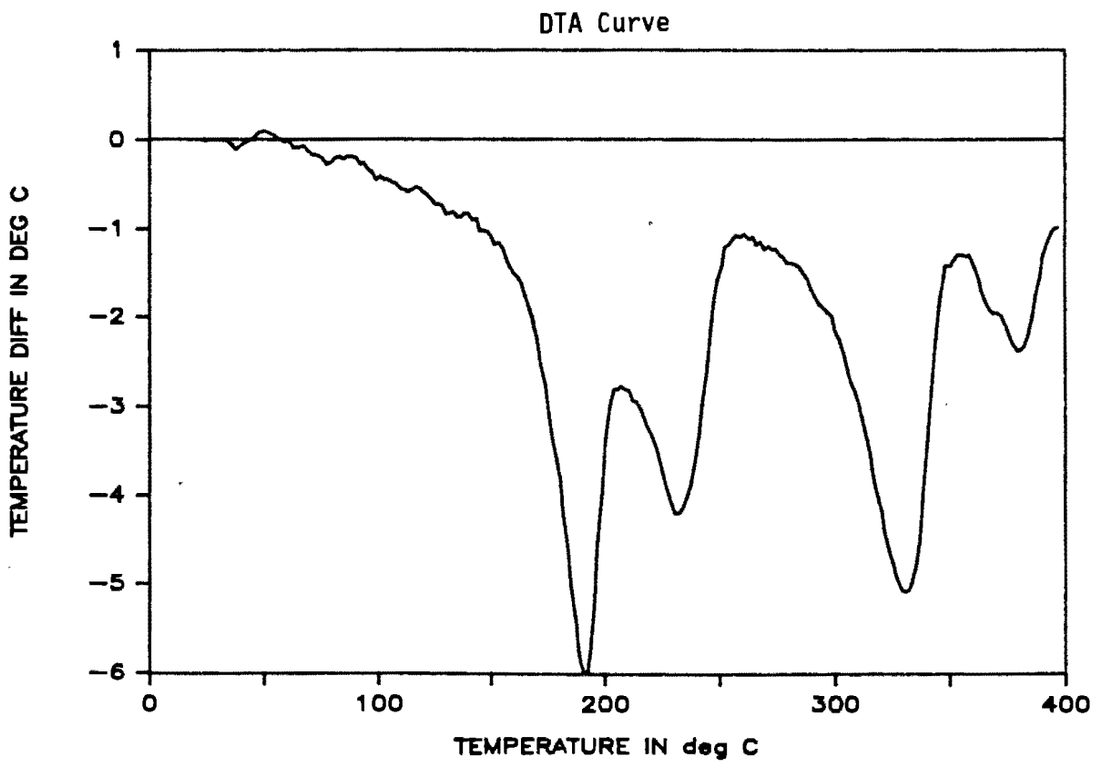

Fig 5.28 Thermogravimetric (TG) and Differential Thermal Analysis (DTA) curves for Compound (IX).

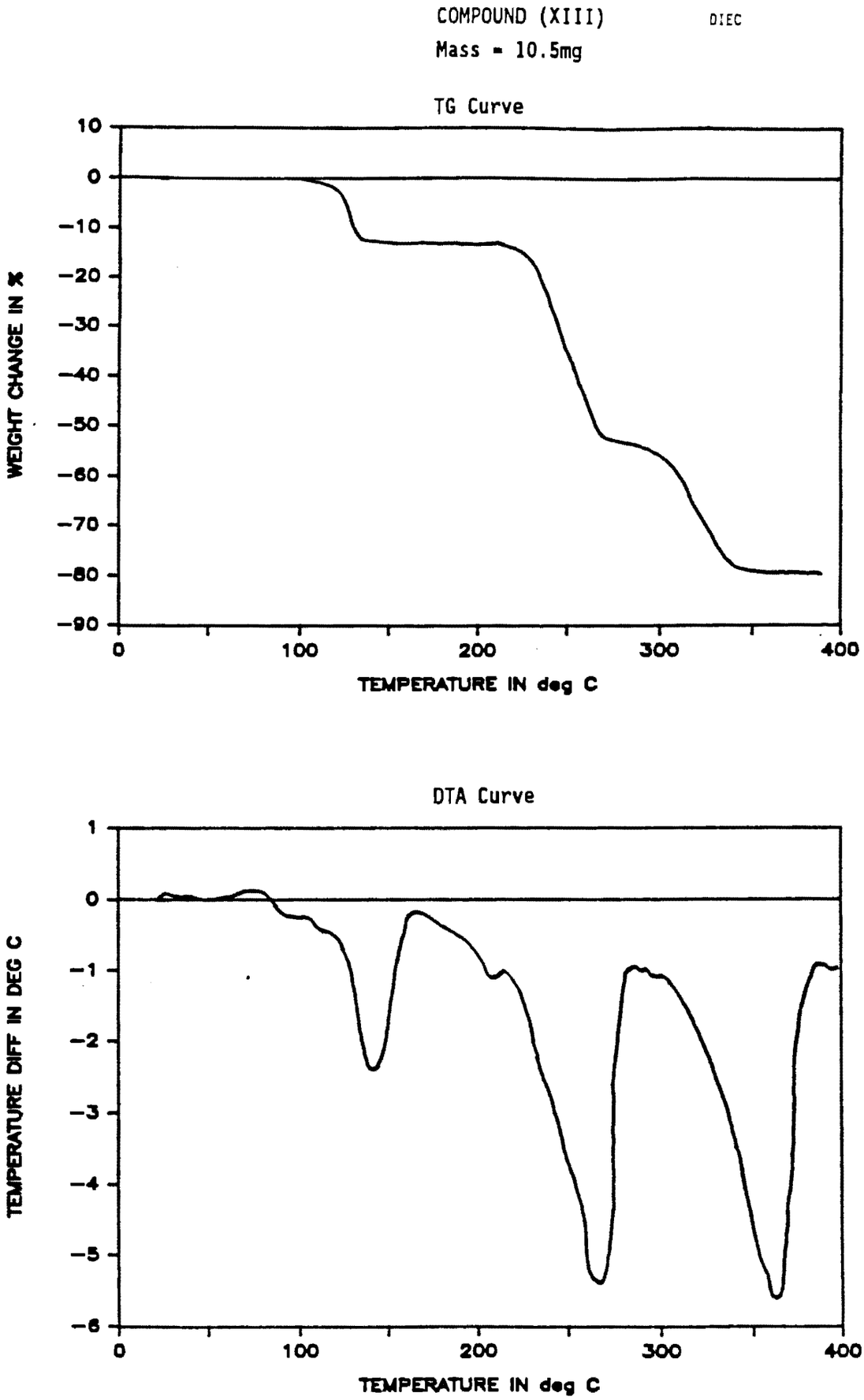

Fig 5.29 Thermogravimetric (TG) and Differential Thermal Analysis (DTA) curves for Compound (XIII).

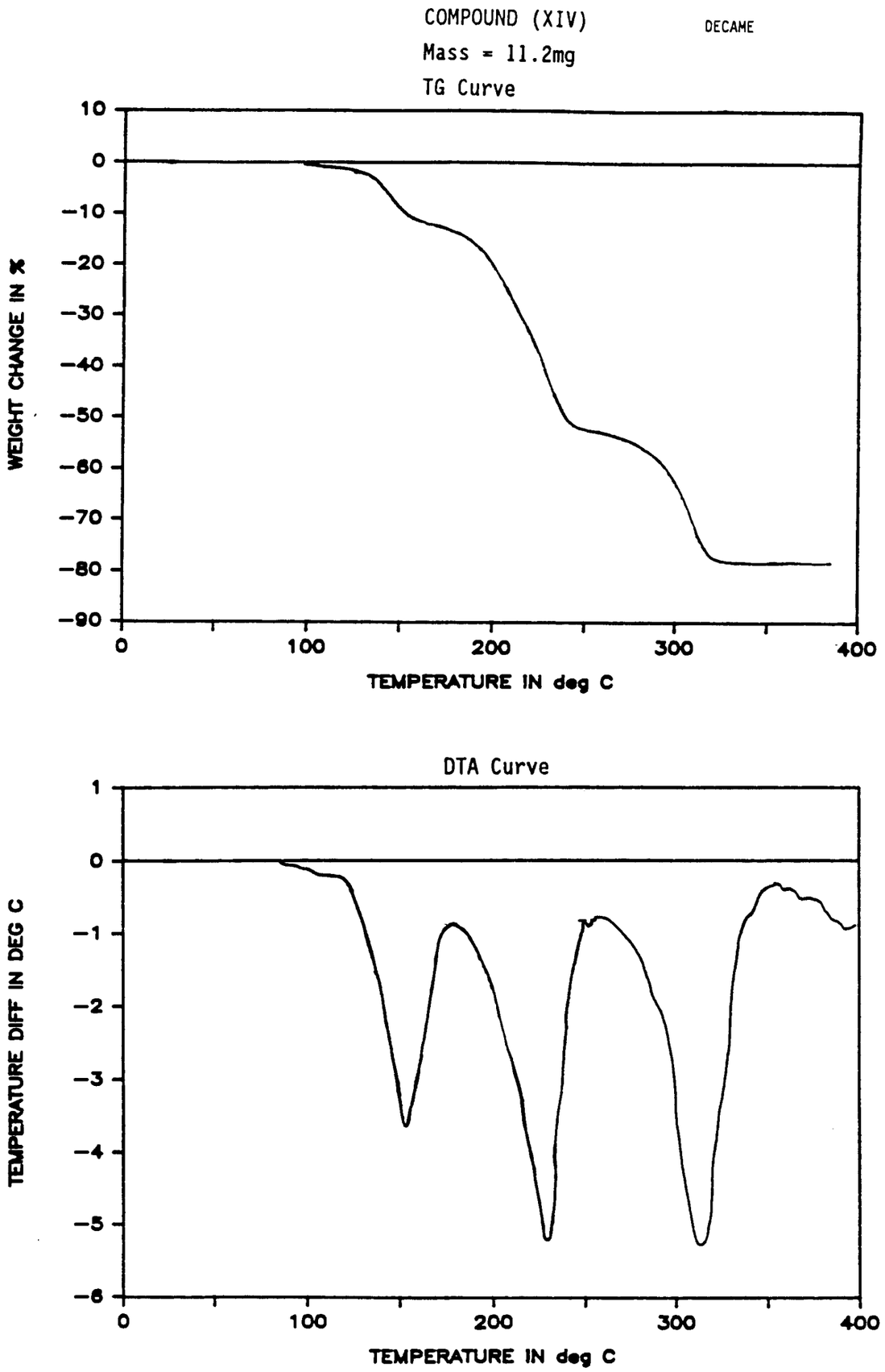

Fig 5.30 Thermogravimetric (TG) and Differential Thermal Analysis (DTA) curves for Compound (XIV).

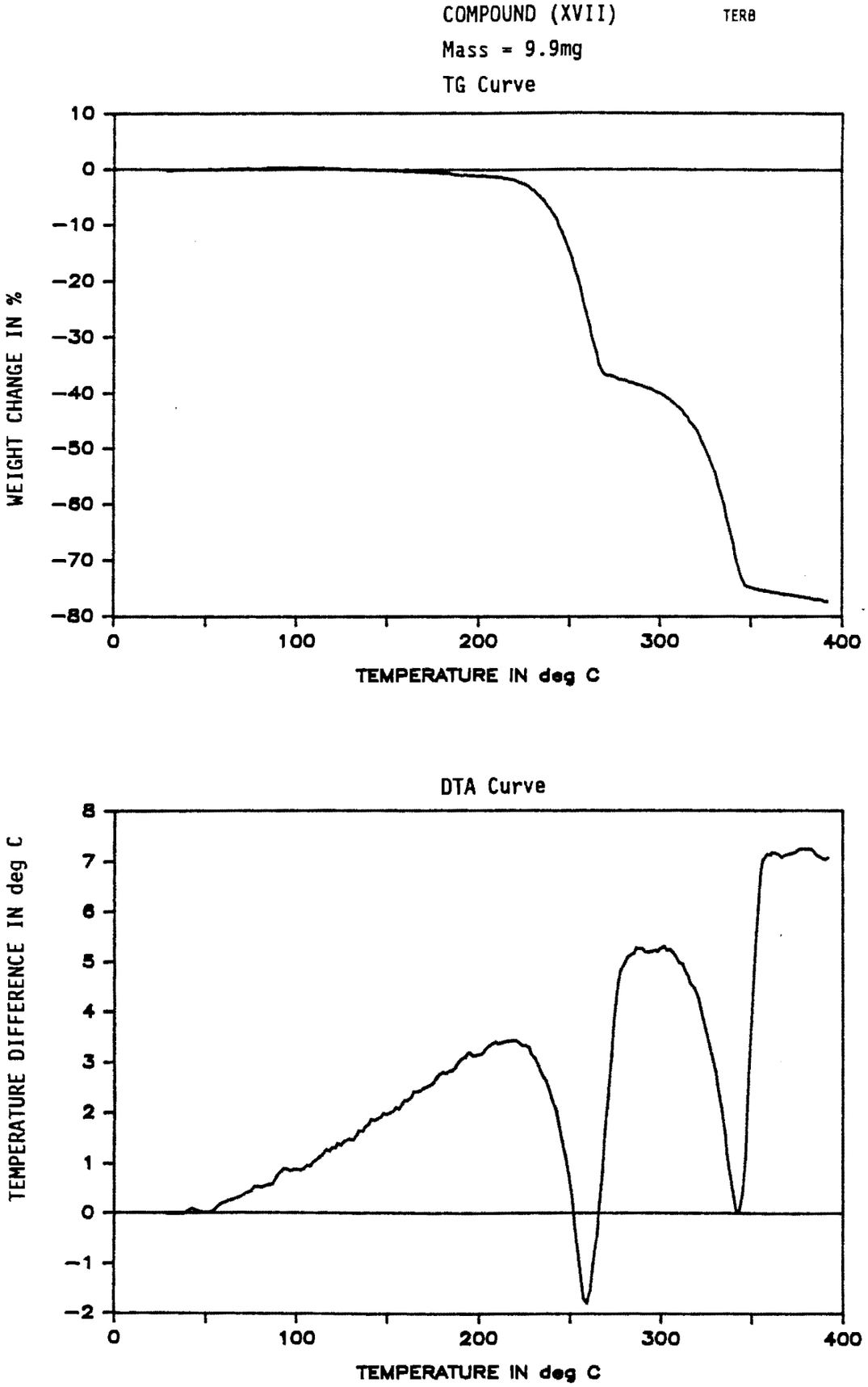

Fig 5.31 Thermogravimetric (TG) and Differential Thermal Analysis (DTA) curves for Compound (XVII).

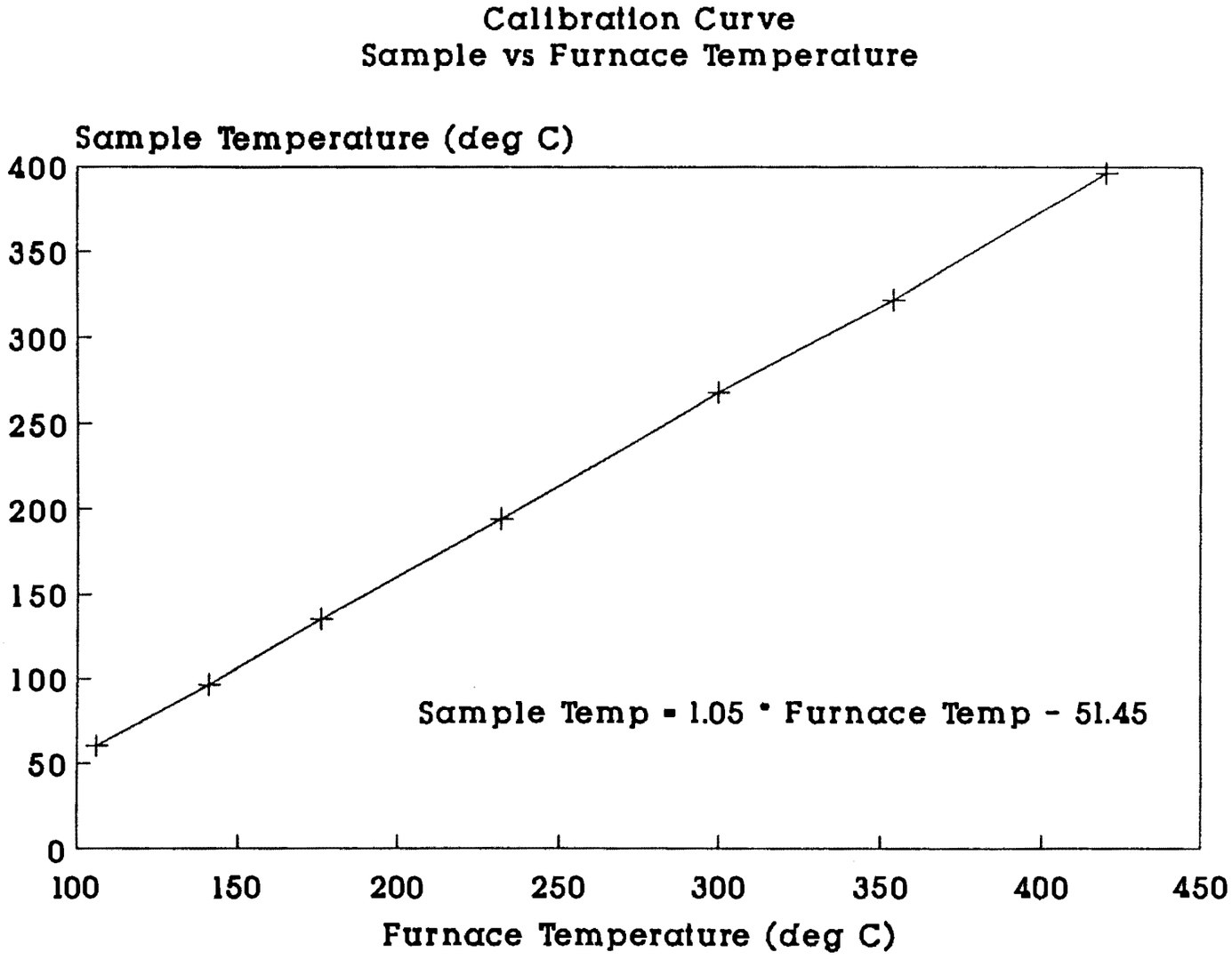

Fig 5.32 Calibration curve of Sample *vs* Furnace Temperature for Thermal Analysis.

COMPOUND (IX)

$z = 0.5$

Fig 4.9d Sections of the unit cell of Compound (IX) indicating the regions occuppied by the host molecules and the channels remaining in which the guest molecules are located.

REFERENCES

5.1 L. Lavelle, L.R. Nassimbeni and M.L. Niven, *Inorg Chim Acta.*, submitted.

5.2 D.R. Bond, G.E. Jackson and L.R. Nassimbeni, *S. Af. J. Chem.*, 36, 19 (1983).

5.3 'Structure-Activity Relationships in Werner Clathrates', M.H. Moore, Ph.D thesis, University of Cape Town (1987).

5.4 M.W. Taylor, unpublished results.

5.5 F. Casellato and B. Casu, *Erdol Kohle Erdgas Petrochem*, 22, 71 (1969).

5.6 E. Giglio, *J. Mol. Struct.*, 75, 39 (1981).

5.7 H.L. Wiener, L.Ilardi, P. Liberati, L. Dengler, S.A. Jeffas, S. Saba and N.O. Smith, *J. Incl. Phenom.*, 4, 415 (1986).

APPENDIX A

TABLE 5.1a Competition Experiments.

Guests: p-Xylene [A] / Benzene [B]

Host: 4-MePy [H]

Run	mass (g)		mmoles		mass	moles	Ratio	Ratio	mmoles	mmoles	Ratio
	A	B	A	B	H	H	area	liquid	A	B	solid
			m_A^T	m_B^T		m_S		R_L	m_A^C	m_B^C	R_S
1	0.481	1.183	4.527	15.145	1.096	2.005	0.240	0.185	1.769	0.236	7.491
2	0.545	1.123	5.130	14.382	1.094	2.001	0.299	0.237	1.775	0.226	7.855
3	0.629	1.045	5.924	13.376	1.096	2.005	0.384	0.313	1.801	0.204	8.834
4	0.775	0.948	7.301	12.137	1.097	2.007	0.548	0.458	1.825	0.182	10.053
5	1.073	0.727	10.108	9.311	1.098	2.008	1.044	0.899	1.866	0.142	13.092
6	1.372	0.478	12.918	6.125	1.095	2.003	2.101	1.838	1.882	0.121	15.585
7	1.566	0.366	14.750	4.682	1.096	2.005	3.189	2.805	1.903	0.102	18.662
8	1.593	0.287	15.000	3.674	1.094	2.001	4.153	3.661	1.904	0.097	19.656
9	1.646	0.243	15.506	3.111	1.095	2.003	5.097	4.500	1.913	0.090	21.188

TABLE 5.2a Competition Experiments.

Guests: p-Xylene [A] / Toluene [B]

Host: 4-MePy [H]

Run	mass (g)		mmoles		mass	moles	Ratio	Ratio	mmoles	mmoles	Ratio
	A	B	A	B	H	H	area	liquid	A	B	solid
			m_A^T	m_B^T		m_S		R_L	m_A^C	m_B^C	R_S
1	0.526	1.923	4.959	20.872	1.095	2.003	0.288	0.182	1.290	0.713	1.809
2	0.696	1.348	6.555	14.635	1.094	2.001	0.476	0.360	1.476	0.525	2.808
3	0.931	1.145	8.769	12.428	1.094	2.001	0.725	0.595	1.608	0.393	4.093
4	1.006	1.015	9.476	11.011	1.097	2.007	0.871	0.734	1.653	0.354	4.677
5	1.063	0.842	10.015	9.134	1.099	2.011	1.094	0.945	1.688	0.323	5.232
6	1.336	0.546	12.582	5.923	1.096	2.005	2.078	1.876	1.819	0.186	9.787
7	1.611	0.433	15.177	4.696	1.095	2.003	3.200	2.937	1.846	0.157	11.757
8	1.661	0.324	15.644	3.517	1.094	2.001	4.411	4.083	1.860	0.141	13.187
9	1.808	0.287	17.032	3.111	1.096	2.005	5.462	5.078	1.878	0.127	14.813

TABLE 5.3a Competition Experiments.

Guests: p-Xylene [A] / Ethylbenzene [B]

Host: 4-MePy [H]

Run	mass (g)		mmoles		mass	moles	Ratio	Ratio	mmoles	mmoles	Ratio
	A	B	A	B	H	H	area	liquid	A	B	solid
			m_A^T	m_B^T		m_S		R_L	m_A^C	m_B^C	R_S
1	0.460	2.072	4.334	19.516	1.097	2.007	0.222	0.172	1.128	0.879	1.284
2	0.751	1.488	7.075	14.012	1.095	2.001	0.505	0.405	1.573	0.428	3.679
3	0.910	1.283	8.570	12.086	1.096	2.005	0.709	0.583	1.701	0.304	5.597
4	1.040	1.127	9.794	10.612	1.099	2.011	0.923	0.771	1.786	0.225	7.929
5	1.107	0.968	10.423	9.122	1.096	2.005	1.143	0.968	1.796	0.209	8.575
6	1.464	1.464	13.785	6.074	1.094	2.001	2.270	1.979	1.922	0.079	24.211
7	1.716	0.500	16.164	4.711	1.094	2.001	3.431	3.052	1.948	0.053	36.717
8	1.805	0.404	17.004	3.801	1.095	2.003	4.474	4.000	1.962	0.041	48.335
9	1.927	0.342	18.147	3.221	1.098	2.009	5.634	5.057	1.984	0.025	79.802

TABLE 5.4a Competition Experiments.

Guests: p-Xylene [A] / Benzene [B]

Host: 4-ViPy [H]

Run	mass (g)		mmoles		mass	moles	Ratio	Ratio	mmoles	mmoles	Ratio
	A	B	A	B	H	H	area	liquid	A	B	solid
			m_A^T	m_B^T		m_S		R_L	m_A^C	m_B^C	R_S
1	0.479	1.190	4.513	15.236	1.192	2.002	0.249	0.193	1.642	0.360	4.560
2	0.560	1.1225	5.272	14.401	1.193	2.004	0.318	0.254	1.693	0.311	5.446
3	0.646	1.046	6.080	13.393	1.189	1.997	0.407	0.333	1.714	0.283	6.057
4	0.777	0.950	7.315	12.156	1.197	2.010	0.558	0.467	1.757	0.253	6.930
5	1.085	0.726	10.216	9.292	1.191	2.000	1.073	0.925	1.802	0.198	9.082
6	1.400	0.479	13.183	6.134	1.192	2.002	2.180	1.908	1.822	0.180	10.139
7	1.583	0.368	14.913	4.717	1.194	2.005	3.266	2.873	1.839	0.166	11.059
8	1.587	0.287	14.945	3.679	1.191	2.000	4.224	3.724	1.840	0.160	11.504
9	1.622	0.244	15.281	3.122	1.195	2.007	5.085	4.489	1.872	0.135	13.874

TABLE 5.5a Competition Experiments.

Guests: p-Xylene [A] / Toluene [B]

Host: 4-ViPy [H]

Run	mass (g)		mmoles		mass	moles	Ratio	Ratio	mmoles	mmoles	Ratio
	A	B	A	B	H	H	area	liquid	A	B	solid
			m_A^T	m_B^T		m_S		R_L	m_A^C	m_B^C	R_S
1	0.508	1.927	4.787	20.913	1.195	2.007	0.282	0.176	1.241	0.766	1.620
2	0.692	1.339	6.522	14.527	1.195	2.007	0.481	0.365	1.430	0.577	2.479
3	0.940	1.140	8.857	12.376	1.191	2.000	0.744	0.613	1.548	0.453	3.418
4	1.024	1.029	9.641	11.173	1.193	2.004	0.881	0.743	1.622	0.381	4.262
5	1.032	0.848	9.717	9.205	1.197	2.010	1.064	0.916	1.632	0.378	4.314
6	1.283	0.542	12.088	5.879	1.195	2.005	1.997	1.799	1.829	0.176	10.376
7	1.570	0.430	14.785	4.672	1.191	2.000	3.208	2.945	1.753	0.247	7.100
8	1.580	0.321	14.880	3.483	1.195	2.007	4.307	3.985	1.805	0.202	8.938
9	1.716	0.285	16.164	3.096	1.193	2.004	5.268	4.894	1.836	0.168	10.909

TABLE 5.6a Competition Experiments.

Guests: p-Xylene [A] / Ethylbenzene [B]

Host: 4-ViPy [H]

Run	mass (g)		mmoles		mass	moles	Ratio	Ratio	mmoles	mmoles	Ratio
	A	B	A	B	H	H	area	liquid	A	B	solid
			m_A^T	m_B^T		m_S		R_L	m_A^C	m_B^C	R_S
1	0.389	2.063	3.660	19.428	1.191	2.000	0.164	0.153	0.862	1.138	0.757
2	0.603	1.499	5.675	14.123	1.197	2.010	0.346	0.327	1.292	0.718	1.798
3	0.798	1.290	7.519	12.154	1.192	2.002	0.541	0.512	1.535	0.467	3.288
4	0.966	1.128	9.094	10.626	1.191	2.000	0.766	0.726	1.641	0.359	4.563
5	1.005	0.963	9.464	9.073	1.194	2.005	0.933	0.885	1.702	0.303	5.624
6	1.381	0.638	13.007	6.009	1.193	2.004	2.006	1.906	1.849	0.155	11.937
7	1.552	0.502	14.620	4.728	1.189	1.997	2.907	2.763	1.880	0.117	16.061
8	1.675	0.402	15.780	3.786	1.195	2.007	3.921	3.728	1.935	0.072	26.810
9	1.759	0.342	16.567	3.225	1.193	2.004	4.854	4.616	1.946	0.058	33.779

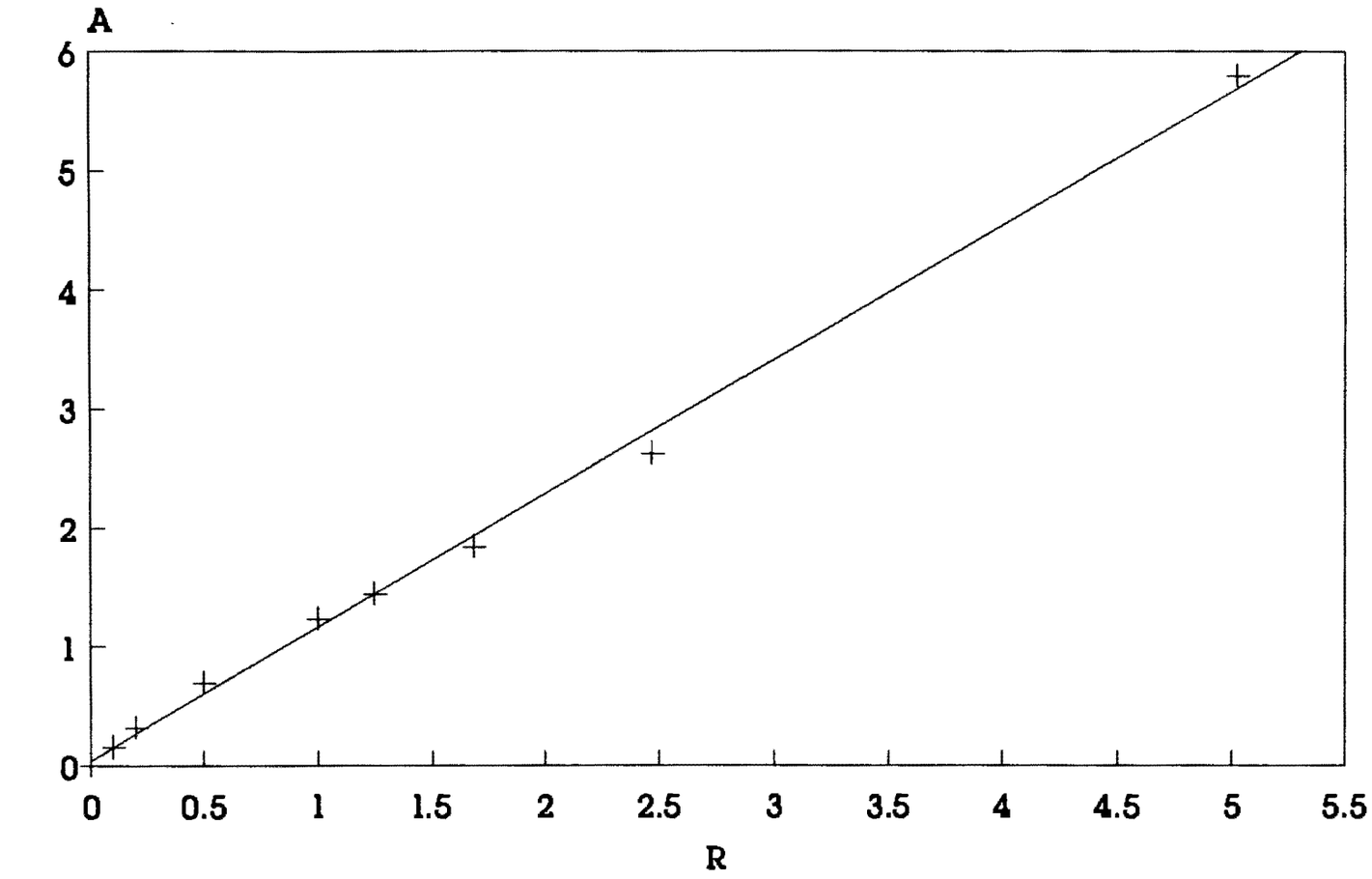

R = mole ratio (p-Xylene / Benzene)
A = area ratio (from G.C.)

Fig 5.7 Calibration curve of area ratio (A) vs mole ratio (R) for *p*-xylene/benzene from G.C.

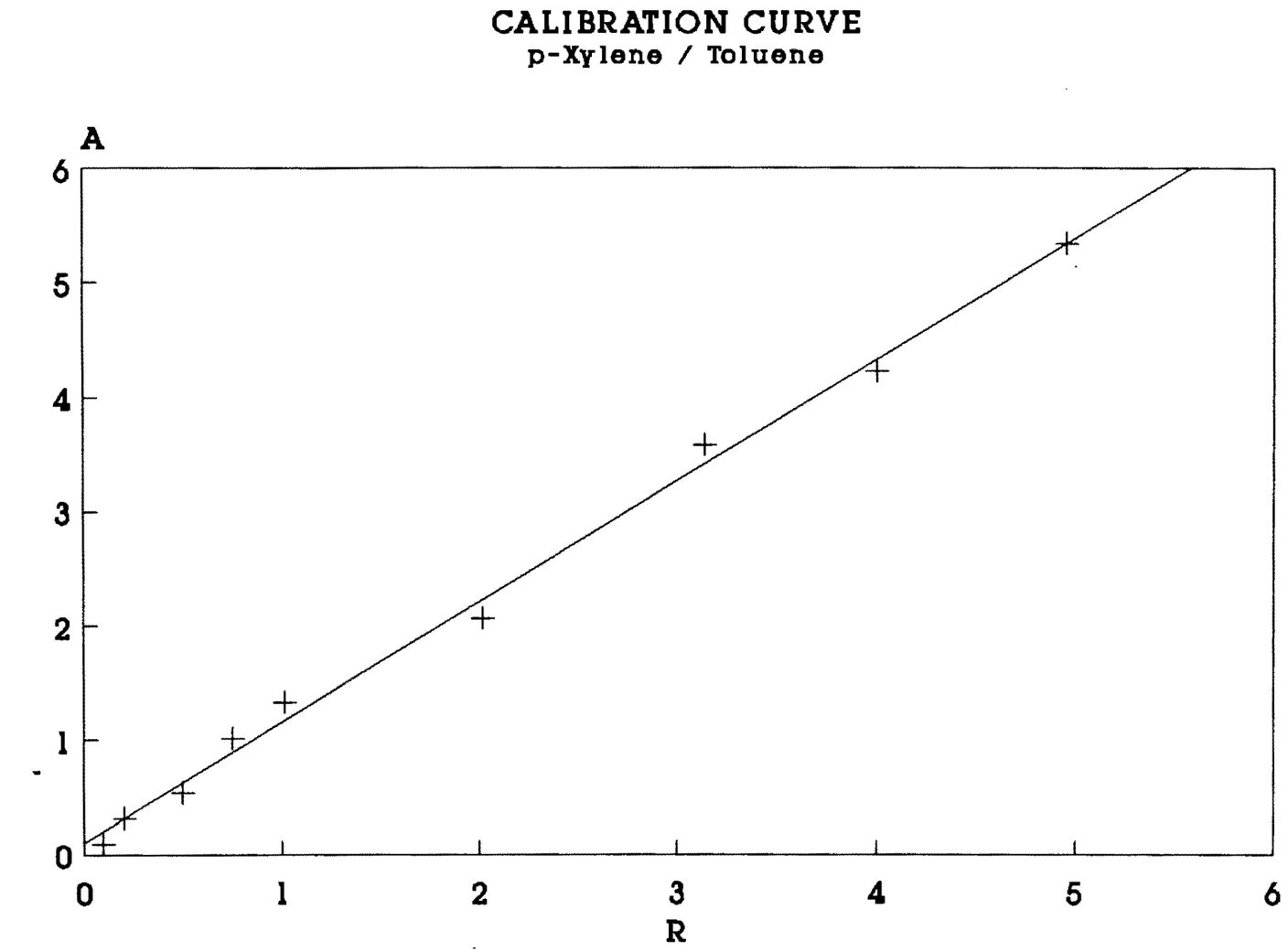

R = mole ratio (p-Xylene / Toluene)
A = area ratio (from G.C.)

Fig 5.8 Calibration curve of area ratio (A) vs mole ratio (R) for *p*-xylene/toluene from G.C.

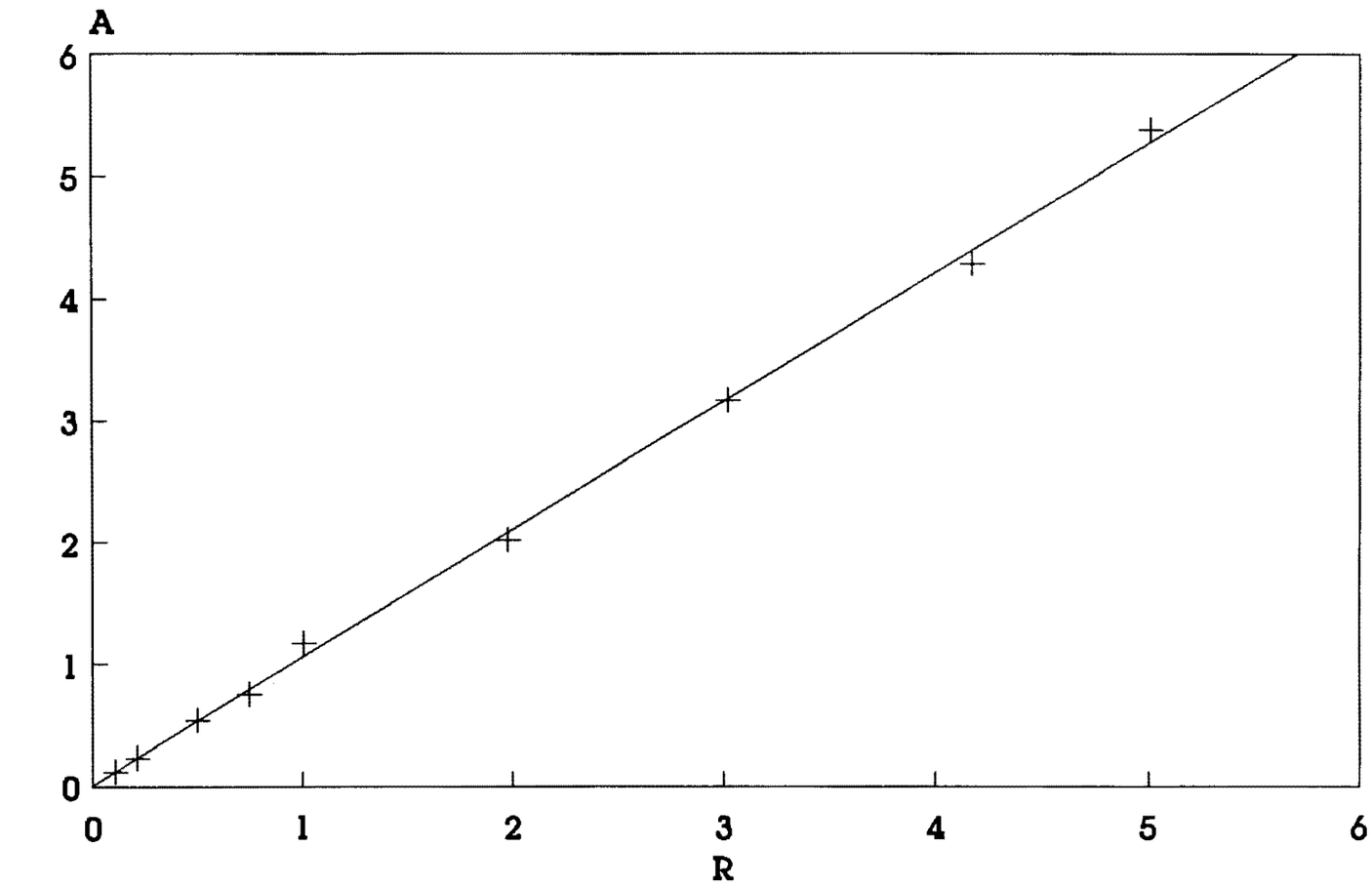

R = mole ratio (p-Xylene / Ethylbenzene)
A = area ratio (from G.C.)

Fig 5.9 Calibration curve of area ratio (A) vs mole ratio (R) for *p*-xylene/ethylbenzene from G.C.

TABLE 2.1 Compound Classes, Numbers and Codenames for all Structures reported in this work.

HOST	COMPOUND	GUEST	CODE.
Class A			
$[Ni(NCS)_2(4\text{-}PhPy)_4]$	I	-	PHEN
	II	*o*-xylene	PHENOX
	III	*m*-xylene	PHENMEX
	IV	*p*-xylene + dmso	PHENPAX
	V	4-PhPy + 2-methoxyethanol	DILUT
	VI	4-PhPy + dmso	PHENALC
	VII	Phenylacetylene + dmso	PHENACR
	VIII	Benzene	PHENBEN
Class B			
$[NiCl_2(4\text{-}PhPy)_4]$	IX	Methanol	PHENSAY
	X	*m*-xylene	FENMEX
	XI	*p*-xylene	FENPAX
	XII	4-PhPy	FENTET
Class C			
$[Ni(NCS)_2(4\text{-}MePy)_2(4\text{-}PhPy)_2]$	XIII	Acetylacetone	DIEC
	XIV	1-chlorobutane	DECAME
Class D			
$[Ni(NCS)_2(dmso)_2(4\text{-}PhPy)_2]$	XV	-	METAG
$[NiCl_2(dmso)_2(4\text{-}PhPy)_2]$	XVI	-	PHENDIM
$[Ni(NCS)_2(4\text{-}t\text{-}BuPy)_4]$	XVII	-	TERB
$[Ni(NCS)_2(4\text{-}BzPy)_4]$	XVIII	-	BENNEY